PhD-FSTC-2016-29
The Faculty of Sciences, Technology and Communication

DISSERTATION

Defense held on 15/07/2016 in Luxembourg

to obtain the degree of

DOCTEUR DE L'UNIVERSITÉ DU LUXEMBOURG

EN BIOLOGIE

by

Sylvie DELCAMBRE
Born on 08th of March 1989 in Messancy (Belgium)

In vitro METABOLIC STUDIES OF DOPAMINE SYNTHESIS AND THE TOXICITY OF L-DOPA IN HUMAN CELLS

Dissertation defense committee

Dr Karsten Hiller, dissertation supervisor
Associate Professor, Université du Luxembourg

Dr Serge Haan, Chairman
Professor, Université du Luxembourg

Dr Marcel Leist, Vice Chairman
Professor, University of Konstanz, Germany

Dr Katrin Marcus
Professor, Ruhr University Bochum, Germany

Dr Carole Linster
PhD, Université du Luxembourg

UNIVERSITY OF LUXEMBOURG

DOCTORAL THESIS

In vitro Metabolic Studies of Dopamine Synthesis and the Toxicity of L-DOPA in Human Cells

Author:
Sylvie DELCAMBRE

Supervisor:
Dr. Karsten HILLER

A thesis submitted in fulfilment of the requirements
for the degree of Doctor of Philosophy

in the

Metabolomics Group
Luxembourg Centre for Systems Biomedicine

July 15, 2016

Declaration of Authorship

I, Sylvie DELCAMBRE, declare that this thesis titled, "*In vitro* Metabolic Studies of Dopamine Synthesis and the Toxicity of L-DOPA in Human Cells" and the work presented in it are my own. I confirm that:

- This work was done wholly while in candidature for a research degree at this University.

- Where any part of this thesis has previously been submitted for a degree or any other qualification at this University or any other institution, this has been clearly stated.

- Where I have consulted the published work of others, this is always clearly attributed.

- Where I have quoted from the work of others, the source is always given. With the exception of such quotations, this thesis is entirely my own work.

- I have acknowledged all main sources of help.

- Where the thesis is based on work done by myself jointly with others, I have made clear exactly what was done by others and what I have contributed myself.

Signed:

_____

Date:

_____

"One of the deep secrets of life is that all that is really worth the doing is what we do for others"

Lewis Carroll

Abstract

In vitro Metabolic Studies of Dopamine Synthesis and the Toxicity of L-DOPA in Human Cells

by Sylvie DELCAMBRE

This work is divided in two parts. In the first, I investigated the effects of 2,3-dihydroxy-L-phenylalanine (L-DOPA) on the metabolism of human tyrosine hydroxylase (TH)-positive neuronal LUHMES cells. L-DOPA is the gold standard treatment for Parkinson's disease (PD) and its effects on cellular metabolism are controversial. It induced a re-routing of intracellular carbon supplies. While glutamine contribution to tricarboxylic acid (TCA) cycle intermediates increased, glucose contribution to the same metabolites decreased. Carbon contribution from glucose was decreased in lactate and was compensated by an increased pyruvate contribution. Pyruvate reacted with hydrogen peroxide generated during the auto-oxidation of L-DOPA and lead to an increase of acetate in the medium. In the presence of L-DOPA, this acetate was taken up by the cells. In combination with an increased glutamate secretion, all these results seem to point towards a mitochondrial complex II inhibition.

In the second part of this work, I studied and compared dopamine (DA)-producing *in vitro* systems. First, I compared gene and protein expression of catecholamine (CA)-related genes. Then, I performed molecular engineering to increase TH expression in LUHMES and SH-SY5Y cells. This was sufficient to induce DA production in SH-SY5Y, but not in LUHMES cells, indicating that TH expression is not sufficient to characterize dopaminergic neurons. Therefore I used SH-SY5Y cells overexpressing TH to study substrates for DA production. Upon overexpression of aromatic amino acid decarboxylase (AADC), LUHMES cells produced DA after L-DOPA supplementation. This model was useful to study L-DOPA uptake in LUHMES cells and I showed that L-DOPA is imported via large amino acid transporter (LAT). In conclusion, the expression of TH is not sufficient to obtain a DA-producing cell system and this work opened many and answered some questions about DA metabolism.

Acknowledgements

I first would like to thank Ass. Prof. Karsten Hiller, without whom this work would not have been possible. You gave me the opportunity to work in this great team, to write my own grant and carry my work over these three and a half year.

My gratitude also goes to Dr. Carole Linster and Prof. Marcel Leist who were both part of my Comité d'encadrement de Thèse (CET) and provided valuable ideas and comments to this work. I also would like to thank Prof. Katrin Marcus, Prof. Jochen Klucken and Prof. Serge Haan for joining my defense committee and their critical review of my thesis.

I promised a whole paragraph in the acknowledgements section to Christian, so here it is... Thank you for being so patient with me, teaching me how to take care of these (at first, so impressive and scary) GC-MS instruments, taking so much time to help me set up some crazy methods, MetaboliteDetector issues and always checking if I would make it home safely on the tough days...

I thank Johannes, who started this whole project, helped me getting comfortable with the LUHMES cells and always providing good advice concerning experimental design. I would have never been able to survive three years in the lab without the help of Jenny, who taught me pretty much everything I know about lab work, who agreed to be my godmother when I started at the LCSB and got me settled next to my "desk partner" Sean. Sean, well, well, well... So many things to say... You started your master thesis when I started my PhD and now, it looks like we will be finishing pretty much together. I had three great years sitting next to you (this of course does not take into account the months you abandoned me on the fifth floor in BT1...) and would like to thank you for our great conversations and time spent together. Xiangyi and Jean-Pierre, we started our master together and were reunited in this lab, I would like to thank you for all the fun we had. JP, I seem to recall that I had to thank you for some Latex coding, I cannot recall exactly which part, but I thank you anyway. I would like to thank Lisa and Yannic for laughs and conversations we had in the lab. I thank Andre for trying to teach me German through sayings on post-it notes (I kept them all throughout my PhD). Here is one of them, the first one I received: "*Morgen morgen nur nicht heute sagen alle faulen Leute*". This thesis would have never been there today if it was not for Daniel Weindl, who fixed my computer countless times. I owe you crates and crates of beers... I would like to thank Thekla Cordes for accompanying me to the

swimming pool each Tuesdays for a year, it was a great way to change my mind.

I thank Nadia who was a great support through this writing phase. Maybe because we went though it together, or because we would build our futures around a bottle of beer, most probably because the two of them... Last but not least, I thank Elodie. During this last year, I really enjoyed working with you. I valued your comments on my thesis and am super thankful for listening whenever I had a hard time or was excited about something. So overall, I would like to thank the Metabolomics group to be the Metabolomics group. I am still amazed by the fact that so many great people can be gathered together and can have such a great time working together as well as doing so many other things together...

During the time spent on my thesis, I also had the chance to participate in teaching activities. It concerned high school, bachelor, master and PhD students. Therefore, I would like to thank Elisabeth John, Alexandre Salsmann, Laurent Vallar, Serge Haan, Jean-Luc Bueb and Karsten Hiller for giving me the opportunity to spend some time in a classroom on the other side of the student desk.

I realize this is a really long acknowledgement section, but I could not finish without thanking my family and especially my parents, Cécile et Danny, for supporting me throughout all these years of studying and working. You gave me the opportunity and the tools to study anything I wanted and to become whatever I wanted to. There is no word strong enough to express what I think, so I will simply say: Merci pour tout ce que vous avez fait pour moi toutes ces années, je vous revaudrai ça au centuple!

There are so many people I would like to thank that I could fill another thesis, so I will just stop there and let you go on with your reading.

Contents

Acronyms

α-**KGDH**	α-ketoglutarate dehydrogenase
ATP13A2	ATPase type 13A2
LRRK2	leucine-rich repeat kinase 2
PINK1	PTEN-induced putative kinase 1
3-MT	3-methoxytyramine
3-NP	3-nitropropionic acid
3-OMD	3-*o*-methyldopa
4F2hc	heavy chain of 4F2 cell surface antigen
5-HT	serotonin
5-HTP	5-hydroxytryptophan
6-OHDA	6-hydroxydopamine
AA	ascorbic acid
AADC	aromatic amino acid decarboxylase
AAV	adeno-associated virus
AC	adenylyl cyclase
Aco	aconitase
ACSS2	acetyl-CoA synthetase
ADH	alcohol dehydrogenase
ADHD	attention deficit and hyperactivity disorder
AIDS	acquired immune deficiency syndrome
ALDH	aldehyde dehydrogenase
ALT	alanine aminotransferase
ANLSH	astrocyte-neuron lactate shuttle hypothesis
AP-1	activator protein 1

ATP	adenosine triphosphate
BBB	blood brain barrier
BDNF	brain-derived neurotrophic factor
BH$_2$	7,8-dihydrobiopterin
BH$_4$	6R-L-erythro-5,6,7,8-tetrahydrobiopterin
BME	β-mercaptoethanol
BSA	bovine serum albumine
CA	catecholamine
cAMP	cyclic adenosine monophosphate
CaMPKII	calcium/calmodulin-dependent protein kinase II
CMA	chaperone-mediated autophagy
CMV	cytomegalovirus
CNS	central nervous system
COMT	catechol-o-methyl transferase
CRE	cAMP response element
CREB	cAMP response element binding protein
D-DOPA	3,4-dihydroxy-D-phenylalanine
DA	dopamine
DAergic	dopaminergic
DAG	diacylglycerol
DARRP-32	dopamine- and cAMP-regulated neuronal phosphoprotein
DAT	dopamine transporter
db-cAMP	dibutyryl cAMP
DBH	dopamine-β-hydroxylase
DBS	deep brain stimulation
DDC	DOPA decarboxylase
DHFR	dihydrofolate reductase
DMEM	Dubelcco's Modified Eagle's Medium
DOPAC	3,4-dihydroxyphenylacetic acid
DOPAL	3,4-dihydroxyphenylacetaldehyde
DOPET	3,4-dihydroxyphenylethanol
DT-diaphorase	NAD(P)H:quinone oxidoreductase

EI	electron ionization
En	Engrail
ER	endoplasmic reticulum
ERK	extracellular signal-regulated kinase
FBS	fetal bovine serum
FGF	fibroblast growth factor
FGF8	fibroblast growth factor 8
GAPDH	glyceraldehyde-3-phosphate dehydrogenase
GC-MS	gas chromatography - mass spectrometry
GDNF	glial cell line-derived neurotrophic factor
GFP	green fluorescent protein
GFRP	GTPCH feedback regulatory protein
GPx	glutathione peroxidase
GR	glutathione reductase
GSH	reduced L-glutathione
GSSG	glutathione disulfide
GST M2-2	glutathione S-transferase M2-2
GTP	guanosine triphosphate
GTPCH	GTP cyclohydrolase 1
HIF	hypoxia-inducible factor
HIP	hypoxia-inducible protein
HRP	horseradish peroxidase
HVA	homovanillic acid
IDH	isocitrate dehydrogenase
IL-1β	interleukine-1 beta
iNOS	inducible nitric oxide synthase
IP$_3$	inositol triphosphate
iPSC	induced pluripotent stem cells
L-DOPA	2,3-dihydroxy-L-phenylalanine

LAT	large amino acid transporter
LC-MS	liquid chromatography coupled to mass spectrometry
LDH	lactate dehydrogenase
LMX1B	LIM Homeobox Transcription Factor 1 β
LOD	limit of detection
LPS	lipopolysaccharide
M-PER	mammalian protein extraction reagent
m/z	mass over charge ratio
MAO	monoamine oxidase
MAPKAPK	mitogen-activated protein kinase activated protein kinase
MCT	monocarboxylate transporter
MID	mass isotopomer distribution
MPDP$^+$	1-methyl-4-phenyl-2,3-dihydropyridinium
MPP$^+$	1-methyl-4-phenylpyridinium
MPPP	1-methyl-4-phenyl-4-propionoxypiperidine
MPTP	1-methyl-4-phenyl-1,2,3,6-tetrahydroxypyridine
MSD	Movement Disorder Society
MSTFA	N-methyl-N-(trimethylsilyl)trifluoroacetamide
MTBSTFA	N-tert-butyldimethylsilyl-N-methyltrifluoroacetamide
NAA	N-acetyl-aspartate
NAC	N-acetyl-L-cysteine
NF-$\varkappa$B	nuclear factor $\varkappa$B
NM	neuromelanin
NMR	nuclear magnetic resonance
nNOS	neuronal nitric oxide synthase
NO	nitric oxide
NOS	nitric oxide synthase
NURR1	nuclear receptor related 1 protein
P/S	Penicillin/Streptomycin
PARP-1	poly (ADP-ribose) polymerase-1
PBMC	peripheral blood mononuclear cell
PBS	Phosphate Buffer Saline

PC	pyruvate carboxylase
PCBP	poly-C binding protein
PCD	pterin-4a-carbinolamine dehydratase
PD	Parkinson's disease
PDH	pyruvate dehydrogenase complex
PDPK	proline-directed serine/threonine kinase
PEG	poly-ethylene glycol
PHD	prolyl hydroxylase
PheH	phenylalanine hydroxylase
PIP_2	phosphaditylinositol-4,5-biphosphate
PITX3	Paired-Like Homeodomain 3
PK	pyruvate kinase
PK-A	protein kinase A
PK-C	protein kinase C
PK-G	protein kinase G
PLC	phospholipase C
PLO	poly-L-ornithine
PLP	pyridoxal phosphate
PNMT	phenylethanolamine N-methyltransferase
PP	protein phosphatase
PP1	protein phosphatase 1
PPP	pentose phosphate pathway
PTP	permeability transition pore
PTPR	6-pyruvoyltetrahydropterin 2′-keto reductase
PTPS	6-pyruvoyltetrahydropterin synthase
PVDF	polyvinylidene fluoride
$q\text{-}BH_2$	quinoid dihydropteridine
QDPR	quinoid dihydropteridine reductase
RA	retinoic acid
RNS	reactive nitric oxide species
ROS	reactive oxygen species
S/N	signal-to-noise ratio

SAH	S-adenosyl homocysteine
SAM	S-adenosyl methionine
SCFA	short chain fatty acid
SCO2	cytochrome c oxidase 2
SDH	succinate dehydrogenase
SDS-PAGE	sodium dodecylsulfate-polyacrylamide gel electrophoresis
SIM	selected ion monitoring
SNCA	synuclein α
SOD	superoxide dismutase
SR	sepiapterin reductase
SSH	sonic hedgehog
STEP	striatal-enriched protein tyrosine phosphatase
SV40	simian virus 40
TAE	Tris-acetate-EDTA
TBDMS	tert-butyl dimethylsilyl
TCA	tricarboxylic acid
TH	tyrosine hydroxylase
TIC	total ion current
TIGAR	TP53-induced glycolysis regulator
TMS	trimethylsylil
TNFα	tumour necrosis factor alpha
TRE	12-O-tetradecanoylphorbol-13-acetate (TPA) response element
TrpH	tryptophan hydroxylase
UbC	ubiquitin C
UCH-LI	ubiquitin C-terminal hydrolase I
UPDRS	Unified Parkinson's Disease Rating Scale
VMAT	vesicular monoamine transporter
VMAT1	vesicular monoamine transporter 1
VMAT2	vesicular monoamine transporter 2
VTA	ventral tegmental area

List of Figures

List of Tables

1

Introduction

In this section, I introduce the scientific background and state of the art related to my PhD project. After a description of Parkinson's disease (PD) etiology and state of the art treatment, I focus on dopaminergic systems. This latter part includes a short historic overview, a brief description of dopamine-producing cells in the body, a more detailed introduction of dopaminergic neurons in the *substantia nigra pars compacta* and finally, a description of the models currently available.

Then, I describe in more detail the biochemistry around dopamine: its synthesis and degradation as well as its action in synaptic clefts. 2,3-dihydroxy-L-phenylalanine (L-DOPA) is the direct precursor of dopamine (DA) and is used as a drug to manage the symptoms of PD. Since L-DOPA is a compound of high interest in the context of my PhD thesis, I shortly introduce its history together with its toxic effects on cells.

Finally, I introduce the analytical methods used in this work: gas chromatography - mass spectrometry as well as stable isotope-assisted metabolomics.

1.1 Parkinson's disease

1.1.1 Etiology of Parkinson's disease

PD is a common neurodegenerative disease affecting 1-2% of the worldwide population with an age above 65 years [1] and about 5% of the population over 85 years old in Western Europe [2]. The disease was first reported by James Parkinson in his "Essay on the shaking palsy" [3] in which he described, through 6 cases, the main motor symptoms of the disease: bradykinesia (slowness of movements), rigidity, tremor and

postural instability. These motor symptoms are associated with the death of dopaminergic neurons within the *substantia nigra pars compacta* located in the midbrain as well as with the presence of Lewy bodies [2]. These neurons project their axons to the striatum where they release a neurotransmitter responsible for movement control: DA [4]. Lewy bodies are cytoplasmic inclusions formed by the aggregation of ubiquitinated proteins [5] as well as full length and truncated forms of the protein synuclein α (SNCA) [6]. By the time of death, 50 to 70% of these neurons degraded leading to a depletion of about 80 to 85% of the DA content in the striatum [7].

Motor symptoms are not the only manifestation of PD. Indeed, other symptoms such as sleep disorder, loss of taste and smell, constipation and depression can occur before the start of motor symptoms [8]. The longitudinal course of PD can be followed using the Unified Parkinson's Disease Rating Scale (UPDRS), which was developed in the 1980s. In 2008, a revised version sponsored by the Movement Disorder Society (MSD) was published. It was designed to be more comprehensive, clearer and more detailed. It comprises four parts, namely (1) non-motor experiences of daily living, (2) motor experiences of daily living, (3) motor examination and (4) motor complications. Some parts are filled by the patient, and a 30-minutes interview with a practitioner is sufficient to complete the survey [9]. The results of this test help the practitioner to define treatment options.

The etiology of PD is not fully understood, although it seems clear that genetic and environmental factors can be involved. A genetic component is thought to be causative of the disease in approximately 5 to 10% of cases [2]. About 28 chromosomal regions are known to be linked to PD. From those, only six of these regions are linked to mutations in genes that can individually cause the disease. These genes are *SNCA/PARK1*, leucine-rich repeat kinase 2 (*LRRK2*)/*PARK8*, *Parkin/PARK2*, PTEN-induced putative kinase 1 (*PINK1*)/*PARK6*, *DJ1/PARK7* and ATPase type 13A2 (*ATP13A2*)/*PARK9* [10]. Interestingly, many of these genes are coding for mitochondrial proteins or for proteins associated with mitochondria and a mutation in their sequence disrupts mitochondrial function [11]. PINK1 has a putative serine-threonine kinase domain and is able to recruit Parkin. Parkin has an E3 ubiquitin ligase activity and is recruited to damaged mitochondria where it promotes mitochondrial fission and mitophagy by ubiquitinating mitofusin proteins [12]. Moreover, PINK1 has been directly linked to mitochondrial

complex I activity [13]. Loss of function of PINK1 correlated with a loss of phosphoryla-tion of a subunit of complex I. This impaired reduction of ubiquinone lead to decreased mitchondrial potential and to mitochondrial dysfunction [13].

DJ1 is an oncogene and when over-expressed, protects cells from oxidative stress. When causing PD, however, the mutation induces a loss of function, which increases intracellular oxidative stress and promotes cell death [14]. An overexpression of α-synuclein, the main component of Lewy bodies, was also found to alter mitochondrial function and increase the levels of oxidative stress [15].

Environmental factors include pesticides such as paraquat or rotenone. The for-mer is a herbicide, which can poorly cross the blood brain barrier (BBB) and its mode of action is thought to be via the generation of superoxide radicals [16]. Rotenone, however, is a fish poison and insecticide, which is highly lipophylic and can reach all organs. It inhibits complex I of the mitochondrial respiratory chain in all cells of the brain, but only dopaminergic neurons are sensitive and selectively die upon rotenone intoxication [17]. It binds to the quinone-binding site of complex I [18]. The conse-quences of this binding are an interruption of movement of electrons leading to a drop in the availability of adenosine triphosphate (ATP) and an accumulation of superoxide radicals [19]. Another drug that induces PD-like symptoms is 1-methyl-4-phenyl-1,2,3,6-tetrahydroxypyridine (MPTP). It was first discovered in 1982 when young drug users developed parkinsonian symptoms. It appeared that MPTP was a contami-nation obtained during the synthesis of 1-methyl-4-phenyl-4-propionoxypiperidine (MPPP), a synthetic opioid drug. Once in the brain, MPTP is oxidized to 1-methyl-4-phenyl-2,3-dihydropyridinium (MPDP$^+$) by the isoform B of the monoamine oxidase (MAO) in glial cells or serotonergic neurons, which are the only cell types expressing this enzyme. Then, MPDP$^+$ spontaneously oxidizes to 1-methyl-4-phenylpyridinium (MPP$^+$). MPP$^+$ can be taken up by dopaminergic neurons via the dopamine trans-porter (DAT) where it inhibits complex I of the mitochondrial respiratory chain [20].

1.1.2 State of the art treatment

To date, there is no cure for PD. The available treatments aim at improving the quality of life of the patients, but their benefits are limited in time and most of them present major side effects.

The "gold standard" treatment is L-DOPA, the precursor of DA. Due to its amino acid-like structure, it has the ability to replenish the neurotransmitter pool by crossing the BBB while DA cannot [21]. The half-life of L-DOPA in plasma is only 60 to 90 minutes [22], but can be improved using several adjunct therapies. One of them is to use a *decarboxylase inhibitor* such as carbidopa which will prevent decarboxylation in the periphery [23]. Aromatic amino acid decarboxylase (AADC) is expressed in the gastrointestinal tract, blood vessels and liver, which together decarboxylate 90% of the orally administered dose of L-DOPA [24]. Treatment can be further improved by using *inhibitors of catechol-o-methyl transferase (COMT)*, one of the enzymes involved in L-DOPA and DA degradation. It is administered together with L-DOPA and carbidopa and prevents the conversion of L-DOPA to 3-O-methyldopa by COMT in the gastrointestinal tract [25]. Another way to improve L-DOPA half-life is by *inhibiting the action of MAO-B*, another enzyme responsible of DA degradation in the brain. Rasagiline and selegiline lead to an increased synaptic concentration of DA reducing motor fluctuations in PD patients [25]. *DA receptor agonists* can be used in early PD and delay the need for L-DOPA treatment. The action of pramipexole and ropimirole is based on the fact that they stimulate the DA receptors and thus mimic the action of DA. Among the five DA receptors known, D1 and D2 regulate voluntary movements. Thus, DA receptor agonists act through these receptors and regulate the activity of neurons in the basal ganglia [25].

Aside from pharmacological interventions, surgical methods are also available to cope with the symptoms of PD. They include pallidotomy. It consists of the destruction of cells in the *globus pallidus* responsible for dyskinesia. However, this intervention has minor effects on bradykinesia and rigidity. Other interventions include thalamotomy and thalamic stimulations. The former involves removal of the thalamus, while the latter consists of the introduction of an electrode into the thalamus, which stimulates the gland and allows management of tremors [26].

Stem cell transplantation has been studied in order to replenish the dopaminergic neuron pool in the putamen [27]. Li *et al.* reported that graft-derived dopaminergic innervation can be maintained for 24 years [28]. The patient was engrafted unilaterally in the putamen with ventral mesencephalic tissue issued from four abortions [28]. The patient showed substantial benefits for up to 12 years with L-DOPA withdrawal from year 5 to 6 post-transplantation [28]. However, after 12 years, L-DOPA doses were increased to those used before transplantation and by 18 years after grafting, no

graft-related improvement remained [28]. Autopsy revealed that the putamen was still strongly innervated and that 76% of neuromelanin (NM)-containing neurons from the graft were tyrosine hydroxylase (TH)-positive, while the nontransplanted putamen did not contain any TH-positive neurons. Interestingly, the transplanted neurons contained Lewy bodies, suggesting that the disease could be transferred to the transplant [28].

The most promising procedure is currently deep brain stimulation (DBS). A thin electrode is implanted into the brain, which generates high frequency waves. They simulate the effects of a lesion without damaging the brain and prevent the transmission of impulses responsible for involuntary movements [26]. However, this treatment is only available for 5 to 10% of PD patients. The selection is based on: response to L-DOPA therapy, age, mental health and predominant symptoms [26]. The most effective DBS is obtained through stimulation of the subthalamic nucleus or *pars interna* of the *globus pallidus*. Stimulation of both regions lead to significant motor benefits as well as reduced dyskinesia and motor fluctuation in patients with advanced PD (Figure **1.1**) [29].
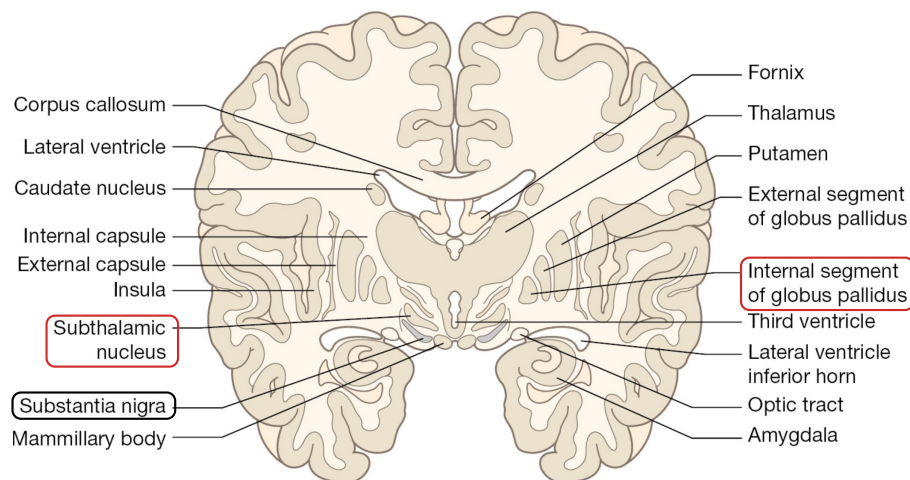
FIGURE 1.1: **Deep brain stimulation areas.** Oblique section at the level of the basal ganglia. The *substantia nigra* is circled in black. Under deep brain stimulation, stimulation of the subthalamic nucleus and the *pars interna* of the *globus pallidus* have shown the best improvement of motor symptoms in patients with PD. These reagions are circled in red (adapted from [30]).

Gene therapy has also been considered for treatment of PD. So far, nine clinical trials using gene therapy for patients with advanced PD have been completed. 60% of them used adeno-associated virus (AAV)-NRTN, a gene coding for the neurotrophic factor neurturin. Neurotrophic factors might protect against neurodegeneration and improve neuronal function. For example, neurturin has been shown to protect

dopaminergic neurons in animal models of PD [31]. Although this could not help to restore DA production in the *substantia nigra pars compacta* of advanced PD patients, the analysis of post-mortem brains enabled important discoveries [32]. (1) Viral vectors can be delivered safely using stereotactic surgical procedures and the proteins transduced are expressed and active on the long term. (2) Another major finding of these clinical trials was that gene therapy might be most profitable for patients with early PD: these patients still possess some TH-positive neurons and the stimulation with NRTN can increase DA production. However, in patients with advanced PD, the dopaminergic neuron loss is too important to observe any benefits [32].

1.2 Dopaminergic systems

1.2.1 Short history of dopamine research

It is nowadays clear that DA is a neurotransmitter and many of its roles in the human body have been revealed. However, this was not always the case: for a long time, DA was considered to be a precursor of norepinephrine and epinephrine, without any biological effects. Arvid Carlsson had to strongly argue in order to prove that DA can act as a neurotransmitter on its own. This section gives a short overview on the discovery of DA and its role in signal transduction.

DA was first synthesized by Mannich and Jacobsohn as well as by Barger and Ewins in 1910 as a by-product in an effort to synthesize other compounds. In 1938, Holtz, Heise and Lüdtke isolated AADC, the enzyme responsible for conversion of L-DOPA to DA, in human kidney. The following year, Holtz and Blaschko identified L-DOPA and DA as intermediates of norepinephrine and epinephrine synthesis. From this time, DA was accepted as a neurotransmitter precursor. In 1942, Holtz confirmed the presence of DA in the human body by demonstrating that DA is a normal constituent of human urine [33].

In 1957, the work of Carlsson revolutionized research on DA. At that time, he was investigating the effects of reserpine, an antipsychotic drug, on the depletion of serotonine and norepinephrine. Together with Lindqvist and Magnusson, they hypothesized that if reserpine is really depleting serotonine and norepinephrine stores, administering these amines should counteract its effects. Since these amines do not cross the BBB, they used the precursors 5-hydroxytryptophan (5-HTP) and L-DOPA. Interestingly, the supplementation with 5-HTP did not rescue the effects of the drug, while

L-DOPA counteracted its effects [33]. They concluded that the lack of norepinephrine, but not serotonine is responsible for reserpine's sedative effects. However, they could not observe any noticeable increase in norepinephrine. Therefore they decided to focus on the study of the role of DA. In 1958, Carlsson and Waldeck developed a staining technique allowing for specific coloration of DA in tissue and bodily fluids. This fluorimetric characterization showed a different localization of norepinephrine and DA. In 1959, Bertler and Rosengren, both students of Carlsson, studied the localization of DA in the brain and other tissues. They found that (1) DA was present in all studied species, (2) that the basal ganglia contained the highest levels of DA and (3) that 80% of the brain DA is located in the caudate nucleus [33]. In 1960, Hornykiewicz analysed the coloration of brain of PD and control patients and found no coloration in the *corpus striatum*, indicating the absence of DA in this region in PD patients only. His observations were accepted only in 1964: the main argument used to discredit these findings was that DA is unstable, it was possible that his observations resulted from a factor unique to PD patients such as medication or cause of death, which could accelerate the degradation of DA. However, in 1964, Bernheimer showed the same trend in levels of homovanillic acid (HVA), which is a more stable degradation product of DA. This lead to the conclusion that DA is involved in PD. Finally, in 1966, Poirier and Sourkes demonstrated the existence of the nigrostriatal DA system and its importance in normal movement. This was linked to the motor control issues in PD and it was hypothesized that the death of dopaminergic neurons in that brain regions is responsible for motor impairments [33].

For his work on DA, Arvind Carlsson received the Nobel Prize in Physiology in 2000. The prize was shared with Paul Greengard and Eric Kandel for "their discoveries concerning signal transduction in the nervous system" [33].

1.2.2 Where is dopamine produced and what is its role in the human body?

DA is a neurotransmitter belonging to the catecholamines (CAs). CA refers to organic compounds containing a catechol nucleus and an amine group. The catechol nucleus is composed of a benzene group with two adjacent hydroxyl groups. Aside from DA, norepinephrine and epinephrine are the other CA found *in vivo*, and both of them are synthesized from DA [34]. DA is synthesized from tyrosine and plays two important roles in the body: first, it is the precursor of norepinephrine and epinephrine. Second, it is an important neurotransmitter. This section highlights the regions where DA is produced as well as its role in these particular regions.

In the brain. Dopaminergic neurons represent less than 1% of the cell population in the brain [35]. In mammalian brain, there exists nine dopamine-containing neuronal cell groups. The localization of these groups varies between mammals, but the nomenclature used to define them allows cross-species comparisons [36]. These areas are called A8 to A16. In primates, A8 is located in the retrorubral field, A9 in the *substantia nigra pars compacta* and A10 in the ventral tegmental area (VTA). These three groups project to the forebrain and contain 400,000 to 600,000 TH-positive cells in human compared to 20,000 to 30,000 in mouse [37]. Among those, 70% are located in the *substantia nigra* [36]. A11-13 are located in the hypothalamus, A14 near the preoptic periventricular nucleus and A15 is distributed between the paraventricular hypothalamic nucleus and supraoptic nucleus. Finally, A16 is located in the olfactory bulb [38].

To illustrate the different functions of DA, the role of some regions producing this neurotransmitter is further developed hereafter. Dopaminergic neurons from the *substantia nigra pars compacta* form the nigrostriatal pathway by projecting to the dorsal *striatum* (*caudate* and *putamen*). Their major role is to control motor planning and execution of movement, but they also play a role in cognition [39]. Dopaminergic neurons located in the VTA give rise to two distinct signalling pathways. The first is the meso-cortic pathway where the neurons project to the frontal and temporal cortices. This pathway plays an important role in concentration and executive functions such as working memory [39]. The second pathway arising from neurons from the VTA is the meso-limbic pathway. The neurons project to the nucleus accubens, hyppocampus, amygdala and septum [39]. This pathway plays an important role for motivation, experience of pleasure and reward [39] (Figure **1.2**). DA can also act on hormone release: neurons from A12 innervate the median eminence of the hypothalamus and inhibit the secretion of prolactin [39]. Finally, the neurons from A13 project to the amygdaloid and hypothalamic nuclei and are involved in sexual behaviour [39].

The DA system is involved in movement control, motor learning, reward-seeking, motivation, memory and cognition. If DA signalling is compromised, it can lead to PD (hypodopaminergic activity), schizophrenia (hyperdopaminergic activity), Huntington's disease, drug addiction, obsessive-compulsive disorder, depression or attention deficit and hyperactivity disorder (ADHD) [41]. In PD, 5 to 10% of patients suffer of severe depression and an additional 10 to 30% experience depressive symptoms [39].

In the gastrointestinal tract. DA is also produced in the gastrointestinal tract, spleen and pancreas, where TH, the rate-limiting enzyme in the synthesis of DA, is present
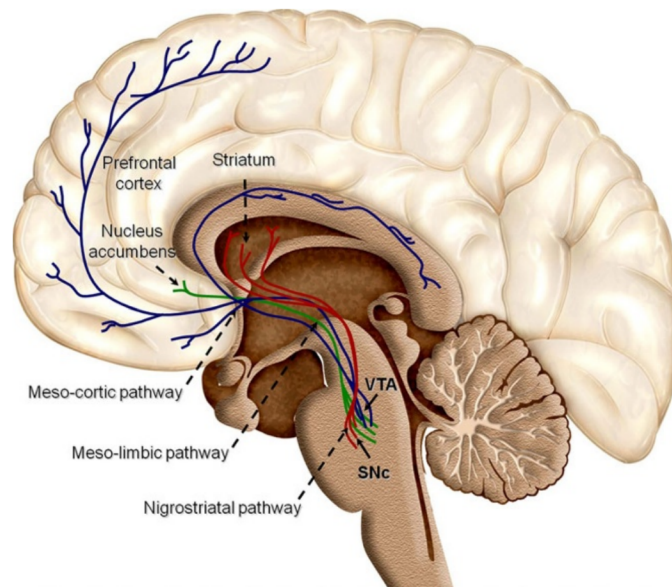
FIGURE 1.2: **Dopaminergic pathways.** Dopaminergic neurons from the *substantia nigra pars compacta* (**SNc**) project to the dorsal *stiatum* and form the nigrostriatal pathway (**in red**). Dopaminergic neurons from the ventral tegmental area (**VTA**) project either to the cortex via the meso-cortic pathway (**in blue**) or to the *nucleus accumbens* via the meso-limbic pathway (**in green**) (adapted from [40]).

and active. About 46% of the DA synthesized in the body is synthesized by the gastrointestinal tract, the spleen and the pancreas and has various roles. DA stimulates exocrine secretions, inhibits gut motility, modulates sodium absorption and mucosal blood flow and has been shown to be protective against gastroduodenal ulcer disease [42]. PD is associated with gastrointestinal dysfunctions such as weight loss, dysphagia (difficulty in swallowing), gastroparesis (impaired gastric emptying) or defecatory dysfunction. The origin of most of these non-motor symptoms is unknown. Weight loss is common in PD and affects 52% of the patients. It could be explained by the fact that DA regulates appetite, thus the loss of dopaminergic neurons in the brain could lead to lower appetite in PD patients. Moreover, DBS and DA agonists induced weight gain in PD patients [43]. Interestingly, treatment with dopamine receptor antagonists, which do not cross the BBB, accelerates gastric emptying, therefore providing a treatment for gastroparesis, presumably via effects on gastric dopamine receptors [43].

In renal cells. Epithelial cells of the proximal convoluted renal tubules synthesize DA from circulating L-DOPA [44]. DA is secreted towards the tubule lumen where it induces sodium excretion by inhibiting its reabsorption through activation of DA receptor. DA controls about 50% of sodium excretion. Dysfunctions in the renal DA

system lead to sodium retention and hypertension. This happens through two distinct mechanisms: either the expression of AADC, responsible for the decarboxylation of L-DOPA to DA, is decreased or the signal transmission through the DA receptor is ineffective [45].

In immune cells. Lymphocytes, neutrophils and macrophages possess DA receptors, DA transport system and are able to synthesize DA [46]. In these cells, DA exerts immunosuppressive functions by down-regulating proliferation and differentiation and increasing apoptosis [47]. In regulatory T-cells, DA has an autocrine function that leads to inhibition of cytokine production and capacity to suppress effector T cells [47]. Altered dopaminergic signalling is associated with autoimmune diseases such as multiple sclerosis [47]: one of the inhibitory DA receptors is downregulated in T cells of patients with multiple sclerosis leading to a hyper-responsiveness of these cells, characteristic of the disease [47].

In the bone marrow. DA is present in bone marrow and originates from nerve endings and bone marrow cells. Interestingly, the amounts of DA follow the circadian rythm, with peak values occurring during the night [46]. The role of DA in hematopoiesis is to stimulate erythropoiesis and platelet production [46].

In retinal cells. A subset of amacrine cells are able to synthesize DA as a chemical messenger for light adaptation. The daily frequency of DA production depends on interaction between dopaminergic cells and photoreceptors. DA and melatonin follow the circadian rhythm: melatonin levels are high at night while DA levels are high during the day. Each compound can act to inhibit secretion of the other [48].

1.2.3 Dopaminergic neurons in the *substantia nigra pars compacta* and their development

It has been postulated that during the course of PD, dopaminergic cell death occurs through apoptosis, but data rely on morphological analysis, which do not provide conclusive evidence [49]. The mechanisms inducing selective cell death in dopaminergic neurons are not yet elucidated. They could involve energy metabolism deficiencies (through mitochondrial complex I inhibition), inadequate control of redox state (due to low levels of antioxidants), environmental toxins (such as rotenone or MPP^+) or low amounts of neurotrophic factors [49].

The development of midbrain dopaminergic neurons is quite complex and not yet fully elucidated. However, the main transcription factors involved have been identified. The developmental process can be divided into four stages: (1) pluripotent stem cells located at the ventricular mesencephalic surface give rise to multiple cell types. (2) Some of these cells commit to dopaminergic neuron precursor cell fate, characterized by the expression of specific markers. (3) The precursor cells exit cell cycle and start expressing early midbrain dopaminergic neuron characteristics. (4) The mature cells express a specific set of markers and project axons to establish connections with target tissues [50] (Figure **1.3**). In the second step, where stem cells commit to dopaminergic neuron differentiation, two factors play a major role: sonic hedgehog (SSH) and fibroblast growth factor 8 (FGF8). Their spatio-temporal expression trigger signalling cascades that lead to commitment to either VTA or *substantia nigra* dopaminergic neurons [37]. The third step is the exit from cell cycle and expression of phenotypic markers such as TH in early stages and DAT at a later time. It is interesting to note that DAT expression is specific to midbrain dopaminergic neurons and is not expressed in other catecholaminergic cell types [50]. Important transcription factors at this stage include nuclear receptor related 1 protein (NURR1), which induces the expression of TH and c-RET, a component of glial cell line-derived neurotrophic factor (GDNF) receptor. GDNF is a growth factor involved in neuronal survival and arborization. LIM Homeobox Transcription Factor 1 β (LMX1B) is initially expressed throughout the midbrain region. Later in the development, it is specifically expressed in dopaminergic neurons. It is essential for the expression of Paired-Like Homeodomain 3 (PITX3). PITX3 is essential for TH expression in the *substantia nigra* but not in the VTA. It is hypothesized that other factors induce TH expression in VTA, but they are unknown [50]. The functional maturation of dopaminergic neurons is characterized by axonal pathfinding, formation of synapses and release of DA induced by depolarization. Several factors are involved in guiding the axons: Engrail (En)-1 and -2 induce the expression of guidance molecule receptors, while slits and nestins are involved in target recognition. The topographical innervation of the *striatum* by midbrain dopaminergic neurons is ensured by the ephrin ligand and receptor system. Dopaminergic cells from the VTA do not express this ligand and thus, cannot form synapses with striatal cells. This final stage is also characterized by a wave of apoptotic cell death. It is highly likely that the axons compete to establish synapses and this ensures cell survival through growth factors such as GDNF and brain-derived neurotrophic factor (BDNF) [50].

1) Pluripotent stem cells

2) Commitment to dopaminergic neuron precursor

SSH, FGF8

VTA   *SNpc*

3) Cell cycle exit
   Expression of early dopaminergic neuron characteristics

NURR1   PITX3 ← LMX1B

TH   TH
cRET   cRET: receptor for GDNF
DAT   DAT

4) Mature neurons project axons to establish connections

En 1,2   En 1,2: guidance molecule
Nestin   Nestin: target recognition
Slit   Slit: target recognition
          Ephrin ligand: topographical innervation

5) Apoptosis cell death wave
         Neurons from the *striatum*:
             a) express Ephrin receptor
             b) produce GNDF and BDNF
      ⇒ Survival of neurons producing the ephrin ligand and
growth factor receptors

FIGURE 1.3: **Development of dopaminergic neurons. (1)**: Pluripotent stem cells give rise to multiple cell types. **(2)**: The commitment to dopaminergic neurons precursor is mediated by sonic hedgehog (**SHH**) and fibroblast growth factor 8 (**FGF8**). Their spatio-temporal expression induce migration to the ventral tegmental area (**VTA**) or *substantia nigra pars compacta* (**SNpc**). **(3)**: The precursors exit cell cycle and start to express neuronal cell markers such as tyrosine hydroxylase (**TH**), GDNF receptor protein (**cRET**) and dopamine transporter (**DAT**). The expression of the two first is induced by nuclear receptor related protein 1 (**NURR1**) in both lineages while TH expression in SNpc is also mediated by paired-like homeodomain 3 (**PITX3**). **(4)**: The mature neurons project axons to their target regions and are guided by engrail 1 and 2 (**En 1, 2**), nestin and slit. Neurons from the SNpc also produce ephrin ligands which is recognized by receptors in the striatum. **(5)**: A wave of apoptotic cells characterizes the last stage of the maturation of dopaminergic neurons.

Deregulation in neurogenesis of dopaminergic cells can have grave consequences on the development of DA-producing brain regions. Hegarty *et al.* summarized the effects of about fifty mutations of genes involved in midbrain dopaminergic neuron development in mice and their effects on neuronal development [37]. Most of them

induced midbrain dopaminergic loss at various stages of neuronal development. Interestingly, the effects of mutations in PITX3 and En-1 were stronger in neurons from the *substantia nigra* than in the VTA, correlating with the highest sensitivity to cell death of these neurons during the course of PD.

A better understanding of dopaminergic neurogenesis is needed to develop cell therapies in PD and to evaluate whether these factors could play a role in the development of PD. Lower levels of development-associated factors could be associated with a lower number of dopaminergic neurons and early neurodegeneration observed in PD patients. It cannot be excluded that supplementation with the potentially missing factors could prevent or decrease cell death [49].

1.2.4 Currently available cell models

The effects of PD-associated mutations or toxins are often studied *in vitro* using cell models. Several cell lines are available and have been characterized. However, many of them are originating from tumours or from non-human organisms. This induces some drawbacks concerning their use: (1) cancer cells are proliferating and therefore do not mirror the quiescent state of mature neurons. (2) The regulation of genes related to DA synthesis pathway, including TH, are organism specific, thus studying the effects of a drug or mutation in mice or rats might not reflect the results that would have been obtained in human cells [51]. (3) Mice and rats do not produce NM, a pigment present in the *substantia nigra pars compacta* [51].

I describe here five cell lines that have been used as model of dopaminergic neurons. NB69 cells are human neuroblastoma cells derived from a sixteen-month old male [52]. They are positive for TH staining and DA has been measured by electrochemical detection [52]. These cells have been used among others to characterize the neurotoxicity of L-DOPA [53]. Another human neuroblastoma cell line commonly used is the SH-SY5Y cell line. These cells were isolated from a four-year old female and can be differentiated to TH expressing cells using low concentrations of fetal bovine serum (FBS) and retinoic acid (RA) [54]. PC-12 are pheochromocytoma cells isolated from the adrenal gland of a male rat. These cells produce DA and norepinerphrine [55]. A fourth model commonly used are the Neuro-2a cells, isolated from mouse neuroblastoma. Neuro2a cells have been reported to be more sensitive to MPP^+ treatment than PC-12 and SH-SY5Y cells [56]. Differentiation of Neuro-2a with low FBS and cyclic

adenosine monophosphate (cAMP) leads to TH-positive cells producing DA, but without expression of PITX3, indicating that they do not differentiate into the same type of dopaminergic neurons as in the *substantia nigra* [57]. A last model used to study dopaminergic neurons are the LUHMES cells. They were derived from the mesencephalon of an eight-week old foetus and immortalized using a *v-myc* vector. This vector is repressible using tetracycline, and these cells can be differentiated to non-proliferative post-mitotic neurons using cAMP [58]. Although these cells are positive for TH, no DA could be measured using our gas chromatography - mass spectrometry (GC-MS) instruments [1].

1.3   Synthesis and degradation of dopamine

DA is synthesized from tyrosine in a two-step reaction (Figure **1.4**). The first and rate-limiting enzyme in this pathway is TH which hydroxylates tyrosine to L-DOPA, using 6R-L-erythro-5,6,7,8-tetrahydrobiopterin (BH$_4$) as cofactor. The second enzyme is AADC, which decarboxylates L-DOPA to DA. The synthesized neurotransmitter can then be packaged into vesicles via the vesicular monoamine transporter 2 (VMAT2), be further enzymatically processed or can oxidize and polymerize to NM. Futher enzymatic processes include synthesis of other catecholamines such as norepinephrine and epinephrine by dopamine-β-hydroxylase (DBH) and phenylethanolamine N-methyltransferase (PNMT), respectively. Several enzymes are involved in degradation of DA: COMT, MAO, aldehyde dehydrogenase (ALDH) and alcohol dehydrogenase (ADH).

This section further describes these pathways starting with a description and regulation of the enzymes responsible for DA synthesis as well as the synthesis of BH$_4$. Then, an overview of the fate of DA within the cells is given, including its packaging, action and transport. Finally, the enzymatic degradation is described as well as the auto-oxidation process and the production of NM.

---

[1]The limit of detection of these instruments is discussed in section 1.5.3
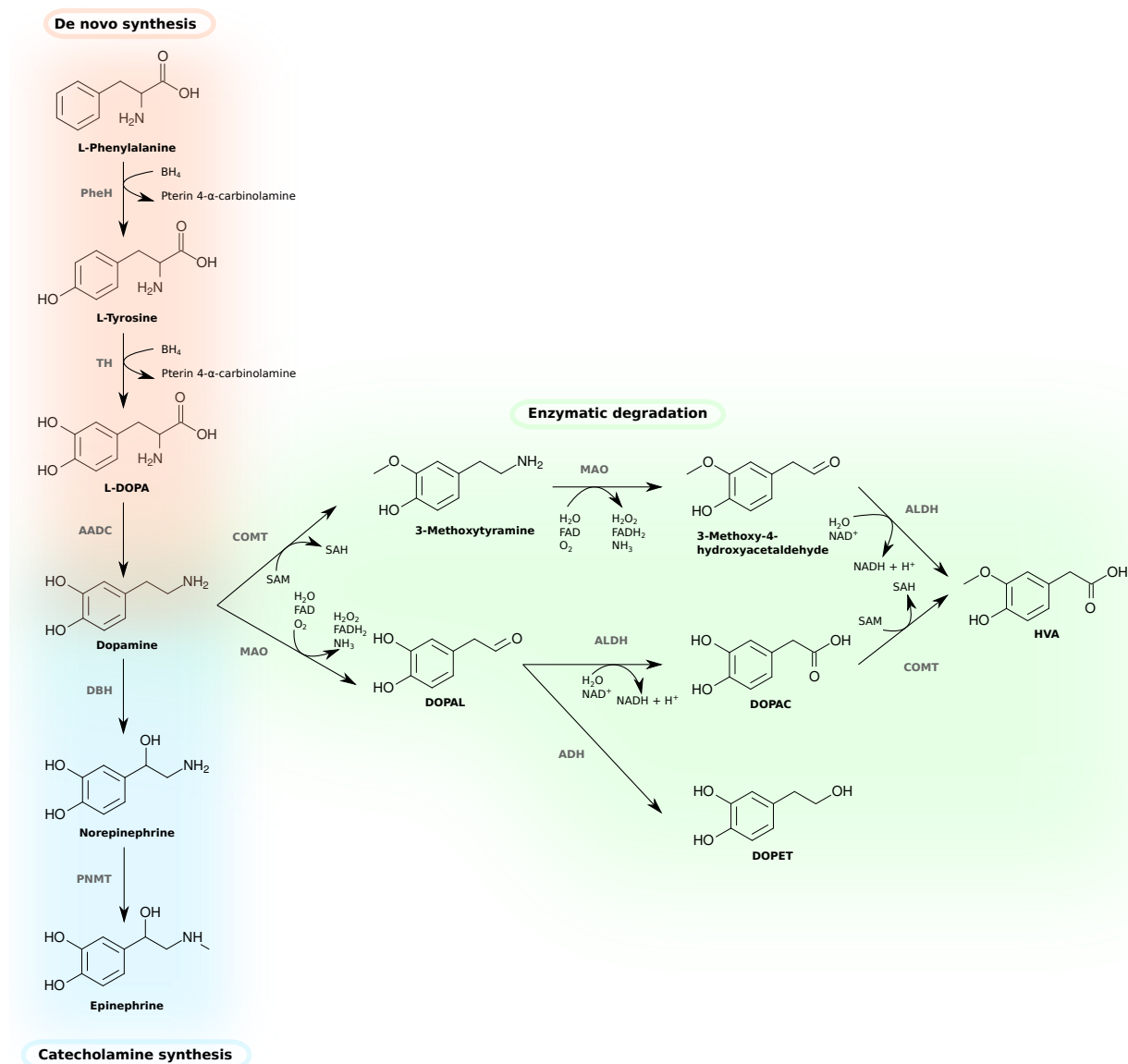
FIGURE 1.4: **Synthesis and degradation of dopamine.** Dopamine can be synthesized from L-phenylalanine or L-tyrosine. In the first case, L-phenylalanine is hydroxylated to L-tyrosine by phenylalanine hydroxylase (**PheH**). L-tyrosine is then further hydroxylated to L-3,4-dihydroxyphenylalanine (**L-DOPA**) by tyrosine hydroxylase (**TH**). Both enzymes require tetrahydrobiopterin (**BH₄**) as cofactor and produce pterin 4-α-carbinolamine. L-DOPA is decarboxylated to dopamine by aromatic amino acid decarboxylase (**AADC**). Dopamine can be degraded via several pathways. First, it can serve as precursor for the synthesis of norepinephrine by dopamine β-hydroxylase (**DBH**), which can be further methylated to epinephrine by the phenylethanolamine N-methyltransferase (**PNMT**). A second degradation pathway is via catechol-*o*-methyltransferase (**COMT**), which methylates dopamine to 3-methoxytyramine using S-adenosyl methionine (**SAM**) and releasing S-adenosyl homocysteine (**SAH**). 3-Methoxytyramine can be further metabolized to 3-methoxy-4-hydroxyacetaldehyde by monoamine oxidase (**MAO**), therefore producing ammonia (**NH₃**) and hydrogen peroxide (**H₂O₂**). 3-Methoxy-4-hydroxyacetaldehyde is finally converted to homovanillic acid (**HVA**) by the aldehyde dehydrogenase (**ALDH**). A third pathway involving the same enzymes leads to the generation of 3,4-dihydroxyphenylacetaldehyde (**DOPAL**) by MAO which is converted to 3,4-dihydroxyphenylacetic acid (**DOPAC**) by the ALDH. Finally, DOPAC is methylated to HVA by COMT. DOPAL can also be reduced to 3,4-dihydroxyphenylethanol (**DOPET**) by alcohol dehydrogenase (**ADH**).

1.3.1   Dopamine synthesis

1.3.1.1   Tyrosine hydroxylase, a key player in dopamine synthesis

TH is the first and rate-limiting enzyme in the synthesis of DA. It belongs to the
family of iron-containing, biopterin dependent amino acid hydroxylases together with
phenylalanine hydroxylase (PheH) and tryptophan hydroxylase (TrpH). TH consists of
three domains: a regulatory (R) domain of 100 to 160 amino acids, a catalytic (C) do-
main of 330 residues and a 40 amino acids coiled-coil domain at the carboxyterminus.
TH is a tetrameric enzyme predominantly found in the cytoplasm [59]. In human, four
isoforms of the enzyme exist and they differ in the length of the regulatory domain.
This is species specific since two isoforms were found in *Drosophila* and one in rat. All
isoforms arise from splicing variants of a single gene [59].

TH is a tightly regulated enzyme and its activity can be regulated by transcrip-
tional and post-translational modifications [34]. Transcriptional activation involves
response to growth factor, hormones and trans-synaptic signals. The major second
messengers involved in this pathway are cAMP, diacylglycerol (DAG) and calcium.
The promoter sequence of *TH* contains binding sites for cAMP response element (CRE)
and 12-O-tetradecanoylphorbol-13-acetate (TPA) response element (TRE). Intracellular
levels of cAMP regulate the transcription of *TH* by activating cAMP response element
binding protein (CREB) [60]. Another transcription factor involved in *TH* regulation is
the activator protein 1 (AP-1) complex, composed of c-Fos and c-Jun, which binds to
TRE. Interestingly, oxygen plays an important role in the transcriptional regulation of
TH: low oxygen levels induce functional activation of CREB and stimulate expression
of c-Fos and AP-1 activity, and thus, increase *TH* transcription. Hypoxia also stabilizes
the mRNA transcript of *TH* through the binding of hypoxia-inducible protein (HIP), a
66 kDa cytosolic protein, to the 3' untranslated region of *TH* mRNA, which prolongs
its half-life from 10 to 30 hours [61]. Interestingly, the effects of low oxygen levels seem
to be organ-specific: Hui *et al.* reported that exposing rats to 10% oxygen for 30 days
induced an increase in DA in the carotid bodies, but not in the sympathetic ganglia or
adrenal glands [62].

At the post-translational level, TH can be regulated by substrate or product in-
hibition, phosphorylation or cofactor availability [34]. TH regulation by tyrosine, its
substrate, occurs *in vitro* for concentrations higher than 50 μM and acts through an al-
losteric mechanism [63]. All three CAs (i.e. DA, norepinephrine and epinephrine) can

induce down-regulation of TH by product inhibition. They can only exert their inhibitory role if the iron is oxidized. In this case, they bind to the active site at a position that overlaps with binding of the cofactor [51]. Since BH_4 is essential for TH activity, preventing binding of BH_4 inhibits TH [34]. The most widely studied post-translational modification of TH is phosphorylation. In rat, TH can be phosphorylated at ser8, -19, -31 and -40, while in human, position eight contains a threonine [51]. Phosphorylation at ser40 induces an increase in TH activity by increasing its affinity for BH_4 [51]. Upon depolarization, phosphorylation at ser40 increases from 5 to 10% *in situ* [59]. Eight kinases can phosphorylate this site *in vivo*, such as protein kinase A (PK-A), protein kinase G (PK-G) or protein kinase C (PK-C). The two phosphatases responsible for the dephosphorylation are protein phosphatase (PP)2A and 2C [59]. Phosphorylation at ser31 also increases TH activity through increased affinity for BH_4. It is modulated by extracellular signal-regulated kinase (ERK)1 and 2, but the phosphatase involved in its dephosphorylation has not been identified [59]. Phosphorylation at ser19 is carried out by calcium/calmodulin-dependent protein kinase II (CaMPKII) and mitogen-activated protein kinase activated protein kinase (MAPKAPK)1 and 2. Dephosphorylation is carried out by PP2A and 2C. Phosphorylation at ser19 does not alter TH activity *in vitro*. Binding of 14-3-3 protein to TH phosphorylated at ser19 increased TH activity *in vitro*. However, this could not be validated *in vivo* [59]. Finally, ser8 can be phosphorylated by proline-directed serine/threonine kinase (PDPK) and ERK1 and 2. The enzymes responsible for its dephosphorylation have not been identified. Phosphorylation at ser8 does not induce any modification in TH activity *in vitro* or *in vivo* [59]. The close proximity of these phosphorylation sites within the regulatory domain raised the question whether they could influence each other. Investigation of hierarchical phosphorylation showed that phosphorylation at ser19 by CaMPKII increased three-fold the rate of phosphorylation of ser40 by the same kinase, while this has not been investigated for ser31 [59].

	Ser8	Ser19	Ser31	Ser40	528
TH					

	Ser8	Ser19	Ser31	Ser40
Kinase	PDPK ERK1 ERK2	CaMPKII MAPKAPK1 MAPKAPK2 14-3-3	ERK1 ERK2	PK-A PK-C PK-G
Phosphatase	?	PP2A PP2C	?	PP2A PP2C
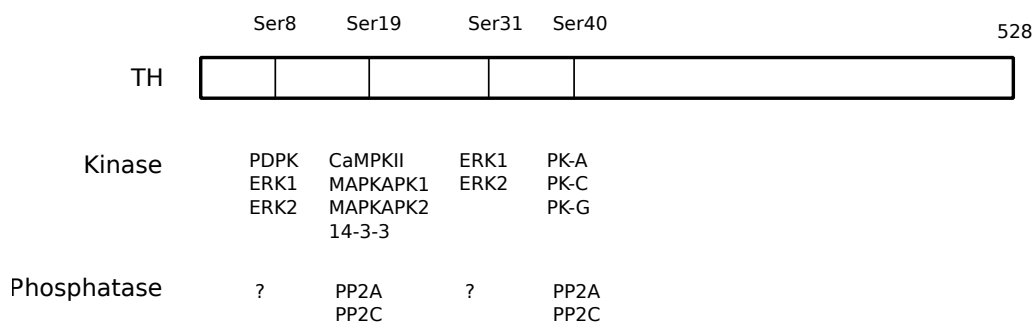
FIGURE 1.5: **Post-translational modifications of TH.** Tyrosine hydroxylase (**TH**) is a protein composed of 528 amino acids. It can be activated by phophorylation at different serine residues. Rat TH can be phosphorylated at ser8, 19, 31 and 40, while human TH contains a threonine at position 8, and therefore can only be phosphorylated at ser19, 31 and 40. The kinases involved in the phosphorylation differ depending on the serine position. At ser8, proline-directed serine/threonine kinase (**PDPK**) and extracellular signal regulated kinases 1 and 2 (**ERK1, ERK2**) are responsible for the phoshporylation. At ser19, calcium/calmoduline-dependent kinase II (**CaMPKII**), mitogen-activated protein kinase activated protein kinase (**MAPKAPK**) and protein 14-3-3 (**14-3-3**) phosphorylate TH. At ser31, ERK1 and ERK2 are responsible for the phosphorylation, while protein kinases A, C and G (**PK- A, PK-C and PK-G**) are involved in the phosphorylation at ser40. Phosphatases involved in dephosphorylation of ser19 and 40 include protein phosphatases 2A and 2C (**PP2A, PP2C**). The phosphatases involved in ser8 and 31 dephosphorylation have not yet been identified.

1.3.1.2 Synthesis of tetrahydrobiopterin

BH_4 is synthesized from guanosine triphosphate (GTP) (Figure **1.6**) [64]. The first and rate limiting enzyme in this pathway is GTP cyclohydrolase 1 (GTPCH) which catalyzes the reaction of GTP to 7,8-dihydroneopterin triphosphate. The activity of this enzyme can be regulated by cooperative binding of GTP. BH_4 and phenylalanine also modulate GTPCH activity via GTPCH feedback regulatory protein (GFRP). It inhibits GTPCH by binding to it and inducing conformational changes [64]. Interestingly, lipopolysaccharide (LPS) and H_2O_2 downregulate the expression of GFRP, rendering BH_4 synthesis independent of phenylalanine levels. However, in the context of dopaminergic neurons, GFRP is not of importance: it was shown to regulate BH_4 in the synthesis of serotonin, but not that of DA [64]. Mutations in GTPCH, the rate-limiting enzyme in BH_4 synthesis, is associated with impaired motor activity, characteristic of low DA levels [34]. The next step in the synthesis of BH_4 is the reaction of 6-pyruvoyltetrahydropterin synthase (PTPS) leading to 6-pyruvoyltetrahydropterine.
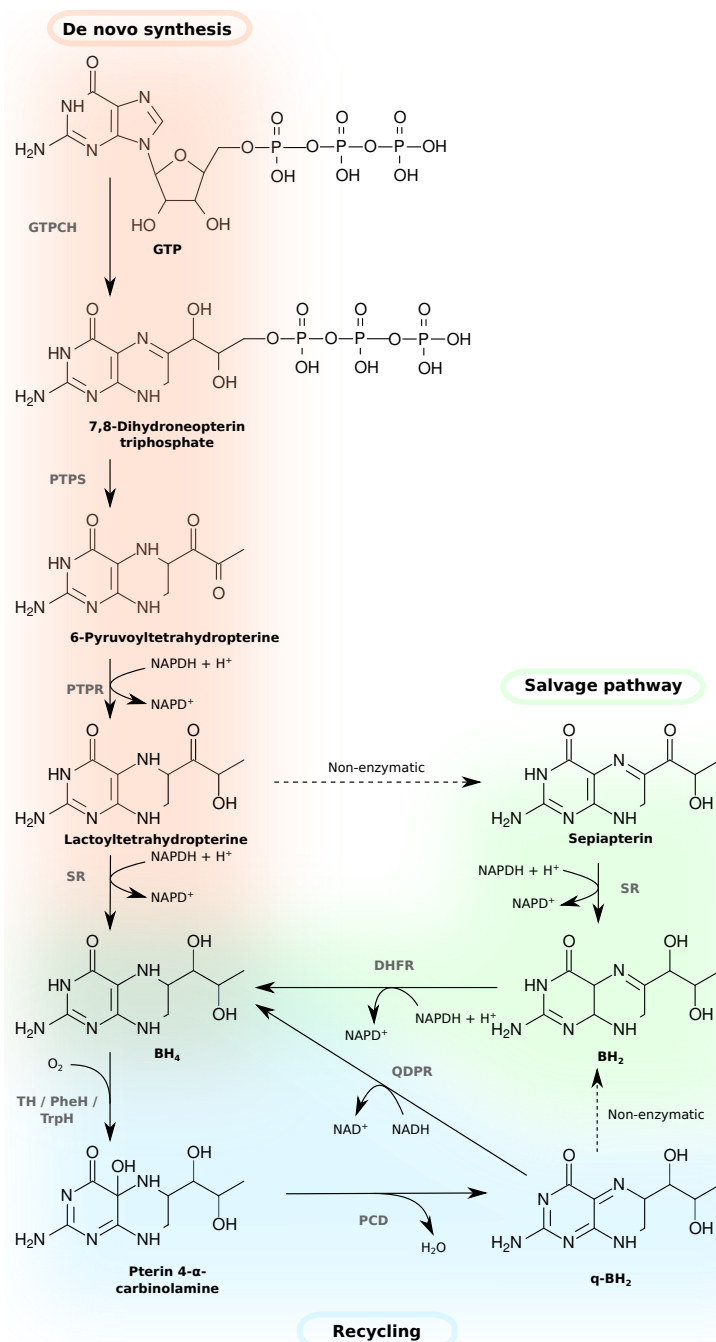
FIGURE 1.6: **Synthesis of tetrahydrobiopterin.** Tetrahydrobiopterin (**BH$_4$**) can be synthesized *de novo* (**red box**) from guanosine triphosphate (**GTP**). GTP is metabolized by GTP cyclohydrolase 1 (**GPTCH**) to 7,8-dihydroneopterin triphosphate which serves as substrate for the 6-pyruvoyl-tetrahydropterin synthase (**PTPS**) to generate 6-pyruvoyltetrahydropterine. Then, 6-pyruvoyltetrahydropterine is converted to lactoyltetrahydropterin by 6-pyruvoyl tetrahydropterin 2′-keto reductase (**PTPR**). Finally, sepiapterin reductase (**SR**) converts lactoyltetrahydropterin to BH$_4$. BH$_4$ can be used as cofactor by tyrosine hydroxylase (**TH**), phenylalanine hydroxylase (**PheH**) or tryptophane hydroxylase (**TrpH**) which then generate pterin 4-α-carbinolamine. To regenerate BH$_4$ (**blue box**), pterin 4-α-carbinolamine is dehydrated to quinoid dehydropterin (**q-BH$_2$**) by the pterin 4-α-carbinolamine dehydratase (**PCD**). q-BH$_2$ can either be converted to BH$_4$ by the quinoid dihydropteridine reductase (**QDPR**) or spontaneously converts to dihydrobiopterin (**BH$_2$**). A third pathway involved in generation of BH$_4$ is the salvage pathway (**green box**), where sepiapterin can be used as substrate of SR to produce BH$_2$. BH$_2$ is then used by the dihydrofolate reductase (**DHFR**) to produce BH$_4$.

The last two steps are catalyzed by 6-pyruvoyltetrahydropterin 2′-keto reductase (PTPR) and sepiapterin reductase (SR) and lead to the production of lactoyltetrahydropterine and BH_4 respectively, both enzymes use NADPH as cofactor. BH_4 can then be used by aromatic amino acid hydroxylases which contain non-haem iron. BH_4 donates two electrons to activate oxygen and exits the reaction as pterin 4-α-carbinolamine. A second class of enzymes using BH_4 as cofactor is nitric oxide synthase (NOS). These enzymes contain a haem iron, and in this case, BH_4 does not induce oxygen activation, but rather gives one electron for each of the two-step reaction from arginine to citrulline [64].

After reaction with either aromatic amino acid hydroxylases or NOS, pterin 4-α-carbinolamine can be recycled to BH_4 in a two-step reaction via the pterin-4a-carbinolamine dehydratase (PCD) and quinoid dihydropteridine reductase (QDPR) to form quinoid dihydropteridine (q-BH_2) and BH_4, respectively. This recycling pathway has two main roles: (1) it ensures continuous supply of reduced cofactor and (2) it prevents accumulation of harmful metabolites produced by rearrangement of pterin 4-α-carbinolamine [64].

BH_4 can also be synthesized via a salvage pathway: sepiapterin can serve as precursor for 7,8-dihydrobiopterin (BH_2) synthesis by the SR. BH_2 can then be metabolized by dihydrofolate reductase (DHFR) [64]. In the case of low enzymatic activity of SR or QDPR, both lactoyltetrahydropterine and q-BH_2 can be non-enzymatically converted to sepiapterin and BH_2 respectively [64].

1.3.1.3   Aromatic L-amino acid decarboxylase

The second enzyme involved in DA synthesis is AADC previously referred to as DOPA decarboxylase (DDC). This multimeric enzyme forms homodimers and uses pyridoxal phosphate (PLP) as cofactor to increase its activity [65]. It catalyzes the reaction of L-DOPA to DA and 5-HTP to serotonin (5-HT) as well as the formation of trace amines from phenylalanine, tyrosine and tryptophan to phenylethylamine, *p*-tyramine and tryptamine, respectively [66]. Interestingly, about 50% of AADC is membrane bound and catalyzing the production of 5-HT, while 35% of the enzyme is found in synaptosomes and catalyzes the production of DA [66]. It is expressed in a wide range of cell types including neurons and glial cells.

AADC is not the rate-limiting enzyme in the DA synthesis pathway. Therefore, it was assumed for a long time that it is not regulated. Recent evidence suggests that

it is regulated at both the transcriptional and post-translational levels. In mammals, genetic regulation of *AADC* is not well established [66]. Different promoter regions are expressed in different tissues suggesting a tissue-specific expression of *AADC* [66]. Among tissues, there exist different ratios of *AADC* activity to L-DOPA and 5-HTP suggesting that there exists several isoforms of the enzyme. Some studies have shown that isoforms are produced by alternative splicing of exon 3 [66], although further work is needed to confirm these data. At the post-translational level, the activity of AADC can be modulated by phosphorylation: AADC contains recognition motifs for PK-A, PK-C and CaMPKII. Phosphorylation can be mediated through the DA receptors: activation of D_2 receptors inhibits adenylyl cyclase (AC). AC is responsible for cAMP synthesis, which then activates PK-A that can phosphorylate AADC. Therefore, activation of D_2 receptors decreases the activity of AADC, while inhibition of D_2 receptors increases the activity of AADC [66]. PK-C activation could be modulated through the 5-HT receptor, which is known to use PK-C as second messenger [66].

Although AADC is not involved in the etiology of PD, it plays a crucial role during L-DOPA treatment. It might become rate-limiting upon degeneration of neurons and L-DOPA supplementation. Glial cells also express AADC and it cannot be excluded that they play a role in DA synthesis when only few dopaminergic neurons are left [66].

1.3.2 Packaging, action and transport of dopamine

Upon synthesis, DA can either be packaged into vesicles via the VMAT2 or can auto-oxidize in the cytoplasm and be incorporated into NM granules (Figure **1.7**). Upon depolarization stimuli, DA-containing vesicles are released into the synaptic cleft where it activates DA receptors. This reaction can be stopped by DA reuptake via the DAT in either neurons or astrocytes. This section describes the role of the different receptors and transporters involved in these processes.
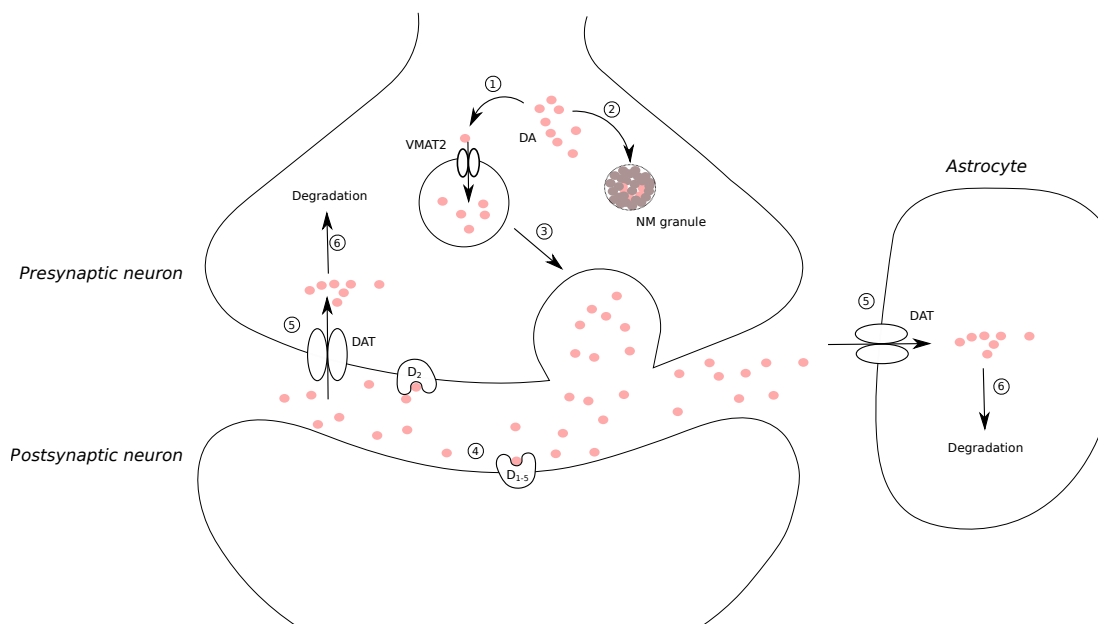
FIGURE 1.7: **Packaging, action and transport of dopamine.** Upon synthesis, dopamine (**DA**) is either **(1)** packaged into vesicles via vesicular monoamine transporter 2 (**VMAT2**) or **(2)** can oxidize and polymerize to melanin which gathers in neuromelanin (**NM**) granules. **(3)** Influx of calcium triggers the release of vesicular DA which **(4)** can activate the membrane bound dopamine receptors (**D$_{1-5}$**). **(5)** The neurotransmition is controlled by the dopamine transporter (**DAT**) which can stop it by transporting DA back into the cells. Both neuronal and astrocytic cells possess DAT. **(6)** Finally, DA can be enzymatically degraded.

1.3.2.1 Vesicular monoamine transporter 2

Vesicular monoamine transporters (VMATs) are H$^+$-ATPase antiporters which package monoamines into vesicles [67]. These transporters evolved from a bacterial antiporter that excretes toxins. The function of VMATs inside the cell is very similar: they sequester molecules that otherwise would be toxic to the cells if left free in the cytoplasm [68]. The vesicle concentrates monoamines about 10,000 fold and possesses a pH of 5.5, which prevents auto-oxidation inside the vesicle [68]. There exists two transporters: vesicular monoamine transporter 1 (VMAT1) and VMAT2. The former is located in peripheral neuroendocrine cells and absent in the central nervous system (CNS) while the latter is present in the central and peripheral sympathetic nervous systems [68]. VMAT2 is present in all neurons in the brain that produce DA, 5-HT, norepinephrine, epinephrine, histamine and trace amines such as tyramine and phenylethylamine [68]. Complete knockout of *VMAT2* is lethal, while a 95% reduction of *VMAT2* in mice leads to a dramatic decrease in the amounts of monoamines in the brain. Interestingly, the amounts of *VMAT2* are decreased in patients with advanced

PD. In patients under L-DOPA medication, VMAT2 levels further decreased shortly after administration of the treatment [68]. It was thus hypothesized that increasing *VMAT2* expression in PD patients could protect them from oxidative stress due to auto-oxidation of DA products, improve the efficacy of L-DOPA treatment and increase DA neurotransmission from the remaining neurons [67]. Moreover, mice overexpressing *VMAT2* showed a beneficial outcome on depression and anxiety behaviours, both mediated by monoamines [67].

1.3.2.2 Dopamine receptor

The DA released into the synaptic cleft upon depolarization can activate DA receptors. These can be divided into two families: the $D_{1\text{-like}}$ receptors containing D_1 and D_5 variants and the $D_{2\text{-like}}$ receptors containing D_2, D_3 and D_4 variants. The major difference is that $D_{1\text{-like}}$ receptors are coupled to AC and thus, exert their activity through cAMP accumulation, while $D_{2\text{-like}}$ receptors are cAMP-independent [69]. The two families possess distinct pharmacological, biochemical and physiological properties as well as distinct anatomical distribution [70]. The affinity to DA is also receptor-specific: DA has a ten times higher affinity for D_5 than for D_1 receptors and a twenty times higher affinity for D_3 than D_2 receptors [70]. The signal transduction of these receptors is quite complex and displayed in Figure **1.8** A. As mentioned, $D_{1\text{-like}}$ receptors can activate AC via activation of the $G_{s\alpha}$ subunit of the G-protein and AC catalyses the production of cAMP from ATP. cAMP activates PK-A which phosphorylates dopamine- and cAMP-regulated neuronal phosphoprotein (DARRP-32). DARRP-32 activates ERK through inhibition of protein phosphatase 1 (PP1), an activator of striatal-enriched protein tyrosine phosphatase (STEP), which negatively regulates ERK [70]. PK-A also plays another role following the activation of $D_{1\text{-like}}$ receptors activation: it induces an increase in cytoplasmic calcium concentration by increasing calcium uptake from the extracellular space and by increasing calcium release from the intracellular storage of the endoplasmic reticulum (ER) lumen. $D_{2\text{-like}}$ receptors, on the other hand, decrease the activity of AC, PK-A and calcium uptake from the extracellular space [70]. The increase of intracellular calcium levels can also be mediated by activation of phospholipase C (PLC) which catalyzes the degradation of phosphaditylinositol-4,5-biphosphate (PIP$_2$) to DAG and inositol triphosphate (IP$_3$). IP$_3$ then binds to calcium channels of the ER and triggers calcium release [70] .

$D_{1\text{-like}}$ and $D_{2\text{-like}}$ receptors also act on other ion channels: potassium channels, sodium/proton exchange and sodium-potassium-ATPase [70]. The effect of $D_{1\text{-like}}$ on

potassium channels is not well documented, but $D_{2\text{-like}}$ receptors increase the outward of potassium leading to cell hyperpolarization. This causes prolactin secretion in the pituitary and DA release inhibition by autoreceptors [70]. $D_{1\text{-like}}$ receptors agonists inhibit sodium/proton exchange while $D_{2\text{-like}}$ agonists activate this transporter. It is responsible for pH and cell volume regulations [70]. Finally, both $D_{1\text{-like}}$ and $D_{2\text{-like}}$ receptor agonists inhibit sodium-potassium-ATPases, which maintain the electrochemical gradient and are responsible for excitability. It has also been suggested that $D_{2\text{-like}}$ receptors play a role in neuronal differentiation, although their roles remain to be clarified [70].

1.3.2.3   Dopamine transporter

DAT is responsible for reuptake of DA from the synaptic cleft into presynaptic neurons. Therefore, it controls the spatio-temporal dynamic of DA neurotransmission [71]. Reuptake is driven by a concentration gradient generated by the sodium-potassium-ATPase allowing co-transport of DA together with 2 sodium ions and 1 chloride ion through the DAT [72]. In mammalian brains, DAT expression is restricted to dopaminergic (DAergic) neurons and astrocytes [73] and the directionality of the flux depends on cellular concentrations. DA can be bidirectionally transported, but at normal membrane potential and sodium gradient, the inward transport is favoured [74]. Regulation of the activity of the DAT can be mediated via several pathways (Figure **1.8** B). First, DAT can be negatively regulated via PK-C: upon extended activation of PK-C, DAT is internalized and targeted for lysosomal degradation, thus this is a long term regulation. PK-C also exerts its effects by increasing efflux of DA through the DAT or by phophorylating ser7, leading to a decrease in DA uptake. Positive regulation of DAT is mediated by $D_{2\text{-like}}$ receptors in two ways: activation of ERK by $D_{2\text{-like}}$ receptors induces phosphorylation of thr53 of the DAT and thus, increasing DA influx. The second role of $D_{2\text{-like}}$ receptors is by G protein-mediated promotion of DAT surface expression, therefore increasing the uptake capacity of the cell [71].
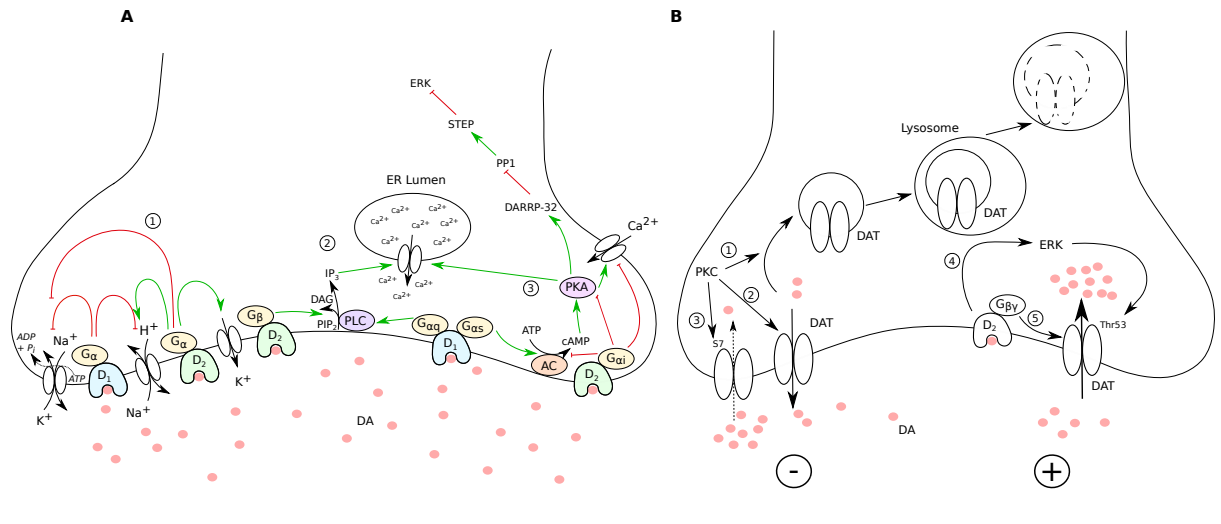
FIGURE 1.8: **The role of dopamine receptor and dopamine transporter. (A)**: *Activation of D_{1-2} receptors*. **(1)** Upon binding of DA, DA receptors regulate ion transport channels. D_{1-like} (**D_1**) receptors inhibit both Na^+/H^+ exchange and Na^+-K^+-ATPase. D_{2-like} (**D_2**) receptors inhibit Na^+-K^+-ATPase and K^+ channels and activate Na^+/H^+ exchange. **(2)** D_{1-like} and D_{2-like} receptors activate phospholipase C (**PLC**) through $G_{\alpha q}$ and G_β, respectively. PLC catalyzes the degradation of phosphatidylinositol-4,5-bisphosphate (**PIP_2**) to diacylglycerol (**DAG**) and inositol triphosphate (**IP_3**). IP_3 can then trigger the release of intracellular stores of calcium from the endoplasmic reticulum (**ER**) lumen. **(3)** D_{1-like} can also activate adenylyl cyclase (**AC**) through $G_{\alpha s}$. AC catalyzes the production of cAMP, which in turn activates protein kinase A (**PK-A**). PK-A phosphorylates dopamine- and cAMP-regulated neuronal phosphoprotein (**DARRP-32**), which inhibits protein phosphatase 1 (**PP1**). PP1 activates striatal-enriched protein tyrosine phosphatase (**STEP**), which inhibits ERK. Thus, activation of DARRP-32 activates ERK. **(B)**: *Regulation of DAT.* Dopamine transporter (**DAT**) can be negatively regulated in several ways by protein kinase C (**PK-C**). **(1)**: The bioavailability of the transporter can be modified by PK-C by targeting it for lysosomal degradation. **(2)**: PK-C can also stimulate the reverse transport of DA from the intracellular matrix to the synaptic cleft, thus increasing the synaptic concentration of DA. **(3)**: Finally, PK-C can decrease the influx of DA by phosphorylation of serine 7 (**Ser7**). DAT can be positively regulated by D_2 in two ways. **(4)**: The binding of DA to the receptor induces activation of extracellular-signal-regulated kinase (**ERK**) which phosphorylates threonine 53 (**Thr53**) of DAT. **(5)**: DAT can also be activated via G-protein $\beta\gamma$ (**$G_{\beta\gamma}$**) to increase DA influx.

1.3.3 Dopamine degradation

After reuptake by DAT, DA can either be packaged into synaptic vesicles via VMAT2 to be reused or it can be degraded either enzymatically or non-enzymatically. The former involves MAO, COMT and ALDH, while the latter occurs spontaneously in the cytoplasm by auto-oxidation. This section describes the degradation pathways of DA as well as the formation of melanin.

**1.3.3.1   Monoamine oxidase, catecholamine-o-methyl transferase and aldehyde de-
hydrogenase**

Degradation of DA occurs via several pathways (Figure **1.4**). The first pathway
involves methylation of DA to 3-methoxytyramine by COMT. S-adenosyl methio-
nine (SAM) is used as a methyl donor in this reaction leading to the formation of
S-adenosyl homocysteine (SAH). Then, 3-methoxytyramine is oxidized by MAO to
3-methoxy-4-hydroxyacetaldehyde. This reaction consumes oxygen, water and FAD
and produces H_2O_2, ammonia and $FADH_2$. Finally, ALDH oxidizes 3-methoxy-
4-hydroxyacetaldehyde to HVA using water and NAD^+ and releasing NADH. An
alternative pathway uses the same enzymes and cofactors, but in a different order.
MAO can oxidize DA to 3,4-dihydroxyphenylacetaldehyde (DOPAL), which is then
either oxidized to 3,4-dihydroxyphenylacetic acid (DOPAC) by ALDH or reduced to
3,4-dihydroxyphenylethanol (DOPET) by ADH. DOPAC is then further methylated by
COMT to HVA.

Monoamine oxidase. MAO are flavoenzymes located at the outer mitochondrial
membrane [75]. There exists two forms of MAO: A and B. Their localization is cell-type
specific: noradrenergic neurons of the *locus coruleus* stain for MAO-A, serotoninergic
neurons of the *raphe nuclei* stain for MAO-B, while the staining of dopaminergic neu-
rons from the *substantia nigra* for both isoforms of MAO is extremely low [76]. This
low expression of the enzyme does not prevent an increase in DA levels upon selec-
tive MAO inhibition. Neurons are not the only cells expressing MAO: microglial cells
express predominantly MAO-B, whereas astrocytes contain both forms of the enzyme
[76]. Metabolism of MAO generates H_2O_2, which can lead to defects in the mitochon-
drial electron transport chain. H_2O_2 is naturally formed during respiration: around
1 to 2% of the oxygen consumed is diverted to superoxide, which dismutes to H_2O_2.
However, the activity of MAO leads to H_2O_2 production largely exceeding that pro-
duced during electron flow [75]. Glutathione peroxidase (GPx) detoxifies H_2O_2 using
reduced L-glutathione (GSH). The products of this reaction are glutathione disulfide
(GSSG) and water. If H_2O_2 production exceeds the rate of detoxification by GPx, it
can be toxic to the mitochondrial electron transport chain in particular by inhibiting
complex I and II [77].

Catechol-o-methyl transferase. COMT catalyzes the methylation of one of the hy-
droxyl groups of a catechol substrates. It can thus methylate DA and DOPAC as well as
L-DOPA. Methylation of L-DOPA leads to the production of 3-*o*-methyldopa (3-OMD)

[78]. COMT exists in two forms: soluble and membrane-bound. In human, the soluble form is more abundant in peripheral tissues, whereas the membrane-bound form is more prevalent in the brain and is predominantly associated with methylation of dopamine and norepinephrine [79]. In all areas of the brain, COMT expression is low in astrocytes and microglial cells express the highest levels [80]. The expression of COMT is the highest in the *striatum* and *substantia nigra pars compacta* [79]. The cells expressing this enzyme differ between brain regions: in the *striatum*, GABAergic neurons express COMT [80], while in the *substantia nigra pars compacta*, it is not expressed in dopaminergic neurons, but in microglia and astrocytes [79].

Aldehyde dehydrogenase. ALDH catalyzes the reaction of 3-methoxy-4-hydroxy-acetaldehyde to HVA and from DOPAL to DOPAC. DOPAL can also be metabolized by ADH to DOPET. Inhibition of ALDH leads to an accumulation of toxic aldehydes and dopaminergic neuron loss *in vitro* and *in vivo* [81].

1.3.3.2   Dopamine auto-oxidation and neuromelanin

In the cytosol, L-DOPA, DA, norepinephrine and epinephrine can undergo non-enzymatic oxidation or auto-oxidation (Figure **1.9** A). This pathway includes quinones, leukochromes and chrome intermediates, which can polymerize and be included into NM vesicles. These intermediates are highly reactive and induce cell death via protein inactivation, mitochondrial dysfunction or depletion of antioxidants. The effects of quinones will be further discussed in section 1.4.2.1.

Melanins are cytoplasmic dark coloured granules that can be found in the skin or in the brain. Because of its location, melanin in the brain is referred to as NM. Melanins can be classified into four groups: (1) eumelanin (formed from L-DOPA), (2) pheomelanin (formed from 5-S-cysteinyl-DOPA), (3) neuromelanin (formed by oxidative polymerization of DA or norepinephrine and a mixture of eumelanin and pheomelanin) and (4) allomelanin (formed from polyphenols) [82]. The brain region containing the highest levels of NM is the *substantia nigra pars compacta*, but no correlation was found between degree of pigmentation and TH immunoreactivity. Knowledge about NM is limited, partly because the most common animal models including rodents do not possess this pigment [82]. In the scope of PD, there is an inverse relationship between the amount of NM contained in the neurons and their vulnerability to cell death [82]. The current hypothesis concerning the role of NM is that it has a protective role through scavenging of toxic phenols, which can be integrated into the polymer. NM also binds
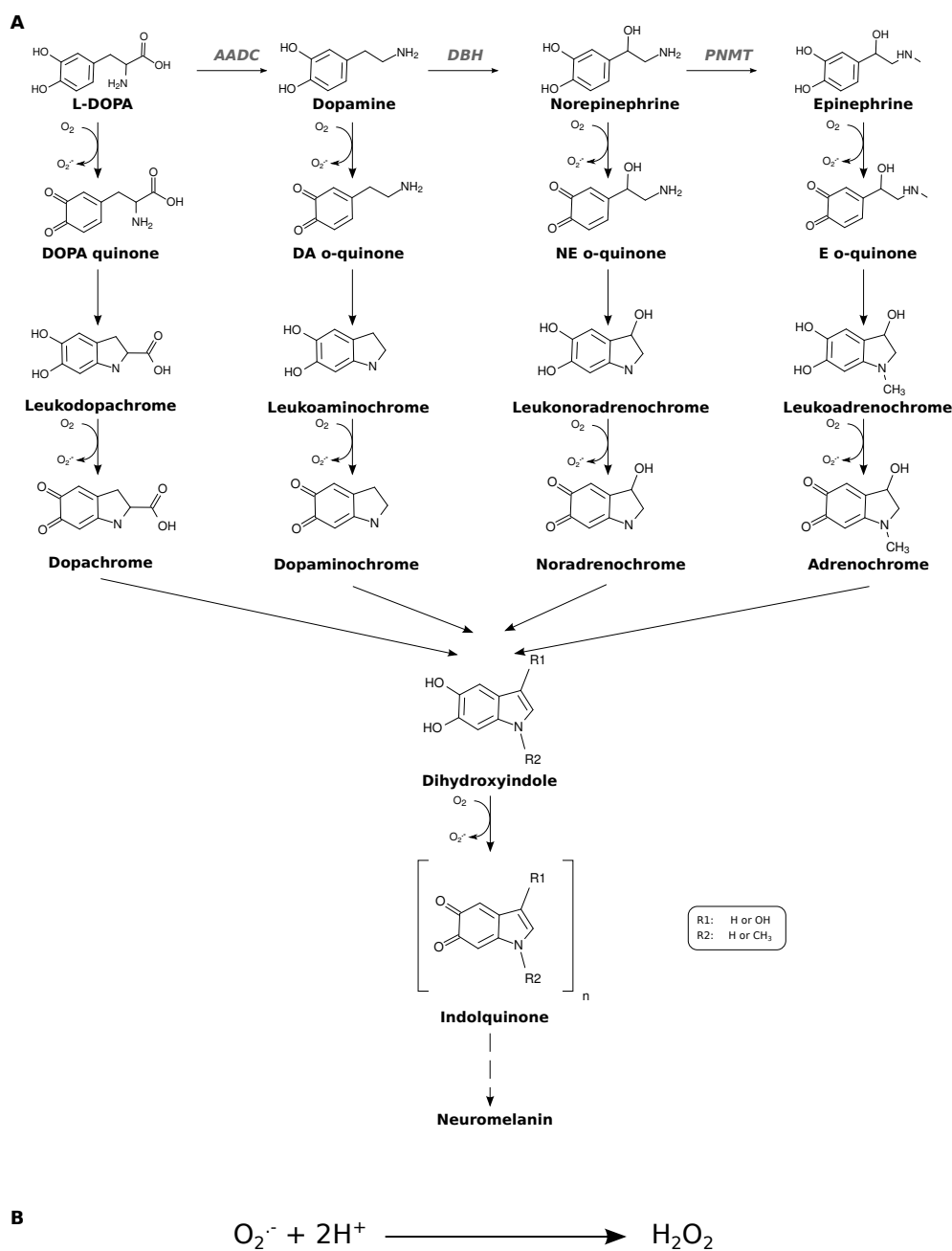
FIGURE 1.9: **Auto-oxidation of catecholamines. (A)**: The synthesis of epinephrine from tyrosine enzymatically occurs as described in Figure **1.4**. Each of the metabolites of the catecholamine synthesis pathway can auto-oxidize and form the respective quinones. Quinones then cyclize into leukochrome intermediates, which further oxidize into chrome intermediates. The next step in the pathway is the formation of dihydroxyindole, which oxidizes to form indolquinone. These can polymerize to form neuromelanin. Depending on the precursor, R1 represents either H or OH and R2 represents H or CH$_3$. **(B)**: The superoxide radicals ($O_2^{\cdot-}$) generated during the auto-oxidation can react with proton (**H$^+$**) to generate hydrogen peroxide (**H$_2$O$_2$**).

toxic cations such as iron, zinc, copper or manganese as well as hydroxyl radicals [82].

It has also been proposed that NM plays a role in iron homeostasis: NM is only partially saturated with iron, and thus binds excess and prevents its toxicity [82]. NM also contains protein and lipids.

1.4 L-DOPA

1.4.1 Short history on L-DOPA as a treatment

L-DOPA was first synthesized by Funk in 1911. Two years later, Guggenheim isolated the compound from the legume *Vicia fabra*. Both considered L-DOPA to be related to epinephrine and biologically inactive, although Guggenheim noticed that it had a very strong emetic capacity after ingesting 2.5 g. This reaction was later associated with the fact that DA acts on the emetic center of the *medulla oblongata*. In 1939, Holtz discovered that AADC catalyzes the decarboxylation of L-DOPA to DA. In 1942, the same investigator showed that treatment of animals with L-DOPA leads to excretion of DA in urine. The first link between L-DOPA administration and DA replenishment in the brain was established by Raab and Gigee in 1951. They treated rats with a large range of compounds and found that only L-DOPA could increase DA concentration in the brain. In 1959, Bertler, Rosengren and Sano demonstrated that brain DA was located mostly in the basal ganglia. They also observed that upon reserpine treatment, a molecule depleting catecholamine stores and causing parkinsonism-like symptoms, there was a drop in DA in the basal ganglia, therefore linking DA and motor control activity [83].

The missing link between L-DOPA and PD was established in 1960 when Erhingen and Hornykiewicz analyzed brains of healthy individuals and PD patients and observed that PD patients suffered from a severe loss of DA in the *corpus striatum*. In 1961, Hornykiewicz and Birkmayer launched a clinical trial and observed that L-DOPA treatment in PD patients improved motor symptoms for at least several hours. The major breakthrough that allowed the use of L-DOPA as treatment for PD is attributable to Colzia: instead of using a single high dose treatment which made the patients sick, he started with low L-DOPA concentrations and steadily increased them over time. The dose was thus adjusted for each patient to maximize motor improvements and minimize side effects [84].

However, the role of L-DOPA in mediating symptoms of PD stayed matter of debate until 1975 when Lloyd published the results of a study in the *striatum* of PD patients treated with L-DOPA and showed that: (1) DA levels were nine to fifteen-fold higher in patients treated with L-DOPA than in non-treated patients, (2) DA levels were depending on the duration between the last L-DOPA dose and the time of death and (3) DA content was higher in good responders to the treatment than in poor responders [85]

1.4.2   L-DOPA toxicity

Reactive oxygen species (ROS) are by-products of DA metabolism that are either enzymatically or non-enzymatically produced. The main source of toxicity depends on the intracellular concentration of DA: under low concentrations, the toxicity is mediated by activity of MAO. Increasing concentrations of DA lead to non-enzymatic toxicity caused by the auto-oxidation of L-DOPA and DA [86]. This section describes the sources of ROS issued from L-DOPA and DA metabolism as well as the means of detoxification.

1.4.2.1   Via auto-oxidation

At cytosolic pH, protons of the hydroxyl groups of catechol rings dissociate. This promotes oxidation of CA, including L-DOPA, DA, norepinephrine and epinephrine, to their respective quinones (see Figure **1.9** A) [87]. This auto-oxidation step can either occur via a one- or two- electron oxidation. Both reactions lead to production of quinones, but the former has an intermediate semiquinone radical [87]. Semiquinones rapidly oxidize in the presence of oxygen to form quinones and superoxide radicals [88]. Quinone residues are not stable at cytosolic pH and their amino chain cyclizes to form leukoaminochrome, which can further oxidize to aminochromes. Aminochromes can oxidize to dihydroxyindoles and indolquinones, which can polymerize and be integrated to NM [87]. Quinones are highly reactive compounds and each oxidation step causes release of superoxide radicals ($O_2^{\cdot-}$) causing GSH depletion and enzymatic inactivation further discussed in section 1.4.2.3. Furthermore, $O_2^{\cdot-}$ reacts with protons to form H_2O_2 (Figure **1.9** B)

Auto-oxidation can be enhanced by high concentrations of metal ions such as manganese, iron or copper [87]. ROS and reactive nitric oxide species (RNS) such as H_2O_2, hydroxyl radicals ($^{\cdot}OH$), peroxynitrite (ONOO) or nitrite ($NO_2^{\cdot-}$) can also increase oxidation rates [87]. RNS are generated by the activity of neuronal nitric oxide synthase

(nNOS), which synthesizes nitric oxide (NO) as mediator of response to excitatory amino acids [89].

1.4.2.2   Via enzymatic degradation

As mentioned in section 1.3.3.1, MAO is one of the main enzymes involved in DA degradation. This protein, located at the outer membrane of the mitochondrium, increases cellular H_2O_2 production 100 times when activated [90]. H_2O_2 can then react with iron via the Fenton reaction and generate hydroxyl radicals [91]. These compounds have several cellular targets and induce DNA mutations, lipid peroxidation or amino acid modifications [91]. Due to the loss of DAergic neurons during the course of PD, the turnover of DA is increased, leading to higher expression of MAO and therefore increased oxidative stress levels [92]. H_2O_2 can be detoxified via reaction with 2 GSH by the GPx to form GSSG and 2 H_2O. However, GSSG can react with sulfydryl residues of proteins leading to their inactivation. This can be avoided by recycling of GSSG to GSH using NADPH via glutathione reductase (GR).

DA can be enzymatically oxidized to DA-quinone by flavoenzymes such as prostaglandin H synthase, lipoxygenase or xhantine oxidase [93]. Aminochromes can also be enzymatically reduced back to leukaminochromes by NAD(P)H:quinone oxidoreductase (DT-diaphorase) or via NADPH cytochrome P450. DT-diaphorase catalyzes a two-electron reduction of aminochrome to leukoaminochrome, while NADPH cytochrome P450 catalyzes a one-electron reduction of aminochrome to the corresponding semiquinone radical, which is not generated upon two-electron reduction [87].

1.4.2.3   Consequences

DA-quinones and DOPA-quinones are electron deficient compounds that react with nucleophiles such as cysteine, GSH or cysteinyl residues of proteins to form 5-cysteinyl-dopamine and 5-cysteinyl-DOPA, respectively [93]. If cysteine residues are located in the active site of an enzyme, the reaction with the quinone leads to its inactivation. Affected proteins include enzymes involved in energy metabolism such as succinate dehydrogenase (SDH), NADH dehydrogenase, ATPase, isocitrate dehydrogenase (IDH), pyruvate dehydrogenase complex (PDH), α-ketoglutarate dehydrogenase (α-KGDH) or aconitase (Aco), which leads to inhibition of tricarboxylic acid (TCA) cycle and mitochondrial electron transport chain.

A second class of proteins affected by quinones include enzymes of the catecholamine synthesis pathway: TH, DAT, QDPR and COMT. They are involved in L-DOPA synthesis, DA reuptake from the synaptic cleft, recycling of the BH_4 cofactor and degradation of L-DOPA and DA, respectively. Inhibition of the three first enzymes is beneficial because it reduces the amount of L-DOPA and DA produced and limits the amount of quinones produced. Inhibition of COMT is detrimental since it prevents degradation of L-DOPA and DA [93, 94].

A third class of proteins affected by quinones are permeability transition pores (PTPs). These proteins, located at the inner membrane of mitochondrium, are involved in the transport of solutes smaller than 1500 kDa. Quinones and oxidants cause an increase in PTP permeability, which induce swelling of the mitochondria, proton leak and subsequent depolarization [95]. The direct consequence of this process is a loss of oxidative phophorylation and uncoupling of ATP synthesis [95].

The activity of DT-diaphorase and NADPH cytochrome P450 also have deleterious effects on the cells: the NADPH used by DT-diaphorase depletes the pool of electron donors for GSSG reduction and the NADH used by both enzymes exhausts the electron donors needed for ATP synthesis in the mitochondria [87].

Quinones have detrimental effects on another important cellular process: autophagy. This includes recycling of cytoplasmic proteins and organelles, which are transported to lysosomes. Quinones can bind to different proteins and inhibit their activity: (1) Quinones can form adducts with SNCA, which subsequently forms fibrils. This complex inhibits chaperone-mediated autophagy (CMA). (2) Quinones can bind to ubiquitin C-terminal hydrolase I (UCH-LI) which also inhibits CMA. (3) Adduct formation between quinones and DJ-1 indirectly alters autophagy by disrupting regulation of oxidative stress. (4) Finally, by binding to β-tubulin, quinones disrupt the cytoskeleton and prevent fusion of autophagosomes with lysosomes by accumulation of microtubules [87].

1.4.2.4   Detoxification

Antioxidants are playing a crucial role in quinone detoxification. GSH and ascorbic acid (AA) can exert their antioxidant effects via enzymatic reaction with GPx and AA peroxidase respectively (although AA peroxidase is expressed only in plants) [96] and via non-enzymatic reaction [97]. Besides the fact that AA and GSH can scavenge

free radicals [98, 99], they can also directly interact with quinone derivatives (Figure **1.10**). AA can react with quinones to generate hydroquinones and dehydroascorbic acid (Figure **1.10** A) [100]. Dehydroascorbic acid can be recycled back to AA via a two-electron reduction by glutaredoxin, a GSH-dependent enzyme [101]. In the case of DOPA-*o*-quinone, the hydroquinone formed by the reaction with AA is L-DOPA itself (Figure **1.10** B) [102, 103], and thus, stabilizes this compound.

Astrocytes possess a great antioxidant capacity [104] and their interaction with neurons is important to assure protection of the neurons against oxidative stress. In the brain, astrocytes are responsible for the recycling of AA [105]. For that, they import dehydroascorbic acid through dedicated transporters, reduce it to AA and export it back to the extracellular space where it can be used to protect neurons [106].

GSH is the most abundant antioxidant in the body [107] and its concentration can reach concentrations of 10 mM inside the cells [108]. Astrocytes also support neurons for GSH synthesis, but the compound cannot be transported across cell membranes [109]. Thus, *in vivo*, astrocytes provide precursor for GSH synthesis to the neurons in the form of the dipeptide CysGly [110]. In co-culture systems of neurons and astrocytes, L-DOPA treatment stimulates the production of GSH by astrocytes [111]. GSH plays an important role in the cellular redox cycle, free radical reactions, thio-transfer reactions and conjugation [99]. It can be conjugated to DA-quinone, DOPA-quinone or aminochrome either non-enzymatically or enzymatically by glutathione S-transferase M2-2 (GST M2-2) to form 5-glutathionyl-dopamine, 4-*S*-5,6-dihydroxyindoline and 5-glutathionyl DOPA (Figure **1.10** C) [112], respectively. These products are stable in the presence of oxidizing agents suggesting that they are final elimination products. All GSH conjugates can be degraded to glutamate, glycine and 5-cysteinyl-DA or 5-cysteinyl-DOPA. *In vivo* 5-S-cysteinyl DOPA has been found in melanoma cells [112], in cerebrospinal fluid and in brain regions containing high amounts of DA such as the *substantia nigra* or the *putamen* [87]. 5-S-cysteinyl DOPA can also be directly formed via interaction of DOPA-quinone with the thiol group of cysteine or cysteinyl residues in proteins. This leads to the protein inactivation if the residue is located within the active site of the enzyme [113].
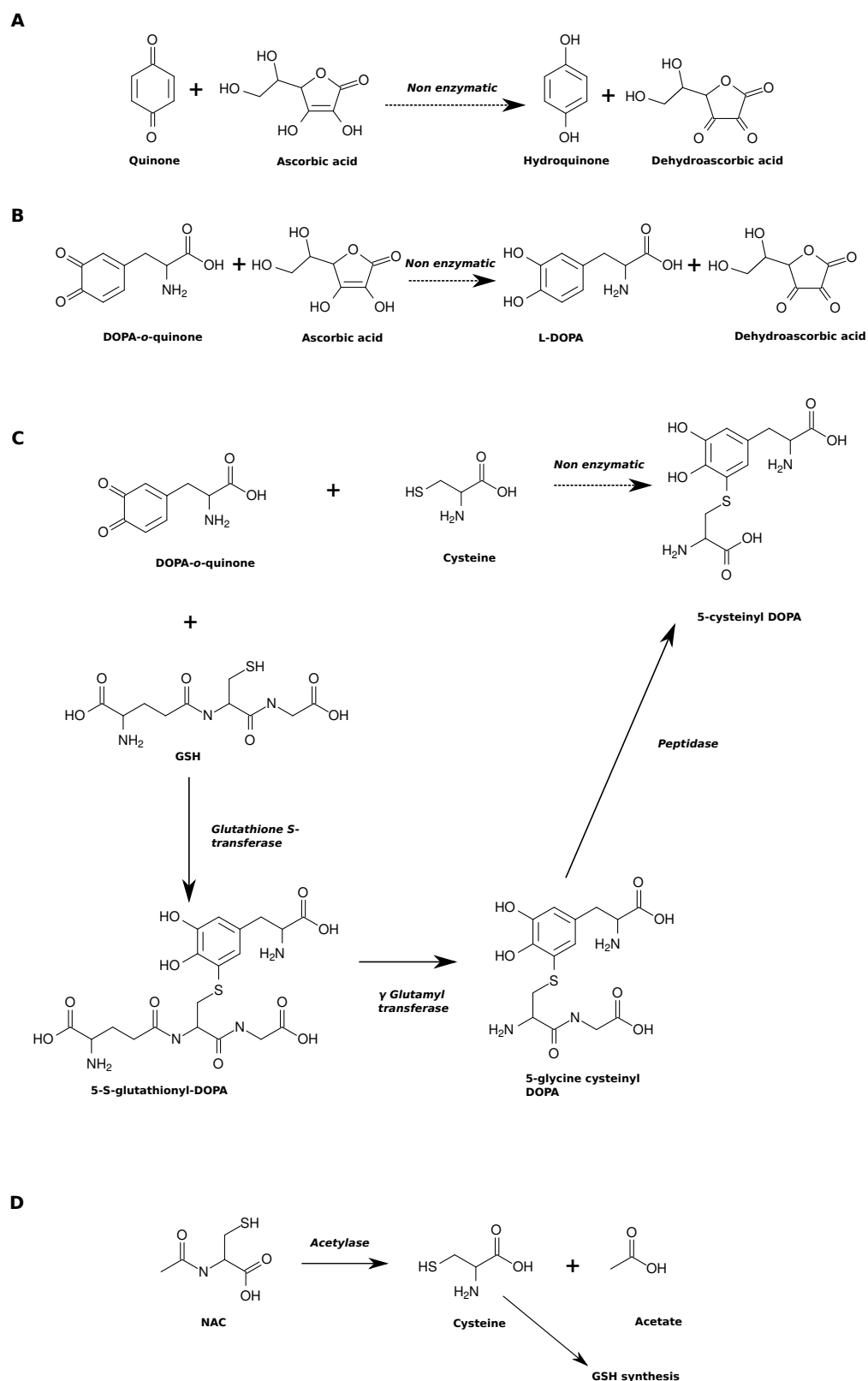
FIGURE 1.10: **Mechanism of action of antioxidants on DOPA-*o*-quinone. (A)**: Ascorbic acid (**AA**) reacts with quinones to form hydroquinones and dehydroascorbic acid. **(B)**: In the case of reaction with DOPA-*o*-quinone, AA forms L-DOPA back and dehydroascorbic acid. **(C)**: Reduced L-glutathione (**GSH**) and cysteine react with DOPA-*o*-quinone to form 5-S-glutathionyl-DOPA and 5-cysteinyl-DOPA respectively. The first can be further metabolized by γGlutamyl transferase and peptidase to 5-cysteinyl-DOPA. **(D)**: N-acetyl-L-cysteine (**NAC**) is cleaved to cysteine and acetate upon entry into the cells and the cysteine residue can be used for GSH synthesis.

The third antioxidant considered is N-acetyl-L-cysteine (NAC). It prevents the toxicity of L-DOPA in two ways: as a synthetic compound, NAC can enter the cell where it is deacetylated to cysteine, (Figure **1.10** D) [109] and thus, promotes GSH synthesis. Secondly, like GSH and cysteine, NAC contains a thiol group which directly reacts with the quinones to stabilize them.

Reactive quinones are inactivated by conjugation via methylation by COMT or transfer of sulfo group by sulfotransferase [114]. Superoxide dismutase (SOD) and catalase also possess a protective role by limiting the amount of H_2O_2 and free superoxide radicals in the cytosol [115]. Metallothioneins are a last class of enzymes important for the prevention of quinone toxicity: they are responsible for metal homeostasis by binding to heavy metals. These proteins are rich in cysteine residues, which can make up to 40% of the protein content. Therefore, they can sequester quinones and prevent further oxidation [93].

Antioxidant systems are important when considering cell viability in the context of ageing. Levels of GSH, SOD and catalase specifically decrease in the *substantia nigra pars compacta* with increasing age rendering these neurons more sensitive to oxidative stress and neurotoxic insults over time [116]. In PD patients, it has been shown that the levels of GSH are further reduced in the *substantia nigra* compared to healthy individuals [117] and a correlation has been established between the extent of neuronal loss and the depletion of GSH [118]. The decrease in GSH levels has been linked to an altered remethylation of homocysteine to methionine and transsulfuration to cysteine [119] (Figure **1.11**). This mechanism was identified through elevated levels of homocysteine in the plasma of PD patients. Plasma levels of homocysteine were further increased in patients under L-DOPA medication, indicating a further decrease in antioxidant levels [120].

The increased levels of homocysteine can be routed back to L-DOPA and DA degradation by COMT, the methyltransferase that uses SAM as cofactor and produces SAH [79]. SAH can be hydrolyzed to homocysteine which can be remethylated to methionine as mentioned above and finally coupled to an adenosyl group to form back SAM [121]. It is therefore possible that the further increase in homocysteine plasma levels observed in PD patients under L-DOPA treatment is due to an increased activity of COMT coupled to an altered remethylation of homocysteine.
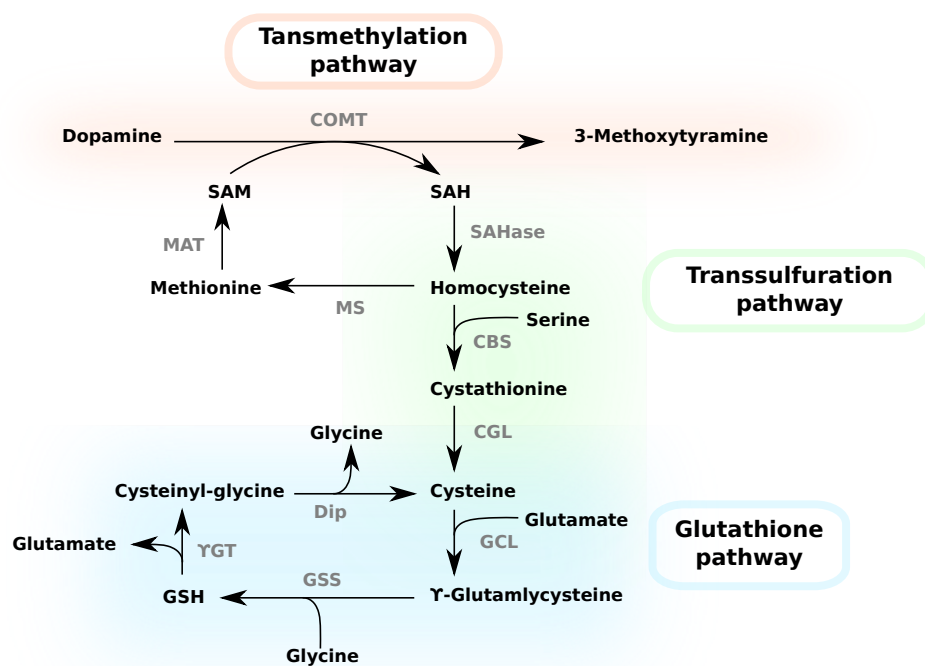
FIGURE 1.11: **Transsulfuration of S-adenosyl-homocysteine and glutathione biosynthesis.** Degradation of dopamine via catechol-*o*-methyltransferase (**COMT**) is dependent on the use of S-adenosyl-methionine (**SAM**) for methylation (**in red**). S-adenosyl-homocysteine (**SAH**) is produced by this reaction and can be recycled. First, SAH is metabolized to homocysteine by S-adenosyl hydrolase (**SAHase**) which can either be converted to methionine by methionine synthase (**MS**) or to cystathionine by cystathionine β-synthase (**CBS**) by addition of serine. Methionine can finally be recycled to SAM by methionine adenosyltransferase (**MAT**). The second pathway involved is the transsulfuation pathway (**in green**) where cystathionine enters the glutathione synthesis pathway (**in blue**) via cystathionine γ-lyase (**CGL**) to form cysteine. γ-glutamylcysteine is formed by addition of glutamate to cysteine by glutamate-cysteine ligase (**GCL**). Finally, glutahione (**GSH**) is synthesized by further addition of glycine by glutathione synthase (**GSS**). GSH can be degraded into the three original amino acids by γ-glutamyl transpeptidase (γ**GT**) which releases glutamate and produces the dipeptide cysteinyl-glycine. This compound can finally be cleaved by dipeptidase (**Dip**) to release glycine and cysteine.

1.5 Metabolomics

After describing the biological background, these last sections focus on the analytical methods applied in this work. I will start with a general introduction on metabolomic studies followed by a more detailed description of GC-MS studies. Finally, I will give an overview of stable isotope-assisted metabolomics and its application in the context of this work.

1.5.1 Metabolomics studies

Metabolites are small molecules that can serve as substrate for enzymatic reactions [122]. Therefore, metabolomics is the study of metabolites within cells, body fluids, tissues or organisms. Metabolites are considered as the direct signature of biochemical activity since they are the final products of epigenetic regulation of genes and post-translational modification of proteins [122].

Depending on the goal and design of the experiment, metabolomics studies can be divided into two classes: targeted and untargeted approaches. In targeted metabolomics, the interest is focused on a selected subset of metabolites. These experiments are designed to answer a specific question directed towards a particular pathway. In untargeted metabolomics, the approach is slightly different: instead of being interested in a subset of compounds, the goal is to detect as many metabolites as possible to obtain a broad overview of metabolic adaptation upon treatment for example [122]. Given the different approaches, the obtained data sets are really different and require different pipelines for data processing and analysis.

In metabolomics studies, sample preparation is critical: the metabolite composition can quickly change due to enzymatic activity, thermo-sensitivity, high reactivity or breakdown of metabolites [123]. To increase reproducibility, extractions are performed using solvents under cold conditions to denature enzymes and preserve metabolites [123]. Once the samples are extracted, they are dried under vacuum and stored under cold temperature to prevent metabolite degradation [123].

Several metabolomics platforms are available for measurements of biological samples. The most commonly used being nuclear magnetic resonance (NMR), GC-MS and liquid chromatography coupled to mass spectrometry (LC-MS) [123]. Each of them presents advantages and disadvantages: NMR requires minimal sample preparation. However, NMR is less sensitive than mass spectrometry [123]. GC-MS and LC-MS are more suitable techniques for measuring and quantifying a broad range of molecules. None of the aforementioned methods is powerful enough to cover the full metabolome. The best approach so far is to use a combination of techniques [123]. GC-MS was the technique of choice during my PhD thesis. Therefore, I will further discuss this technique using DA as example.

1.5.2 Gas chromatography - mass spectrometry

GC-MS can be divided into two parts: the gas chromatograph and the mass spectrometer. The chromatography consists of a column composed of a specific stationary phase. The sample is transferred to the gas phase and loaded on the column, where a temperature gradient is applied to induce migration of metabolites on the column depending on their affinity with the stationary phase. Therefore, the chromatography allows for compound separation based on retention.

The second component of GC-MS is the mass spectrometer. This can be divided into three parts: (1) an ionization step by electron ionization (EI), (2) a ion selection step by quadrupole and (3) finally, the detector records all ions reaching it. The role of EI is to fragment the metabolites eluting from the column: the metabolites are bombarded with electrons generated from a filament and are fragmented in highly reproducible ion patterns. It is therefore the most commonly used mode of ionization [123]. Upon fragmentation, the ions travel through the quadrupole, which allows either all ions to migrate to the detector or selects for specific ions. Finally, the detector records the ions reaching it as well as their intensity. A detector is characterized by its scan rate, which is how fast it scans a mass spectrum: the faster it is, the more data points are recorded and available for analysis.

The complexity of a sample can be visualized by the total ion current (TIC) chromatogram. This is obtained by summing up the intensity of all ions detected at each recording point. The TIC of DA 4TMS [2] is displayed in Figure **1.12** A.

In optimal conditions, one peak represents one metabolite, which can be further visualized by its mass spectrum. This is the plot of intensity against mass over charge ratio (m/z). The patterns obtained in the mass spectra are compound specific and can be used for metabolite identification along with the retention time. Identification is performed by comparison of obtained spectra and retention times with compound libraries. The compound libraries used in this work were built in house.

---

[2]Sample derivatization is further discussed in section 1.5.4
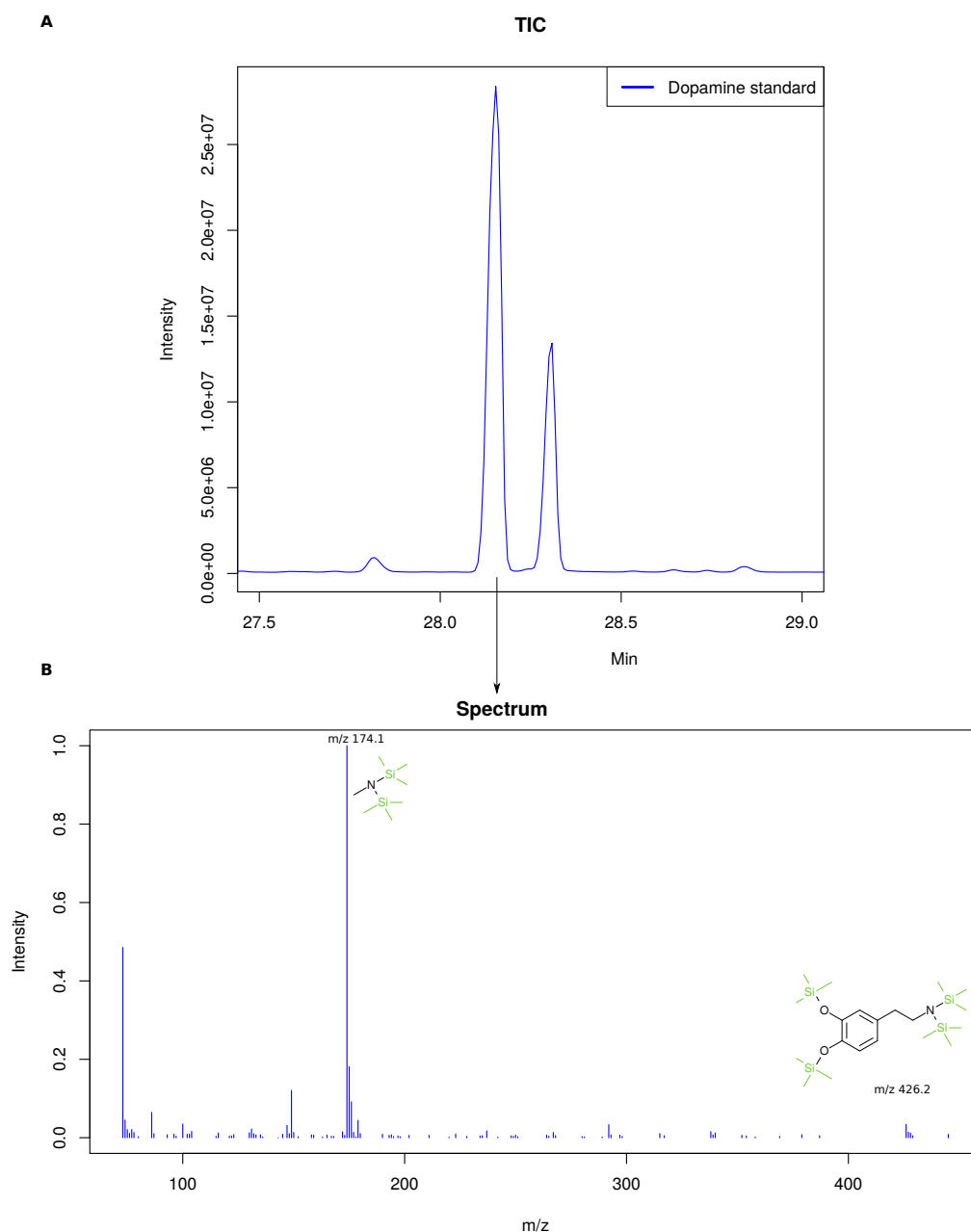
FIGURE 1.12: **Chromatogram and spectrum of dopamine. (A)**: The sum of all ions recorded at a given time point can be visualized by the total ion current (**TIC**) chromatogram, plotting signal intensity in function of the time. A compound can first be characterized by its retention time: in this temperature gradient, the retention time for dopamine is 28.16 min. **(B)**: A second characteristic of a compound is its spectrum obtained by fragmentation in the ion source. The spectrum of dopamine is displayed. Specific ions of dopamine include 174.1 and 426.2.

Figure **1.12** B represents the mass spectrum of DA. This plot displays the intensity of the signal in function of the m/z. Ion m/z 426.2 represents the fragment of DA 4TMS in which the full carbon backbone of the metabolite is present. Ions m/z 427.2 and 428.2 are the isotopic peaks of this molecule. Upon fragmentation in the ion source, other

fragments are formed: ion m/z 174.1 can also be used to identify DA and this molecule contains only a fragment of the original DA. Isotopic peaks are m/z 175.1 and 176.1.

The isotopic peaks obtained in the mass spectrum are due to natural occurrence of stable isotopes. Isotopes are obtained upon addition of neutron within the nucleus of an atom. For example, 98.9% of the naturally occurring carbon contains six protons and six neutrons, called ^{12}C. Around 1.1% of carbon atoms are formed by six protons and seven neutrons, giving rise to ^{13}C. For hydrogen, 99.99% of the atoms contain only one proton and are called ^{1}H. The second possible isotope contains one proton and one neutron and is called ^{2}H or deuterium. The presence of this extra neutron can be visualized on GC-MS mass spectrum due to a shift of one mass unit.

The spectrum in Figure **1.12** B was obtained in full SCAN mode, meaning that all the ions hitting the detector are recorded. The detector can also be operated in selected ion monitoring (SIM) mode: specific ions can be selected and only those are recorded. This increases the sensitivity of the measurement and allows to detect low amounts of metabolites [124]. In the case of DA, specific ions used for SIM measurement are 174.1 and 426.2.

1.5.3   Limit of detection

Limit of detection (LOD) is the lowest quantity of analyte that can be distinguished from the background signal. This value is instrument specific, analyte dependent and can be calculated from the signal-to-noise ratio (S/N) [125]. I calculated this value for ion 426.2 of DA in SIM mode. The LOD is 234.3 fmol (30 μL in vial), which is equivalent to 7.8 fmol on column (1 μL injected). Given the fact that 1 μL is injected, this corresponds to a LOD of 7.8 nM. Using electrochemical detection, Kim *et al.* estimated the LOD of DA to be 2.64 μM [126]. Using nanoparticles and modified electrodes, Guo *et al.* reported an LOD of 30 nM [127]. The addition of a microfluidic device can decrease the LOD to 3.5 nM [128]. Therefore, the LOD obtained using GC-MS is in the range of LOD obtained with other methods. The advantage of GC-MS is that the spectrum allows for specific identification, while using electrochemical detection, this identification is based on elution profile [129].

1.5.4 Sample preparation: derivatization

To perform GC-MS analysis, samples need to be transferred to the gas phase. Most compounds containing polar functional groups are thermally labile or not volatile at all [123]. This can be circumvented by the use of chemical derivatization.
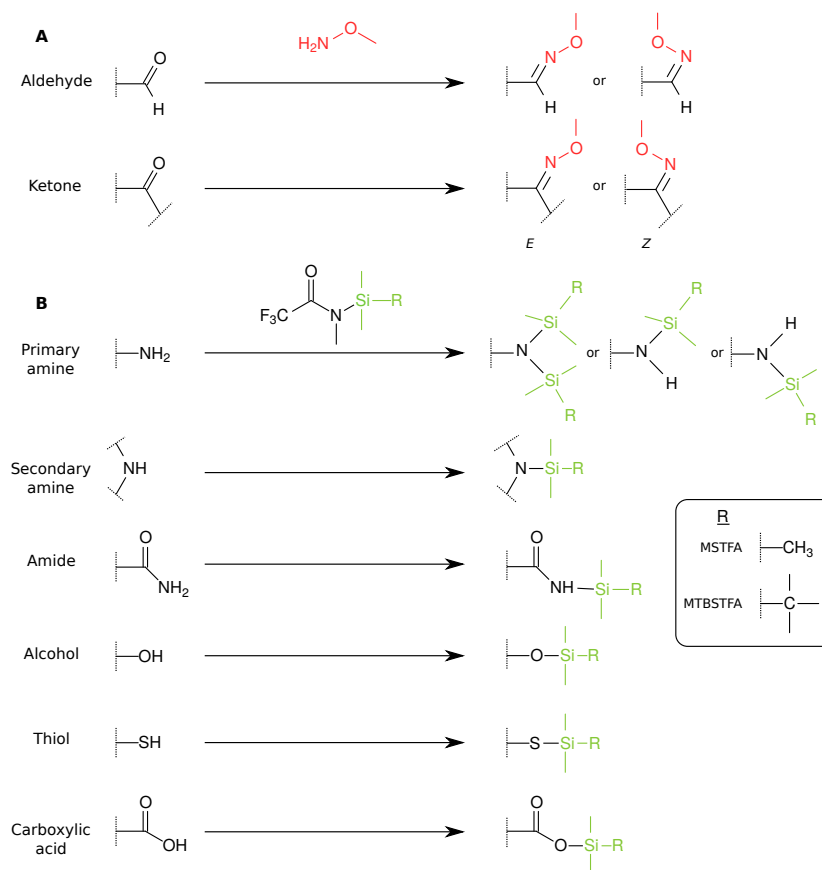
FIGURE 1.13: **Derivatization of functional groups in GC-MS.** Derivatization is necessary in order to bring metabolites to the gas phase. **(A)**: Methoxyamine prevents keto-enol tautomerization of aldehydes and ketones. **(B)**: MSTFA or MTBSTFA can be used for alkylsilylation on a wide range of functional groups.

Common derivatization methods in GC-MS are based on oximation followed by silylation [123]. Oximation can be performed by methoxyamine which modifies aldehyde and ketone groups (Figure **1.13** A). This allows for example to keep sugars in open chain form. Methoxyamine can exist in two different configuration (*E/Z*), which give two derivatives. Silylation can be performed with N-methyl-N-(trimethylsilyl)trifluoroacetamide (MSTFA) or N-tert-butyldimethylsilyl-N-methyltrifluoroacetamide (MTBSTFA), both modifying amine, amide, alcohol, thiol and carboxylic acid groups (Figure **1.13** B) and give rise to trimethylsylil (TMS) or

tert-butyl dimethylsilyl (TBDMS) derivatives, respectively. In order to perform a complete silylation, the samples must be completely dry: silylation reagents are extremely sensitive to hydrolysis and the presence of water can use up to twenty times its volume in derivatization reagent.

1.6 Stable isotope-assisted metabolomics

Results from non-targeted metabolomics experiments give indication about intracellular or extracellular metabolite levels. In addition, information about consumption, secretion and transport reactions are obtained. This does not provide any information on metabolic fluxes nor which carbon source is preferably used for specific pathways and how this could change upon stimulation. These can be investigated using stable isotope labeled nutrients [130]. The most commonly used isotope is ^{13}C. In this work, the tracers used were fully labeled glucose ([U-$^{13}C_6$]-glucose), fully labeled glutamine ([U-$^{13}C_5$]-glutamine), fully labeled pyruvate ([U-$^{13}C_3$]-pyruvate), glucose labeled at positions 1 and 2 ([1,2-$^{13}C_2$]-glucose), fully labeled phenylalanine ([U-$^{13}C_9$]-phenylalanine) and fully labeled tyrosine ([U-$^{13}C_9$]-tyrosine).

1.6.1 Isotopic steady state

In order to perform stable isotope-assisted metabolomics, the cells need to be at metabolic and isotopic steady state. When a tracer is supplemented to cells, intracellular enrichment of downstream metabolites increases over time until it reaches a stable level, which is the isotopic steady state. Using [U-$^{13}C_6$]-glucose as tracer, isotopic steady state within glycolysis is reached within minutes while it takes up to several hours to reach this point in TCA cycle intermediates [130]. To assess the isotopic steady state precondition in LUHMES cells, I incubated these cells with [U-$^{13}C_6$]-glucose or [U-$^{13}C_5$]-glutamine for 2 min, 15 min, 30 min, 1 h, 6 h, 18 h, 24 h and 48 h. I established that cells were at isotopic steady state after 24 hours for both tracers (Appendix A).

1.6.2 Mass isotopomer distribution

The use of stable isotope tracers leads to the formation of labeling patterns in target metabolites. Metabolites only differing in their isotopic compositions are called *isotopologues* or *mass isotopomer*. As isotopologues have different masses, they can be separated on a mass spectrum [130]. On the other hand, *isotopomers* are positional isomers with the same isotopic composition, therefore, they have the same mass. These cannot be resolved by GC-MS, which does not provide any positional information [130].
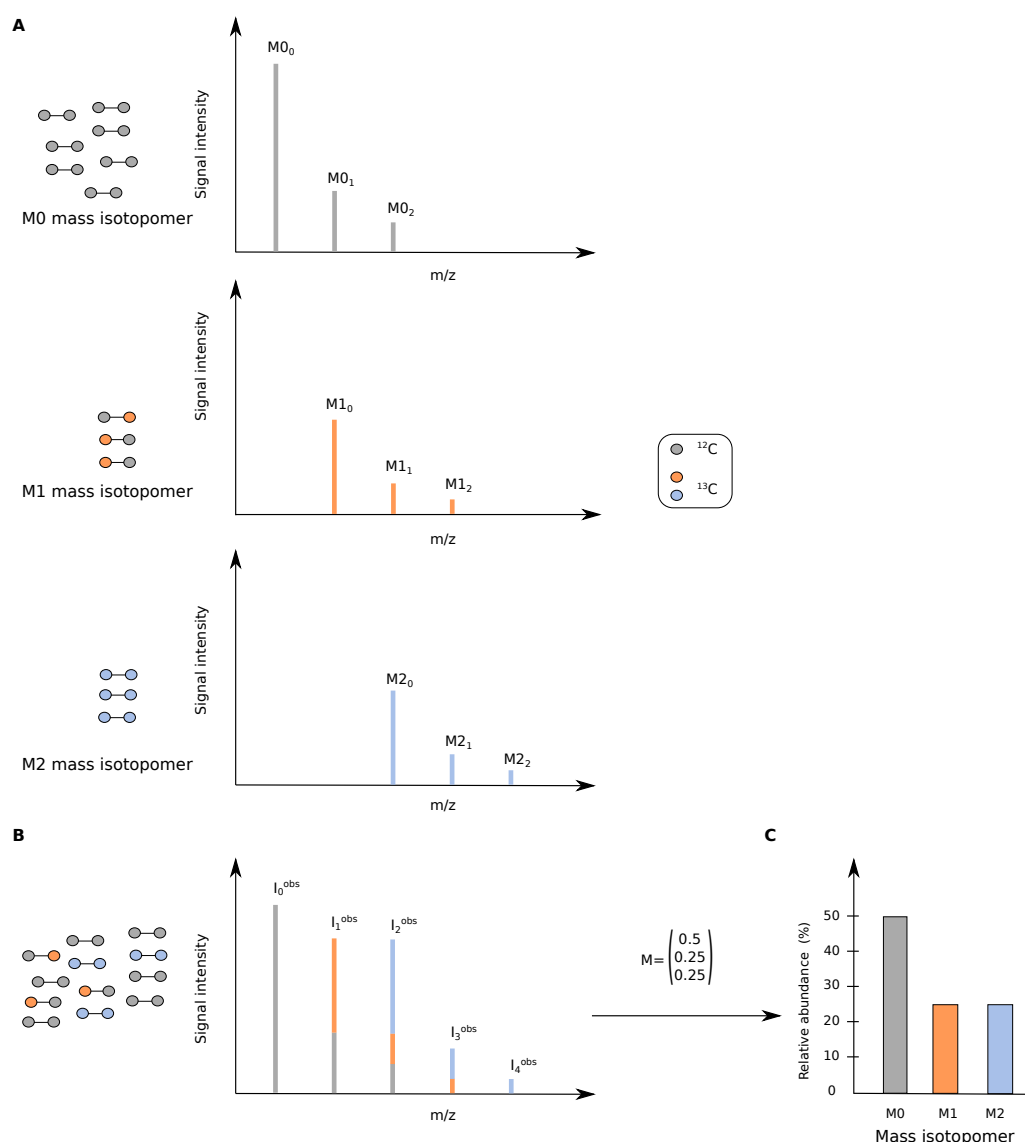
FIGURE 1.14: **Mass isotopomer distribution. (A)**: A metabolite composed of two carbons gives rise to three different isotopologues or mass isotopomers: either none of the carbons is labeled (**M0**), one of them is labeled (**M1**) or both of them are labeled (**M2**). If a stable isotope tracer is used, the abundance of labeled carbons increases and the different mass isotopomer can be separated by the different spectra. **(B)**: When a metabolite elutes from the chromatographic column, the spectrum obtained is a mix of all isotopomers. **(C)**: The isotopomers can be separated by solving a linear equation system and data can be visualized using barplots for example. Adapted from [131].

Mass isotopomer distributions (MIDs) vector can be determined and describe the fractional abundance of each isotopologue normalized to the sum of all possible iso-topologues [130]. Therefore, the sum of all MIDs of a metabolite is always 1 or 100%. An example is given in Figure **1.14**. In Figure **1.14** A, different isotopologues give rise to different spectra, with shift of one m/z unit for each heavy isotope added to the

metabolite. A sample is usually constituted of a mixture of isotopologues which gives rise to complex MID pattern (Figure **1.14** B). This can be computationally solved using linear equation systems. In the resolution of these equations, the natural abundance of isotopes needs to be taken into account and corrected for. The results can then be displayed in the form of barplots for example (Figure **1.14** C), where M0 is the non-labeled fraction of metabolites, M1 represents the fraction of metabolites containing one atom labeled and M2 represents the fraction of metabolites containing two labeled atoms.

1.6.3 Compartmentalization

Stable isotope assisted-metabolomics can be used to evaluate compartmentalization of metabolites. For example, pyruvate can be found in the cytosol and in the mitochondrium. Upon extraction and calculation of pyruvate MIDs, it is not possible to evaluate from which compartment they derive. However, this can be estimated by proxy: lactate dehydrogenase (LDH), the enzyme converting pyruvate to lactate is strictly cytosolic while the expression of alanine aminotransferase (ALT) appears to be mainly mitochondrial in some cell lines [130]. Indeed, knock down of the pyruvate mitochondrial transporter in cultured myoblasts leads to a strong decrease in alanine levels, suggesting a strong contribution of the mitochondrial ALT in alanine synthesis in these cells [132]. Therefore, the labeling of lactate reflects the cytosolic pool of pyruvate labeling, while the labeling of alanine reflects the mitochondrial pyruvate pool [130].

1.6.4 Fractional contribution

MIDs are also informative on nutrient contribution to a certain metabolite. This can be calculated by a weighted average of all isotopologues, as follows:

$$\frac{1}{n} \times \sum_{i=1}^{n} M_i \times i$$

Where n is the number of carbon atom of the molecule and M_i is the ith mass isotopomer. This gives information on fractional contribution of a substrate to a metabolite and allows to determine whether a treatment or conditions induce metabolic switches [130].

Finally, stable isotope-assisted metabolomics experiments give information on pathway activity. This can be inferred by the ratio of two alternative and converging pathways. This implies that a specific pathway can be identified by a specific isotopologue and that a metabolite of the targeted pathway can be measured [130].

Aim of the thesis

Although described for the first time in 1817 by James Parkinson, the mechanisms underlying the development of Parkinson's disease (PD) are still unknown. This neurodegenerative disease primarily affects dopaminergic neurons within the *substantia nigra pars compacta*. The death of dopaminergic neurons causes a drop in the amounts of dopamine (DA) in the *striatum*, leading to impaired movement control. Genetic and environmental factors are involved in some cases and molecular mechanisms include increased oxidative stress, mitochondrial dysfunction or disruption of proteasomal degradation. So far, there exists no cure for PD, but symptoms can be managed for several years using 2,3-dihydroxy-L-phenylalanine (L-DOPA), the precursor of DA, as a treatment.

In vitro models for PD include cell lines derived from different organisms (human, mouse, rat), different organs (brain, adrenal gland) or different cell types (neuroblastoma, pheochromocytoma, immortalized mesencephalon cells). The most commonly used *in vivo* models include mice and rats unilaterally treated with PD-inducing drugs, such as 1-methyl-4-phenylpyridinium (MPP^+), 6-hydroxydopamine (6-OHDA) or rotenone. Both *in vitro* and *in vivo* models present some disadvantages: most of the cell lines used are of cancer origin and therefore proliferate in culture. Proliferating and resting cells have distinct metabolism. Therefore, the use of cancer cells to study neurons under cell cycle arrest is not ideal. Concerning *in vivo* studies, it is important to bear in mind that enzymatic regulation of tyrosine hydroxylase (TH), the rate-limiting enzyme in the DA synthesis pathway, is organism-specific. Moreover, mouse and rat do not produce neuromelanin (NM), a pigment typical for DA producing cells.

Given cell type and organism specificity of central carbon metabolism as well as regulation of DA synthesis, **it is of crucial importance to have a study model that reflects the human dopaminergic neurons from the** *substantia nigra* **as best as possible**. A second important point to address is **the interplay between the different enzymes involved in DA synthesis**. Therefore, I decided to focus this work on the **human LUHMES immortalized mesencephalon cells**. These cells can be differentiated into post-mitotic TH-expressing neurons, but they do not produce DA in amounts detectable by gas chromatography - mass spectrometry (GC-MS).

In the **first part of my PhD**, I investigated the **effects of L-DOPA on the metabolism of LUHMES cells**. LUHMES cells were treated with L-DOPA for 24 hours and metabolites were extracted for GC-MS measurement. I used a **non-targeted approach** to assess the overall changes in the metabolism as well as **stable isotope-assisted metabolomics** in order to follow the fate of carbon sources throughout central carbon metabolism.

In the **second part**, I focused on the **generation of a human DA-producing cell system** that would not be of cancer origin. After comparing gene and protein expression of available systems, I used lentiviral-mediated systems to increase expression of genes involved in DA synthesis. In the course of this project, I also evaluated **the role of enzymes involved in the synthesis of DA**.

2

<div style="text-align: right;">*2*</div>

Material and Methods

Contents

2.1   Cell culture

2.1.1   LUHMES cell line

LUnd Human Mesencephalon (LUHMES) cells [58] were kindly provided by Professor Marcel Leist (University of Konstanz, Germany). They are issued from a

8-week old foetus and were conditionally immortalized using a *v-myc* vector. Thus the cells are proliferating. Upon addition of tetracycline, the cells stop proliferating and differentiation can be initiated.

The cells are always cultivated in flasks and plates coated with 5 μg/mL poly-L-ornithine (PLO) (Sigma Aldrich, P4957) and 1 μg/mL fibronectine (Sigma Aldrich, F1141) for minimum 3 hours and dried before use.

Proliferating cells were cultivated in Advanced Dubelcco's Modified Eagle's Medium (DMEM)/F-12 (Life Technologies, 12634) supplemented with 2 mM L-Glutamine (Sigma Aldrich, G7513), 1x N2 (Life Technologies, 17502-048) and 40 ng/mL fibroblast growth factor (FGF) (R&D Systems Europe, 4114-TC). Cells were passaged twice a week. They were dissociated with 0.05% Trypsin-EDTA (1X) (Life Technologies, 25300) for 5 min, 500.000 cells were centrifuged for 5 min at 200 x g and resuspended in 10 mL of fresh proliferation medium in a coated T75 flask.

For differentiation, 8 million cells were transferred to a T175 flask and medium was exchanged to differentiation medium on the next day. This medium consists of Advanced DMEM/F-12 supplemented with 1 mM L-Glutamine, 1X N2, 1 mM dibu-tyryl cAMP (db-cAMP) (Sigma Aldrich, D0627), 1 μg/mL tetracycline (Sigma Aldrich, T7660) and 2 ng/mL glial cell line-derived neurotrophic factor (GDNF) (R&D Systems Europe, 212-GD-050). 48 h later, cells are seeded in plates, unless otherwise stated, with the following densities: 1 million cells per well in 6-well plates, 500.000 cells per well in 12-well plates, 250.000 cells per well in 24-well plates and 125.000 cells per well in 48-well plates. Cells were kept in culture for additional 4 days (day 6 of differentiation) or 8 days (day 10 of differentiation) prior to experiments.

2.1.2 IMA2.1 cell line

The mouse immortalized astrocyte IMA2.1 cell line [133] was kindly provided by Professor Marcel Leist (University of Konstanz, Germany). They were culti-vated in DMEM low glucose (Sigma Aldrich, D6046) supplemented with 10% heat inactivated fetal bovine serum (FBS) (Gibco, 10500-064, Lot #1096628K) and 1% Peni-cillin/Streptomycin (P/S) (Sigma Aldrich, P0781). They were passaged twice a week and dissociated using 0.05% Trypsin-EDTA (1X) (Life Technologies, 25300).

For experiments, the cells were seeded at a density of 50.000 cells per well in 48-well plates for cell viability assay and 100.000 cells per well in 12-well plates for metabolite extraction 24 hours before the start of the treatment.

2.1.3 BV2 cell line

The retroviral immortalized microglia BV2 cell line [134] was kindly provided by Dr Wolfgang Wurst (Helmholtz Centre, Munich, Germany) were cultivated in Advanced DMEM/F-12 (Life Technologies, 12634) supplemented with 2mM L-Glutamine (Sigma Aldrich, G7513). Cells were passaged twice a week and dissociated using a cell scraper.

For experiments, cells were seeded 24 hours before treatment at the density of 100.000 cells per well in 24-well plates for cell viability assay and at the density of 200.000 cells per well in 12-well plates for metabolite extraction 24 h before the start of the treatment.

2.1.4 SH-SY5Y cell line

The neuroblastoma cell line SH-SY5Y [135] was kindly provided by Dr Aleksandar Rakovic (University of Luebeck, Germany). They were cultivated in DMEM high glucose (Sigma Aldrich, D5796) supplemented with 10% FBS and 1% P/S. They were passaged twice a week and dissociated using 0.05% Trypsin-EDTA (1X).

For experiments, the cells were seeded at a density of 50.000 cells per well in 48-well plates for cell viability assay and 100.000 cells per well in 12-well plates for metabolite extraction 24 hours before the start of the treatment.

2.1.5 P-C12 cell line

The rat pheochromocytoma cell line PC-12 was obtained from ATCC (CRL-1721.1®). They were cultivated in ATCC-formulated F-12K medium (ATCC, 30-2004) completed with 2.5% FBS and 15% horse serum. Cells were passaged twice a week and dissociated using a cell scraper.

For experiments, cells were seeded at a density of 50.000 cells per well in 48-well plates for cell viability assay 24 h before the start of the treatment and 300.000 cells per well in 12-well plates for metabolite extraction 48 hours prior to extraction.

2.1.6 CCF-STTG1 cell line

The human astrocytoma cell line CCF-STTG1 was obtained from ATCC (CRL-1718®). They were cultivated in ATCC-formulated RPMI-1640 medium (ATCC, 30-2001) completed with 10% FBS. Cells were passaged twice a week and dissociated using 0.05% Trypsin-EDTA (1X).

For experiments, cells were seeded at a density of 150.000 cells per well in 48-well plates for cell viability assay 24 h before the start of the treatment.

2.2 Treatments

2.2.1 L-DOPA

2,3-dihydroxy-L-phenylalanine (L-DOPA) (Sigma Aldrich, D9628) was freshly prepared unless otherwise stated and reconstituted in cell culture medium. Treatments were carried out for 24 h.

When assessing the role of anti-oxidants on the viability of LUHMES cells upon L-DOPA treatment, ascorbic acid (AA) (Sigma Aldrich, 255564), reduced L-glutathione (GSH) (Sigma Aldrich, G6013) and N-acetyl-L-cysteine (NAC) (Sigma Aldrich, A7250) were reconstituted in cell culture medium and applied to the cells at the same time as L-DOPA at the concentration of 1 mM.

When evaluating the transport of L-DOPA, cells were co-treated with 1 mM L-leucine (Sigma Aldrich, L8912) reconstituted in cell culture medium or 5 μM GBR 12909 dihyrdrochloride (Sigma Aldrich, D052). GBR12909 was reconstituted in DMSO (Sigma Aldrich, D2438) at the concentration of 5 mM and diluted to the final concentration in cell culture medium. These compounds were used to inhibit the large amino acid transporter (LAT) and the dopamine transporter (DAT) respectively. To evaluate if the toxicity is due to enzymatic degradation products, cells were treated with 3,4-dihydroxy-D-phenylalanine (D-DOPA) (Sigma Aldrich, D9378) at the same concentrations as L-DOPA. superoxide dismutase (SOD) (Sigma Aldrich, S7571) was reconstituted in cell culture medium at the concentration of 1000 U/mL and was further diluted to 500 U/mL for treatment for 24 h.

2.2.2 Others

LPS: BV2 cells were treated with lipopolysaccharide (LPS) from *E.coli* (Sigma Aldrich, L6529) to induce inflammatory response. It was reconstituted in Phosphate Buffer Saline (PBS) without calcium and magnesium (Sigma Aldrich, D1408) at the stock concentration of 1 mg/mL. The final concentration used was 10 ng/mL for 6h. When an additional L-DOPA treatment was performed, the L-DOPA was reconstituted in cell culture medium and applied to the cells 18 h before the LPS treatment.

MPP$^+$: LUHMES cells were treated with 1-methyl-4-phenylpyridinium (MPP$^+$) (Sigma Aldrich, D048) to induce mitochondrial complex I inhibition. Stock solutions of 13.5 mM were prepared in water and stored at -20 °C. The solution was then diluted 1:10 in cell culture medium and 5.6 μL were added in 1 mL of medium in each well to the final concentration of 10 μM. Incubation was carried for 24 h before metabolite extraction.

Rotenone: LUHMES cells were treated with rotenone (Sigma Aldrich, R8875) to induce mitochondrial complex I inhibition. Stock solutions were prepared in DMSO at the concentration of 10 mM. This solution was stored at -20 °C. Upon utilization, it was diluted in cell culture medium to 1 mM and 1 μL was added in 1 mL of medium in each well to the final concentration of 1 μM. Incubation was carried for 6 h before metabolite extraction.

Heptelidic acid: LUHMES cells were treated with heptelidic acid (Abcam, ab144269) to induce glyceraldehyde-3-phosphate dehydrogenase (GAPDH) inhibition. Stock solutions were prepared in water at the concentration of 1 mM. This solution was stored at -20 °C. Upon utilization, 3.6 μL was diluted in 1 mL of medium to the final concentration of 3.6 μM. Incubation was carried for 24 h before metabolite extraction.

H$_2$O$_2$: LUHMES cells were treated with H$_2$O$_2$ (Sigma Aldrich, 216763) for cell viability assays. Cells were treated for 24 h with concentrations ranging from 12.5 μM to 200 μM.

Glutamate: LUHMES cells were treated with glutamate (Sigma Aldrich, G8415) for cell viability assay. Cells were treated with concentrations ranging from 100 μM to 400 μM for 24 h.

Acetate: LUHMES cells were treated with acetate (Sigma Aldrich, S8750) for metabolite extraction. Cells were treated for 24 h with 800 μM acetate and 400 μM pyruvate (instead of the usual 1 mM) before metabolite extraction. These concentrations correspond to the concentrations of acetate and pyruvate measured in Advanced DMEM/F-12 incubated without cells for 24 h with 200 μM L-DOPA.

Tyrosine hydroxylase (TH) cofactors: LUHMES AADCox cells were treated for 5 h with 200, 400 or 600 μM sepiapterin (Sigma Aldrich, S154) before metabolites were extracted. The same cell line was also treated with 100 μM and 200 μM *6R*-L-erythro-5,6,7,8-tetrahydrobiopterin (BH_4) (Sigma Aldrich, T4425) for 30 min before metabolite extraction. For both compounds, solutions were prepared freshly in cell culture medium.

2.3 Molecular Biology

2.3.1 RNA extraction

RNA was extracted either directly from cells or from interphases after metabolite extraction using the RNeasy Mini Kit[1] (Qiagen, 74106) following manufacturer's instructions. If the RNA was extracted from the cells, they were seeded, treated and washed once with PBS before 350 μL RLT buffer supplemented with 10 μL/mL β-mercaptoethanol (BME) (Sigma Aldrich, M3148) was added. If the RNA was extracted from the interphase, the interphase contained in methanol was centrifuged for 5 min at 16,000 x g at 4 °C. All the methanol was removed and the interphase was left to dry before 350 μL RLT/BME buffer was added. The rest of the extraction was done following the manufacturer's instruction and the RNA was eluted in 40 μL of RNase free water. RNA concentration was measured using the Nanodrop. Samples were stored at -80 °C.

2.3.2 cDNA synthesis

cDNA was synthesized by using SuperScript III Reverse Transcriptase® kit[2] (Thermo Scientific, 18080-044) and following manufacturer's instruction. 0.1 to 0.5 μg of RNA were used per reaction and the final product was diluted in 180 μL of RNase free water to obtain a final volume of 200 μL. Samples were stored at -20 °C.

---

[1]https://www.qiagen.com/us/shop/sample-technologies/rna/rna-preparation/rneasy-mini-kit

[2]https://www.thermofisher.com/order/catalog/product/18080085

2.3.3 qPCR using LigthCycler 480

All primers used for qPCR were designed using the NCBI Primer-BLAST tool[3]. They were sent for synthesis to Eurogentec[4] at a concentration of 100 µM. All human and mouse primer sequences used in this thesis can be found in tables 2.1 and 2.2.
A master mix solution was prepared for each primer pair containing per sample in a 384-well plate: 0.25 µL of 10 µM forward and reverse primer, 5 µL of IQ SYBR Green Supermix (Bio-Rad, 170-8885) and 3.5 µL of H_2O. 9 µL of master mix and 1 µL of cDNA were added per well. The plate was then sealed and centrifuged before being loaded on the LightCycler 480 (Roche). The program used to run the PCR can be found in Table 2.3.

TABLE 2.1: Sequences of human primers used for qPCR

Gene symbol		Sequence
DAT	fwd	5'-GTCACCAACGGTGGCATCTA-3'
	rev	5'-CTGGATGTCGTCGCTGAACT-3'
DDC	fwd	5'-CTGTCCCATGAGTTTGAGTC-3'
	rev	5'-CACTTTGTTGGAACCCTTTAG-3'
GTPCH	fwd	5'-GCTGTAGCAATCACGGAAGC-3'
	rev	5'-TTTGGATCCTCCCGGAACAC-3'
L27	fwd	5'-CTGGTGGCTGGAATTGAC-3'
	rev	5'-ACAGAGTACCTTGTGGGC-3'
TH	fwd	5'-TGTAAGCAGAACGGGGAGGT-3'
	rev	5'-CTGGATGCGTGAGGCATAGC-3'
VMAT2	fwd	5'-CCTTCTGCTGGTGGTGCTAT-3'
	rev	5'-AGGGCAGTTGTGATCCATGA-3'

TABLE 2.2: Sequences of mouse primers used for qPCR

Gene symbol		Sequence
IL1b	fwd	5'-TGCCACCTTTTGACAGTGATG-3'
	rev	5'-TGATGTGCTGCTGCGAGATT-3'
iNOS	fwd	5'-ACATCGACCCGTCCACAGTAT-3'
	rev	5'-CAGAGGGGTAGGCTTGTCTC-3'

---

[3]http://www.ncbi.nlm.nih.gov/tools/primer-blast/
[4]http://www.eurogentec.com/eu-home.html

TABLE 2.2: (continued)

Gene symbol		Sequence
L27	fwd	5'-ACATTGACGATGGCACCTC-3'
	rev	5'-GCTTGGCGATCTTCTTCTTG-3'
TNFa	fwd	5'-GGTTCTGTCCCTTTCACTCAC-3'
	rev	5'-TGCCTCTTCTGCCAGTTCC-3'

TABLE 2.3: Run protocol for qPCR on the LightCycler 480

Step	Temperature	Duration	Repetition
Denaturation	95 °C	5 min	
Amplification	95 °C	30 sec	
	60 °C	30 sec	x 45
	72 °C	30 sec	
Melting curve	95 °C	15 sec	
	40 °C	90 sec	
	95 °C	continuous	
Cooling	40 °C	30 min	

2.3.4   Western Blot

2.3.5   Protein extraction

Proteins were extracted using mammalian protein extraction reagent (M-PER) (Thermo Fischer Scientific, 78501) supplemented with cOmplete Mini EDTA-free protease inhibitor (Roche, 11836170001, 1 tablet diluted in 10 mL of M-PER). Cells in 6-well plates were extracted with 120 µL of M-PER-cOmplete and cells from 12-well plates were extracted with 60 µL. The extract was transferred to a tube and vortexed for 10 min at 4 °C and 1400 rpm on a Thermomixer (Eppendorf). The extract was centrifuged for 10 min at 4 °C and 16,000 x g. The supernatant was finally transferred to a new tube and the samples were stored at -80 °C. Before loading on a sodium dodecylsulfate-polyacrylamide gel electrophoresis (SDS-PAGE) gel, the samples were quantified using the spectrophotometer Nanodrop 2000C UV-V15 (Thermo).

2.3.5.1 SDS-PAGE

The protein extracts were denatured by dilution in self-made 5X Laemmli buffer and heated at 95 °C for 5 min. Then, 10 or 20 μg were loaded on self-made 10% acrylamide gels. The precision plus protein kaleidoscope standard (Bio-Rad, 161-0375) served as marker. Gels were run for 20 min at 90V, then at 120V until the Laemmli buffer reached the end of the gel.

2.3.5.2 Transfer

The proteins were transferred to a 0.45 μm polyvinylidene fluoride (PVDF) membrane (Merck Millipore, IPFL00010) at 80V for 1 h. The membranes were then blocked in 5% skim milk (Fluka, 70166) (w/v) for 1 h at room temperature or overnight at 4 °C.

2.3.5.3 Antibodies and detection

The list of antibodies and their respective dilutions can be found in table 2.4.

TABLE 2.4: Antibodies and dilution used.

	Antibody	Supplier	Dilution
Primary	mouse anti-TH	Millipore MAB318	1:5000 in 5% Milk
	rabbit anti-DDC	Cell Signaling 13531	1:1000 in 5% BSA
	mouse anti-V5 HRP	Invitrogen 46-0708	1:5000 in 5% Milk
	mouse anti-GAPDH HRP	Sigma G9295-25UL	1:1000 in 5% Milk
	mouse anti-beta actin	Sigma A5451	1:3000 in 5% Milk
Secondary	anti-mouse HRP	Cell Signaling 7076P2	1:10.000 in 5% Milk
	anti-rabbit HRP	Cell Signaling 7074P2	1:10.000 in 5% Milk

Antibodies were incubated for 1 h at room temperature or overnight at 4 °C. They were diluted either in 5% skim milk or in 5% bovine serum albumine (BSA) (VWR, A6588,0100), following the recommendation from the antibodies provider. After incubation with primary antibodies, the membranes were washed three times for 5 min with TBS-Tween. Then the secondary antibody was added and the membranes were incubated for 1 h at room temperature or overnight at 4 °C. After three additional washing steps, detection was done using the Odyssey Fc Imager (LI-COR), the standard was detected at 700 nm for 30 sec and the horseradish peroxidase (HRP)-conjugated antibodies were detected with the chemiluminescence channel for 10 min, after a 1-min

incubation in self-made pCA-ECL detection reagent. Data were analysed using Image Studio software (LI-COR).

2.4   Cell viability assay

Cell viability was assayed using resazurin (Sigma Aldrich, R7017). Resazurin, a blue and non-fluorescent dye, can be reduced to resorufin, which is pink and fluorescent, proportionally to the cell density [136]. Stock solutions of 1 mg/mL were prepared, filtered with a 0.22 µm filter and stored at 4 °C protected from light. Cells were then treated for 1 h with a final concentration of 5 µg/mL. Fluorescence was measured with excitation wavelength of 570 nm and emission wavelength of 590 nm using Synergy Mx microplate reader (BIOTEK).

2.5   Cloning

The plasmids used for cloning were purchased from Harvard Medical School Plasmid[5]. Plasmids used:

- THox: clone HsCD00378692

- Aromatic amino acid decarboxylase (AADC)ox: clone HsCD00003768.

2.5.1   Bacterial growth

All bacterial plasmid amplifications were carried using the One Shot® MAX Efficiency® DH5α™-T1® competent cells (Invitrogen, 12297016). Culture plates were prepared with LB agar (Sigma, L2897) and supplemented with the corresponding antibiotic. Liquid cultures were carried out in LB broth (Sigma L3022) supplemented with antibiotics. A single colony was picked from the plate and transferred to 5 mL culture for minimum 10 hours before being transferred to 200 mL liquid culture for an overnight incubation. Liquid cultures were incubated at 37 °C with constant shaking (200rpm). Liquid cultures were incubated at the same temperature with constant shaking (200rpm). Before purification of the plasmids by maxiprep, glycerol stocks were made: 700 µL of bacteria were mixed with 300 µL of glycerol (Sigma Aldrich, G6279) and stored at -80 °C.

---

[5]`https://plasmid.med.harvard.edu/PLASMID/Home.xhtml`

2.5.1.1 Transformation

25 µL of DH5α™ bacteria were transformed with 1 µL of plasmid and incubated on ice for 30 min. Heat shock was performed for 30 sec at 42 °C. 125 µL of SOC medium (Invitrogen, PIN 46-0700) were then added and the bacteria were incubated for 1 h at 37 °C with constant shaking (900rpm). 100 µL of the transformation were plated on agar plates and incubated overnight at 37 °C.

2.5.1.2 Plasmid purification

Plasmids were purified using the NucleoBond Xtra Midi/Maxi kit[6] (Macherey Nagel, 740414.50) following manufacturer's instructions. Plasmids were reconstituted in 400 µL water.

2.5.2 Gateway cloning

2.5.2.1 Attachment sites addition

For the AADC plasmid that was not compatible with the Gateway system, *attB* sites needed to be added to the gene of interest. This was done by PCR. The run protocol can be found in table 2.5. A description of the master mix follows.

TABLE 2.5: Run protocol for to attach *attB* sites

Step	Temperature	Duration	Repetition
Denaturation	95 °C	3 min	
Amplification	95 °C	30 sec	
	60 °C	45 sec	x 45
	68 °C	1 min 30 sec	
Final elongation	68 °C	10 min	
	10 °C	pause	

A master mix was prepared containing 2.5 µL of 10X *Pfx* AccuPrime™ Reaction mix (Invitrogen, 55013), 0.5 µL of AccuPrime™ *Pfx* DNA Polymerase (Invitrogen, 12344-02A), 0.5 µL of 50 mM MgSO$_4$, 0.5 µL of DNA template diluted 1:200, 1.5 µL of 10 µM attB1 primer (5'-GGG GAC AAG TTT GTA CAA AAA AGC AGG CTG GAT

---

[6] http://www.mn-net.com/ProductsBioanalysis/DNAandRNApurification/ PlasmidDNApurificationeasyfastreliable/NucleoBondXtraplasmidMidiprepMaxiprepkits/ tabid/1479/language/en-US/Default.aspx

GAA CGC AAG TGA ATT CCGA-3'), 1.5 μL of 10 μM attB2 primer (5'-GGG GAC CAC TTT GTA CAA GAA AGC TGG GTA CAA CTC CCT CTC TGC TCGC-3') and 18 μL of water.

2.5.2.2   PCR product isolation and purification

PCR products were isolated by agarose gel. 0.8 % agarose (Sigma Aldrich, A9539) gel containing 1:10.000 SYBR®Safe DNA Gel Stain (Thermo Fisher, S33102) (v:v, i.e: 5 μL in 50 mL) was prepared. The 20 μL of PCR products were mixed with 4 μL of 6X MassRuler DNA Loading Dye (Thermo Fisher, R0621). The mix was loaded on the gel together with GeneRuler 1kb Plus DNA Ladder (Thermo Fisher, SM1331). The gel was run 1 h at 100 V in Tris-acetate-EDTA (TAE) buffer. A picture of the gel was taken using UV light and the PCR product was cut out of the gel. The DNA was then purified using the QIAquick Gel Extraction Kit[7] (Quiagen, 28704) following the manufacturer's instructions. The DNA was eluted in 20 μL of water and the samples were stored at -20 °C.

2.5.2.3   BP reaction

BP reaction was performed using an *attB*-flanked DNA fragment and an *attP*-containing donor vector (pDONR207) to generate an *attL*-containing entry vector.
In a microcentrifuge tube, the reaction was started by mixing 1 μL to 7 μL of attB-PCR product (15-150 ng), 1 μL of pDONR207 (150 ng/μL) and TE buffer pH 8 up to 8 μL. Then, 2 μL of Gateway ® BP clonase™II Enzyme mix (Invitrogen, 56481) were added and the reaction was incubated for 1 h at 25 °C. The reaction was terminated by adding 1 μL of proteinase K (Invitrogen, 59895) and incubated for 10 min at 37 °C. The product was amplified using *E.coli* DH5α and purified by maxiprep.

2.5.2.4   LR reaction

LR reaction was performed using an *attL*-containing entry clone and an *attR*-containing destination vector to generate an expression vector.
In a microcentrifuge tube, reaction was started by mixing 1 μL to 7 μL of entry clone (15-150 ng), 1 μL of pLenti6.3/TO/V5-DEST or pLenti6/UbC/V5-DEST (150 ng/μL) and TE buffer pH 8 up to 8 μL. Then, 2 μL of Gateway ® LR clonase™II Enzyme mix (Invitrogen, 56484) were added and the reaction was incubated for 1 h at 25 °C.

---

[7]https://www.qiagen.com/us/shop/sample-technologies/dna/dna-clean-up/qiaquick-gel-extraction-kit

The reaction was terminated by adding 1 μL of proteinase K (Invitrogen, 59895) and incubating for 10 min at 37 °C.

The maps for the pDONR207, pLenti6.3/TO/V5-DEST and pLenti6/UbC/V5-DEST are available in Appendix B.

2.5.2.5 Sequencing

To ensure proper gene insertion, plasmids were sent to Eurofins Genomics[8]. Primers were designed to cover the plasmid before and after the attachment sites. The primers used for the sequencing can be found in table 2.6

TABLE 2.6: Sequences of the mouse primers used for qPCR

Gene symbol	Position		Sequence
	plamsid	fwd	5′-CGCGTTAACGCTAGCATGGA-3′
DDC	on gene	fwd	5′-GCTCACACAGGCCGCTATCA-3′
	on plasmid	rev	5′-ATTTTGAGACACGGGCCAGA-3′
	plamsid	fwd	5′- CGACGGCCAGTCTTAAGCTCG-3′
TH	on gene	fwd	5′-GTGATGACACTTGTCCAGCTCTG-3′
	on plasmid	rev	5′- GAGCTGCCAGGAAACAGCTATG-3′

2.5.3 Virus production

Viruses were produced using the ViraPower™Lentiviral Gateway® Expression kit[9] (Thermo Fisher, K4960-00) using the reverse transfection procedure following manufacturer's instruction in a volume of 10 mL. After filtration with a 0.45 μm cellulose acetate membrane filter (VWR International, 28145-481), the viruses were concentrated. First, 1/5 of the final volume of 40% poly-ethylene glycol (PEG)10.000 (Fluka, 81280) was added to the filtered viruses and incubated overnight. Then, the samples were centrifuged for 30 min at 1500 x g, 4 °C. The supernatant was discarded and the samples were centrifuged once again for 5 min at the same speed and temperature. The remaining supernatant was discarded and the viruses were resuspended in 100 μL of PBS, aliquoted by 10 μL and stored at -80 °C.

---

[8]https://eurofinsgenomics.eu/?countryCode=LU
[9]https://www.thermofisher.com/order/catalog/product/K497500

2.5.4   Cell transduction

For viral transduction, cells were seeded in a 12-well plate at the density of 50.000 cells per well. 10 µL of virus were added to the cells at the same time. On the next day, cell culture media were exchanged. Two days later, the antibiotic selection was started.

2.5.5   Antibiotic selection

pLenti6.3/TO/V5-DEST and pLenti6/UbC/V5-DEST carry a blasticidine resistance gene. To assess the concentration needed for selection, 50.000 cells were seeded per well in a 24-well plate. On the next day, blasticidin was applied with a concentration range from 0 to 5 µg/mL. The concentration that kills the cells within 5 days was used. For the LUHMES cells, this corresponds to 2 µg/mL.

2.6   Metabolite extraction and measurements

2.6.1   Stable isotope labeled compounds

TABLE 2.7: Stable isotope labeled compounds and internal standards used

Tracer	Supplier
U-^{13}C$_6$ D-Glucose	Cambridge Isotope Laboratories, CLM-2250-0,25
1,2-^{13}C$_2$ D-Glucose	Sigma Aldrich, 453188
U-^{13}C$_5$ L-Glutamine	Cambridge Isotope Laboratories,CS01-183-434
U-^{13}C$_9$ L-Phenylalanine	Cambridge Isotope Laboratories,CLM-2250-0,25
U-^{13}C$_3$ Sodium pyruvate	Cambridge Isotope Laboratories, CLM-2440-0,5
U-^{13}C$_9$ L-Tyrosine	Cambridge Isotope Laboratories, CLM-2263-0,1
Internal Standard	**Supplier**
Pentanedioic D$_6$ acid	CDN Isotopes, D-5227
2-(3,4-dihydroxyphenyl)ethyl-1,1,2,2-D$_4$-amine HCl	CDN Isotopes, D1540
U-^{13}C$_5$ Ribitol	Omiron Biochemicl Inc., ALD062
2-Ethylbutyric acid	Sigma Aldrich, 109959

Advanced DMEM/F-12 for experiments using labeled glucose, glutamine or pyruvate was prepared in house, omitting these metabolites [10]. Glucose, glutamine and

---

[10]Formulation of the complete medium can be found here: `http://www.thermofisher.com/lu/en/home/technical-resources/media-formulation.227.html`

pyruvate were then supplemented at the concentrations of 17.5, 2 and 1 mM respectively, either as tracers or as unlabled compounds.

Advanced DMEM/F-12 for experiments using labeled phenylalanine and tyrosine was prepared in house, omitting these metabolites as well as glucose, glutamine and pyruvate. Glucose, glutamine and pyruvate were then supplemented at the concentrations of 17.5, 2 and 1 mM respectively as unlabled compounds. Labeled or unlabeled tyrosine and phenylalanine were supplemented at the concentrations of 213 and 215 µM respectively.

After adjustment of the pH to 7.4, all media were filtered with a 0.22 µm pore size filter and supplemented with necessary additives (depending on the cell lines).

2.6.2 Non-targeted approach

2.6.2.1 Metabolite extraction

Metabolites were extracted from 12-well plates. First, the cells were washed using room temperature 0.9% NaCl (Sigma Aldrich, S5886) solution (w:v), then metabolism was quenched with 200 µL of ice-cold methanol (Sigma Aldrich, 34860). The plate was transferred to an ice plate (CoolSink$^®$ XT 96F, Biocision) and 200 µL of 4 °C water containing 1 µg/mL pentanedioic D_6 acid were added. Cells were scraped and transferred to a reaction tube containing 200 µL of chloroform (Sigma Aldrich, 650498). Samples were vortexed for 20 min at 4 °C, 1400 rpm on a Thermomixer (Eppendorf). They were then centrifuged for 5 min at 4 °C, 16,000 x g. 150 µL of the upper phase were transferred to a 1.8 mL glass vial with 5-250 µL micro-insert (further referred to as GC glass vials) and dried in a refrigerated rotary vacuum evaporator (Labconco) at -4 °C. The samples were finally capped and stored at -80 °C until measurement. If the interphases were kept for RNA extraction, the rest of the upper phase as well as the lower phase were removed, methanol was added and the samples were centrifuged once more to pellet the interphases. Supernatant was removed and replaced with fresh methanol. Samples were transferred to -80 °C until further sample processing.

2.6.2.2   Sample derivatization

The dried samples were derivatized using a multipurpose sampler (Gerstel) for 1 hour at 40 °C under constant shaking using 15 µL pyridine (Sigma 270970) containing 20 µg/mL methoxyamine (Sigma Aldrich 226904). Then 15 µL N-methyl-N-(trimethylsilyl)trifluoroacetamide (MSTFA) (Macherey-Nagel 701270.110) were added for 30 min at 40 °C under constant shaking.

2.6.2.3   GC-MS measurement

Gas chromatography - mass spectrometry (GC-MS) analysis was performed using an Agilent 7890A GC equipped with a 30 m DB-35MS capillary column (Agilent 122-3832). The GC was connected to an Agilent 5975C mass selective detector operating under electron ionization (EI) at 70 eV. The MS source was held at 230 °C and the quadrupole at 150 °C. A sample volume of 1 µL was injected into a split/splitless inlet in splitless mode. Helium was used as carrier gas at a constant flow rate of 1 mL/min. The GC oven temperature was held on 80 °C for 6 min and increased to 300 °C at 6 °C/min. After 10 min, the temperature was increased to 325 °C at 10 °C/min for 4 min. The detector was operated in scan mode with a mass over charge ratio (m/z) of 70 to 800. The run time of one sample was 59 min.

2.6.3   Stable isotope-assisted metabolomics

2.6.3.1   Metabolite extraction

Metabolites were extracted following the same procedure as in section 2.6.2.1.

2.6.3.2   Sample derivatization

Sample that were incubated with tracers were derivatized for 90 min with methoxyamine at 55 °C, and silylation was performed with 15 µL N-tert-butyldimethylsilyl-N-methyltrifluoroacetamide (MTBSTFA) (Restek) for 1 hour at 55 °C under constant shaking.

2.6.3.3   GC-MS measurement

For samples incubated with a tracer and derivatized with MTBSTFA, the GC oven temperature was held on 100 °C for 2 min and increased to 300 °C at 10 °C /min and held at this temperature for 4 min. The run time of one sample was 26 min. Labeled

samples were measured in selected ion monitoring (SIM) mode, the fragment ions used are displayed in table 2.8. Data were acquired using the Agilent MassHunter Software.

TABLE 2.8: SIM method settings for TBDMS derivatives of intermediates of central carbon metabolism

Metabolite	Ions	Dwell time (ms)	Formula
Pyruvate	174-180	15	$C_6H_{12}O_3NSi$
Lactate	261-267	15	$C_{11}H_{25}O_3Si_2$
Alanine	260-266	15	$C_{11}H_{26}NO_2Si_2$
Glycine	246-252	15	$C_{10}H_{24}NO_2Si_2$
GABA	274-281	15	$C_{12}H_{28}NO_2Si_2$
Succinate	289-296	15	$C_{12}H_{25}O_4Si_2$
Fumarate	287-294	15	$C_{12}H_{23}O_4Si_2$
Pentanedioic D_6 acid	235,309,351	15	
Serine	390-396	15	$C_{17}H_{40}NO_3Si_3$
Methionine	320-328	10	$C_{13}H_{30}NO_2SSi_2$
α-Ketoglutarate	346-354	15	$C_{14}H_{28}NO_5Si_2$
Malate	419-426	15	$C_{18}H_{39}O_5Si_3$
Aspartate	418-425	15	$C_{18}H_{40}NO_4Si_3$
Cysteine	406-413	15	$C_{17}H_{40}NO_2SSi_3$
Glutamate	432-440	10	$C_{19}H_{42}NO_4Si_3$
Glutamine	431-439	10	$C_{19}H_{43}N_2O_3Si_3$
Citrate	591-600	10	$C_{26}H_{55}O_7Si_4$

2.6.4 Dopamine extraction

2.6.4.1 Metabolite extraction

Metabolites were extracted following the procedure as described in section 2.6.2.1, with slight adaptations. The water was replaced by 0.1 M HCl and the internal standard was replaced by 0.5 μM 2-(3,4-dihydroxyphenyl)ethyl-1,1,2,2-D_4-amine HCl. 200 μL of the polar phase were transferred to GC glass vials.

This extraction procedure was also used upon labeling with [U-$^{13}C_9$]tyrosine and [U-$^{13}C_9$]phenylalanine.

2.6.4.2 Sample derivatization

The samples were derivatized following procedure described in section 2.6.2.2.

2.6.4.3 GC-MS measurement

Measurements were performed using the same temperature profile as in section 2.6.2.3. The samples were measured in SIM mode with the following target ions within the same measurement window: 176.1 and 430.2 for the internal standard and 174.1 and 426.2 for dopamine (DA) with dwell times of 20 ms.

Upon labeling with [U-^{13}C$_9$]tyrosine and [U-^{13}C$_9$]phenylalanine, samples were measured in SIM mode, the fragment ions used are displayed in table 2.9.

TABLE 2.9: SIM method settings for TMS derivatives of intermediates of central carbon metabolism

Metabolite	Ions	Dwell time (ms)	Formula
Phenylalanine	217-223	30	$C_{15}H_{17}NO_2Si_2$
Tyrosine	217-223	30	$C_{18}H_{35}NO_3Si_3$
Dopamine	425-437	15	$C_{20}H_{43}NO_2Si_4$

2.6.5 Medium extraction

Metabolites from medium were obtained from LUHMES cells cultivated in 400 μL of medium in 24-well plates. Control samples were prepared with the same volume of medium and incubated in wells without cells. The media were transferred to a reaction tube. The cells were washed once with PBS before trypsinization with 100 μL of trypsin. After 7 min of incubation, 400 μL of medium was added and two wells were pooled for cell counting using the Vi-CELL XR 2.03 (Beckman Coulter, Inc.).

The media were filtered with a 0.2 μm pore size 4 mm regenerated cellulose filter (Phenomenex, AF0-3203-52) to remove cells and cell debris. Quantification was performed using a calibration curve prepared in Advanced DMEM/F-12. It was supplemented with 8 mM L-Lactate (Sigma Aldrich, L7022) and 450 μM L-Glutamate (Sigma Aldrich, G8415) to obtain a final concentration of 500 μM L-Glutamate. Concentration in the original medium of L-Pyruvate was 1 mM, D-Glucose: 17.5 mM and L-Glutamine: 2 mM. The initial stock was diluted 1:2, 1:4, 1:8, 1:16 and 1:32 to obtain a five-point calibration curve.

2.6.5.1 Metabolite extraction for GC-MS measurement

20 μL of medium were extracted with 180 μL of extraction fluid composed of 5:1 methanol:water (v:v) containing 50 μg/mL of $^{13}C_5$ Ribitol and 20 μg/mL Pentanedioic D_6 acid. Samples were incubated for 10 min at 4 °C, 1400 rpm on a Thermomixer. They were then centrifuged for 5 min at 4 °C, 16,000 g. 50 μL were transferred to a GC glass vial dried in a refrigerated rotary vacuum evaporator at -4 °C.

2.6.5.2 Sample derivatization

Samples were derivatized following the procedure in section 2.6.3.2.

2.6.5.3 GC-MS measurement

Medium samples were derivatized with MTBSTFA and measured with a split ratio of 10:1. The GC oven temperature was held on 100 °C for 2 min and increased to 300 °C at 10 °C /min and held at this temperature for 4 min. The run time of one sample was 26 min. Samples were measured in SIM mode, the fragments ions are displayed in table 2.10.

TABLE 2.10: SIM method settings for TBDMS derivatives of metabolites extracted from cell culture medium

Metabolite	Quant ion	Qual ion	Qual ion	Dwell time (ms)	Formula
Pyruvate	174.1	89	115	50	$C_6H_{12}NO_3Si$
Lactate	261.1	189.1	233.1	50	$C_{11}H_{25}O_3Si_2$
Alanine	260.2	158.1	232.1	70	$C_{11}H_{26}NO_2Si_2$
Glycine	246.1	189.1	218.1	50	$C_{10}H_{24}NO_2Si_2$
Valine	288.6	186.1	260.2	70	$C_{13}H_{30}NO_2Si_2$
Leucine	302.2	200.2	274.2	70	$C_{14}H_{32}NO_2Si_2$
Isoleucine	302.2	200.2	274.2	70	$C_{14}H_{32}NO_2Si_2$
Threonine	290.2	159.1	303.2	50	$C_{12}H_{28}NO_3Si_2$
Proline	286.2	184.1	258.2	50	$C_{13}H_{28}NO_2Si_2$
Succinate	289.1	215.1	331.2	50	$C_{12}H_{25}O_4Si_2$
Pentanedioic D_6	309.2	235.2	351.3	70	
Phosphoric acid	383.2	425.1	440.2	50	$C_{14}H_{36}O_4PSi_3$
Serine	390.2	302.2	362.2	50	$C_{17}H_{40}NO_3Si_3$
Threonine	404.2	376.3	417.3	70	$C_{18}H_{42}NO_3Si_3$
Methionine	320.2	218.1	292.2	50	$C_{13}H_{30}NO_2SSi_2$

continued …

Metabolite	Quant ion	Qual ion	Qual ion	Dwell time (ms)	Formula
Malate	419.2	287.1	403.2	50	$C_{18}H_{39}O_5Si_3$
Phenylalanine	336.2	308.2		50	$C_{17}H_{30}NO_2Si_2$
Aspartate	418.2	316.2			$C_{18}H_{40}NO_4Si_3$
Cysteine	406.2	304.2	378.2	50	$C_{17}H_{40}NO_2SSi_3$
Ornithine	474.4	184.1	286.2	50	$C_{23}H_{54}N_2O_2Si_3$
Glutamate	432.3	330.2	404.3	50	$C_{19}H_{42}NO_4Si_3$
Lysine	431.3	300.2	488.4	70	$C_{20}H_{47}N_2O_2Si_3$
Glutamine	431.3	329.2	473.3	50	$C_{19}H_{43}N_2O_3Si_3$
Arginine	442,3	169.2	340.3	50	$C_{20}H_{44}N_3O_2Si_3$
Tyrosine	466.3	302.2	438.3	50	$C_{23}H_{44}NO_3Si_3$
Histidine	440.3	338.3	196.1	70	$C_{20}H_{42}N_3O_2Si_3$

2.6.5.4   Medium quantification using YSI Bioanalyzer

120 μL of filtered medium were loaded on a 96-well plate and measured with a 2950D Biochemistry Analyzer (YSI). Membranes for quantification of glucose (YSI, 2365), lactate (YIS, 2329), glutamine (YSI, 2735) and glutamate (YSI, 2754) were used. Quantification was performed using an external calibration curve prepared in the Advanced DMEM/F-12 containing 17.5 mM D-Glucose, 2 mM L-Glutamine, 500 μM L-Glutamate and 8 mM L-Lactate.

2.6.5.5   Determination of uptake and secretion rates

Uptake rates for glucose and glutamine as well as secretion rates for glutamate and lactate were calculated. First, concentrations in each sample were determined using an external calibration curve. Second, the concentration of metabolites obtained in media incubated without cells were subtracted from the samples in order to control for temperature-associated metabolite degradation. Third, this difference was divided by the respective cell number at the beginning of the experiment and by 24 h to obtain rates in mol/cell/hour.

2.6.6 Short chain fatty acid extraction

2.6.6.1 Metabolite extraction

Quantification of short chain fatty acid (SCFA) was performed using a volatile acid standard mix (Supelco, 46975-U). Each compound is present in the mix at the concentration of 10 mM. For extraction, the standard mix was diluted 1:10 to a final concentration of 1 mM. A calibration curve of concentrations 0, 0.2, 0.4, 0.6, 0.8 and 1 mM were used for extraction. 95 µL of filtered medium were transferred to a new tube. 5 µL of 200 mM 2-Ethylbutyric acid (internal standard), 5 µL of 1 M HCl and 500 µL of diethyl ether (VWR, 1.00921.1000) were added to each sample. Samples were vortexed for 10 min at room temperature, 1400 rpm on a Thermomixer. They were then centrifuged for 5 min at 4 °C, 16,000 x g. 450 µL were transferred to a new tube and 500 µL of diethyl ether were added a second time to the first tubes. Samples were vortexed for 10 min at room temperature, 1400 rpm. They were then centrifuged for 5 min at 4 °C, 16,000 x g and 450 µL were transferred to the second tube. 250 µL of the second reaction tube were transferred to a GC glass vial and the samples were derivatized by adding 25 µL of MTBSTFA and incubated for 1 h at room temperature before measurement.

2.6.6.2 GC-MS measurement

GC-MS analysis was performed using an Agilent 7890A GC equipped with a 20 m DB-1MS capillary column (Agilent, 121-0122). Samples were measured with a split ratio of 20:1. The GC oven temperature was held on 80 °C for 0.75 min and increased to 150 °C at 15 °C /min and held at this temperature for 2 min, then temperature was increased to 280 °C at 50 °C /min and held at this temperature for 2 min. The run time of one sample was 12 min. Samples were measured in SIM mode, the fragments used are displayed in table 2.11. The detector was switched off between 2.2 and 2.6 min, corresponding to the elution of MTBSTFA.

TABLE 2.11: SIM method settings for MTBSTFA derivatives of SCFA extracted from cell culture medium

Metabolite	Quant ion	Qual ion	Qual ion	Dwell time (ms)	Formula
Formate	103	75	99	20	$C_3H_7O_2Si$
Acetate	117	75	99	20	$C_4H_9O_2Si$
Propionate	131	75	115.1	20	$C_5H_{12}O_2Si$
Butyrate	145.1	75	115.1	20	$C_6H_{14}O_2Si$

TABLE 2.11: (continued)

Metabolite	Quant ion	Qual ion	Qual ion	Dwell time (ms)	Formula
Isobutyrate	145.1	75	115.1	20	$C_6H_{14}O_2Si$
Valerate	159.1	75	201.1	20	$C_7H_{16}O_2Si$
2-Ethylbutyrate	173.1	75	115.1	20	$C_8H_{18}O_2Si$
4-Methylvalerate	173.1	75	215.1	20	$C_8H_{18}O_2Si$
Hexanoate	173.1	75	131	20	$C_8H_{18}O_2Si$
Heptanoate	187.1	75	131	20	$C_9H_{20}O_2Si$
Lactate	261.1	233.1	189.1	20	$C_{11}H_{25}O_3Si_2$
Succinate	289.1	331.2	331.2	20	$C_{12}H_{25}O_4Si_2$

2.6.7   Limit of detection calculation

Limit of detection (LOD) of DA was determined following the procedure described by Wells *et al.* [125]. Briefly, a concentration curve of fresh DA was measured to determine which concentration of DA would give a signal between 5 and 10 times above background signal for ion 426.2. This concentration was 4.63 ng/mL. Then, a fresh solution of DA with this concentration was prepared and 200 μL were transferred to an eppendorf tube and dried under vacuum at -4 °C. The sample was derivatized for 90 min with 150 μL of 20 mg/mL methoxyamine dissolved in pyridine followed by a 30-min derivatization with MSTFA. Finally, 30 μL of sample were aliquoted in 8 GC glass vials and measured in SIM mode as described in section 2.6.4.3.

The LOD was calculated using the following formula:

$$\frac{t_\alpha \times S_{\bar{X}} \times A}{\bar{X}}$$

Where t_α is 2.998, equivalent to the test statistic for 7 degrees of freedom and a 99% confidence interval. $\bar{X}$ and $S_{\bar{X}}$ are the average and standard deviation of the eight peak areas, respectively. A is the concentration of standard in the vial (1.19 ng/mL).

2.6.8 Data analysis

Acquired data were processed using the MetaboliteDetector [137] software package. Deconvolution settings for SCAN and SIM measurement are displayed in Table **2.12**. Setting for batch quantification and mass isotopomer distribution (MID) calculations are displayed in Table **2.13**.

TABLE 2.12: Deconvolution settings for SCAN and SIM measurement

Settings	SCAN	SIM
Peak Threshold	5	1
Mininum Peak Height	5	1
Bins/Scan	10	10
Deconvolution width	5	7

TABLE 2.13: Batch quantification and MID settings for SCAN and SIM measurement

Settings	*Batch quantification*		*MID calculation*
	Non-targeted	**SIM medium DA, SCFA**	**SIM TCA**
Δ RI	50	3	3
Pure/Impure	0.50	0.50	0.50
Scoring Method	RI + Seq	RI + Seq	RI + Seq
Req. score	0.85	0.85	0.60
Compound Reproducibility	0.75	1	1
Req S/N	0.0	0.0	0.0
Max. peak discr. index	100	100	100
Min. # ions	15	1	1

The data can be visualized by integrating the carbon contributions from each tracer in the metabolites of interest. This is a weighted average of the MIDs calculated as follows:

$$\frac{1}{n} \times \sum_{i=1}^{n} M_i \times i$$

Where n is the number of carbon atoms of the molecule and M_i is the ith mass isotopomer.

2.7   Statistics

Experiments were performed in biological triplicates. Each replicate contained technical triplicates. The data displayed in this work display a representative experiment. Figures were created using LibreOffice Calc, QtiPlot and Inkscape. Statistical analysis were performed using LibreOffice Calc and the R statistical environment [138].

3

<div style="background:#d9d9d9">

Results and discussion

</div>

This chapter is divided in two sections which correspond to the main research projects I participated in | . The first section focuses on the effects of 2,3-dihydroxy-L-phenylalanine (L-DOPA) on the metabolism of tyrosine hydroxylase (TH)-positive neuronal cells, LUHMES. First of all, we assayed cell viability to assess the sensitivity of neuronal cells against L-DOPA and determined the rescuing effect of antioxidants. Furthermore, we compared its toxicity in neurons to that in cell lines of other cell types. Then, I performed a metabolic study of these neurons to evaluate their response to L-DOPA using non-targeted, targeted and stable isotope-assisted metabolomics.

In the second part of this work, I focused on the engineering of a human dopamine-producing cell system which is not of cancer origin. First, we performed a comparison of catecholamine (CA) metabolism in LUHMES cells with that in other models (induced pluripotent stem cells (iPSC) and SH-SY5Y) to evaluate the strengths and weaknesses of the LUHMES cell model. Second, we used a genome-engineering approach to increase catecholamine-related gene expression.

3.1 Effects of L-DOPA on the metabolism of TH-positive neurons

3.1.1 The effects of L-DOPA on cell viability

Although it is the most widely used treatment for Parkinson's disease (PD), L-DOPA has been shown to be toxic *in vitro* [53, 107, 139–142]. Dopaminergic neurons are the most sensitive cells, but other cell types such as melanoma cells [140] were sensitive to high L-DOPA concentrations (500 μM), while fibroblasts or ovarian cancer cells [142]

died upon long term L-DOPA treatment at lower concentrations (10 μM for 6 days). In order to compare the response to L-DOPA in different cell types, we performed a cell viability assay for different concentrations in a 24 h-treatment (Figure **3.1**). The two first assays (Figure **3.1** A and B) were performed with the support of Xiangyi Dong and Jenny Ghelfi. In the first assay (Figure **3.1** A), we compared the effects of L-DOPA on three cells lines derived from neuronal cells and one human cell line which was not derived from the central nervous system (CNS): rat PC-12 pheochromocytoma cells, human SH-SY5Y neuroblastoma cells, human LUHMES immortalized mesencephalon cells and human A549 lung cancer cells. Overall, the LUHMES cells were the most sensitive to the treatment and the viability already dropped at 25 μM. It should be noted that LUHMES cells are the only cell type studied which is in a cell cycle arrest state. The three other cell types are of cancer origin and are proliferative. At 200 μM L-DOPA, SH-SY5Y cells started to be affected and their viability dropped to 20%, the same level as LUHMES cells. A549 were sensitive to 100 μM and higher concentrations of L-DOPA, with a drop in viability to 50%, but their viability did not further decrease for higher concentrations. PC-12 cells were not affected at all by the applied concentrations of L-DOPA. At this stage, we could not rule out an organism-specific effect of L-DOPA in which human-derived cells would be more sensitive than cells derived from other organisms.

In order to test other cell types of CNS origin, the same assay was performed with mouse IMA2.1 immortalized astrocytes, mouse BV2 immortalized microglia and human CCF-STTG1 astrocytoma cells (Figure **3.1** B). LUHMES cells were plotted again for comparison. We observed that IMA2.1 and BV2 cells were sensitive to high (250 μM) concentrations of L-DOPA and that CFF-STTG1 were not sensitive to the applied L-DOPA treatment.

L-DOPA quickly auto-oxidizes in cell culture media. The auto-oxidation pathway involves generation of free radicals and mixtures of quinones and semi-quinones [140, 143]. Antioxidants have been shown to protect cells against oxidation products of L-DOPA [107]. Their mechanism of action was described in section 1.4.2.4. I tested whether providing LUHMES cells with antioxidants would prevent L-DOPA toxicity. Ascorbic acid (AA) and reduced L-glutathione (GSH) were tested as well as N-acetyl-L-cysteine (NAC). Unlike GSH, NAC passively enters the cells where it is cleaved to generate cysteine, which can then be used for GSH synthesis [109]. Figure **3.1** C shows that all three antioxidants tested rescued cell viability upon L-DOPA treatment.
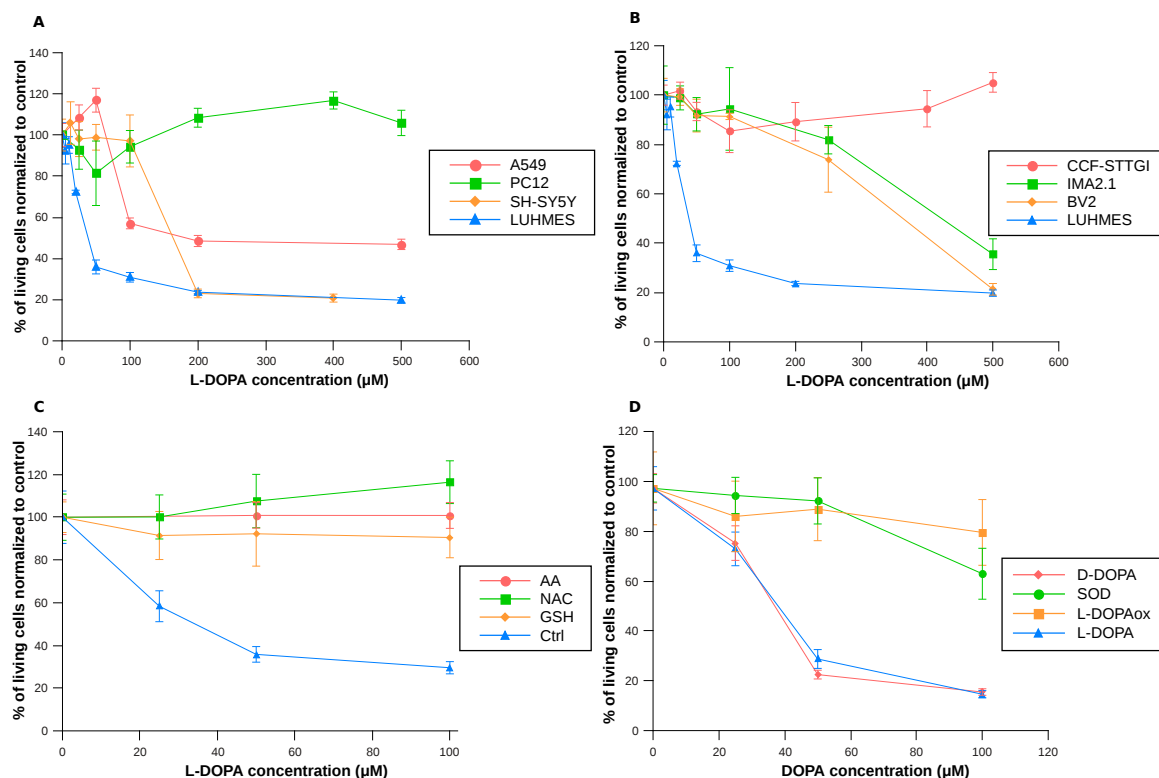
FIGURE 3.1: **Cell viability upon L-DOPA treatment. (A)**: Human A549 lung cancer, rat PC-12 pheochromocytoma, human SH-SY5Y neuroblastoma and human LUHMES immortalized mesencephalon cells were treated for 24 h with different L-DOPA concentrations. **(B)**: Human CCF-STTG1 astrocytoma, mouse IMA2.1 immortalized astrocytes, mouse BV2 immortalized microglia and human LUHMES immortalized mesencephalon cells were treated for 24 h with different L-DOPA concentrations. **(C)**: LUHMES cells were treated for 24 h with different concentrations of L-DOPA and 1 mM of ascorbic acid **(AA)**, N-acetyl-L-cysteine **(NAC)** or L-glutathione reduced **(GSH)**. (**D**): LUHMES cells were treated for 24 h with different concentrations of L-DOPA, D-DOPA, L-DOPA previously oxidized for 7 days (**DOPAox**) or L-DOPA supplemented with 500 units per mL of superoxide dismutase **(SOD)**.

Impaired serine metabolism has also been associated with decreased GSH levels in the cell: loss of DJ-1 in LUHMES cells induced a decrease in serine synthesis from glycolysis and an increase in serine uptake from the extracellular space. It also induced an increase in glutathione disulfide (GSSG) to GSH ratio, indicative of impaired GSH regeneration or increased reactive oxygen species (ROS).Therefore, serine was proposed to be used for transsulfuration to cysteine which can then be used for GSH synthesis [144][1].

I performed a final assay to ensure that the observed toxicity is mediated by intermediates of L-DOPA auto-oxidation in the extracellular space and not via its intracellular enzymatic degradation. Therefore, I incubated LUHMES cells in the presence of

---

[1]More details on this subject in the manuscript I co-authored in Appendix D

superoxide dismutase (SOD), 3,4-dihydroxy-D-phenylalanine (D-DOPA) or L-DOPA oxidized for seven days. First, L-DOPA was incubated with SOD, an enzyme responsible for superoxide detoxification (Figure **3.1** D). The presence of this enzyme rescued the cell loss induced by L-DOPA. In this case, the protection was entirely at the extracellular level since SOD cannot cross the cell membrane as such [145]. Secondly, replacing L-DOPA by its stereoisomer D-DOPA did not modify the cell viability pattern. D-DOPA auto-oxidizes in a similar fashion than L-DOPA and Shindo *et al.* reported that it cannot be enzymatically metabolized [146]. In this publication, they studied the transport and metabolism of D- and L-DOPA in rat intestine. Upon treatment of the animals with radio isotopically labeled D-DOPA, they could not observe any labeled dopamine (DA), 3-methoxytyramine (3-MT), nor 3,4-dihydroxyphenylacetic acid (DOPAC) (products of the activity of aromatic amino acid decarboxylase (AADC), catechol-o-methyl transferase (COMT) and aldehyde dehydrogenase (ALDH), respectively). These three metabolites could all be detected upon L-DOPA stimulation [146]. Finally, viability of cells was not affected when I treated them with L-DOPA that was left to oxidize for seven days prior to supplementation to the cells, indicating that the final products of the oxidation pathway are not toxic.

Further evidence points to an extracellular effect of L-DOPA oxidation independent of DA synthesis. Basma *et al.* reported that L-DOPA is toxic to PC-12 in culture due to its auto-oxidation, independently of DA formation since addition of carbidopa, an inhibitor of AADC, did not affect cell viability. On the other hand, toxicity was not mediated by enzymatically generated oxidative products of DA metabolism since inhibition of both isoforms of monoamine oxidase (MAO) (MAO-A and -B) by pargyline did not change cell viability. Cytotoxicity was decreased by supplementation of catalase and SOD indicating that the toxicity comes from auto-oxidation products of L-DOPA [139].

In summary, we demonstrated that LUHMES cells are the most sensitive to L-DOPA treatment among all cell lines tested. Moreover, we showed that the toxicity generated by L-DOPA treatment could be prevented by using antioxidants. Neurons possess less antioxidant capacity than astrocytes [110] and microglia [147] and thus are more sensitive to oxidative stress [110]. Given the fact that antioxidant levels are already decreased in PD patients [117], they have been suggested as potential co-drugs before [148] or during L-DOPA treatment [149].

The higher resistance against L-DOPA in BV2 and IMA2.1 cell lines can be explained by the increased antioxidant capacities of astrocytes and microglia. The other cell lines, A549, PC-12, SH-SY5Y and CFF-STCG1 are of various cancer origin, thus are prone to proliferation. It has been reported by Miller *et al.* that the expression of the oncogene *ras* induces oxidative stress resistance without involving the GSH pathway [150], indicating that cancer cells are able to adapt to stress conditions.

Finally, the toxic effects induced by L-DOPA treatment were due to its auto-oxidation which could be prevented by SOD, AA, GSH and NAC. We demonstrated that this process mainly occurred in the extracellular space, by the use of D-DOPA as negative control [146]. Eumelanin itself, as final product of the oxidation pathway of L-DOPA was not toxic to the cells.

3.1.2 The effects of L-DOPA on the metabolism of LUHMES cells

After evaluating the effects of L-DOPA on the viability of human TH-positive neurons LUHMES, I investigated the effects of L-DOPA on the metabolism of these neurons, focusing primarily on the central carbon metabolism.

3.1.2.1 Non-targeted metabolomics approach

It has been reported that the concentration of L-DOPA in the plasma of PD patients under treatment ranges between 5 and 50 μM [151]. Therefore, in this section, I used concentrations ranging from 0 to 100 μM. LUHMES cells were treated for 24 h with 0, 25, 50 or 100 μM of L-DOPA before quenching of metabolism and metabolite extraction. Significantly altered metabolites (one-way ANOVA, p-value < 0.05) are displayed in Figure **3.2**. This heatmap shows profound changes in the levels of many metabolites. L-DOPA treatment induced increased levels of essential amino acids such as valine, leucine, isoleucine, phenylalanine and lysine (Figure **3.3** A-E) and decreased levels of non-essential amino acids such as alanine, serine and glycine (Figure **3.3** F-H). Another interesting compound in the context of neuronal cells is N-acetyl-aspartate (NAA), which levels decreased (Figure **3.3** I). The levels of tricarboxylic acid (TCA) cycle intermediates, citrate, glutamate, fumarate, malate and aspartate decreased with increasing L-DOPA concentrations, while the level of succinate increased upon treatment (Figure **3.4** B-G). Citrate and succinate are not included in the heatmap (Figure **3.2**) because these data were obtained using a targeted metabolomics approach.
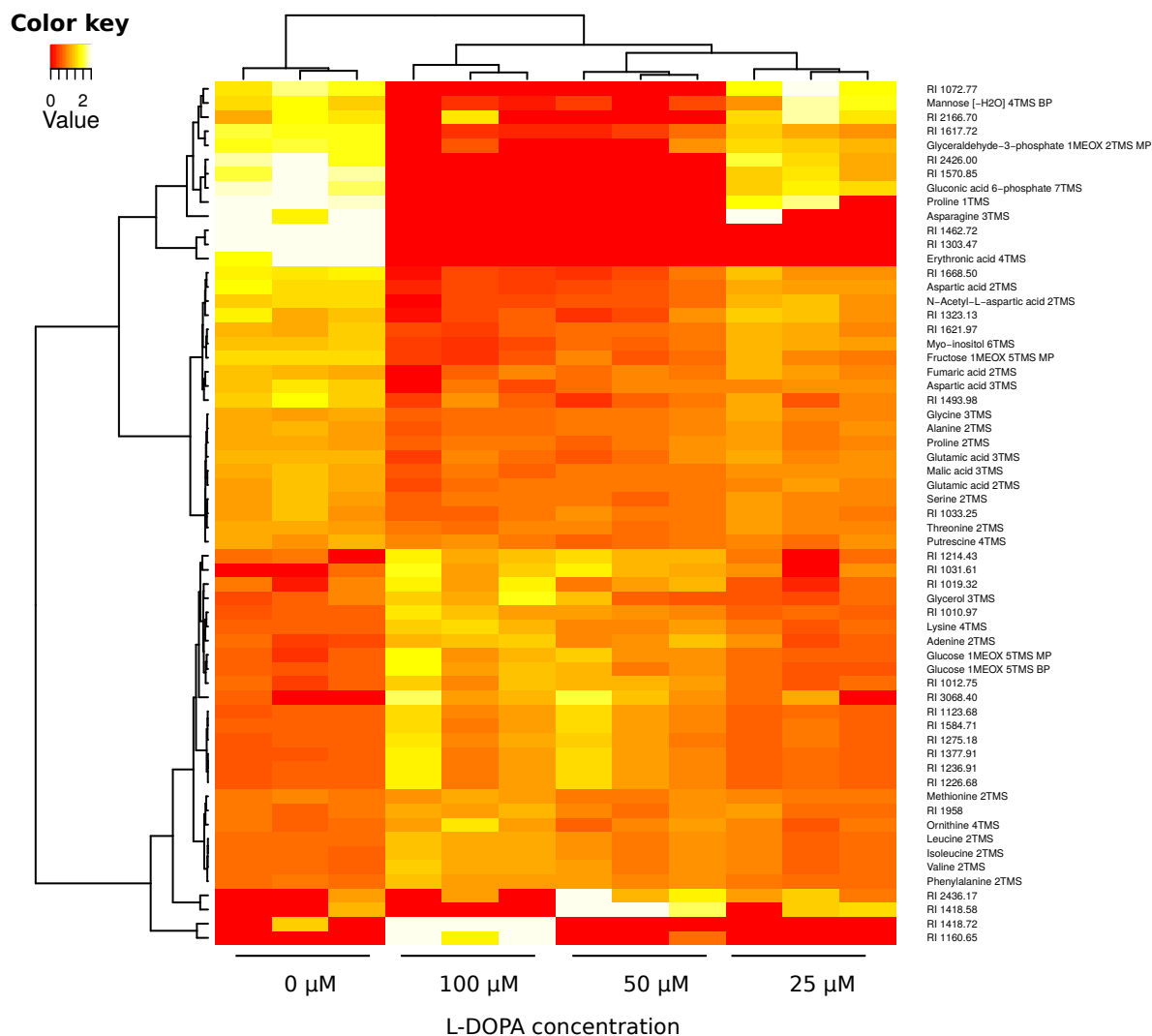
FIGURE 3.2: **Effects of L-DOPA treatment on the metabolism of LUHMES cells.** LUHMES cells were treated for 24 h with 0, 25, 50 or 100 µM L-DOPA. This heatmap displays the metabolites that show a significance level below 0.05 by one-way ANOVA. Signal intensities were normalized using the summed sample signal and row mean.

The increase of free essential amino acids could indicate a decrease in protein synthesis. In opposite, I observed a significant decrease of serine, glycine and alanine levels, which are non-essential amino acids synthesized from glycolytic intermediates. Most of the intermediates of the TCA cycle showed lower abundance upon L-DOPA treatments, except for succinate, which increased. Interestingly, increased succinate levels have been associated with succinate dehydrogenase (SDH) inhibition, which acts as complex II of the mitochondrial electron transport chain [152].
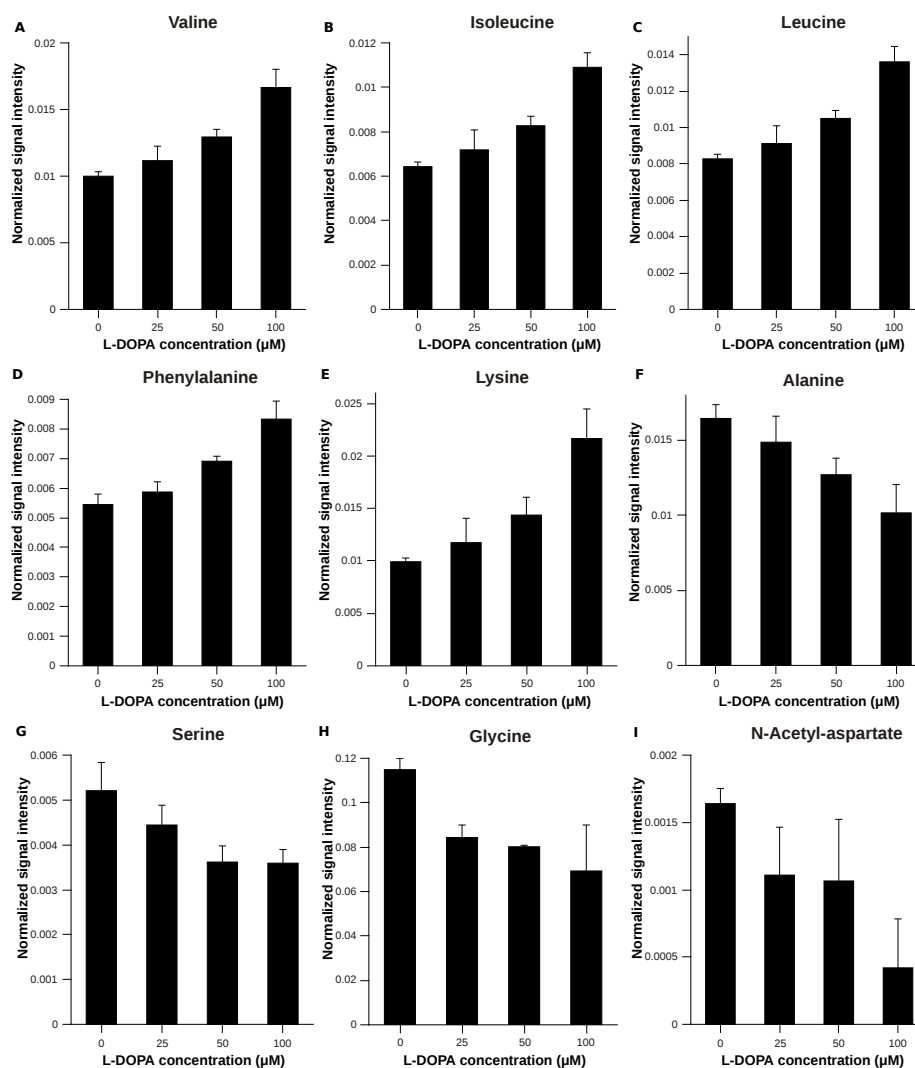
FIGURE 3.3: **Effects of L-DOPA treatment on the levels of amino acids.** LUHMES cells were treated for 24 h with 0, 25, 50 or 100 μM L-DOPA. Levels of valine **(A)**, isoleucine **(B)**, leucine **(C)**, phenylalanine **(D)**, lysine **(E)**, alanine **(F)**, serine **(G)**, glycine **(H)** and N-acetyl-aspartate **(I)** are displayed. Signal intensities were normalized using the sum sample signal normalization. All changes were significant by one-way ANOVA, p-value <0.05.

In cancer, inhibition of SDH leads to accumulation of succinate which can stabilize hypoxia-inducible factor (HIF)-1α expression by inhibiting prolyl hydroxylase (PHD) through a product inhibition feedback. Stabilization of HIF-1α leads to its translocation to the nucleus where it promotes expression of tumor survival-associated genes [152]. On the other hand, inhibition of SDH decreases the activity of coenzyme Q10, which can act as antioxidant by scavenging ROS. Upon inactivation of coenzyme Q10 and increased ROS levels, p53 is activated and has two major impacts on central carbon metabolism. First, it leads to the activation of the glycolysis inhibiting gene TP53-induced
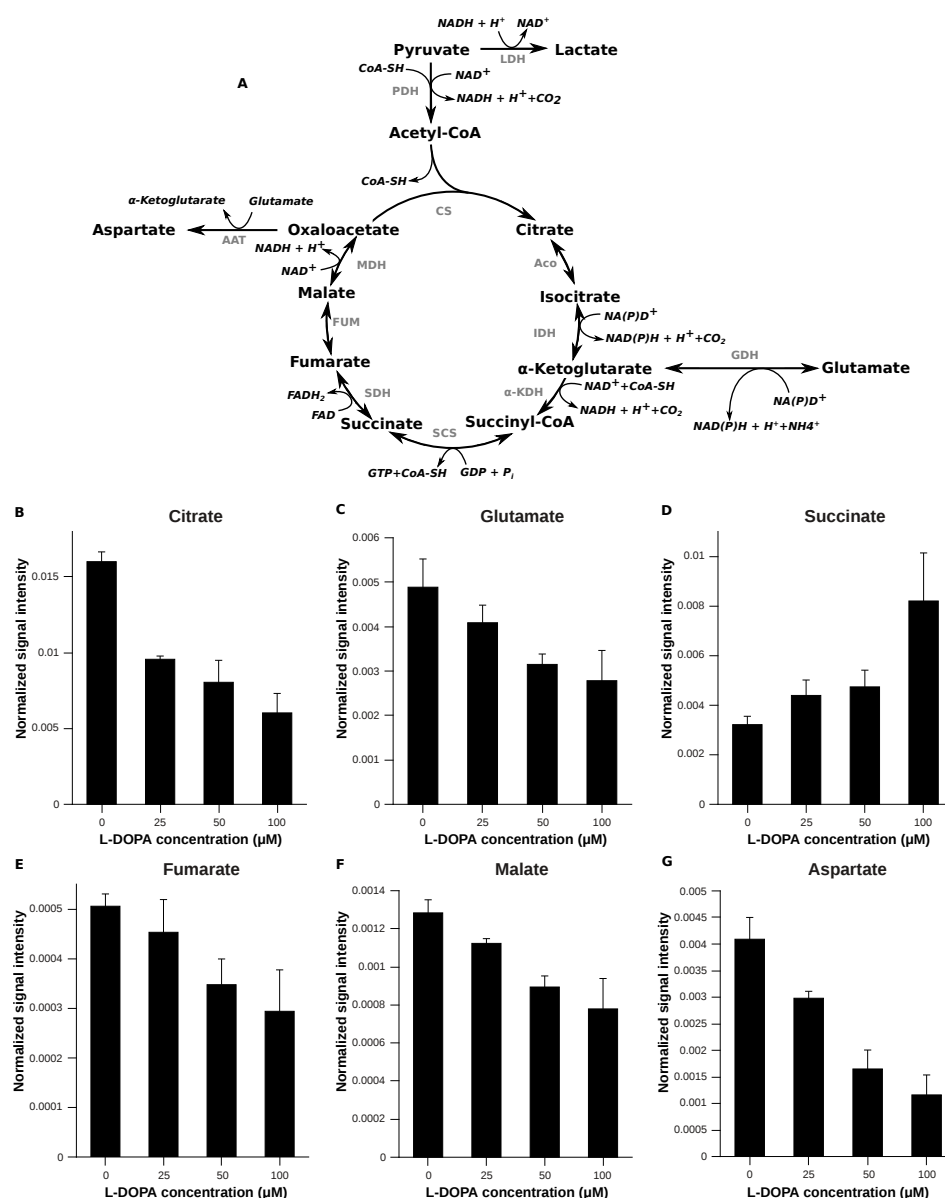
FIGURE 3.4: **Effects of L-DOPA treatment on the levels of intermediates of the TCA cycle and associated metabolites. (A)**: Scheme of the TCA cycle. LUHMES cells were treated for 24 h with 0, 25, 50 or 100 μM L-DOPA. Levels of citrate **(B)**, glutamate **(C)**, succinate **(D)**, fumarate **(E)**, malate **(F)** and aspartate **(G)** are displayed. Signal intensities were normalized using the sum sample signal normalization. **LDH**: lactate dehydrogenase, **PDH**: pyruvate dehydrogenase complex, **CS**: citrate synthase, **Aco**: aconitase, **IDH**: isocitrate dehydrogenase, **GDH**: glutamate dehydrogenase, α**-KDH**: α-ketoglutarate dehydrogenase, **SCS**: succinyl-CoA synthetase, **SDH**: succinate dehydrogenase, **FUM**: fumarase, **MDH**: malate dehydrogenase, **AAT**: aspartate aminotransferase. All changes were significant by one-way ANOVA, p-value <0.05.

glycolysis regulator (TIGAR) by lowering the levels of fructose-2,6-biphosphate, a regulator of glycolysis [153]. Second, it leads to inhibition of oxidative phosphorylation by inducing gene expression of cytochrome c oxidase 2 (SCO2).

These events induce a decrease in glycolytic and oxidative phophorylation fluxes preventing tumor survival and progression. In the light of L-DOPA treatment, an activation of these enzymes in response to oxidative stress could explain the decrease in TCA cycle intermediates as well as glycolysis-derived amino acids.

Mutations or decreased activity of SDH have also been associated with several neurodegenerative diseases such as Leigh's syndrome, Huntington's disease or Down syndrome [152]. Huntington's disease is characterized by the death of striatal GABAergic neurons which causes a loss of coordination, dystonia and decline in cognitive functions [152]. Patients with Huntington's disease show decreased levels of SDHA and SDHB, two of the four subunits composing SDH. In addition, treatment of animals with specific complex II inhibitors such as 3-nitropropionic acid (3-NP) or malonate induced the same phenotype [152]. These two compounds have been shown to be cytotoxic *in vitro* and *in vivo*. 3-NP is an irreversible inhibitor while the action of malonate is reversible [154] and both compounds induce decreased ATP levels, increased glutamate secretion and oxidative damage [155]. The toxicity could be prevented by using antioxidants and free radical scavengers, preventing ROS accumulation downstream of the mitochondrial complex II inhibition [156]. In the case of L-DOPA treatment, it is interesting to note that, similar to complex II inhibition, succinate accumulated and the toxicity could be prevented by antioxidants. Moreover, as observed for complex II inhibition, I observed an increased glutamate secretion (see section 3.1.4).

Another important metabolite in the context of the CNS is NAA. It is synthesized from aspartate and acetyl-CoA by the N-acetylaspartate synthetase. Arun *et al.* reported that in SH-SY5Y, NAA can be synthesized in both the cytoplasm and the mitochondria with its majority being synthesized in the mitochondria [157]. In the CNS, it has several functions: 1) NAA is a precursor for N-acetylaspartylglutamate, the most concentrated neurotransmitter. 2) NAA has also been correlated to ATP levels and neuronal energy metabolism, although no direct connection between the two components has been found, 3) NAA is a source of acetate for fatty acid (such as myelin) and steroid synthesis in oligodendrocytes [158]. Demougeat *et al.* reported that upon 3-NP treatment, NAA levels decreased in the *striatum* before observation of any cell death and was associated with motor symptoms [159]. Treating rat striatal cells with the same compound, Lee *et al.* firstly observed an increased acetate level [160]. Three hours after the start of the treatment, they observed a decrease in acetate concentrations suggesting that it was used as acetyl donor for membrane repair in neuronal injuries [160]. 3-NP

caused a disruption of cell membranes leading to the release of NAA which could be hydrolyzed to acetate and aspartate. The toxin also induced an increase in free fatty acids which can be metabolized to acetate as well. Interestingly, L-DOPA treatment induced a degradation of the neurite network (suggesting a disruption of cell membranes) as well as an increase in acetate uptake (see section 3.1.4).

To summarize, I showed that L-DOPA treatment caused profound changes in the metabolic profile of LUHMES cells, demonstrated by a decrease in the levels of non-essential amino acids such as alanine, serine and glycine and an increase in the levels of essential amino acids such as valine, leucine, isoleucine, phenylalanine and lysine. This suggests a decreased protein synthesis. Levels of NAA also decreased. The levels of TCA cycle intermediates decreased, except for succinate which increased upon treatment. This indicates that auto-oxidation products of L-DOPA induced a complex II inhibition and lead to decreased glycolytic and TCA cycle activity.

3.1.2.2 Stable isotope-assisted metabolomics

Stable isotopes are a powerful tool in metabolomics and fluxomics studies. They allow to study the utilization of specific substrates by cells or organisms. In order to study the metabolic adaptations of LUHMES cells during L-DOPA treatment, I incubated these cells for 24 h with either [U-^{13}C$_6$]glucose, [U-^{13}C$_5$]glutamine or [U-^{13}C$_3$]pyruvate, the main carbon sources of these cells. To obtain a higher percentage of labeling, Advanced DMEM/F12 free of glucose-, glutamine- and pyruvate was prepared in-house. After incubation of the cells in the presence of the tracer, I extracted intracellular metabolites and measured the polar extracts in selected ion monitoring (SIM) mode to precisely determine mass isotopomer distributions (MIDs). For all experiments described in this section, I cultivated one million cells per well instead of five hundred thousand and increased L-DOPA concentrations to 200 μM. The increase in cell number allowed an increase in signal intensity for compounds of low abundance, such as citrate and succinate, and to better quantify medium uptake and secretion rates. Since LUHMES cells do not proliferate when they are differentiated, their substrate use is really low and precise quantification was not possible over the duration of the treatment with the original cell density. Increased cell number allowed to increase the amount of metabolites consumed and secreted, and thus lead to a more precise quantification. However, when the cells at this density were treated with 50 or 100 μL-DOPA, the morphological changes (neurite degradation) and apparition of

eumelanin in the medium did not occur any more. This is why the concentration of L-DOPA was increased for consistency.

Figure **3.5** depicts the relative carbon contributions from glucose, glutamine and pyruvate to the glycolysis-derived metabolites serine, glycine, alanine and lactate (Figure **3.5** A-D) as well as to the TCA cycle-derived metabolites citrate, succinate, malate and fumarate (Figure **3.5** E-H). "Other" represents other carbon sources that were not labeled by the applied tracers as, for example, carbon derived from protein degradation or β-oxidation of fatty acids.
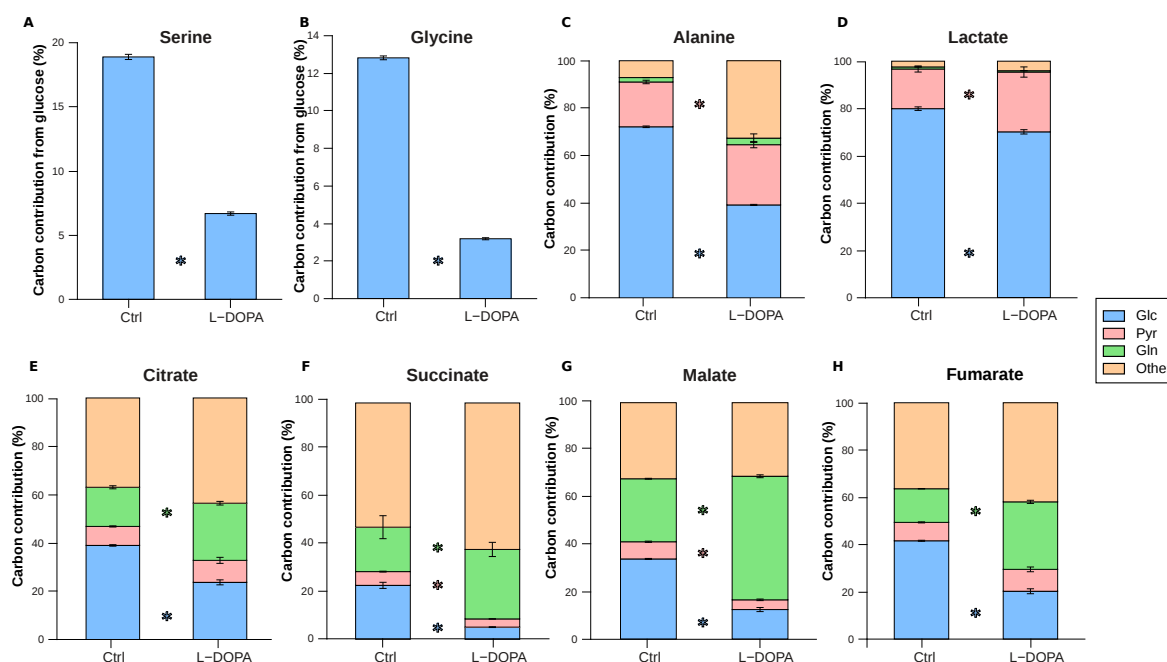

FIGURE 3.5: **Effects of L-DOPA treatment on carbon contribution.** **(A)**: LUHMES cells were treated for 24 h with 200 μM L-DOPA and incubated with [U-^{13}C$_6$]glucose (**Glc**), [U-^{13}C$_5$]glutamine (**Gln**) or [U-^{13}C$_3$]pyruvate (**Pyr**), for the same amount of time. Carbon contributions were calculated by a weighted average of the individual mass isotopomer distribution. **Other** denotes carbon contribution from other sources. Carbon contributions to serine (**A**) and glycine (**B**) only consider glucose since none other applied tracer was detected. Carbon contributions to alanine (**C**), lactate (**D**) and the TCA cycle intermediates citrate (**E**), succinate (**F**), malate (**G**) and fumarate (**H**) are displayed. *: p-value <0.05 by Student t-test.

Serine and glycine are derived from 3-phosphoglycerate and are exclusively labeled from glucose (Figure **3.5** A and B). Neither pyruvate nor glutamine contributed to their labeling pattern. Upon L-DOPA treatment, the carbon contribution from glucose significantly decreased for both amino acids.

Alanine and lactate are derived from pyruvate. For both metabolites, carbon contribution from glucose decreased upon L-DOPA treatment, and the decrease was stronger for alanine (Figure **3.5** C and D). In parallel, carbon contribution from pyruvate increased in both metabolites, but only compensated for the decrease of glucose contribution in the case of lactate. For alanine, however, the carbon contribution from other sources increased, potentially from protein degradation. It is also interesting to note that although no carbon from glutamine was detected in lactate, its contribution to alanine increased upon L-DOPA treatment.

Concerning the TCA cycle intermediates, in all metabolites displayed, glucose contribution decreased upon L-DOPA treatment (Figure **3.5** E-F). There was no significant change in pyruvate contribution to citrate and malate, but a significant decrease in its contribution to succinate and fumarate. Glutamine contribution increased in all metabolites of the TCA cycle upon L-DOPA treatment.

MIDs also provide information on enzymatic activities (Figure **3.6**). Glucose-derived carbons enter the TCA cycle via two distinct routes: via pyruvate dehydrogenase complex (PDH) or pyruvate carboxylase (PC) (Figure **3.6** A). In the first case, pyruvate is decarboxylated to acetyl-CoA and is condensed with oxaloacetate to form citrate. Thus, two labeled carbons originating from glucose end up in citrate. The ratio of M2 citrate over M3 lactate gives information on the activity of PDH. The second route glucose can undertake to enter the TCA cycle is via PC. This enzyme carboxylates pyruvate to oxaloacetate, thus three carbons from glucose end up in citrate. The ratio of M3 citrate over M3 lactate gives an overview of the flux through PC. The relative fluxes through both enzymes are depicted in Figure **3.6** B and C. The activity of both enzymes significantly decreased under treatment with L-DOPA and the decrease in PC activity was stronger than that of PDH.

Glutamine is another important carbon source contributing to the TCA cycle. It enters the cycle after deamidation to glutamate and conversion to α-ketoglutarate. Thus, glutamine-derived carbons enter the TCA cycle as fully labeled α-ketoglutarate, which can be further metabolized through two distinct routes (Figure **3.6** D): (1) in the oxidative glutamine metabolism, α-ketoglutarate is decarboxylated to succinyl-CoA, which is further oxidized to oxaloacetate and then condensed with an unlabeled acetyl-CoA to form M4 citrate. Thus, the ratio of M4 citrate over M5 glutamate gives an estimation of the oxidative metabolism of glutamine. (2) The second metabolic route of glutamine

is the reductive glutamine metabolism in which α-ketoglutarate is reductively carboxy-lated to isocitrate, finally giving M5 citrate. The ratio used to estimate this flux is M5 citrate over M5 glutamate. Since two decarboxylations occur through one complete cycle, the ratio of M2 over M4 citrate indicates the TCA cycling activity. Finally, the ratio of reductive to oxidative glutamine metabolism can be determined using the ratio of M5 over M4 citrate. Upon L-DOPA treatment, the TCA cycle turnover, (figure **3.6** E), as well as the oxidative (figure **3.6** F) and the reductive (Figure **3.6** G) glutamine metabolism decreased. Moreover, the ratio of reductive to oxidative glutamine metabolism decreased (Figure **3.6** H).
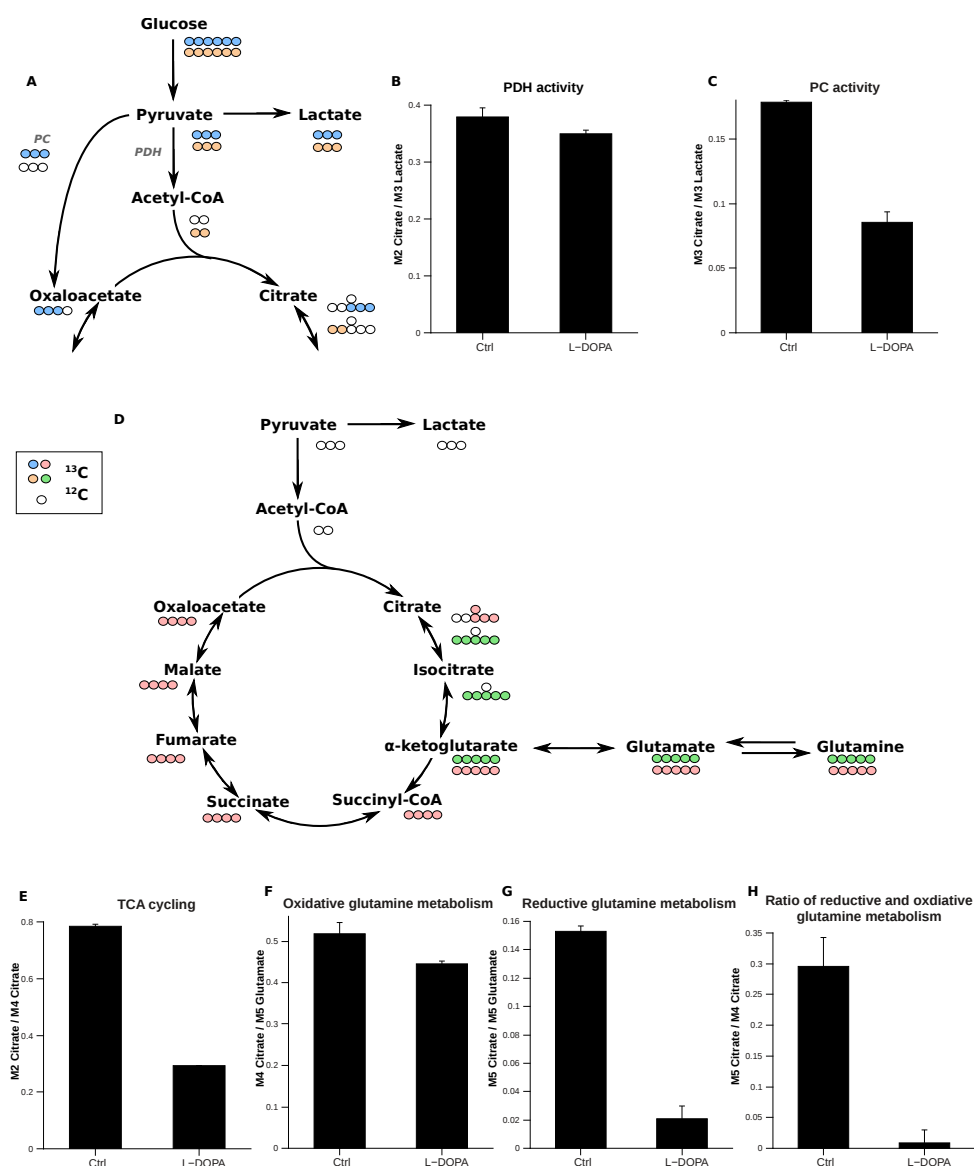
FIGURE 3.6: **Effects of L-DOPA treatment on metabolic fluxes.** LUHMES cells were treated for 24 h with 200 μM L-DOPA and incubated with [U-^{13}C$_6$]glucose or [U-^{13}C$_5$]glutamine. **(A)**: The fluxes through pyruvate dehydrogenase complex (**PDH**) and pyruvate carboxylase (**PC**) can be determined from [U-^{13}C$_6$]glucose labeling. M2 isotopomers in citrate are derived through PDH activity (**orange**) while PC activity induces M3 isotopomers of citrate (**blue**). **(B)**: The ratio of M2 citrate/M3 lactate gives an estimation of PDH activity. **(C)**: The ratio of M3 citrate/M3 lactate gives an estimation of PC activity. **(D)**: Upon its entry into the TCA cycle, glutamine can be metabolized through two different pathways: on the one hand, glutamine can be metabolized oxidatively (**red**), giving rise to M4 labeled citrate. On the other hand, the reaction to isocitrate being reversible, glutamine can be metabolized in a reductive way and gives rise to M5 citrate (**green**). **(E)**: Since a complete cycling through the TCA cycle leads to two decarboxylations, the cycling rate of the TCA cycle can be evaluated by using the ratio of M2 citrate/M4 citrate from [U-^{13}C$_5$]glutamine labeling. **(F)**: The ratio of M4 citrate/M5 glutamate gives an estimate of the oxidative glutamine metabolism. **(G)**: The ratio of M5 citrate/M5 glutamate gives an estimate of the reductive glutamine metabolism. **(H)**: The ratio of M5 citrate/M4 citrate gives an estimate of the ratio of reductive to oxidative glutamine metabolism. All changes were significant by Student t-test, p-value <0.05.

As pointed out in section 3.1.2.1, ROS can inhibit glycolysis through the action of p53. The decrease of glucose contribution to glycolytic intermediates could indicate an inhibition of glycolysis, although uptake and secretion rates of glucose and lactate are necessary to finally draw that conclusion. Inhibition of glyceraldehyde-3-phosphate dehydrogenase (GAPDH) is commonly used to assess metabolic effects of inhibition of glycolysis [161]. In order to assess the effects of glycolysis inhibition and to compare these to the effects of the L-DOPA treatment in LUHMES cells, I treated them for 24 h with 3.6 μM heptelidic acid, a compound binding to the Cys149 residue in the catalytic site of GAPDH [162]. Interestingly, the effects of the GAPDH inhibitor were different to those observed upon L-DOPA treatment. Upon treatment of LUHMES cells with heptelidic acid, the contribution of glucose to serine, glycine, alanine, lactate and TCA cycle intermediates decreased (Figure **3.7** A-G), as seen upon L-DOPA treatment. However, upon [U-^{13}C$_3$]pyruvate labeling, carbon contribution increased not only in lactate and alanine, as seen upon L-DOPA treatment, but also in the TCA cycle intermediates, which was not observed under L-DOPA treatment (Figure **3.7** C-G). This indicates that a decrease in glucose contribution to the TCA cycle is compensated by contribution from pyruvate. I can therefore rule out a complete GAPDH inhibition as only mechanism of L-DOPA-induced metabolic changes.

Przedborski *et al.* showed that chronic L-DOPA treatment in rats induced a decrease of mitochondrial complex I activity without affecting the activity of mitochondrial complexes II and IV [163]. To compare the profile of LUHMES cells treated with L-DOPA with the effects of a complex I inhibitor, I treated the LUHMES cells with rotenone or 1-methyl-4-phenylpyridinium (MPP$^+$). Using [U-^{13}C$_6$]glucose, the contribution of glucose to alanine and lactate as well as the fraction of M3 isotopomer of malate and aspartate increased upon complex I inhibition (Figure **3.7** H-J), which was not observed upon L-DOPA treatment. Moreover, Worth *et al.* showed that rotenone treatment induced an increase in reductive glutamine metabolism [164], which was not observed upon L-DOPA treatment (see Figure **3.6** G). Taken together, these data indicate that L-DOPA did not induce a mitochondrial complex I inhibition in LUHMES cells.

Tretter *et al.* used guinea pig synaptosomes (isolated nerve endings) to show that concentrations of H$_2$O$_2$ below 50 μM block the activity of aconitase, the enzyme that interconverts citrate and isocitrate. To compensate this inhibition, glutamate intake increased to fuel the TCA cycle. This lead to an unaltered NADH production. However,
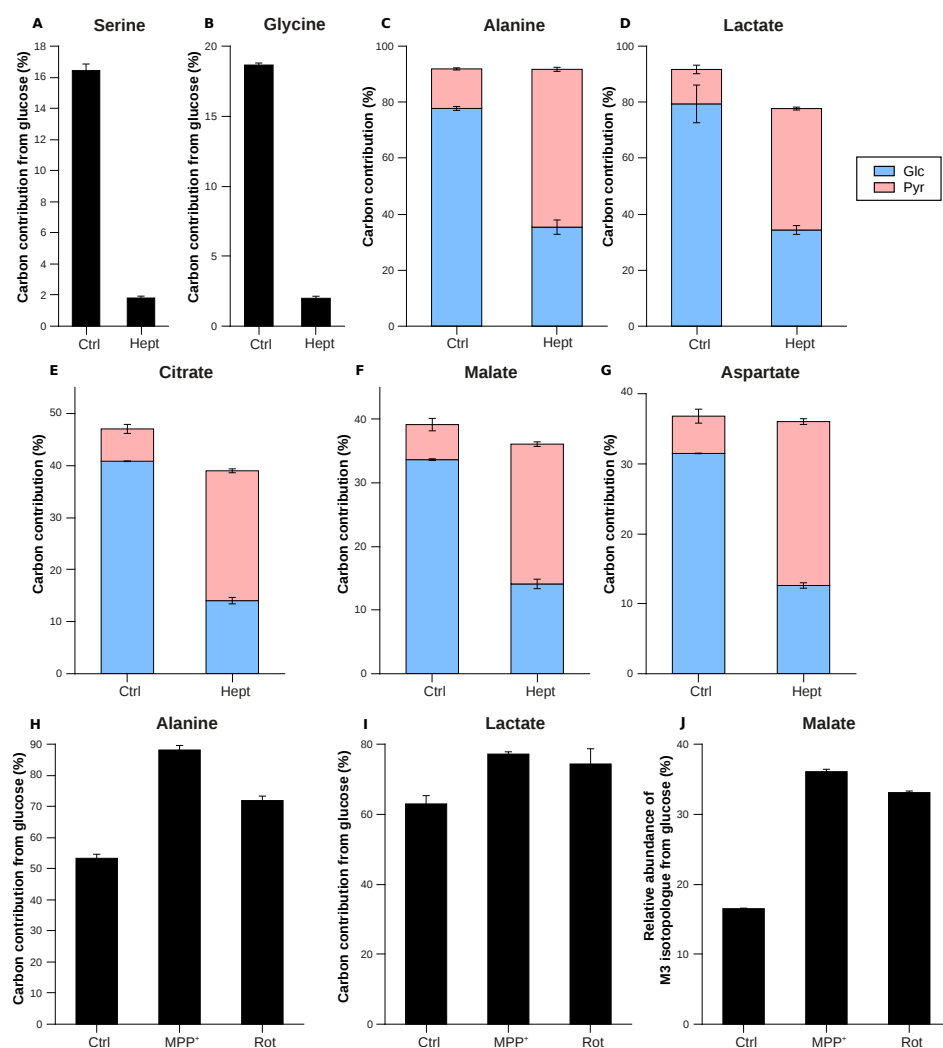
FIGURE 3.7: **Effects of heptelidic acid, rotenone and MPP$^+$ treatment on carbon contribution.** LUHMES cells were treated for 24 h with 3.6 µM heptelidic acid (**Hept**), 10 µM MPP$^+$ or for 6 h with 1 µM rotenone (**Rot**) and incubated with [U-^{13}C$_6$]glucose (**Glc**) or [U-^{13}C$_3$]pyruvate (**Pyr**). Carbon contributions of serine (**A**), glycine (**B**), alanine (**C**), lactate (**D**), citrate (**E**), malate (**F**) and aspartate (**G**) were calculated under glucose and pyruvate tracers after heptelidic acid treatment. Carbon contribution from glucose to alanine (**H**) and lactate (**I**) upon MPP$^+$ and rotenone treatments. (**J**): M3 isotopologue of malate under glucose tracer and MPP$^+$ and rotenone treatment. All were significant by Student t-test, p-value <0.05.

in the case of concentrations of H$_2$O$_2$ higher than 100 µM, the α-ketoglutarate dehydrogenase was also inhibited, leading to a limited NADH generation which caused impaired respiratory capacities [165]. In their study, Tretter *et al.* also observed an inhibition of SDH by H$_2$O$_2$, although this was not further discussed [165]. The inhibition of aconitase by H$_2$O$_2$ lead to a truncated TCA cycle. In that case, the aspartate aminotransferase becomes important to keep the cycle running. This enzyme is responsible for the conversion of oxaloacetate to aspartate, thereby using glutamate and producing

α-ketoglutarate. Yudkoff *et al.* used rat synaptosome and radioactive tracers to show that aspartate aminotransferase is active in those particles and that the malate-aspartate shuttle is functional, but to a considerately lower rate than aspartate aminotransferase [166]. Moreover, Oikawa *et al.* used *substantia nigra* tissue from monkeys to show that ROS induced carbonylation of various proteins including aconitase, glutamate dehydrogenase and aspartate aminotransferase [167]. Protein carbonylation is a modification induced by ROS during which carbonyl amino acid side chains of proteins are oxidized to reactive ketones or aldehydes. It has been linked to several dysfunctions and targets the side chains of lysine, arginine, proline and threonine residues [168]. The inactivation of these enzymes could explain the decreased activity of the TCA cycle.

Another interesting pathway of central carbon metabolism is the pentose phosphate pathway (PPP). On the one hand, it provides precursors for nucleotide biosynthesis from glucose-6-phosphate. On the other hand, it produces the reduced form of the cofactor $NADP^+$, NADPH. The regeneration of this cofactor plays an important role in the context of oxidative stress: oxidants cause an increase in the $NADP^+$/NADPH ratio. NADPH is an important cofactor of the glutathione reductase (GR), the enzyme recycling GSSG to GSH. This increase in the $NADP^+$/NADPH ratio leads to the inhibition of GAPDH and pyruvate kinase (PK), redirecting the glycolytic flux towards the PPP to reduce more $NADP^+$, thereby supporting the stress response and the synthesis of ribose-5-phosphate needed for the repair of DNA damaged upon stress [169, 170]. Ralser *et al.* reported that inhibition of GAPDH in *S. cerevisiae* and *C. elegans* induced a rerouting of carbon fluxes towards the PPP. Upon GAPDH inhibition, this pathway was essential for survival under oxidative stress in order to maintain the cytoplasmic NADPH/$NADP^+$ ratio [170]. Using stable isotopte tracing, the activity of the PPP can be monitored using a $[1,2-^{13}C_2]$glucose tracer. The third reaction of the pathway leads to the decarboxylation of the first carbon of glucose-6-phosphate, thus M1 isotopologues of lactate can be traced back to the activity of the oxidative part of the PPP. On the other hand, M2 isotopologues of lactate are indicative for glycolytic activity (Figure **3.8** A). The ratio of M1 over (M1 + M2) lactate gives an estimation of the flux through the PPP. To test whether L-DOPA treatment affects the activity of the oxidative part of the PPP, I seeded LUHMES cells at the density used in section 3.1.2.1 and treated for 24 h with 0, 25, 50 and 100 μM L-DOPA in the presence of the $[1,2-^{13}C_2]$glucose. I observed an increase in this ratio, indicating an increased activity of the oxidative PPP, and thus a linked increased NADPH production (Figure **3.8** B).
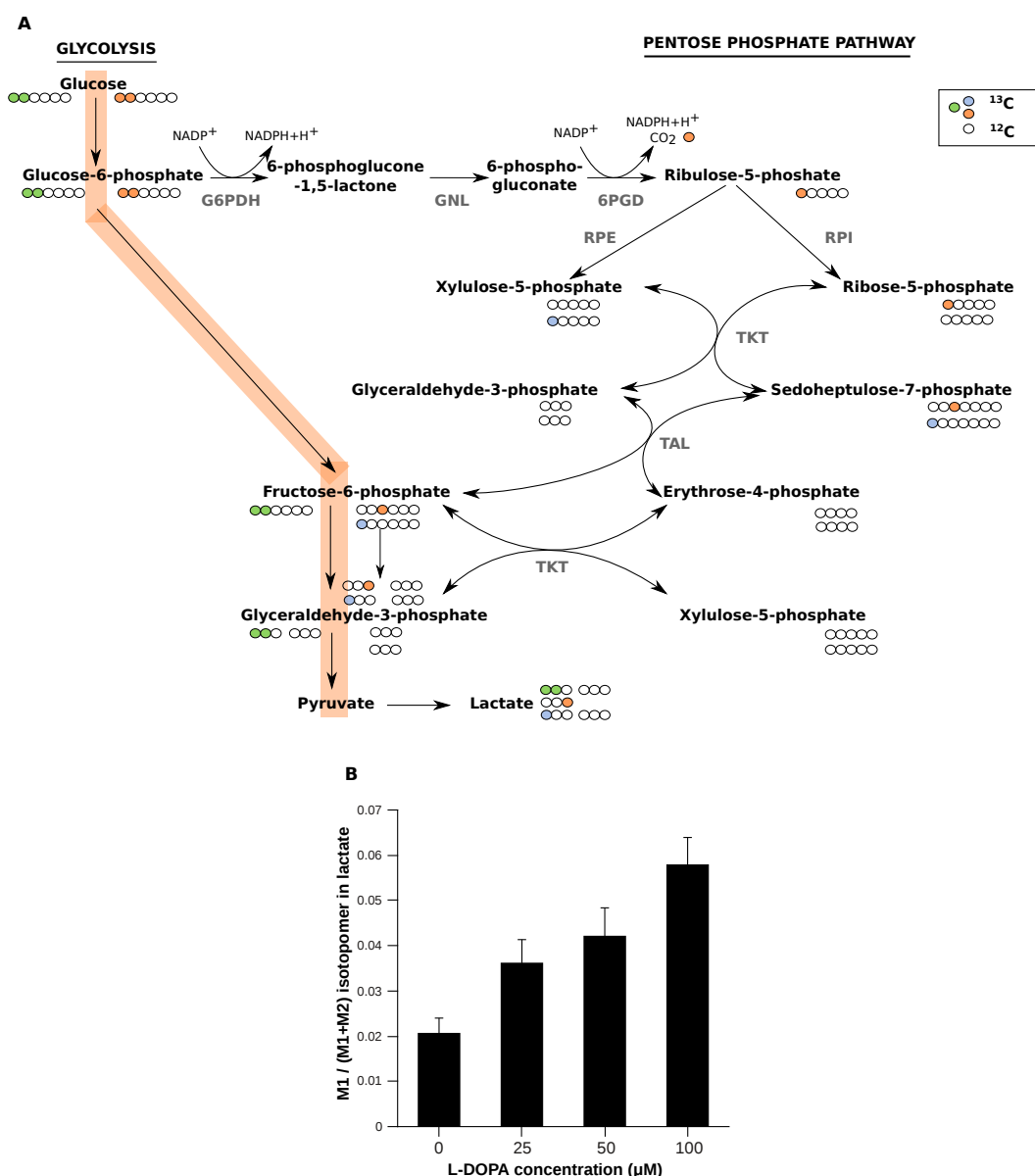
FIGURE 3.8: **Effects of L-DOPA treatment on the pentose phosphate pathway.** LUHMES cells (seeded at the density used in section 3.1.2.1) were treated for 24 h with 0, 25, 50 or 100 μM L-DOPA and incubated with $[1,2\text{-}^{13}C_2]$glucose. **(A)**: A scheme of the pentose phosphate pathway (PPP) is represented: the two times labeled glucose-6-phosphate is decarboxylated upon entry in the PPP, thus only non-labeled or one time labeled fructose-6-phosphate will enter back the glycolysis and M1 of lactate represents the fraction of metabolites that went through the PPP. If glucose goes through glycolysis, lactate is two times labeled. **(B)**: Upon L-DOPA treatment the fraction of carbons that went through the PPP was calculated using the ratio of M1 over (M1 + M2) lactate. **G6PDH**: glucose-6-phosphate dehydrogenase; **GNL**: gluconolactonase; **6PGD**: 6-phophogluconate dehydrogenase; **RPE**: ribulose-5-phosphate-3-epimerase; **RPI**: ribose-5-phosphate isomerase; **TKT**: transketolase; **TAL**: transaldolase; **TIM**: triose-phosphate isomerase. p-value <0.05 by One-way ANOVA.

In summary, I observed that L-DOPA treatment induced (1) a decreased carbon contribution from glucose to glycolysis and TCA-derived metabolites. (2) In alanine

and lactate, carbon contribution from pyruvate increased while in TCA cycle inter-
mediates, glutamine-derived carbon contribution increased. (3) L-DOPA caused a de-
crease in PDH and PC activity as well as a decrease in TCA cycling, oxidative and re-
ductive glutamine metabolism. (4) Although the glycolytic flux might be reduced, an
inhibition of glycolysis cannot account for all these changes observed upon L-DOPA
treatment as observed by comparing L-DOPA and heptelidic acid treatments. (5) L-
DOPA induced changes in TCA cycle activity, but not through a mitochondrial complex
I inhibition as shown by comparison of L-DOPA, rotenone and MPP$^+$ treatments. (6)
The glutamine contribution to TCA cycle intermediates correlates with data obtained
by Tretter *et al.* who showed that ROS inhibits aconitase and SDH and induces gluta-
mate utilization to fuel the TCA cycle [165]. Inhibition of aconitase would thus lead
to the observed decreased activities of PDH and PC. (7) Finally, L-DOPA treatment
induced an increase in the activity of the oxidative part of the PPP.

The decreased TCA cycling, reduction of the oxidative and reductive glutamine
metabolism as well as the increased activity through the PPP upon treatment indicates
an imbalance in the NAD(P)$^+$ /NAD(P)H ratio.

3.1.3 Does pyruvate play a crucial role for cell survival?

As demonstrated in the previous section, L-DOPA treatment induced a signifi-
cant increase in the contribution of pyruvate carbon to lactate and alanine. Wang *et al.*
showed that upon H$_2$O$_2$-induced oxidative stress, pyruvate was essential for survival
of human SK-N-SH neuroblastoma cells [171]. They also observed (1) that pyruvate
helped to maintain the membrane potential of the mitochondria and (2) that pyruvate
rescued the decrease in ATP production induced by oxidative stress. They concluded
from these facts that pyruvate could provide protection by being oxidized and be used
as substrate for energy production to maintain cellular functions under stress condi-
tions [171]. I therefore investigated whether pyruvate could play a role in neuronal
survival upon L-DOPA treatment (Figure **3.9**). First, I treated LUHMES cells with dif-
ferent concentrations of H$_2$O$_2$ for 24 h in the presence or absence of pyruvate (Fig-
ure **3.9** A). Pyruvate was essential for cell survival for all concentrations of H$_2$O$_2$ above
10 μM. However, when I treated LUHMES cells with L-DOPA, the presence or absence
of pyruvate did not play any role in cell survival (Figure **3.9** B). This is in contradiction
with a further article published by Wang *et al.* where they found that ethyl pyruvate
could protect PC-12 cells from DA-induced toxicity by suppressing intracellular oxida-
tive stress and modulating signal pathways of apoptosis [172]. It cannot be excluded

that the protective effect seen in PC-12 was due to the fact that ethyl pyruvate and not pyruvate was used. Sappington *et al.* treated enterocytic Caco-2 cells with a mixture of pro-inflammatory cytokines and showed that ethyl pyruvate inhibited nuclear factor $\varkappa$B (NF-$\varkappa$B) activation, inducible nitric oxide synthase (iNOS) mRNA expression and nitric oxide (NO) production (all being responses to inflammation). When pyruvate was used under the same conditions, it was ineffective and did not reduce the inflammatory state of these cells [173].
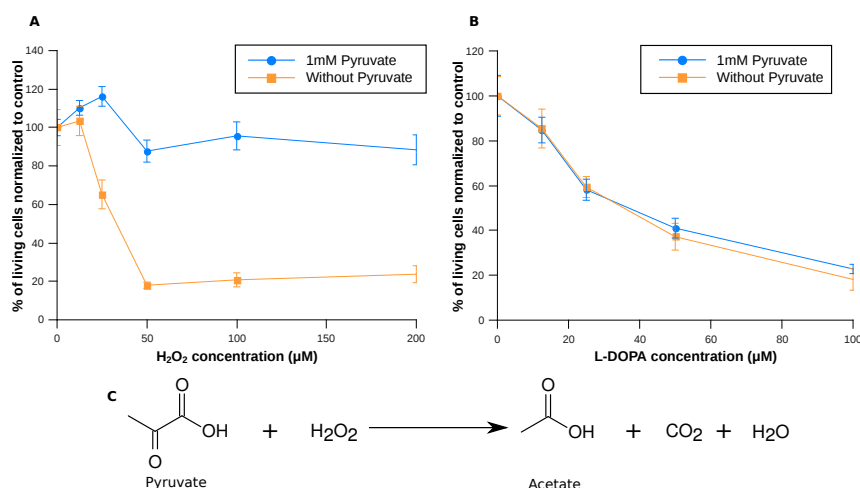

FIGURE 3.9: **Effects of pyruvate on the viability of LUHMES cells. (A)**: LUHMES cells were treated for 24 h with different concentrations of hydrogen peroxide (H_2O_2) in the presence or absence of 1 mM pyruvate. **(B)**: LUHMES cells were treated for 24 h with different concentrations of L-DOPA in the presence or absence of 1 mM pyruvate. **(C)**: Mechanism of action of pyruvate in the scavenging of H_2O_2 to form acetate, carbon dioxide and water.

Pyruvate protects cells through two mechanisms: (1) by scavenging H_2O_2 radicals and (2) by rescuing intracellular energy failure [174]. In the first case, pyruvate can degrade H_2O_2 through a non-enzymatic oxidative decarboxylation leading to the formation of acetate, water and carbon dioxide (Figure **3.9** C) [175]. O'Donnel-Tormey *et al.* showed, that human and murine cancer cell lines cultured in pyruvate-free medium secreted pyruvate to reach the extracellular concentration of 60-150 μM, which corresponds to the human serum and plasma concentrations and that this pyruvate served as extracellular antioxidant [176]. In the second case, pyruvate replenishes the TCA cycle [177]: upon H_2O_2 treatment of rat brain slices, the expression of poly (ADP-ribose) polymerase-1 (PARP-1), a nuclear enzyme expressed abundantly upon DNA damage induced by oxidative stress, increased and lead to the depletion of NAD^+. The NAD^+/NADH redox couple is highly important for energy metabolism and its depletion leads to a drop in ATP production, causing cell death. Zheng *et al.* incubated the

slices with mixtures of glucose and pyruvate or pyruvate alone and could conclude that pyruvate alone was able to replenish the NAD^+ pool, probably via the lactate dehydrogenase, while only the glucose-pyruvate mixture lead to a recovery of both NAD^+ and ATP [177].

In neuronal cells, pyruvate metabolism has not been studied in detail. However, lactate metabolism has been studied in a much greater extend and its particular use in neuronal cells gave rise to the astrocyte-neuron lactate shuttle hypothesis (ANLSH). This process is happening upon glutamatergic activation: neurons synthesize and release glutamate, which is a highly energy-demanding process. The oxidative phosphorylation is thus increased, leading to lower intracellular levels of pyruvate. Glutamate released for neuronal signalling can also activate glycolysis in astrocytes which release lactate for neuronal utilization. Concomitantly, neuronal use of glucose is decreased and lactate is used as carbon source for energy production [178]. In their original work, Pellerin *et al.* demonstrated that glutamate induced an increased glycolytic flux in astrocytes, leading to increased release of lactate. They also reported that astrocytes released pyruvate at a rate three times lower than lactate [179]. Furthermore, Wang *et al.* showed that astrocytes can release pyruvate to protect neurons upon cysteine auto-oxidation-induced toxicity [180].

Although I did not observe any protective effect of pyruvate on cell viability in the presence of L-DOPA, I determined whether pyruvate supplementation impacts intracellular fluxes. For that, I incubated LUHMES cells in the presence and absence of pyruvate, together with L-DOPA and [U-$^{13}C_6$]glucose or [U-$^{13}C_5$]glutamine. Based on the MIDs, I determined carbon contributions (Figure **3.10**). In the following paragraphs, I compare the carbon contributions for control conditions in the presence and absence of pyruvate as well as the carbon contributions for L-DOPA treated cells in the presence and absence of pyruvate. This comparison was performed for alanine, lactate, citrate, fumarate, malate and aspartate.

As shown in section 3.1.2.2, L-DOPA treatment induced a decreased carbon contribution from glucose in both alanine and lactate This is displayed in Figure **3.10** A and B, *ctrl* and *L-DOPA* bars.

When pyruvate was omitted, the contribution of glucose-derived carbon increased in both lactate and alanine (Figure **3.10** A and B, *ctrl* and *wo pyr* bars). This could be

explained by the fact that if one substrate (pyruvate) is omitted, the overall relative contribution of others sources (glucose in this case) increase.

However, upon L-DOPA treatment in the absence of pyruvate, the carbon contribution pattern differed for the two metabolites: while alanine carbon contribution from glucose decreased upon treatment to the levels observed in L-DOPA treated cells in the presence of pyruvate, the carbon contribution from glucose to lactate also significantly decreased, but to a much lesser extend than that of alanine (Figure **3.10** A and B, *wo pyr L-DOPA* bars).

Concerning carbon contribution to TCA cycle intermediates, the absence of pyruvate did not induce a difference in carbon contributions under control conditions for citrate, fumarate, malate and aspartate (Figure **3.10** C-F, *ctrl* and *wo pyr* bars). Upon L-DOPA treatment, the response in the absence of pyruvate showed similar trend as in the presence of pyruvate and L-DOPA treatment. However, citrate, malate and aspartate showed a significant decreased carbon contribution from glucose compared to the condition containing pyruvate. In addition, citrate and malate showed a significant increase in carbon contribution from glutamine compared to the L-DOPA treated conditions with pyruvate (Figure **3.10** C, E, F, *L-DOPA* and *wo pyr L-DOPA* bars).

The absence of pyruvate did not induce any change in the TCA cycling as indicated by the ratio of M2 citrate and M4 citrate from [U-^{13}C$_6$]glucose labeling in control conditions. (Figure **3.10** G, *ctrl* and *wo pyr* bars). However, when the treatment was combined with the absence of pyruvate, the cycling significantly decreased to levels lower than those observed under treatment conditions in the presence of pyruvate (Figure **3.10** G, *L-DOPA* and *wo pyr L-DOPA* bars).

The lower decrease in carbon contribution from glucose to lactate in comparison to the one from glucose to alanine supports the idea that the cells are using the lactate dehydrogenase (LDH) reaction to regenerate NAD$^+$, since the absence of pyruvate deprived the cells of alternative substrate for LDH. Ying *et al.* reported that astrocytes treated with an alkylating agent inducing DNA damage had higher expression of PARP-1, an enzyme facilitating DNA repair. As mentioned earlier in this section, this lead to NAD$^+$ depletion and inhibition of glycolysis. In those cells, glucose was the primary substrate for energy metabolism, thus inhibition of glycolysis lead to mitochondrial dysfunction and permeability transition pore (PTP) opening, eventually leading to cell death. The same authors could partially prevent this toxic effect by supplying
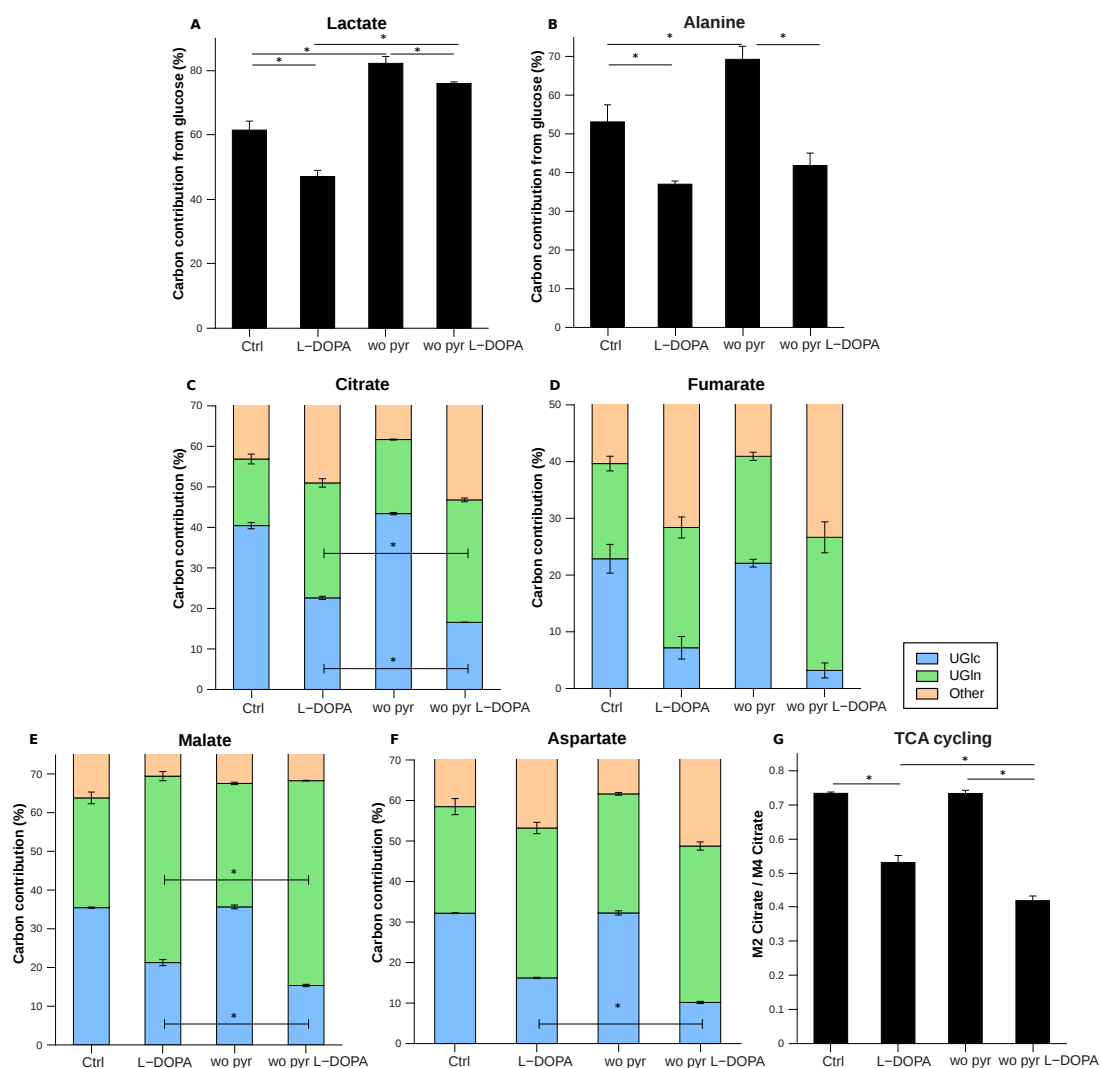
FIGURE 3.10: **Effects of pyruvate on the metabolism of LUHMES cells upon L-DOPA treatment.** LUHMES cells were treated for 24 h with 50 µM L-DOPA in the presence or absence (**wo pyr**) of 1 mM pyruvate. Carbon contribution from glucose to lactate **(A)** and alanine **(B)**. Carbon contribution from glucose (**UGlc**), glutamine (**UGln**) or other sources (**Other**) for citrate **(C)**, fumarate **(D)**, malate **(E)** and aspartate **(F)**. **(G)**: TCA cycling was calculated using the ratio of M2 over M4 citrate from UGlc tracer for each condition. *: p-value <0.05 by Student t-test.

the astrocytes with either pyruvate, glutamate or glutamine, but not lactate [181]. They hypothesized that these three metabolites were all able to replenish the TCA cycle and thus preserve the energy state of the cells. Since NAD$^+$ depletion by PARP-1 did not prevent activation of TCA cycle upon replenishment, this also suggested that the mitochondrial NAD$^+$ pool was spared from the depletion [181]. In the light of our cell system, it is possible that I did not observe any effect on the cell viability upon pyruvate depletion due to the fact that the cell culture medium contains both glutamine and glutamate.

DNA damage via its cleavage has been linked to quinone toxicity by Wang *et al.* [182]. Quinones bind to cysteinyl residues of the toposiamerase II enzymes [183]. These enzymes generate DNA double strand break in order to remove superhelical twists and tangles from the genetic material. Bender *et al.* reported that quinones interfere with this process by covalently attaching to the protein-DNA complex and increase DNA scission [183], which could in turn induce PARP-1 activation.

The decrease in TCA cycling upon L-DOPA treatment in the absence of pyruvate could also be due to lower NAD^+ levels: although NAD^+ as such cannot cross the mitochondrial inner membrane, the malate-aspartate shuttle can transport aspartate to the cytoplasm where it is converted to oxaloacetate, then to malate with the consumption of NADH and production of NAD^+. Malate can then enter the mitochondria back and be converted to oxaloacetate, thereby consuming NAD^+ and producing NADH. This would decrease the amount of NAD^+ available for the TCA cycle activity [184], but the NADH generated could be used for oxidative phosphorylation through the electron transport chain.

To summarize, I observed that pyruvate is not essential for cell survival upon L-DOPA treatment as it is for H_2O_2, indicating that it does not play an antioxidant role in the case of L-DOPA treatment. Its absence, however, induced an increase of glucose-derived carbon contribution to lactate under treated conditions, which was not observed under conditions containing pyruvate. This suggested a compensation of pyruvate absence by glucose for NAD^+ regeneration. Concerning the TCA cycle, the absence of pyruvate induced a decrease in glucose contribution to citrate, malate and aspartate as well as an increased glutamine contribution to citrate and malate. The TCA cycling decreased upon L-DOPA treatment in the absence of pyruvate. This could suggest that quinone induced DNA strand break by binding to the topoisomerase, which lead to the activation of PARP-1 and depletion of the cytosolic NAD^+ pool. The malate-aspartate shuttle, together with lactate production, could contribute to restoration of NAD^+, but at the expense of the TCA cycling.

3.1.4 Effects of L-DOPA on uptake and secretion rates

In section 3.1.2.2, the effects of L-DOPA on the contributions of glucose, glutamine and pyruvate to metabolites of central carbon metabolism were assessed. However, these values only give a partial view of the overall picture. In order to complete it,

uptake and secretion rates for glucose, glutamine, lactate, glutamate and pyruvate were needed.

To measure differences in uptake and secretion rates induced by L-DOPA, I treated LUHMES cells, seeded at the same density as in section 3.1.2.2, for 24 h with 200 μM L-DOPA. Uptake rates for glucose and glutamine, as well as secretion rates of lactate and glutamate are depicted in Figure **3.11** A-D. Upon L-DOPA treatment, I observed that glucose uptake and lactate secretion decreased. Interestingly, the ratio of lactate over glucose, indicating the proportion of glycolysis used for ATP production, increased upon treatment (Figure **3.11** E). This also means that glucose-derived carbon is deviated from oxidation in the TCA cycle towards lactate secretion, thus suggesting a decreased flux through PDH. On the other hand, glutamine uptake was not modified by L-DOPA stimulation, while glutamate secretion highly increased. As a result, glutamine anaplerosis to the TCA cycle, obtained by subtracting glutamate secretion from glutamine uptake, decreased upon treatment (Figure **3.11** F).

The decrease in glucose uptake further pointed towards a decreased glycolytic activity. The lesser decrease in lactate secretion compared to the decrease in glucose uptake, manifested in an increase in the lactate over glucose ratio, confirmed the redirection of glucose carbon towards lactate production rather than towards the TCA cycle. This increased ATP and NAD$^+$ production through glycolysis could be advantageous over short periods of time. Indeed, on the long term, TCA cycle is more efficient both for energy and cofactor synthesis. However, glycolysis runs 100 times faster than TCA cycle, therefore, an increased lactate to glucose ratio lead to rapid, short term increase in NAD$^+$ [185].

Glutamine and glutamate showed different profiles. The unchanged uptake rate of glutamine with and without L-DOPA could be due to an intracellular redirection of fluxes, away from protein synthesis to protein degradation, thus replenishing the TCA cycle. The increased concentrations of glutamate in the medium upon L-DOPA treatment could be due to an inhibition of glutamate transporters. These transporters are responsible for limiting the amounts of glutamate present in the extracellular space [186]. Large amounts of glutamate are secreted under ischemic conditions (i.e. low oxygen and glucose availability), which lead to overexcitation of postsynaptic neurons [187]. Glutamate excitotoxicity is characterized by disrupted calcium homeostasis, mitochondrial dysfunction and generation of ROS [187]. Berman *et al.* studied rat synaptosomes and reported an decreased glutamate uptake upon DA treatment [186]. This decrease
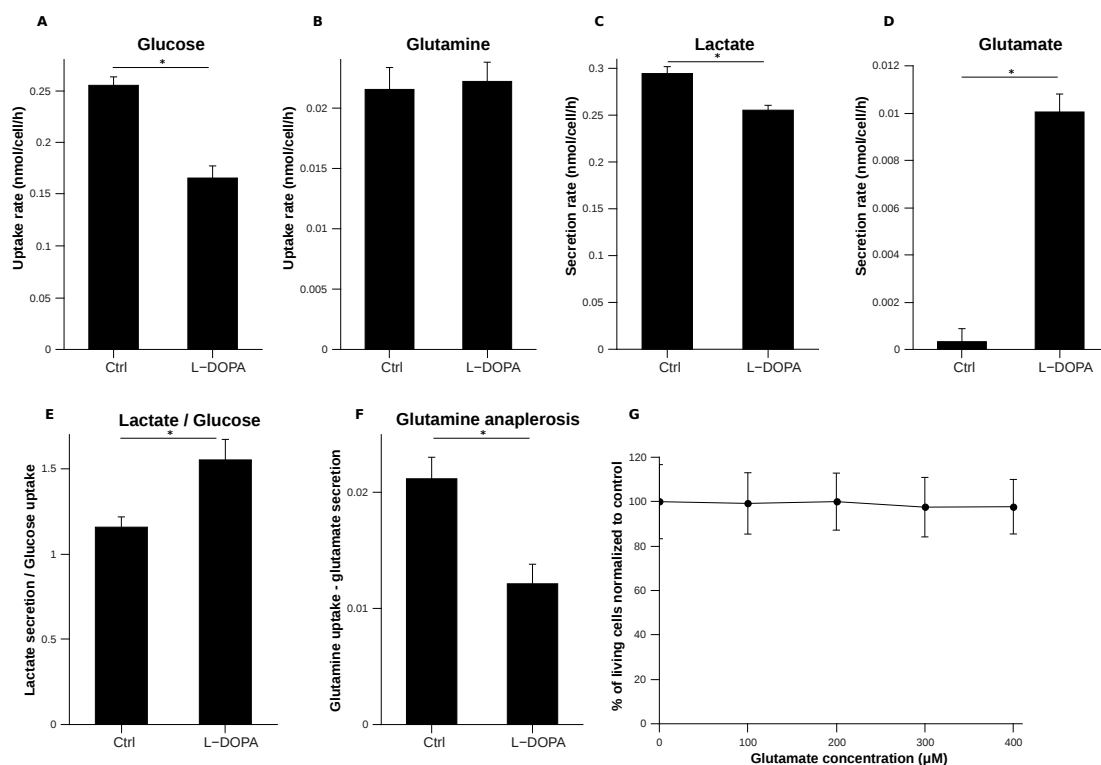
FIGURE 3.11: **Effects of L-DOPA on uptake of glucose and glutamine and secretion of lactate and glutamate.** LUHMES cells were treated for 24 h with 200 μM L-DOPA. Uptake and secretion rates were determined. The concentration of the metabolites did not vary between control and treated conditions in medium without cells. Uptake of glucose **(A)**, glutamine **(B)** as well as secretion of lactate **(C)** and glutamate **(D)** were calculated. **(E)**: The ratio of lactate over glucose indicates the proportion of glucose taken up secreted as lactate. **(F)**: Glutamine anaplerosis can be calculated by subtracting glutamate secretion to glutamine uptake. **(G)**: To test whether the secreted glutamate could be toxic to the cells, LUHMES cells were treated for 24 h with various concentrations of glutamate. *: p-value <0.05 by Student t-test.

was due to inhibition of glutamate transporter by ROS and quinones produced during the oxidation of DA. ROS and quinones can directly inactivate glutamate transporter by binding to cysteinyl residues located in the active site of the protein, therefore preventing re-uptake of glutamate into the cells [186]. Transport of glutamate is bidirectional, therefore, inhibition of the uptake should be accompanied by inhibition of release [188]. However, Rothstein *et al.* reported that a selective inhibition of glutamate transport in rat spinal cord cells lead to an accumulation of glutamate in cell culture medium [189]. Glutamate transporter is a symport with sodium, and therefore its activity is linked to the activity of the Na^+/K^+ ATPase and membrane potential [188]. Disruption of membrane potential is responsible for reverse transport of glutamate, and therefore increased extracellular concentrations of glutamate, under ischemic conditions [188]. Although I could not find evidence of membrane disruption upon L-DOPA treatment

in the literature, Jana *et al.* reported that quinones issued from DA oxidation lead to loss of mitochondrial membrane potential [190]. Interestingly, increased glutamate extracellular concentrations have been associated with SDH inhibition [155].

In order to ascertain that the toxic effects observed on LUHMES cells upon L-DOPA treatment were not due to glutamate excitotoxicity, I performed a cell viability assay with a range of glutamate concentrations covering the concentration measured in medium after L-DOPA treatment (200 μM) (Figure **3.11** G). No cell death was observed, indicating that glutamate excitotoxicity is not involved in L-DOPA toxicity.

Intriguingly, I observed that pyruvate levels decreased in media incubated with L-DOPA, even in the absence of cells (Figure **3.12** A). One hypothesis for the observed pyruvate depletion could be its function as antioxidant as described in section 3.1.3: H_2O_2 produced from redox cycling of quinone can non-enzymatically react with pyruvate to form acetate [175]. In this case, I would expect a production of acetate due to oxidative decarboxylation of pyruvate (see reaction in Figure **3.9** C). To test this hypothesis, I compared the acetate levels in the medium after incubation with and without L-DOPA, in the absence of cells. Figure **3.12** B shows that the concentration of acetate increased if L-DOPA is present in the medium. It is however intriguing that the concentration of acetate measured is about one and a half times higher than the concentration of pyruvate consumed during the same time period. H_2O_2 can also react with other α-ketoacids to form the respective carboxylic acid [175]. It is therefore possible that other compounds from the medium react with H_2O_2 to form acetate.

Taking into account the degradation of pyruvate as well as acetate production in medium containing L-DOPA, I calculated uptake rates of pyruvate and acetate in both treated and untreated conditions (Figure **3.12** C). The consumption of pyruvate was significantly decreased upon L-DOPA treatment. In the case of acetate, the cells secreted it in the absence of treatment, while upon L-DOPA treatment, the uptake of acetate increased.

Since the presence of acetate in the medium of L-DOPA treated cells induced an increased uptake of this metabolite, I tested whether this metabolite could influence neuronal metabolism. Therefore, LUHMES cells were treated for 24 h with 400 μM pyruvate and 800 μM acetate, as measured in incubated medium with L-DOPA. First, I assayed cell viability to evaluate if acetate is toxic to the cells (Figure **3.13** A), then I determined uptake rates for glucose, glutamine and pyruvate as well as secretion
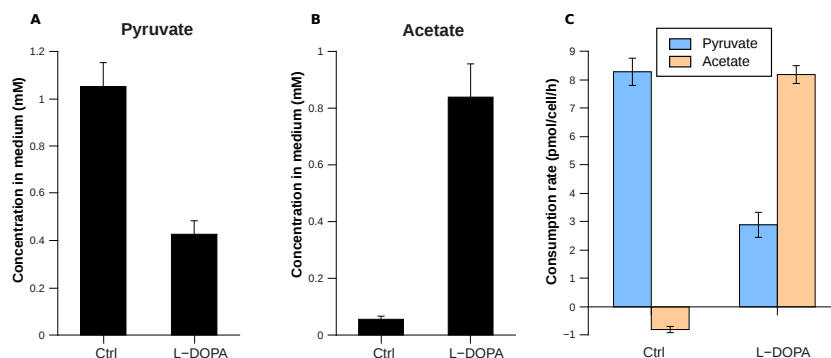
FIGURE 3.12: **Effects of L-DOPA on pyruvate and acetate concentrations.** LUHMES cells were treated for 24 h with 200 μM L-DOPA. **(A-B)**: Concentrations of pyruvate and acetate were measured from media incubated without cells in the presence or absence of L-DOPA. **(C)**: Uptake and secretion rates of pyruvate and acetate. All were significant by Student t-test, p-value <0.05

rates for lactate, glutamate and acetate (Figure **3.13** B-G). I found that 800 μM of acetate did not impair cell viability within a period of 24 h. In addition, glucose, glutamine and pyruvate uptake did not change upon acetate treatment. I observed no change of lactate and glutamate secretion rates. Interestingly, following acetate treatment, the cells did not consume any acetate, but they rather increased its secretion (Figure **3.13** G).

As shown in Figure **3.12** C and Figure **3.13** G, LUHMES cells can either secrete or consume acetate depending on the conditions. It is synthesized by hydrolysis of acetyl-CoA by the cytosolic acetyl-CoA hydrolase, with pyruvate as the predominant precursor of acetyl-CoA [191]. Although acetate was only measured following ischemia and not in healthy brain, it is reported as common metabolite in primary CNS-derived cultures [191].

Upon L-DOPA treatment, LUHMES cells consumed acetate rather than secreting it. Waniewski *et al.* reported that only glial cells can metabolize acetate because neuronal cells do not possess the adequate transport system [192]. However, Rae *et al.* refuted this by showing that acetate can be transported by neurons through the monocarboxylate transporters (MCTs), among which neuronal MCT2 has the highest affinity for acetate. They also showed that acetate is rapidly incorporated into the lipid fraction [191]. Once inside the cell, acetate can be metabolized to acetyl-CoA by the acetyl-CoA synthetase (ACSS2). Acetyl-CoA can then be used to fuel the TCA cycle, for cholesterol and fatty acid synthesis or for protein and histone acetylation [193]. If LUHMES

cells are indeed able to use acetate, a rerouting of acetyl-CoA from TCA cycle fueling to fatty acid synthesis could explain the decreased carbon contribution of pyruvate to TCA cycle intermediates observed upon L-DOPA treatment in Figure **3.5** F and G, section 3.1.2.2.

Zhao *et al.* showed that most enzymes of the central carbon metabolism are acetylated. However, the change in enzymatic activity depended on the enzyme considered [194]. In this case, it seems improbable that the acetate consumed upon L-DOPA treatment goes to protein acetylation. On the other hand, Gu *et al.* showed that upon H_2O_2 treatment, the expression of acetyltransferases p300/cAMP-response element binding protein increased while the expression of histone deacetylases decreased in SH-SY5Y cells [195]. Acetyl-CoA can also be used to synthesize fatty acids. Ischemic injury induced the degradation of membrane phospholipids and release of free fatty acids. Ulloth *et al.* showed that treatment of PC-12 cells with palmitic and stearic acids induced cell death. They used concentrations comparable to those measured following traumatic brain injuries. The mechanisms involved an early activation of the expression of the Fas receptor, followed by cell shrinkage and membrane blebbing. In a third step, the nuclear content condensed and fragmented and finally, the Fas ligand was upregulated. Treatment with oleic and arachidonic acids did not induce any toxicity [196]. Although the levels of free fatty acids as well as the contribution of acetate to their synthesis upon L-DOPA treatment is currently unknown, I cannot rule out a potential toxicity induced by an increase in their concentration.

Finally, I assayed the effect of acetate on the metabolism of pyruvate (Figure **3.13** H). LUHMES cells were incubated with [U-^{13}C$_3$]pyruvate in the presence or absence of acetate. No difference was observed in the MIDs of citrate, malate and NAA, indicating that the presence of acetate alone did not modify intracellular fluxes of pyruvate. To assess if LUHMES cells can metabolize acetate, I incubated them with [U-^{13}C$_2$]acetate for 24 h (Figure **3.13** I). MID of NAA, citrate, glutamate, malate and fumarate showed that, indeed, the neuronal LUHMES cells can metabolize acetate. However, the proportion of labeling is very low, suggesting that the acetate taken up upon L-DOPA treatment is used for other purposes. As mentioned in section 3.1.2.1, acetate can be used as acetyl donor in neurons for membrane repair [160], it is therefore possible that acetate is directed towards fatty acid synthesis.
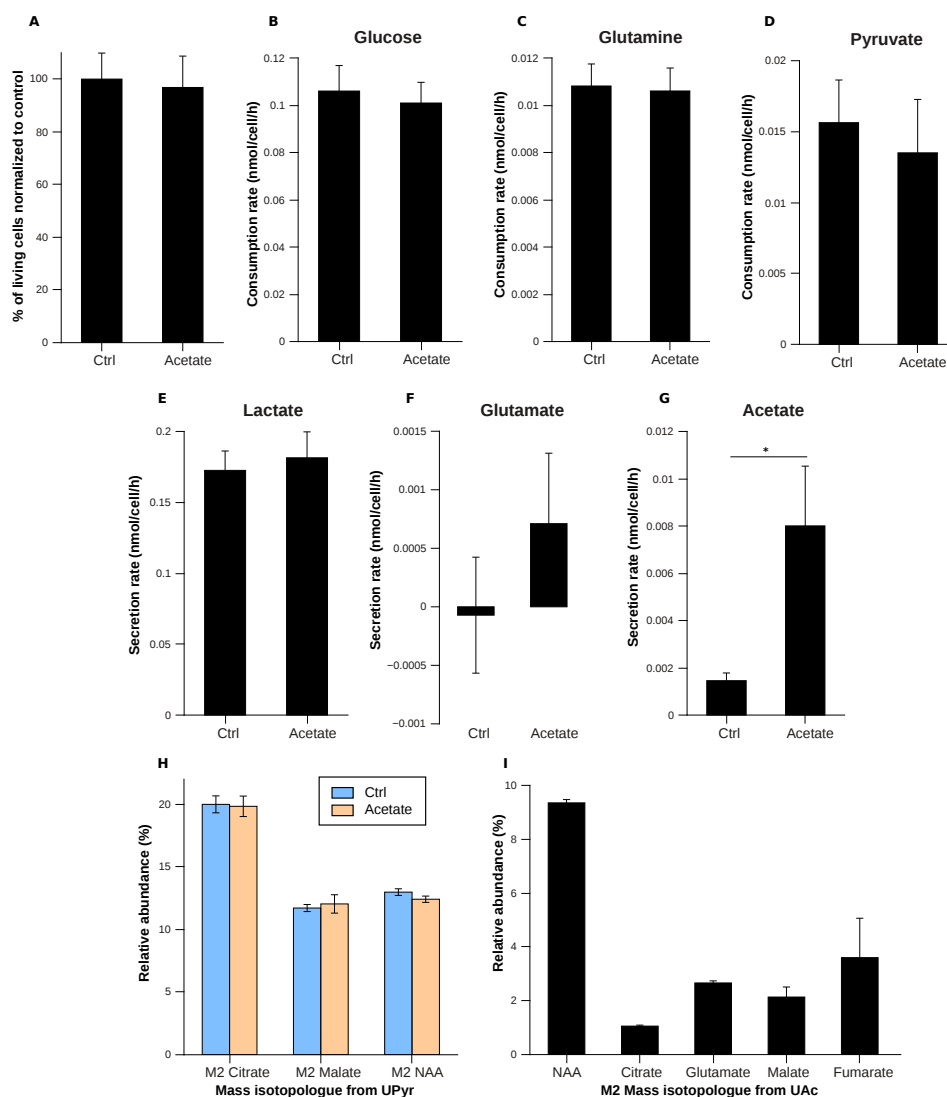
FIGURE 3.13: **Effects of acetate on uptake and secretion rates.** LUHMES cells were treated for 24 h with 800 μM acetate. **(A)**: The viability of treated cells was assayed. Uptake rates for glucose **(B)**, glutamine **(C)** and pyruvate **(D)**, and secretion rates for lactate **(E)**, glutamate **(F)** and acetate **(G)** were calculated. **(H)**: To evaluate if acetate modified the metabolism of the cells, they were incubated with [U-^{13}C$_3$]pyruvate (**UPyr**) in the presence or absence of acetate. M2 isotopomer for citrate, malate and N-acetyl-aspartate (**NAA**) are displayed. **(I):** To evaluate if LUHMES cells can use acetate as carbon source, they were incubated with 800 μM [U-^{13}C$_2$]Acetate (**UAc**) for 24 h. M2 isotopomer for NAA, citrate, glutamate, malate and fumarate are displayed. *: p-value <0.05 by Student t-test

In summary, I observed that L-DOPA treatment induced a decreased glucose and pyruvate consumption as well as lactate secretion, but increased the lactate over glucose ratio, indicating a decreased glycolytic activity but an increased conversion of glucose to lactate possibly for NAD$^+$ regeneration. While the uptake of glutamine did not change upon L-DOPA treatment, the concentration of glutamate in extracellular space highly increased. This increase is rather the result of decreased re-uptake through an

inhibition of glutamate transporters by ROS and quinones [186]. Increase in glutamate concentration in the extracellular space has also been associated with SDH inhibition [155], thus strengthening the idea that L-DOPA toxicity might be mediated through mitochondrial complex II inhibition. Upon L-DOPA treatment, LUHMES cells consumed acetate produced by the reaction of H_2O_2 with pyruvate, possibly for fatty acid synthesis. However, when incubated with acetate, LUHMES cells secreted it, indicating it could be used as carbon source under stress condition.

3.1.5 Effects of L-DOPA on inflammation

The *substantia nigra* possesses the highest microglial density in the brain. About 12% of the cells in this region are microglia, therefore rendering this brain area highly sensitive to immune system activation [197]. Microglial cells are of the same myeloid lineage as macrophages and are the resident immune cells of the brain. Upon activation, these cells release pro-inflammatory cytokines such as tumour necrosis factor alpha (TNFα), interleukine-1 beta (IL-1β), increase the expression of *iNOS* and the generation of ROS, which actively trigger apoptosis in neuronal cell culture [198]. Although the underlying mechanisms of PD are still unknown, it has been hypothesized that the progressive nature of the disease is caused by chronic neuro-inflammation [199]. In PD patients, levels of pro-inflammatory cytokines were elevated in peripheral blood mononuclear cells (PBMCs) [199] and in post-mortem analysis of the *substantia nigra* [198]. Moreover, the use of anti-inflammatory drugs has been associated with decreased risk of PD [197]. Loss of DJ-1 is associated with dopaminergic neuronal cell death and development of PD. Silencing of this gene in neurons increased their susceptibility to oxidative stress, while DJ-1 silencing in microglial BV-2 cells increased pro-inflammatory-associated markers without further stimulation [144].

The effects of neuromelanin (NM) on microglial cells have been investigated *in vivo* and *in vitro*. Viceconte *et al.* reported that synthetic NM triggers and inflammatory reaction in rat brain as well as in BV2 cells [200]. Wilms *et al.* used primary rat microglia to demonstrate that human-isolated NM caused an activation of these cells in a NF-*κ*B-dependent fashion [201]. Bortolanza *et al.* used rat models of PD to show that L-DOPA-induced dyskinesia is accompanied by an activation of glial cells. This activation was characterized by an activation of iNOS. Co-administration of L-DOPA and nitric oxide synthase (NOS) inhibitor could prevent the dyskinesia, therefore showing that NO plays a role in this side-effect of L-DOPA treatment [202].

I showed in section 3.1.1 that mouse immortalized microglial cells BV2 were sensitive to high L-DOPA concentrations. In this section, I investigated whether L-DOPA triggered an inflammatory response in these cells. Therefore, I treated the cells either (1) for 24 h with 50 μM L-DOPA alone, (2) 10 ng/mL lipopolysaccharide (LPS) for 6 h or (3) a combination of both where I added LPS 18 h after the L-DOPA treatment was initiated. I observed that LPS induced a pro-inflammatory response in BV2 cells as shown by the increase in levels of itaconate and succinate as well as increased gene expression of *TNFα*, *IL-1β* and *iNOS* (Figure **3.14**). Itaconate is a metabolic product derived from the TCA cycle and synthesized in macrophages and microglial cells upon pro-inflammatory activation. It has antimicrobial effects through inhibition of the glyoxylate shunt in bacteria [203]. Succinate accumulation is another marker of inflammatory response in macrophages [204]. L-DOPA alone induced a slight non-significant increase in itaconate and succinate levels, without affecting cytokine gene expression. A combination of L-DOPA and LPS did not induce a stronger or weaker inflammatory state than the one generated by LPS alone.
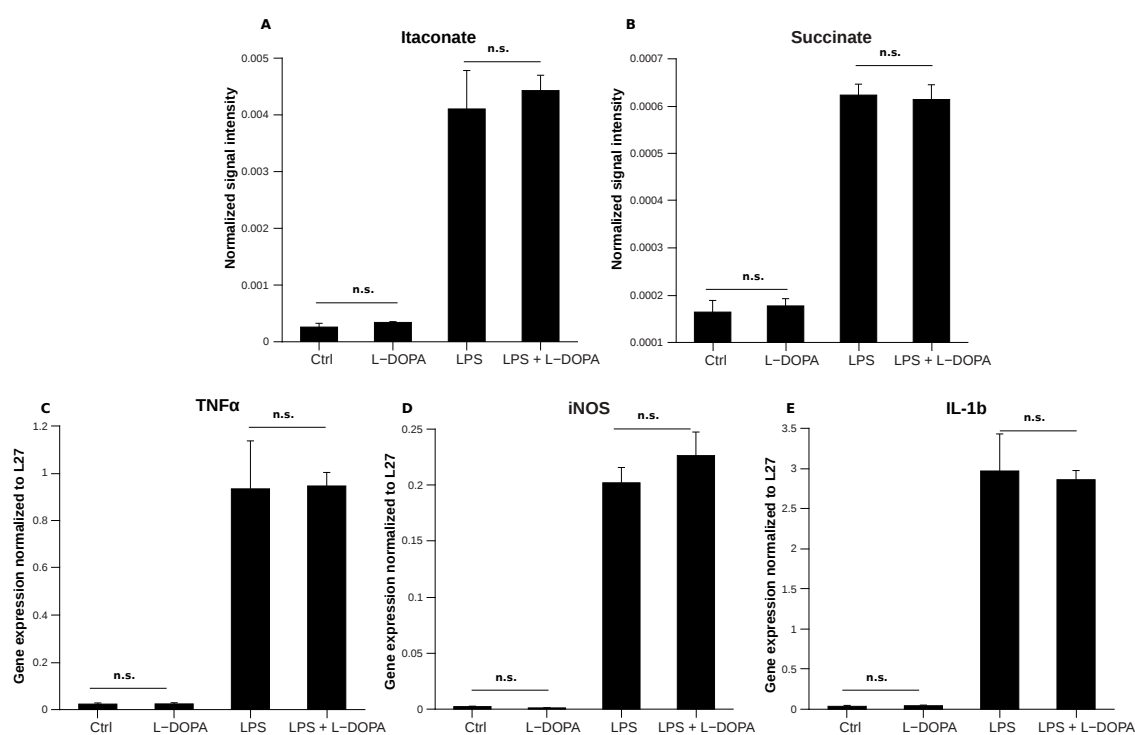

FIGURE 3.14: **Effects of L-DOPA on inflammation.** Mouse microglia BV2 cells were treated for 6 h with 10 ng/mL LPS, for 24 h with 50 μM L-DOPA or with a combination of both: cells were treated with L-DOPA and 18 h later, LPS was added for an additional 6 h. **(A)**: Itaconate levels. **(B)**: Succinate levels. Inflammation can also be viewed at the gene expression level: *TNFα* **(C)**, *iNOS* **(D)** and *IL-1β* **(E)** are displayed. *: p-value <0.05 by Student t-test, n.s.: not significant

In summary, I demonstrated that, in our experimental set up, L-DOPA did not induce an inflammatory response in quiescent cells and that concomitant L-DOPA and LPS stimulation did not induce a inflammatory profile different than in the case of LPS stimulation alone.

3.1.6 Summary: Effects of L-DOPA on the metabolism of TH-positive neurons

In this section, I studied the effects of L-DOPA, the most commonly used drug to treat PD, on the metabolism of the TH-positive neuronal cell model LUHMES. Elucidating the metabolic adaptation of neurons to this compound is of importance in order to understand the effects of L-DOPA and its derivatives on these cells. We first determined the effects of L-DOPA on the viability of cell lines of various origins, including human LUHMES immortalized mesencephalon, human SH-SY5Y neuroblastoma, human A549 lung cancer, human CFF-STTG1 astrocytoma, mouse BV2 immortalized microglia, mouse IMA2.1 immortalized and rat PC-12 pheochromocytoma cells. We could observe that the LUHMES cells were the most sensitive to this drug. This could be partly due to the fact that these cells are in a post-mitotic state. The sensitivity of the different cell lines did not appear to be organism specific: the human CFF-STTG1 cells did not die upon treatment. I also showed that preventing oxidation using AA, GSH, NAC or SOD prevented its toxicity. Application of the DOPA enantiomer D-DOPA did not modify cell viability indicating that the toxicity was independent of enzymatic action on L-DOPA. Moreover, oxidized L-DOPA was not toxic.

I revealed profound changes in the metabolism of LUHMES cells using a non-targeted metabolomics approach. The intracellular amounts of essential amino acids such as valine, leucine, isoleucine, lysine and phenylalanine increased while the amount of non-essential amino acids including alanine, serine and glycine decreased, which is indicative of a decreased protein synthesis. Levels of intermediates of the TCA cycle decreased except for succinate, which showed increased levels upon L-DOPA treatment. Labeling experiment showed that glucose contribution to lactate, alanine, serine, glycine and TCA cycle intermediates decreased upon treatment. Carbon contribution from pyruvate increased in lactate and alanine, while carbon contribution from glutamine increased in TCA cycle intermediates. Flux through the PPP was increased upon treatment indicating an increased need of NADPH. Fluxes through PDH and PC decreased as well as the TCA cycling activity, the reductive and oxidative glutamine metabolism. This indicated a strong reduction in TCA cycle activity.

The same treatment was performed in the absence of pyruvate to determine whether this metabolite is necessary for cell survival in the presence of L-DOPA, as it is the case under H_2O_2 treatment. Although the absence of pyruvate did not modify the cell viability upon L-DOPA treatment, it induced a significant increase in glucose contribution to lactate, but not to alanine. The TCA cycling activity further decreased and carbon contribution from glucose significantly decreased in citrate, malate and aspartate, while carbon contribution from glutamine increased in citrate and malate.

Uptake and secretion rates indicated that glucose and pyruvate uptake as well as lactate secretion decreased upon L-DOPA treatment. However, when calculating the ratio of lactate over glucose, it appeared that the amount of glucose directed to lactate production increased, while the carbon contribution from glucose to lactate decreased. This is due to the fact that although both uptake of glucose and secretion of lactate decreased upon treatment, the decrease in glucose uptake was stronger than the decrease in lactate secretion, leading to an increased ratio. Glutamine uptake was unchanged and glutamate secretion increased. The really strong secretion of glutamate biased the difference of glutamine uptake versus glutamate secretion towards a decreased glutamine anaplerosis into the TCA cycle. However, I observed an increased glutamine-derived carbon contribution to TCA cycle intermediates. These are not exclusive: carbon contribution is a relative value. Although the percentage of glutamine-derived carbon increased in TCA cycle intermediates, the amount of TCA cycle intermediates decreased (see Figure **3.4**). The absolute carbon contribution from glutamine to the different TCA cycle intermediates can be obtained by multiplying the relative carbon contribution with the signal intensity for each metabolite. The absolute carbon contribution from glutamine decreased in citrate, malate, fumarate and aspartate Appendix C.1.

Interestingly, there was an increase in the consumption of acetate, which was produced by the reaction of pyruvate and H_2O_2 (issued from L-DOPA auto-oxidation) in the medium. We could also show that the toxicity was not mediated through glutamate secretion nor acetate production. Moreover, when the cells were treated with acetate, they secreted acetate instead of consuming it.

I also profiled cellular metabolism after mitochondrial complex I and GAPDH inhibition and could show that none of these reproduced the changes observed upon L-DOPA treatment. A promising lead to investigate would be a mitochondrial complex

II inhibition, as shown by increased glutamine contribution to the TCA cycle, accumulation of succinate and increased glutamate secretion.

In the last part of this section, I evaluated whether L-DOPA induces an inflammatory response in mouse microglia BV2 and whether concomitant treatment of L-DOPA and LPS would induce a different inflammation profile than LPS alone. I showed that L-DOPA does not induce an inflammatory response in BV2 cells. It is possible that the increased inflammatory state observed in PD patients is initiated by dying neurons rather than from the L-DOPA itself.
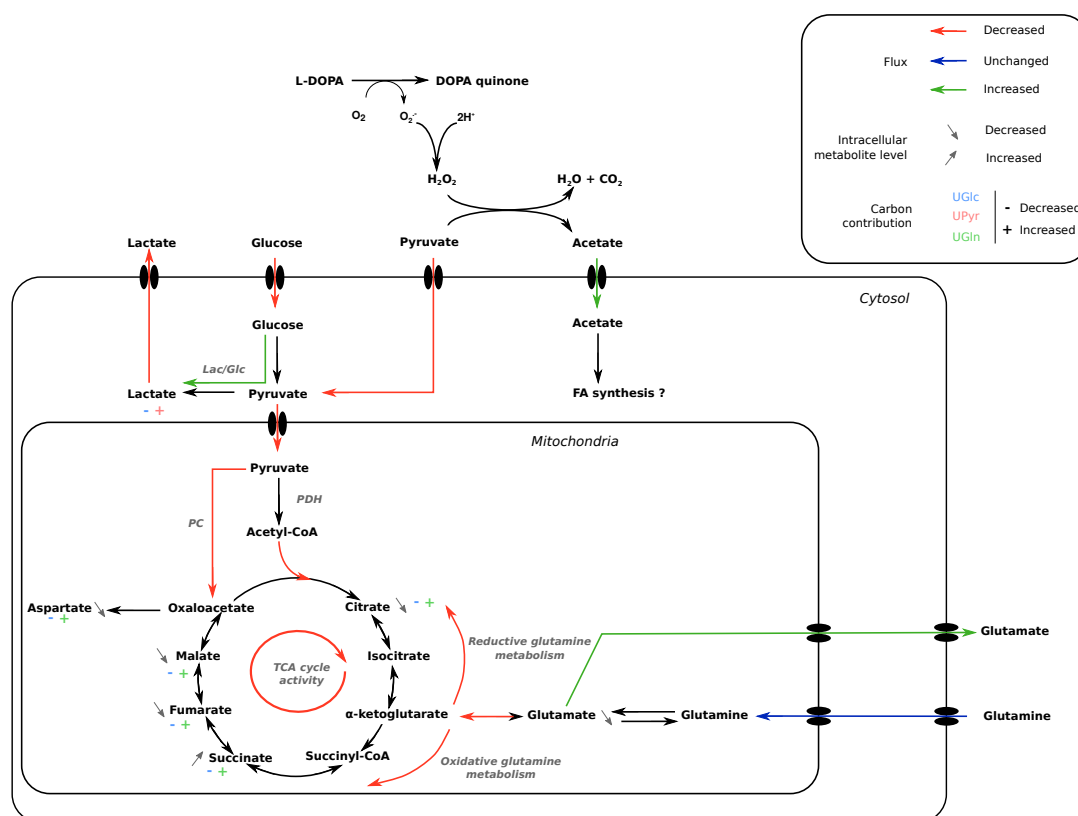

FIGURE 3.15: **Summary: the effects of L-DOPA.** Treatment of LUHMES cells with L-DOPA induced profound metabolic changes. (1) *At the uptake and secretion rate level:* a decrease in glucose, and pyruvate uptake rates, an unchanged uptake rate of glutamine and an increased uptake rate of acetate. It caused an increased secretion rate of glutamate, as well as a decreased secretion rate of lactate. Treatment decreased glutamine anaplerosis in the TCA cycle and increased the glucose to lactate conversion. (2) *At the metabolic flux level:* L-DOPA induced a decrease in the activity of pyruvate dehydrogenase complex (**PDH**) and pyruvate carboxylase (**PC**), a reduced TCA cycle activity as well as a decrease in oxidative and reductive glutamine metabolism. (3) *At the metabolite abundance level:* L-DOPA treatment caused a decrease in the amounts of TCA cycle intermediates citrate, glutamate, fumarate, malate and aspartate as well as an increase in the amount of succinate. (4) *At the carbon contribution level:* in lactate, contribution of glucose to lactate decreased upon treatment, while contribution of pyruvate increased. In all TCA cycle intermediates measured, carbon contribution from glucose decreased upon treatment, while carbon contribution from glutamine increased.

3.2   Generation of a human dopaminergic cell model

This section focuses on the generation of a human dopamine producing cell system. As mentioned in the introduction in section 1.2.4, to date, there exists no cell culture model of human origin derived from non-cancerous brain cells that produces DA. Such a system is of crucial importance in the scope of PD: the dopaminergic neurons selectively degenerate with the progression of the disease and DA is known to increase intracellular oxidative stress [93]. The most widely used systems include human SH-SY5Y neuroblastoma and rat PC-12 pheochromocytoma cells. The goal of this project was to use the human immortalized mesencephalon LUHMES cells to obtain such a model. These cells can be differentiated in post-mitotic neurons and express TH, the rate-limiting enzyme in the DA synthesis pathway. The first part of this section focuses on the comparison of available cell models. Then, in order to induce DA production in LUHMES and SH-SY5Y cells, I undertook a cloning approach to increase the expression of genes involved in DA synthesis.

3.2.1   Comparison with available systems

DA is synthesized from tyrosine in a two-step reaction: first, tyrosine is hydroxylated by TH to L-DOPA, which is then decarboxlated by AADC to DA. The activity of TH depends on the presence of a cofactor, $6R$-L-erythro-5,6,7,8-tetrahydrobiopterin (BH_4). The first and rate-limiting enzyme of the synthesis of this cofactor from guanosine triphosphate (GTP) is GTP cyclohydrolase 1 (GTPCH). Upon synthesis, DA is packaged into vesicles by the vesicular monoamine transporter 2 (VMAT2), where it is stabilized by a lower pH [205].

I first checked gene expression of *GTPCH*, *TH*, *AADC*, *VMAT2* in various cell lines. I compared the iPSC-derived dopaminergic neurons 17608/3 (differentiated by Peter Barbuti, Clinical and Experimental Neuroscience, LCSB) with LUHMES and SH-SY5Y cells (Figure **3.16** A-D). Only iPSC-derived dopaminergic neurons expressed all four genes. SH-SY5Y expressed *GTPCH* and *AADC*, but did not express *VMAT2* nor *TH*. LUHMES cells only expressed *TH*.

I compared protein synthesis of TH in iPSC-derived dopaminergic 17608/3 and SNCA3 (a A30P synuclein α (SNCA)-mutation carrier) with LUHMES, SH-SY5Y and PC-12 (Figure **3.16** E-F). The 17608/3 cells synthesized higher levels of TH than the

SNCA3 mutants, which produced similar levels to LUHMES cells. SH-SY5Y cells did not express any TH, while PC-12 cells had the highest expression.
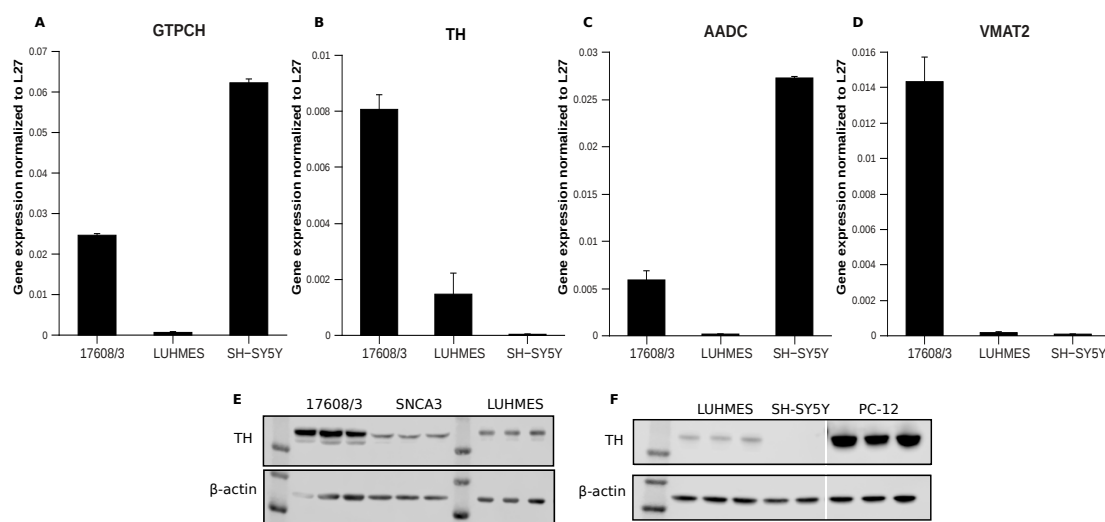

FIGURE 3.16: **Comparison of gene and protein expressions between the iPSC-derived dopaminergic neurons 17608/3, human LUHMES immortalized TH-positive neurons, human SH-SY5Y neuroblastoma and rat PC-12 pheochromocytoma cells.** Comparison of gene expression between 17608/3, LUHMES and SH-SY5Y for GTP-cyclohydrolase (*GTPCH*) **(A)**, tyrosine hydroxylase (*TH*) **(B)**, aromatic amino acid decarboxylase (*AADC*) **(C)** and vesicular monoamine transporter 2 (*VMAT*2) **(D)**. **(E)**: Protein expression of TH in 17608/3, iPSC-derived dopaminergic neurons carrying a α-synuclein mutation SNCA3 and LUHMES. **(F)**: Protein expression of TH in LUHMES, SH-SY5Y and PC-12 cells. Protein samples from the same box were loaded on the same membrane.

I measured DA levels in each cell line using a targeted and highly sensitive method by gas chromatography - mass spectrometry (GC-MS) (Figure **3.17** A). Metabolites were extracted from fully confluent wells in 12-well plates. I observed significant DA production in PC-12 cells and in iPSC-derived dopaminergic neurons 17608/3 cells. The compound was also detected in the SNCA3 cells, but to a much lesser extend. LUHMES and SH-SY5Y cells did not produce any detectable amounts of DA. To test whether AADC was active, I incubated SH-SY5Y and LUHMES cells in the presence of 50 μM L-DOPA for 2 h (Figure **3.17** B). Only SH-SY5Y produced DA by decarboxylation of L-DOPA.

In summary, the iPSC-derived dopaminergic cells are fully mature DA-producing cells. Their gene expression of catecholamine-related genes served as basis for gene expression in the model to be generated. PC-12 cells possessed the strongest TH expression and they produced DA. Gene expression for the considered genes was not
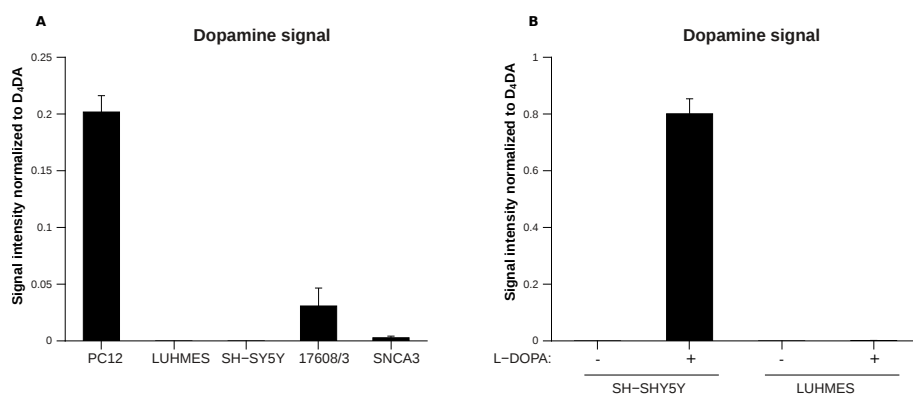
FIGURE 3.17: **Dopamine production across cell lines. (A):** Rat PC-12 pheochromocytoma, human LUHMES mesencephalon, human SH-SY5Y neuroblastoma, iPSC-derived dopaminergic neurons 17608/3 and SNCA3 were extracted. Dopamine could only be detected in PC-12 cells and in iPSC-derived dopaminergic neurons. **(B):** Upon 50 μM L-DOPA stimulation for 2 h on SH-SY5Y and LUHMES cells, only the SH-SY5Y cells produced detectable amounts of dopamine.

investigated in PC-12 because of primer incompatibility between organisms. In SH-SY5Y cells, the expressions of *AADC* and *GTPCH* were the strongest, but no TH was detected neither at gene nor at protein levels. The fact that L-DOPA was decarboxylated to DA indicated that AADC is active in SH-SY5Y. In this case, overexpression of TH may induce endogenous DA production. Finally, in LUHMES cells, only TH was expressed on both gene and protein levels. Moreover, DA synthesis could neither be detected with and without L-DOPA supplementation.

As depicted in Figure **3.17** B, LUHMES cells were incubated with L-DOPA to initiate DA production. I applied several other conditions to induce DA production, such as KCl for depolarization, AA to prevent DA oxidation or culture under 2% oxygen to better simulate the brain environment. Unfortunately, none of these were successful. I then engineered TH overexpressing cell lines using lentiviruses as delivery systems.

3.2.2 Genome engineering to increase gene expression in LUHMES and SH-SY5Y cells

3.2.2.1 TH overexpression in LUHMES and SH-SY5Y cells

SH-SY5Y cells are classically differentiated for 5 days using retinoic acid (RA) and low fetal bovine serum (FBS) [54]. Lopes *et al.* reported that the expression of TH is induced upon 4 days of differentiation, however, we could not detect any synthesis of

TH after 5 days of differentiation. Therefore, I used proliferating SH-SY5Y cells for the following experiments.

TH was the only enzyme of the synthesis pathway of DA missing in SH-SY5Y. Since it is the rate-limiting enzyme in the pathway, I hypothesized that increasing the expression of this enzyme in both LUHMES and SH-SY5Y cell lines could induce DA production. Therefore, the overexpression of this gene was introduced using a lentiviral system which integrated the target sequence into the DNA of the host. Transfected cells were then selected using blasticidine. As a control, I engineered constructs encoding the LacZ gene. The expressed proteins were coupled to a V5-tag, which allows for protein purification and separation of endogenous and overexpressed enzyme by western blot using a specific antibody. Both TH and LacZ overexpression were under the control of a cytomegalovirus (CMV) promoter. LUHMES and SH-SY5Y were seeded at the same density and infected with the same amount of viral particles. Cells overexpressing TH will be referred to as THox and cells overexpressing LacZ will be referred to as LacZox.

Figure **3.18** A-D presents gene and protein expressions of TH in SH-SY5Y and LUHMES cells. The expression of both were much stronger in SH-SY5Y compared to LUHMES cells. DA measurement (Figure **3.18** E) showed that TH overexpression was sufficient to induce endogenous DA production in SH-SY5Y, but not in LUHMES cells.

DA is synthesized from L-DOPA, which itself is produced from tyrosine. Tyrosine is a non-essential amino acid which, in mammals, can only be produced from phenylalanine or supplied by the diet [206]. Using the newly engineered SH-SY5Y THox cells, I characterized the origin of DA depending on substrate availability. I incubated the cells in Advanced DMEM/F12 prepared in house free of tyrosine and phenylalanine. The experiment was divided in four parts: cells were incubated for 24 h in medium containing (1) unlabeled tyrosine and phenylalanine, (2) [U-^{13}C$_9$]tyrosine and unlabeled phenylalanine, (3) unlabeled tyrosine and [U-^{13}C$_9$]phenylalanine and (4) [U-^{13}C$_9$]phenylalanine without tyrosine. This design allowed to evaluate which substrate is preferred and if phenylalanine can compensate for the absence of tyrosine. I observed that none of the conditions modified the amount of phenylalanine measured intracellularly (Figure **3.19** A). When tyrosine was excluded, the intracellular level of this metabolite significantly decreased (Figure **3.19** B) without affecting the total amount of DA produced under this condition (Figure **3.19** C). Figure **3.19** D-F shows the results
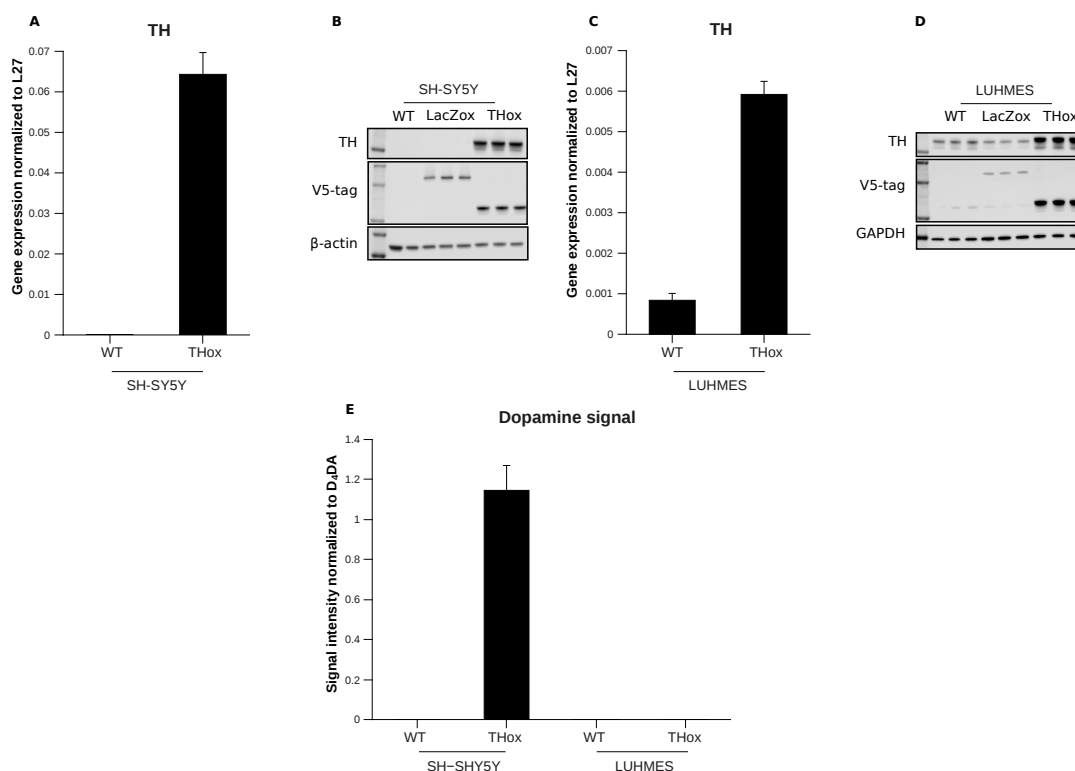
FIGURE 3.18: **TH overexpression in SH-SY5Y and LUHMES cells.** Tyrosine hydroxylase (**TH**) was overexpressed under the control of a CMV promoter. **(A)**: TH gene expression in SH-SY5Y wild type (**WT**) and TH overexpressing (**THox**) cells. The expression of the protein is coupled to a V5-tag which can also be detected by western blot. A vector expressing LacZ was used as control and was also coupled to a V5-tag. **(B)**: TH and V5-tag protein levels in SH-SY5Y WT and THox. **(C)**: TH gene expression in LUHMES WT and THox. **(D)**: TH and V5-tag protein levels in LUHMES WT and THox. **(E)**: Dopamine signal in WT and THox SH-SY5Y and LUHMES cells. Protein samples from the same box were loaded on the same membrane.

obtained from following the fate of each of the tracers. In the case where none of the precursor was labeled, the dopamine produced was totally unlabeled. When phenylalanine was labeled and tyrosine was present in the medium, no labeling in tyrosine nor DA was observed. When tyrosine was labeled, about 80% of the DA produced was labeled. Finally, when phenylalanine was labeled and tyrosine was omitted, about 80% of tyrosine and 75% of DA were labeled.

In SH-SY5Y THox cells, tyrosine was the preferred substrate for DA synthesis. In the absence of tyrosine, phenylalanine was used as substrate and the total amount of DA synthesized was the same as in the presence of tyrosine. However, phenylalanine did not replenish the total amount of tyrosine. Figure **3.19** G summarizes these findings. Fernstrom *et al.* reported that, in PC-12 cells as well as in rat dopaminergic
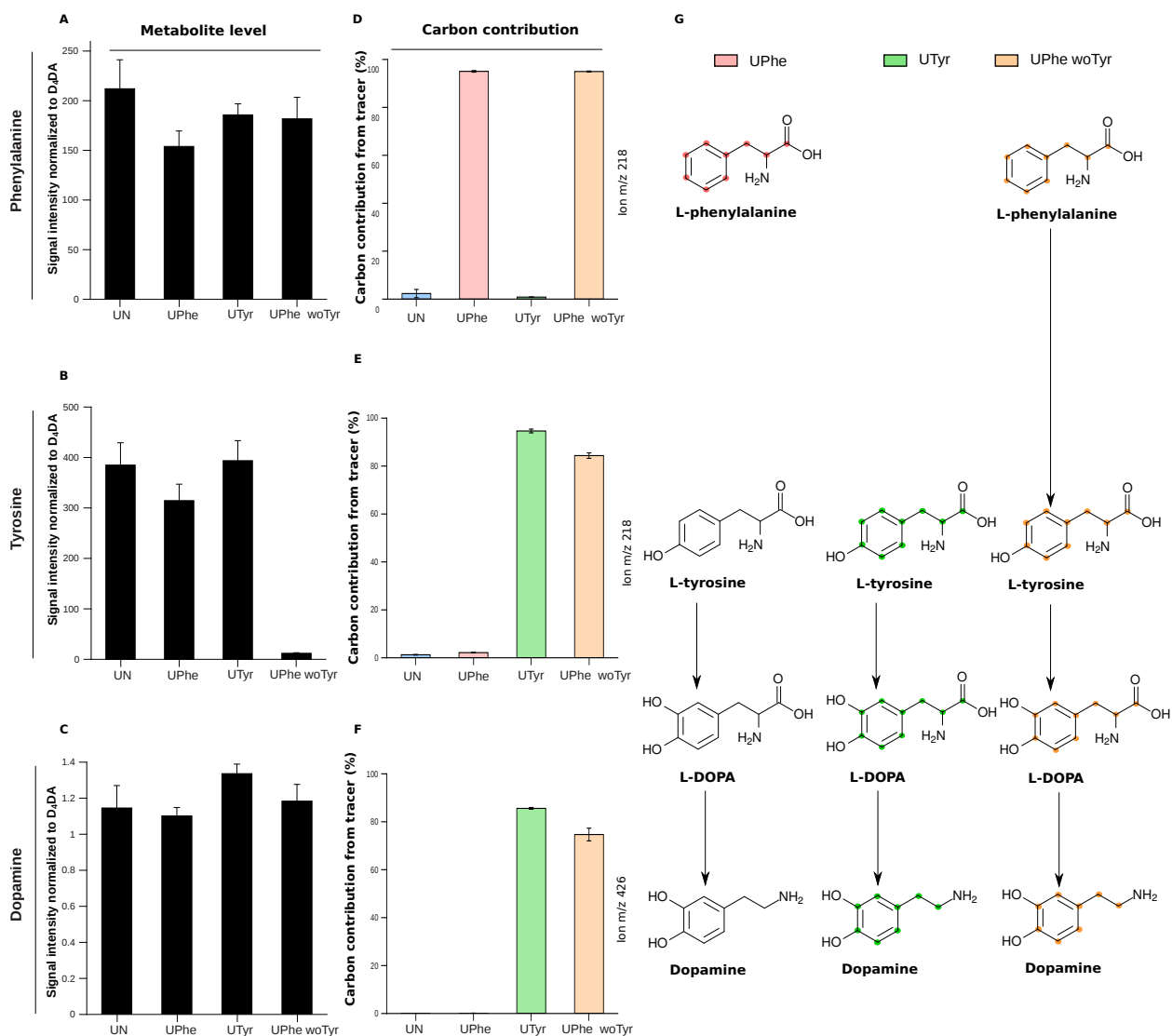
FIGURE 3.19: **Source of dopamine production.** SH-SY5Y cells overexpressing TH were culti-
vated for 24 h without any stable isotope tracer **(UN)**, with [U-^{13}C$_9$]phenylalanine in the pres-
ence of tyrosine in the medium **(UPhe)**, with [U-^{13}C$_9$]tyrosine in the presence of phenylalanine
in the medium **(UTyr)** or with [U-^{13}C$_9$]phenylalanine in the absence of tyrosine in the medium
(UPhe woTyr). **(A-C):** Intracellular amounts of phenylalanine, tyrosine and dopamine. **(D-F)**:
Carbon contribution from the different tracers in phenylalanine, tyrosine and dopamine. **(F)**:
From the labeling, the synthesis of dopamine is primarily issued from extracellular tyrosine.
However, in the absence of tyrosine, phenylalanine is used.

neurons issued from the retina, tyrosine is the preferred substrate for L-DOPA synthe-
sis. Phenylalanine was only used in the absence or at low concentrations of tyrosine
[207]. They also tested several combinations of tyrosine and phenylalanine concentra-
tions. They observed that higher tyrosine concentrations exerted a substrate inhibition
on TH, but only at low phenylalanine concentrations [207]. Kaborath *et al.* reported
that, in rat brain synaptosomes, phenylalanine hydroxylase (PheH) is not expressed.

This enzyme is responsible for the hydroxylation of phenylalanine to tyrosine and can be inhibited by D,L-*p*-chlorophenylalanine. However, this compound had no effect on the tyrosine synthesis suggesting that phenylalanine is hydroxylated by TH [208]. They also reported that the hydroxylation rate of tyrosine and phenylalanine by TH are similar [208].

In summary, upon overexpression of TH, SH-SY5Y produced DA. I showed that these cells use preferentially tyrosine for its synthesis and that phenylalanine can be used in the absence of tyrosine to produce the same amounts of DA. Both reactions are probably mediated by TH, which seems to have a higher affinity for tyrosine than phenylalanine. However, LUHMES cells did not produce any DA upon TH overexpression.

3.2.2.2   Time course differentiation of LUHMES cells

In their original description of the LUHMES cells, Scholz *et al.* reported that, although the LUHMES cells are considered to be mature from day 6 of differentiation, longer differentiation leads to increased TH expression [58]. I hypothesized that a longer differentiation of the LUHMES THox cells could increase TH expression and activity. This experiment was performed with the support of Xiangyi Dong. We differentiated LUHMES WT and THox cells for 0, 2, 6, 10 and 15 days and compared the expression of TH (Figure **3.20** A). As expected, no expression of TH was detected in WT cells at day 0 and 2 of differentiation. The protein was detected after 6 days of differentiation and its expression increased further after 10 days. However, after 15 days, the expression of TH started to decrease. Expression of TH in LUHMES THox cells was already detected after 2 days of differentiation. At day 6, two bands are discernible: the upper one corresponded to the overexpressed protein coupled to a V5-tag that rendered it slightly heavier, while the lower one corresponded to the endogenous TH. At day 10, TH expression was further increased. The expression of the TH construct stayed constant until day 15, while the intensity of the other band, corresponding to the endogenous TH, decreased. Metabolites were extracted after 10 days of differentiation in each cell line, but no DA was detected in any of them.

In the same article, Scholz *et al.* reported that cyclic adenosine monophosphate (cAMP) is essential to induce endogenous TH expression [58]. Since the overexpression of TH is under the control of a CMV promoter, I hypothesized that omitting dibutyryl cAMP (db-cAMP) would result in the exclusive expression of the engineered version
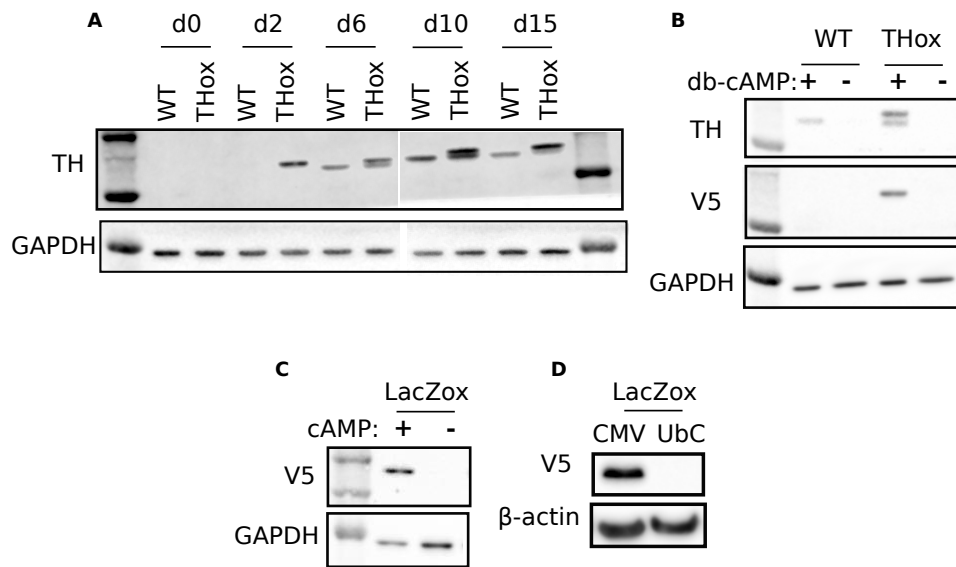
FIGURE 3.20: **Time course differentiation of LUHMES WT and THox cells. (A)**: TH protein expression for LUHMES WT and THox cells differentiated for 0, 2, 6, 10 and 15 days. **(B)**: TH and V5-tag protein expression of LUHMES WT and THox cells differentiated for 6 days in the presence of absence of cAMP. **(C)**: TH protein expression for LUHMES LacZox cells differentiated for 6 days in the presence or absence of db-cAMP. **(D)**: V5-tag protein expression of LUHMES cells overexpressing LacZox under the CMV or UbC promoter. Protein samples from the same box were loaded on the same membrane.

and no expression of endogenous TH. This would be of value to study mutant forms of TH in LUHMES. In order to test this, LUHMES WT and THox cells were differentiated with and without db-cAMP for 6 days and TH protein levels were assessed (Figure **3.20** B). For both cell lines, the absence of db-cAMP impaired TH protein synthesis. Lewis-Truffin *et al.* reported that cAMP regulates TH expression through activation of cAMP response element binding protein (CREB) [60]. Upon activation by cAMP, CREB binds to the cAMP response element (CRE) located at -45 bp in the 5' flanking region of TH and activates its transcription [60]. As expected, endogenous production of TH is absent when db-cAMP was omitted. Intriguingly, however, TH synthesis from the overexpression construct was affected as well.

Tank *et al.* and Chen *et al.* reported that cAMP can regulate TH at the post-transcriptional level [209, 210]. In their adrenal medulla and midbrain dopaminergic neuron models, they did not observe any change in TH mRNA levels upon db-cAMP supplementation. However, they observed increased TH protein levels. They hypothesized that poly-C binding protein (PCBP) is activated by cAMP and binds to the 3'UTR region of TH mRNA. The PCBP-TH mRNA complex can stabilize the mRNA and/or increase its association with polyribosomes leading to increased translation [209]. To

test whether or not TH is targeted for proteasomal degradation because it is not stabilized by PCBP, LUHMES cells overexpressing LacZ were differentiated for 6 days with or without db-cAMP (Figure **3.20** C). The results showed that the absence of db-cAMP lead to no expression of LacZ in those cells. As a consequence, I ruled out a post-translational modification as the reason why TH was not expressed in LUHMES THox cells.

Interestingly, CMV infections have been associated with neurological disorders in people with acquired immune deficiency syndrome (AIDS) as well as with impaired brain growth, mental retardation and progressive motor deficits in infants with congenital disorders [211]. Wheeler *et al.* investigated the mechanisms of CMV production in the brain and found that the CMV promoter possesses five CREs and that mutation in those sites cause a decrease in protein expression of 95% [211]. Thus, the induction of the overexpressed TH is initiated by cAMP at the transcriptional level and is necessary for its expression.

For all these reasons, the CMV promoter was not the most appropriate promoter for the selective study of overexpressed TH in LUHMES cells. Another available promoter is the ubiquitin C (UbC) promoter. Dittgen *et al.* reported that UbC was the best suited promoter for expression in cultured neurons [212] and Wilhelm *et al.* found that the expression of this promoter was specific for neurons [213]. To test this promoter, the LacZ gene was expressed under the control of the UbC promoter in LUHMES cells and the cells were selected with blasticidine. Cells were differentiated for 6 days and protein expression of LacZ using a V5-tag antibody was assessed (Figure **3.20** D). I could not observe any LacZ expression under the control of the UbC promoter. I can here rule out any issue with plasmid insertion into the host DNA since the cells were resistant to blasticidine. However, the gene of interest and the blasticidine-resistance gene are not controlled by the same promoter: the former is under the UbC promoter, while the latter is under the control of simian virus 40 (SV40) promoter (see Figure **B.3**). Therefore, it seems that the UbC promoter is not expressed in LUHMES cells. The reason for the low expression of the CMV promoter and the absence of expression of the UbC promoter in LUHMES cells could be due to promoter methylation. Herbst *et al.* studied the expression of green fluorescent protein (GFP) under the control of different promoters during the differentiation of cardiomyocytes [214]. Although the CMV promoter was expressed at all stages of differentiation, they observed a significant decrease of its expression due to heavy DNA methylation [214].

In the context of SH-SY5Y, the effects of cAMP on the cells are completely different. Cho *et al.* reported that 500 μM of db-cAMP increased cell proliferation rate in SH-SY5Y [215]. The CMV promoter can be activated by other factors than cAMP. Activator protein 1 (AP-1), which also regulates TH expression, has binding sites on the CMV promoter and can therefore activate it [216]. Moreover, Li *et al.* reported a cell type-specific expression of different promoters [217].

In summary, as demonstrated by Scholz *et al.*, the expression of TH in LUHMES cells depend on cAMP and its expression increased with longer differentiation [58]. I observed that TH expression was at maximum after 10 days of differentiation and decreased after day 15. When I overexpressed TH in LUHMES cells under the control of a CMV promoter, I already observed TH synthesis after 2 days of differentiation. As for the endogenous TH, I observed a maximal expression after day 10, but the expression of the construct did not decrease at day 15. Both, the endogenous TH and the engineered construct, depended on cAMP for their expression since both promoters possess CREs. Using a UbC promoter to control gene expression did not lead to any expression in the LUHMES cells although it was reported to be specific to neurons [212, 213].

3.2.2.3 LUHMES: AADC overexpression

As I demonstrated in Figure **3.16** C, LUHMES cells expressed really low levels of AADC. I also showed that, although TH is the rate-limiting enzyme in the DA synthesis pathway, increasing its expression did not lead to any DA production. I thus generated a LUHMES cell line overexpressing AADC, referred to as LUHMES AADCox.
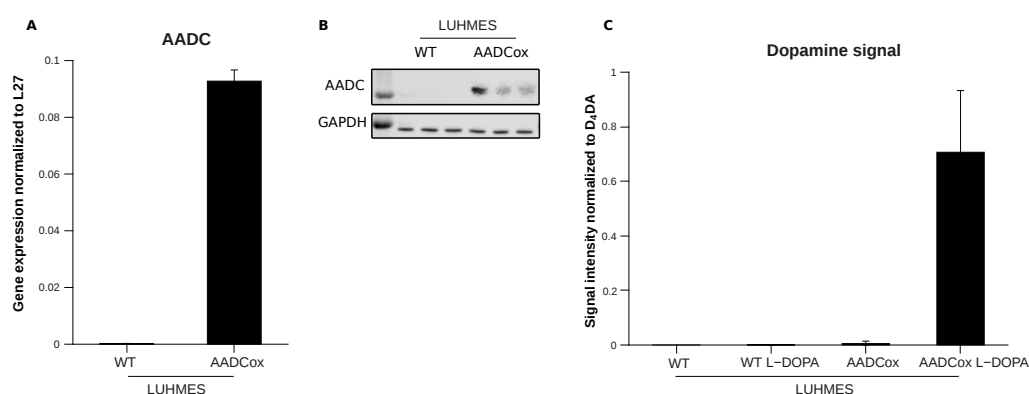

FIGURE 3.21: **AADC overexpression in LUHMES cells. (A)**: *AADC* gene expression levels in LUHMES WT and AADCox cells. **(B)**: AADC protein expression in LUHMES WT and AADCox cells. **(C)**: Dopamine signal in LUHMES WT and AADCox cells with and without 50 μM L-DOPA incubation for 2 h.

Figure **3.21** A and B show significant increase in gene expression and protein of AADC in LUHMES AADCox cells as compared to LUHMES WT. However, no DA signal was detected after metabolite extraction in these cells. To ascertain that the enzyme is active, I incubated LUHMES AADCox cells for 2 h with 50 μM L-DOPA (Figure **3.21** C). In that case, DA was detected in LUHMES AADCox cells, but not in LUHMES WT, indicating that the enzyme is active.

To further evaluate the activity of the enzyme, I incubated LUHMES AADCox with 50 μM L-DOPA for up to 6 h (Figure **3.22** A). DA could be detected as early as after five minutes of incubation and within one hour, the maximal DA production was reached. After four hours, the DA levels decreased slightly. There are several reasons which could explain this plateau. First, the DA synthesis reaches equilibrium with the rate of the enzymes degrading it, thus preventing any further accumulation. Second, the DA produced is secreted and this activates the dopamine receptors. This is supported by Berry *et al.* who reported that AADC activity is increased by dopamine receptor antagonists and its activity is decreased by dopamine receptor agonists [66]. It is highly unlikely that the amount of DA remained constant because of a lack of substrate. At the concentration of 50 μM in 1 mL of medium, this corresponded to a total of 50 nmol of L-DOPA in the medium at the beginning of the experiment, about a thousand-fold higher than the amount of DA intracellularly measured. In order to test whether the amount of DA obtained was the highest that could be produced, I treated LUHMES AADCox cells for 1 h (corresponding to the beginning of the plateau) with a range of L-DOPA concentrations from 50 to 600 μM (Figure **3.22** B). The fact that I obtained higher amounts of DA in this case, suggested that none of the previous hypothesis were correct. Increasing DA in function of L-DOPA concentrations could suggest a feed-forward stimulation: when the substrate concentration was high, the enzyme activity was high as well.

Since AADC is not the rate-limiting enzyme in the CA synthesis pathway, it has been considered as unregulated for a long time [65]. However, Berry *et al.* suggested that the enzyme can be phosphorylated which increases its activity [66]. It is therefore possible that increasing L-DOPA concentrations induce phosphorylation of AADC and increase its activity.
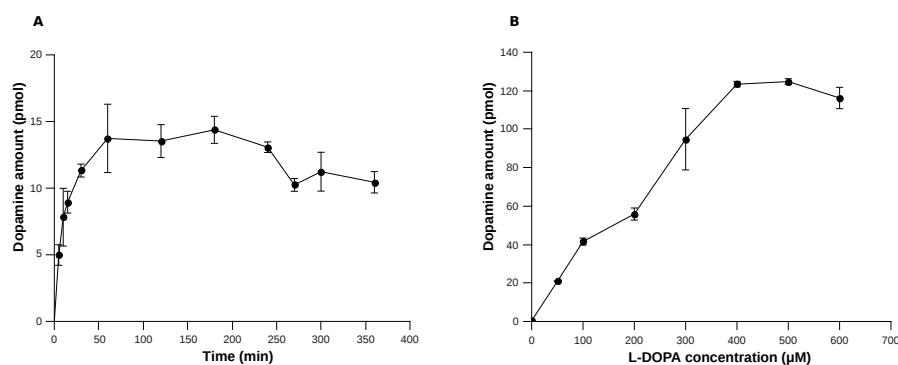
FIGURE 3.22: **Dopamine production in function of time and L-DOPA concentration. (A)**: LUHMES AADCox were treated with 50 μM L-DOPA for 0 to 350 min. **(B)**: LUHMES AADCox cells were treated for 1 h with different L-DOPA concentrations.

In summary, I observed that although AADC expression did not induce endogenous DA production, LUHMES AADCox cells produced DA upon L-DOPA supplementation. The amounts of DA produced were time- and concentration-dependent and reached saturation for longer incubation times and concentrations.

3.2.3 L-DOPA transport in LUHMES cells

The transport of L-DOPA across the blood brain barrier (BBB) has been widely studied [218, 219]. It is mediated by the large amino acid transporter (LAT)1 which transports branched-chain and aromatic amino acids [218]. The expression of LAT1 is restricted to certain tissues such as the brain, placenta or testis [220]. In order to be active, it forms a heterodimeric complex with the heavy chain of 4F2 cell surface antigen (4F2hc) [218] and functions as antiport by exporting glutamine and importing large amino acids [221]. Aside from the BBB, L-DOPA has been shown to be transported via the LAT1 in a porcine renal tubule epithelial cell line [44], teratocarcinoma cells [222] and in human bladder carcinoma cells [220]. However, L-DOPA transport in neurons has been poorly studied. On the one hand, studies have been performed *in vivo*, which makes it difficult to study transport in a particular cell type. On the other hand, the study of L-DOPA *in vitro* has focused on the toxicity of the compound and not on its transport [223]. Sampiao-Maia *et al.* reported that LAT1 is responsible for L-DOPA transport in the mouse neuroblastoma Neuro2A cells [223].

Dopamine transporter (DAT) is responsible for regulating the duration and intensity of DA neurotransmission by rapid re-uptake of DA from the synaptic cleft. Jones *et al.* reported that loss of DAT is associated with a 95% reduction in DA content in

the *striatum* as well as with a 75% reduction in its release. However, extracellular DA levels increased five times due to lack of clearance system [224]. This shows that DAT indirectly regulates intracellular DA levels.
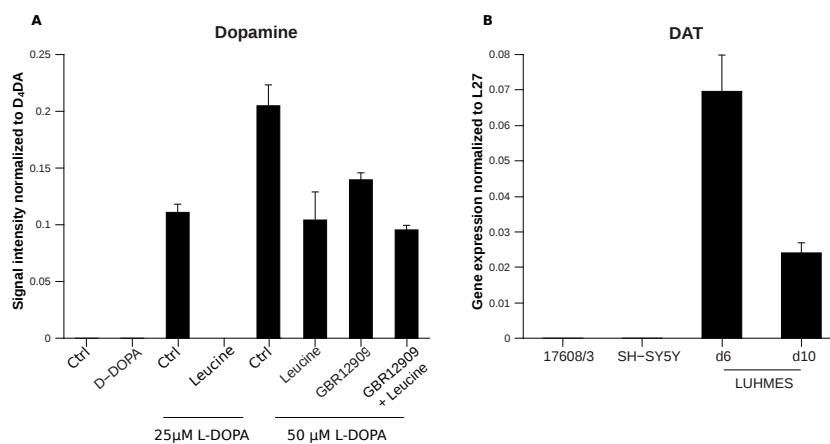

FIGURE 3.23: **Characterization of L-DOPA uptake in LUHMES AADCox cells. (A)**: LUHMES AADCox cells were treated for 1 h with 50 µM D-DOPA, L-DOPA alone or supplemented with 5 µM GBR12909, 1 mM leucine or a combination of both or with 25 µM L-DOPA with or without leucine. **(B)**: Gene expression of the DAT in iPSC-derived dopaminergic 17608/3 cells, SH-SY5Y cells and LUHMES cells after 6 and 10 days of differentiation.

The LUHMES AADCox cells are a good model to study L-DOPA uptake and the response of inhibitors on the metabolism of DA: having a functional AADC, the production of DA can easily be monitored. Therefore, I used these cells to improve our knowledge of L-DOPA transport in LUHMES cells. The uptake of L-DOPA through the LAT1 can be inhibited by substrate competition using 1 mM L-leucine [44]. In rat fetal midbrain neurons, DAT can be inhibited by 5 µM of GBR12909 [225]. I incubated LUHMES AADCox cells for 1 h with (1) 50 µM D-DOPA, (2) 25 µM L-DOPA supplemented or not with 1 mM leucine, (3) 50 µM L-DOPA supplemented with 1 mM leucine, 5 µM GBR12909 or a combination of both (Figure **3.23** A). The supplementation with D-DOPA served as control, since this L-DOPA enantiomer cannot be enzymatically processed. In agreement with Shindo *et al.*, I did not observe DA production from D-DOPA [146]. However, treatment with 25 µM L-DOPA induced DA production, which was completely prevented by competitive inhibition of LAT1 with 1 mM leucine. When the cells were treated with 50 µM L-DOPA, leucine supplementation induced a 50% decrease in DA production. The levels of intracellular DA measured upon DAT inhibition by GBR12909 were decreased by 30%. The combination of leucine and GBR12909 was not additive and the levels of DA measured were the same as those measured upon leucine treatment alone.

These data confirmed the observation made by Sampaio-Maia *et al.* in Neuro2A cells [223] that L-DOPA is transported into LUHMES via the LAT1 transporter. I also observed that 1 mM leucine is enough to completely prevent DA synthesis in medium containing 25 μM L-DOPA and that the same concentration of leucine decreased DA production by a factor of two in cells treated with 50 μM L-DOPA. DAT is selective for DA, but can also participate in the transport of synthetic and natural analogues, such as MPP^+, its pyridine derivatives, isoquinoline derivatives or β-carbinoline derivatives [74]. It is a symporter that translocates one molecule of DA, two sodium and one chloride ions across the membrane. Its major physiological role is to terminate neurotransmission by re-uptake of DA from the synaptic cleft [74]. In mammalian cells, DAT expression is restricted to dopaminergic neurons [74]. It is highly expressed in LUHMES cells at day 6 of differentiation, but its expression decreased at day 10 of differentiation. iPSC-derived dopaminergic neurons and SH-SY5Y did not express DAT at all (Figure **3.23** B). The decreased DA levels observed upon GBR12909 treatment could be due to a decreased re-uptake of DA rather than a decreased uptake of L-DOPA. The decreased re-uptake of DA could have been evaluated by extracting DA from medium. Moreover, loss of DAT has been linked to ageing: the decline of striatal DAT is about 6-7% per decade. DAT neuroimaging is used in the context of PD to evaluate the loss of dopaminergic neurons [226], therefore highlighting its importance. The importance of DAT in the context of PD is not fully elucidated yet: Nutt *et al.* reported that treating PD patients with a DAT inhibitor prolonged the effects of co-administered L-DOPA. However, it also prolonged the duration of dyskinesia [227].

Interestingly, the effects of LAT1 and DAT inhibitions were not additive. One hypothesis could be that upon inhibition of L-DOPA transport by leucine, the amounts of DA produced are not sufficient to induce an active re-uptake by DAT. Therefore, the inactivation of this transport does not change the intracellular levels of DA. This could be verified by treating LUHMES AADCox cells with 25 μM L-DOPA in combination with GBR12909. If the levels of DA do not change, this would confirm our hypothesis.

In summary, in contrary to iPSC-derived dopaminergic neurons and SH-SY5Y cells, LUHMES cells express the DAT. Its expression was the highest after 6 days of differentiation and decreased after 10 days. DA production from supplemented L-DOPA was inhibited by competitive inhibition of LAT1 using leucine, confirming that L-DOPA transport is carried through the LAT1. I could also confirm that the DAT is

active in LUHMES cells since its inhibition using GBR12909 caused a decrease in intracellular amounts of DA.

3.2.4   L-DOPA toxicity on dopamine producing cells and upon L-DOPA uptake inhibition

In section 3.1.1, we evaluated the toxicity of L-DOPA in LUHMES WT cells. The LUHMES AADCox produced DA upon L-DOPA supplementation. In the brain, upon synthesis, DA is packaged into synaptic vesicles. These vesicles have a pH of 5.5, which stabilizes DA and therefore prevents its auto-oxidation. We showed in section 3.1.1 that the effects of L-DOPA are due to its auto-oxidation in the extracellular space. In order to strengthen this affirmation, I first tested whether the production of DA from L-DOPA modified their sensitivity to L-DOPA. If the effect is intracellular, the fact that L-DOPA can be decarboxylated to DA could trigger its packaging and therefore decrease its toxicity. Therefore, I treated LUHMES WT and AADCox cells for 24 h with different L-DOPA concentrations (Figure **3.24** A). The sensitivity to L-DOPA was identical in both cell lines, indicating that DA did not play a role in the L-DOPA-mediated toxicity. However, in this case, I cannot rule out the fact that DA also auto-oxidizes in the cells since LUHMES cells did not express VMAT2.
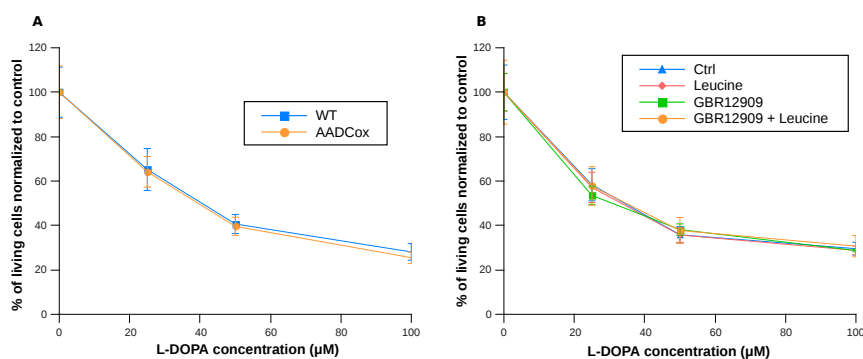

FIGURE 3.24: **Effects of L-DOPA on LUHMES AADCox and on LUHMES WT under inhibition of L-DOPA uptake. (A)**: LUHMES WT and AADCox cells were treated for 24 h with various L-DOPA concentrations and cell viability was assayed. **(B)**: LUHMES WT cells were treated for 24 h with various L-DOPA concentrations alone or supplemented with 5 μM GBR12909, 1 mM leucine or a combination of both and cell viability was assayed.

I performed a final assay to ascertain extracellular effects of L-DOPA. If the effects are extracellular, preventing or reducing L-DOPA uptake should not modify the sensitivity to the treatment. I demonstrated in section 3.2.3 that uptake of L-DOPA can be reduced by 1 mM leucine. I also observed that GBR12909 decreased DA levels intracellularly, potentially by preventing its re-uptake. Therefore, I treated LUHMES

WT cells for 24 h with different concentrations of L-DOPA and with 1 mM leucine, 5 μM GBR12909 or a combination of both (Figure **3.24** B). As expected, the inhibition of GBR12909 did not lead to any change in cell viability: in those cells, AADC is not active, thus L-DOPA is not converted to DA. I could also observe that preventing L-DOPA entry into the cells did not protect against L-DOPA toxicity. As seen in 3.23 A, incubation of 25 μM L-DOPA in combination with 1mM leucine (to inhibit L-DOPA uptake through LAT) did not lead to any detectable amounts of DA in LUHMES AADCox cells, indicating that its uptake is almost completely inhibited. Therefore, preventing or decreasing L-DOPA uptake did not lead to any change in the sensitivity to L-DOPA-mediated toxicity.

In summary, neither the capacity to process L-DOPA to DA nor the decreased capacity to take up L-DOPA lead to any change in sensitivity to L-DOPA treatment. These data strongly support the idea that L-DOPA-mediated toxicity is not due to L-DOPA itself, but rather to its degradation products from oxidation in the extracellular matrix.

3.2.5 Co-factor supplementation

TH is assumed to be the rate-limiting enzyme in the DA synthesis pathway. Rat brain synaptosomes do not express PheH while TH, which hydroxylates tyrosine to L-DOPA, has been reported to also hydroxylate phenylalanine to tyrosine [208]. Tyrosine is more stable than L-DOPA and thus can be measured in a more accurate way. I therefore applied phenylalanine as substrate for this experiment. To test whether LUHMES WT cells can hydroxylate phenylalanine to tyrosine and therefore evaluate whether TH is active in these cells, I incubated the cells for 24 h in unlabeled medium or in medium free of tyrosine and supplemented with [U-^{13}C$_9$]phenylalanine, at twice the concentration present in Advanced DMEM/F12 (i.e. 430 μM) (Figure **3.25**). Levels of tyrosine and phenylalanine were measured (Figure **3.25** A, B). Levels of phenylalanine were higher in the [U-^{13}C$_9$]phenylalanine treated cells, in accordance with the fact that cells were treated with higher concentrations. Tyrosine levels strongly decreased in the absence of tyrosine (Figure **3.25** A), as observed in SH-SY5Y cells in Figure **3.19** B. Concerning labeling data, upon treatment with [U-^{13}C$_9$]phenylalanine, almost all the phenylalanine was labeled (Figure **3.25** C), while none of the tyrosine was labeled (Figure **3.25** D), suggesting that TH is not active.
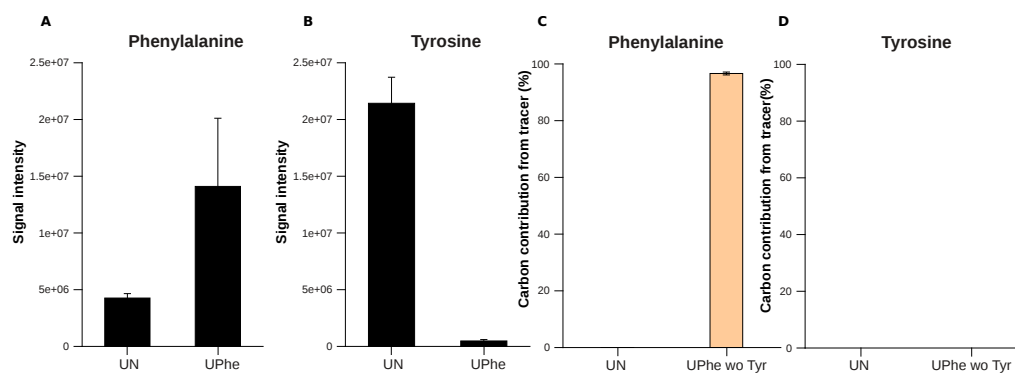
FIGURE 3.25: **Tyrosine hydroxylase activity in LUHMES cells.** LUHMES WT cells were treated for 24 h with regular medium (**UN**) or with medium free of tyrosine and containing [U-$^{13}C_9$]phenylalanine (**UPhe**). **(A)**: Intracellular levels of phenylalanine. **(B)**: Intracellular levels of tyrosine. **(C)**: Carbon contribution in phenylalanine. **(D)**: Carbon contribution of phenylalanine in tyrosine.

The absence of labeling in tyrosine, indicating that TH is inactive, taken together with the low GTPCH gene expression (Figure **3.16** A), could indicate that BH_4, the co-factor of TH, is absent. Sawabe *et al.* reported that sepiapterin, one of the intermediates in BH_4 synthesis, is much more permeable across the cell membrane than BH_4. Upon treatment with sepiapterin or BH_4, they observed an accumulation of sepiapterin in RBL2H3 rat basophilic leukemia cell line, but extremely low levels of BH_4 in the cells [228]. To test whether BH_4 is the limiting step in endogenous DA synthesis in LUHMES AADCox cells, I used sepiapterin for its membrane permeability properties. Once inside the cells, it is metabolized to BH_4 by sepiapterin reductase (SR) and dihydrofolate reductase (DHFR) via the BH_4 salvage pathway (see Figure **1.6**). I supplemented LUHMES AADCox cells with various concentrations of sepiapterin (100 to 600 μM) for 5 h and extracted metabolites. If the two enzymes responsible for sepiapterin metabolism are active and BH_4 is synthesized, this should lead to activation of TH and DA production. However, no DA could be measured.

I cannot exclude that SR or DHFR, the enzymes responsible for the conversion of sepiapterin to BH_4, were inactive in LUHMES cells. Harding *et al.* reported that BH_4 accumulated in primary mouse myotubes and reached a maximum after 30 min [229]. To evaluate whether direct BH_4 supplementation could lead to TH activation and DA production in LUHMES AADCox cells, I incubated them with the cofactor. I supplemented LUHMES AADCox cells differentiated for 10 days, corresponding to the higher TH expression, for 30 min with 100 and 200 μM BH_4 and extracted metabolites for DA measurement. No dopamine could be measured under these conditions.

In summary, I observed that in LUHMES WT cells, TH did not hydroxylate phenylalanine to tyrosine, suggesting that the enzyme is inactive. As observed in section 3.2.1, the gene expression of GTPCH is very low. In order to bypass this reaction and to assess whether BH_4, the cofactor for TH activity, is missing in LUHMES AADCox, I supplemented the cells with the cofactor or its precursor. Unfortunately, this did not lead to an activation of TH and production of DA.

3.2.6 Summary: Generation of a human dopaminergic cell model

This section focused on the generation of a human dopaminergic cell model. Such a model is of critical importance in the scope of the study of neurodegenerative disease. Most of the available cell models are of cancer origin or derived from other organisms than human. Given the organism-specific regulation of enzymes involved in DA synthesis and degradation as well as the proliferative character of cancer cells, such models are not the best suited to study the metabolism of neurons. Human TH exists in four isoforms. From these, isoforms 1 and 2 are predominantly expressed in the brain. Other primates possess two isoforms, while rodents possess only one [205]. The coding region also slightly differs: rodent TH can be phosphorylated at serine 8, 19, 31 and 40. However, in human, position 8 contains a threonine, which cannot be phosphorylated, therefore emphasizing the organism-specific regulation of the enzyme [51].

I focused on the LUHMES cells, derived from the mesencephalon of a eight-week old foetus and conditionally immortalized using a v-myc vector. I compared gene expression levels of *GTPCH*, *AADC*, *TH* and *VMAT2* with those of human SH-SY5Y neuroblastoma and iPSC-derived dopaminergic neurons. iPSC-derived dopaminergic neurons expressed all these genes, while SH-SY5Y expressed neither *TH* nor *VMAT2* and LUHMES cells only expressed *TH*. At protein synthesis level, LUHMES, iPSC-derived dopaminergic neurons and rat PC-12 pheochromocytoma expressed TH while it was absent in SH-SY5Y cells. DA measurements showed that only PC-12 and iPSC-derived dopaminergic neurons produced endogenous DA. SH-SY5Y produced DA upon L-DOPA supplementation, while LUHMES cells did not produce any DA, with or without addition of L-DOPA.

To increase the expression of *TH* in both SH-SY5Y and LUHMES cells, I engineered cell lines overexpressing *TH*. This was sufficient to induce DA production in SH-SY5Y, but not in LUHMES cells. I then used the SH-SY5Y THox cells to demonstrate that these cells preferentially use tyrosine for DA synthesis. Furthermore, in the absence of

tyrosine, they were able to use phenylalanine as substrate. A time course differentiation of LUHMES WT and THox cells showed that TH expression is maximal after 10 days of differentiation and that both the endogenous TH as well as the gene overexpressed under the CMV promoter are under cAMP regulation. The UbC promoter did not lead to any gene expression in LUHMES cells.

I increased the expression of AADC in LUHMES cells to evaluate whether the absence of AADC expression is the missing link for DA production in LUHMES. These cells did not produce any endogenous DA, but produced the neurotransmitter upon incubation with L-DOPA. In this case, DA production was time- and concentration-dependent. I then used these cells to characterize L-DOPA transport in LUHMES cells. I observed that it is LAT1-dependent and that 1 mM of leucine completely abrogated the production of DA when the cells were incubated with 25 μM L-DOPA. Inhibition of the DAT also lead to decreased intracellular DA levels through a decreased DA re-uptake. Interestingly, the effects of LAT1 and DAT inhibition were not additive.

To evaluate whether the capacity of LUHMES AADCox cells to produce DA from L-DOPA would modify their sensitivity to L-DOPA treatment, LUHMES WT and AADCox cells were treated with various concentrations of L-DOPA. The results showed that the ability to degrade L-DOPA to DA did not modify the toxicity of the compound, suggesting that either DA is as toxic as L-DOPA or that the cell viability is primarily affected by oxidation products produced in the extracellular space. To finally confirm this hypothesis, LUHMES WT cells were treated with LAT1 and DAT inhibitors and the results showed that preventing L-DOPA uptake did not affect cell viability. This finally ascertained that the toxic effects of L-DOPA are mediated by its auto-oxidation in extracellular space.

The overexpression of AADC lead to a system able to produce DA upon L-DOPA supplementation. In order to test whether in this case endogenous TH is active, LUHMES WT cells were incubated with a phenylalanine tracer in the absence of tyrosine. PheH has been reported absent in synaptosomes and TH can hydroxylate tyrosine. Moreover, tyrosine is more stable than L-DOPA. I therefore used this system to study TH activity. The results showed that there was no hydroxylation of phenyl-alanine to tyrosine (this hydroxylation was observed in SH-SY5Y THox cells). I thus supplemented LUHMES AADCox cells with BH_4, the cofactor of TH or its precursor, sepiapterin, to circumvent the low expression levels of GTPCH. None of these lead to DA production.

The new LUHMES AADCox cells could be of interest to study the effects of increased AADC expression on the metabolism of neuronal cells. Bankiewicz *et al.* reported that using an adeno-associated virus to overexpress AADC in monkeys lead to an improvement in clinical rating scores and decreased L-DOPA requirements as well as reduced L-DOPA associated side-effects [230]. Mittmeyer *et al.* launched a phase 1 clinical trial using adeno-associated virus overexpression of AADC and found that the overexpression persisted over four years and that although the clinical rating improved over the first twelve months, a slow deterioration was observed over time [231]. This highlights the need to understand the effects of AADC overexpression on the metabolism of neurons.

It is also interesting to note that the basal forebrain, *striatum* and cortical areas contain cell populations of TH-positive neurons that are not expressing AADC and do not produce CA. However, these cells were not reported to be present in the mesencephalon [36].

To conclude, the expression of TH is not sufficient to obtain a DA-producing cell system. A summary of the models used as well as the expression and activity of enzymes tested and the resulting DA production can be found in Figure **3.26**.
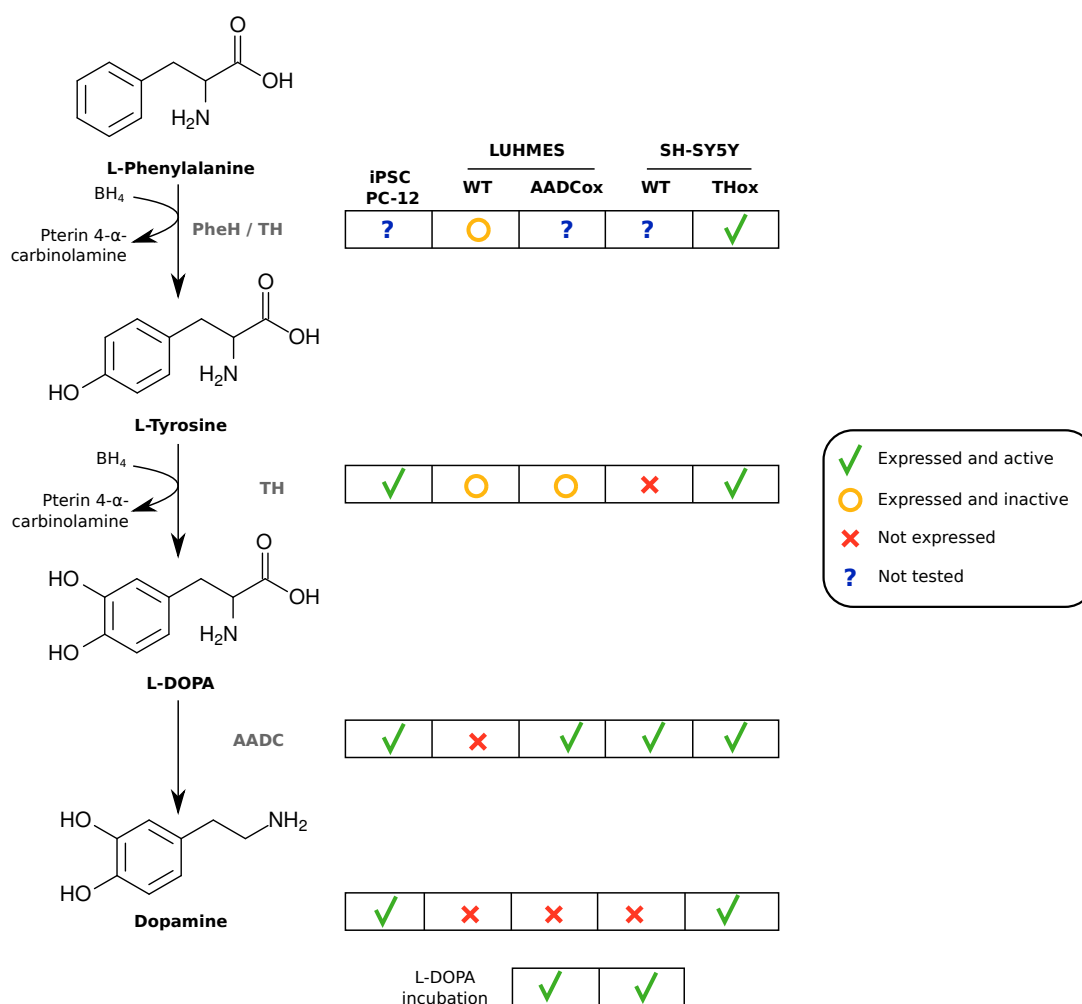
FIGURE 3.26: **Summary: DA-producing systems.** Dopaminergic neurons derived from iPSC as well as PC-12 cells produced DA without further stimulation. LUHMES WT cells expressed only TH, but it was not active. Upon overexpression of AADC, LUHMES AADCox cells produced DA when incubated with L-DOPA. SH-SY5Y WT cells expressed AADC, but did not express TH and did not produce DA. Upon overexpression of TH, SH-SY5Y THox produced DA without further stimulation.

Conclusion and Perspectives

In this work, I first investigated the effects of 2,3-dihydroxy-L-phenylalanine (L-DOPA) on the metabolism of the human tyrosine hydroxylase (TH)-positive LUHMES neuronal cells. I demonstrated that this drug, which is commonly used to cope with the symptoms of Parkinson's disease (PD), is toxic to these cells and that antioxidant treatment can rescue the toxicity. I also established that L-DOPA induced profound changes on the metabolism of LUHMES cells. Indeed, glucose contribution to the tricarboxylic acid (TCA) cycle decreased while glutamine carbon contribution increased upon treatment. Contribution of glucose to lactate decreased, while pyruvate carbon contribution increased. Pyruvate was not essential for cell survival under L-DOPA treatment. In addition, I demonstrated that the effect observed was not due to glyceraldehyde-3-phosphate dehydrogenase (GAPDH) nor mitochondrial complex I inhibition. The observed accumulation of intracellular succinate, the increase in secretion of glutamate and the increase in uptake of acetate point towards a mitochondrial complex II inhibition. To test this hypothesis, a further experiment would be to treat LUHMES cells with 3-nitropropionic acid (3-NP) or malonate, which are inhibitors of mitochondrial complex II.

It is also interesting to note that LUHMES cells consumed acetate upon L-DOPA treatment although the literature suggests that acetate is a substrate used by astrocytes. Upon treatment, acetate is generated through the non-enzymatic and extracellular reaction of pyruvate with H_2O_2 derived from L-DOPA auto-oxidation. After its uptake, acetate can be converted to acetyl-CoA and either be directed towards the TCA cycle or be used for fatty acid synthesis. Given the fact that labeling from pyruvate was not increased in the TCA cycle, I can conclude that acetate is not used for that

purpose. It would therefore be interesting to investigate whether acetate is directed to fatty acid synthesis. This hypothesis could be tested by profiling isotopic enrichment in fatty acids. The measurement of mass isotopomer distributions (MIDs) using [U-^{13}C$_3$]pyruvate as a tracer together with L-DOPA treatment could indicate whether pyruvate and acetate are directed to fatty acid synthesis. If this is the case, acetate could be an additional carbon source supporting the cells upon mitochondrial complex II inhibition.

Finally, in a future study, the redox and energy state as well as levels of reduced L-glutathione (GSH) and glutathione disulfide (GSSG) should be studied in the context of L-DOPA treatment.

In the second part of this work, I investigated dopamine (DA) metabolism in various *in vitro* models. I first compared the expression levels of genes related to DA synthesis in several cell models including human LUHMES mesencephalon cells, human SH-SY5Y neuroblastoma cells, rat PC-12 pheochromocytoma cells and iPSC-derived dopaminergic neurons. TH is responsible for the hydroxylation of tyrosine to L-DOPA, which is decarboxylated to DA by aromatic amino acid decarboxylase (AADC). Upon synthesis, DA is packaged into vesicles by vesicular monoamine transporter 2 (VMAT2). Another important enzyme in the context of DA synthesis is GTP cyclohydrolase 1 (GTPCH), which is the rate-limiting enzyme in the synthesis of 6*R*-L-erythro-5,6,7,8-tetrahydrobiopterin (BH$_4$), the cofactor of TH. LUHMES cells expressed *TH*, but not *GTPCH*, *AADC*, nor *VMAT2*. SH-SY5Y expressed *GTPCH* and *AADC*, but not *TH* nor *VMAT2*. These two cell lines did not produce any endogenous DA. iPSC-derived dopaminergic neurons expressed *GTPCH*, *TH*, *AADC* and *VMAT2*. In PC-12, I only investigated protein expression of TH and showed that these cells express the protein. Both iPSC-derived dopaminergic neurons and PC-12 produced DA.

In a first attempt to induce DA production in LUHMES cells, I increased TH expression under cytomegalovirus (CMV) and ubiquitin C (UbC) promoters and observed that only the CMV promoter was expressed. The increased expression of TH did not lead to endogenous DA production in LUHMES cells. I also observed that the expression of endogenous and CMV-induced expression of TH was dependent on the presence of cyclic adenosine monophosphate (cAMP) and the duration of differentiation.

In SH-SY5Y, among the genes involved in DA synthesis, only TH was missing. TH overexpression was sufficient to induce endogenous DA production. Using this cell system, I determined that tyrosine was the preferential substrate for DA synthesis, but that phenylalanine was used in the absence of tyrosine.

Given the low level of AADC expression in LUHMES cells, this enzyme was overexpressed in these cells. This did not lead to any endogenous DA production. However, upon L-DOPA stimulation, DA was detected. Using this cell model, I characterized L-DOPA transport in LUHMES cells and established that L-DOPA is taken up via the large amino acid transporter (LAT).

The expression of GTPCH was also low in LUHMES cells, it is therefore possible that the activity of TH is impaired due to the low level or absence of its cofactor, BH_4. In order to evaluate this, I supplemented LUHMES AADCox cells with BH_4. This did not lead to any DA synthesis either. This demonstrate that although TH expression has been considered as a sufficient marker to determine dopaminergic populations, it is not sufficient for DA production.

Therefore, despite the fact LUHMES cells are a good model to study 1-methyl-4-phenylpyridinium (MPP^+) due to their high expression of dopamine transporter (DAT) and that the new LUHMES AADCox represents a good model to study L-DOPA uptake, they are not a suitable model for study of DA metabolism. It would be possible to co-overexpress AADC and GTPCH in the same cell line, but the fact that neither BH_4 nor its precursor sepiapterin induced activation of TH suggests that this approach would not give the expected results. It is also possible that the expression of catecholamine (CA)-related genes was turned down with passaged cells. It would therefore be interesting to measure the original cells.

Appendices

A

Isotopic steady state

In order to perform stable isotope-assisted metabolomics, the intracellular fluxes must be at isotopic steady state. This means that the labeling of metabolite is constant over time. The isotopic steady state can be established by incubating cells with tracers of interest and extracting the metabolites at different time point. This experiment was performed for LUHMES cell using either [U-^{13}C$_6$]glucose or [U-^{13}C$_5$]glutamine and extracting metabolites after 2, 15, 30 min, 1, 6, 18, 24 and 48 h. I therefore established that LUHMES cells are at isotopic steady state after 24 h, the incubation time used for 2,3-dihydroxy-L-phenylalanine (L-DOPA) treatment.
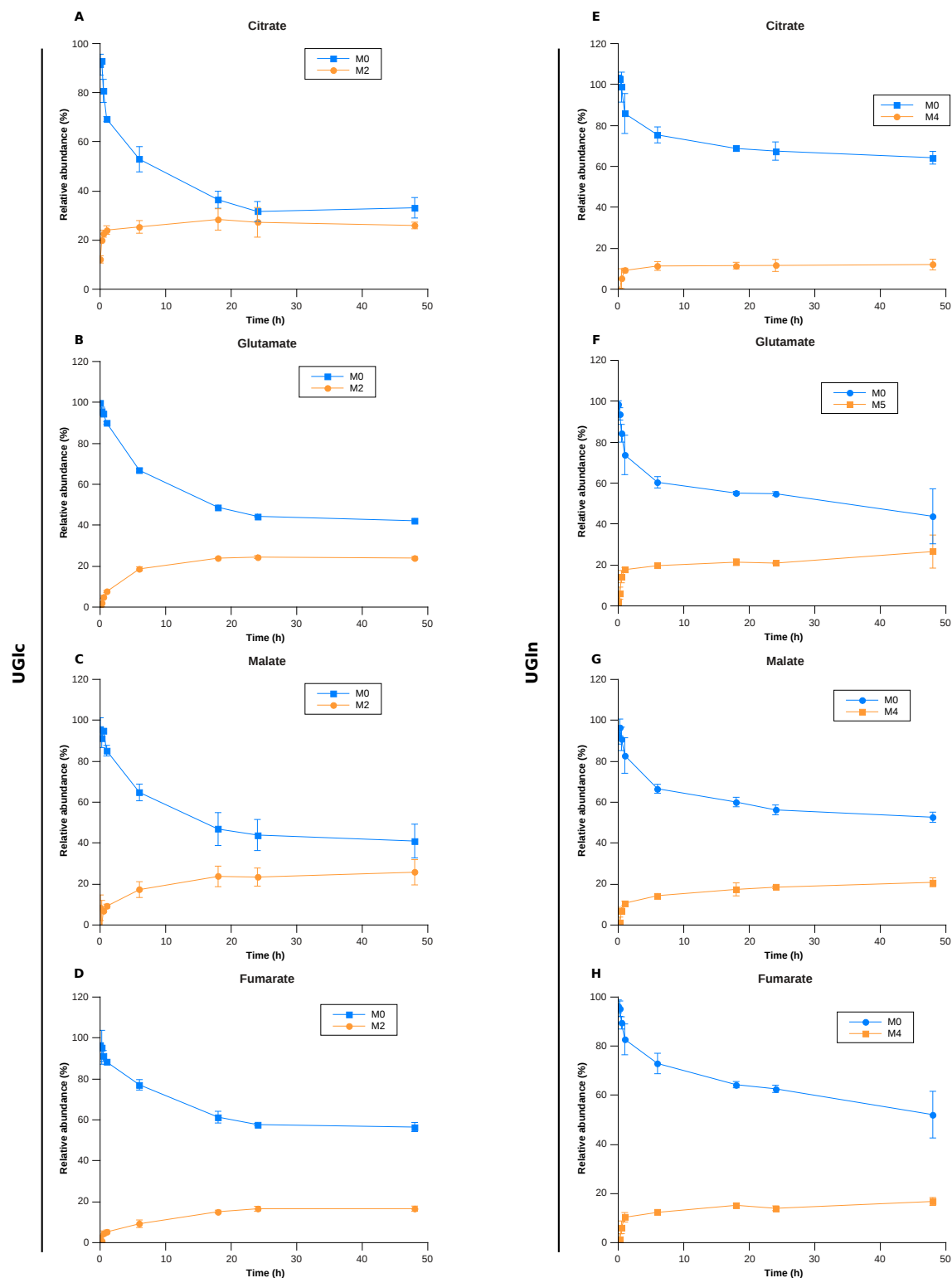
FIGURE A.1: **Isotopic steady state.** LUHMES cells were incubated for different durations (2, 15, 30 min, 1, 6, 18, 24, 48 h) with either [U-$^{13}C_6$]glucose (**UGlc**) or [U-$^{13}C_5$]glutamine **(UGln)**. Mass isotopomer distribution is displayed for citrate, glutamate, malate and fumarate. **(A-D)**: Kinetic of M0 and M2 isotopologues upon UGlc labeling. **(E-H)**: Kinetic of M0 and M4 (citrate, malate, fumarate) or M5 (glutamate) isotopologue upon UGln labeling.
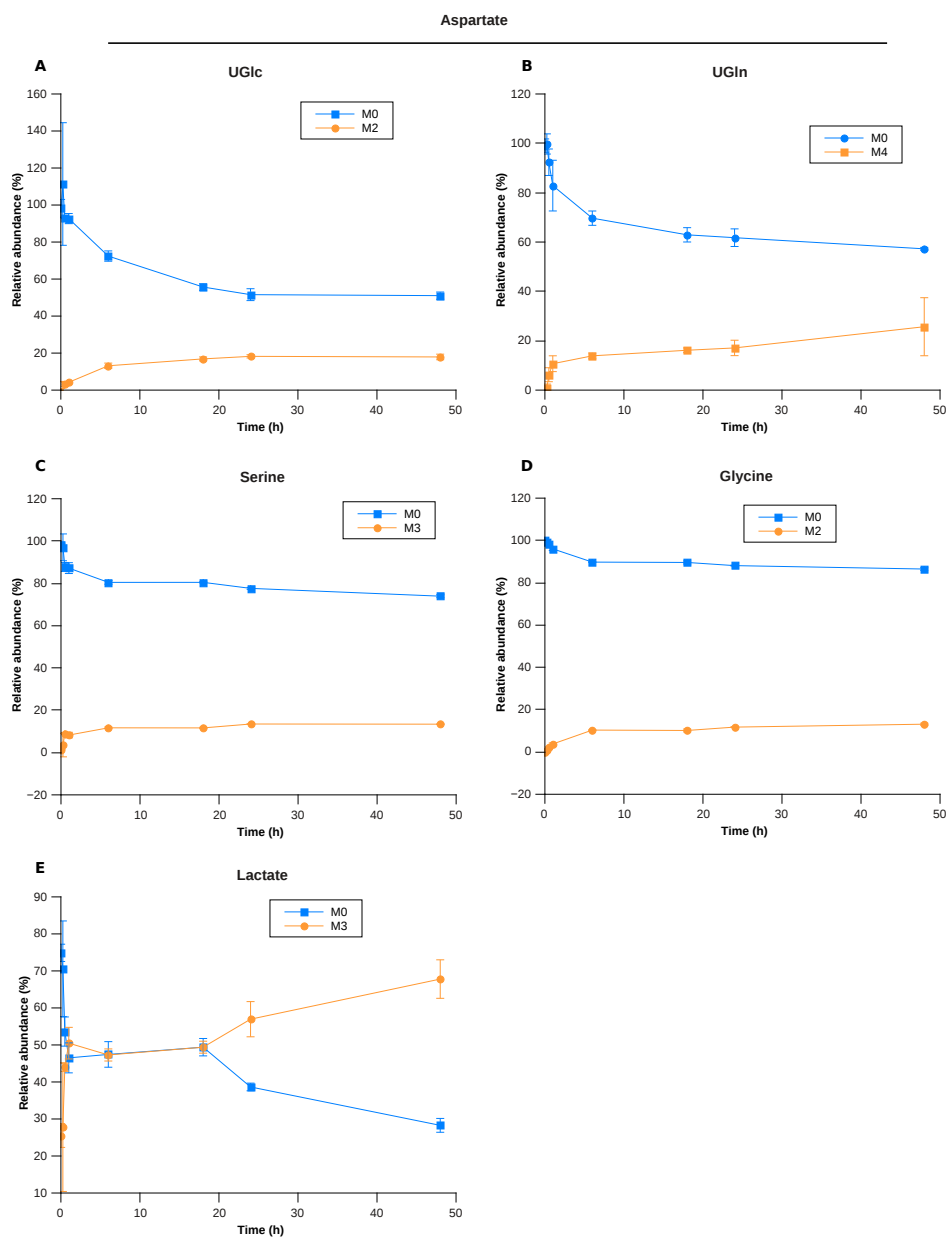
FIGURE A.2: **Isotopic steady state.** LUHMES cells were incubated for different durations (2, 15, 30 min, 1, 6, 18, 24, 48 h) with either [U-^{13}C$_6$]glucose (**UGlc**) or [U-^{13}C$_5$]glutamine **(UGln)**. Mass isotopomer distribution is displayed for aspartate, serine, glycine and lactate. **(A)**: Kinetic of M0 and M2 isotopologues upon UGlc labeling in aspartate. **(B)**: Kinetic of M0 and M4 isotopologues upon UGln labeling in aspartate. Kinetic of M0 and M2 (glycine) or M3 (serine, lactate) upon UGlc labeling in serine **(C)**, glycine **(D)** and lactate **(E)**.

Plasmid maps

This section displays the plasmids used for the cloning of tyrosine hydroxylase (TH) and aromatic amino acid decarboxylase (AADC) into LUHMES and SH-SY5Y cells. pDONR207 (Figure **B.1**) was used to create the entry vector of AADC, while TH was purchased directly in the entry plasmid. pLenti6.3/TO/V5/DEST (Figure **B.2**) was used to produce the expression vector and subsequent lentivirus production. In this plasmid, the expression of the gene inserted is under the control of the cytomegalovirus (CMV) promoter. The last plasmid used was pLenti6/UbC/V5-DEST (Figure **B.3**). It was also used to produce the expression vector. In this case, the expression of the gene of interest was under the control of ubiquitin C (UbC) promoter.
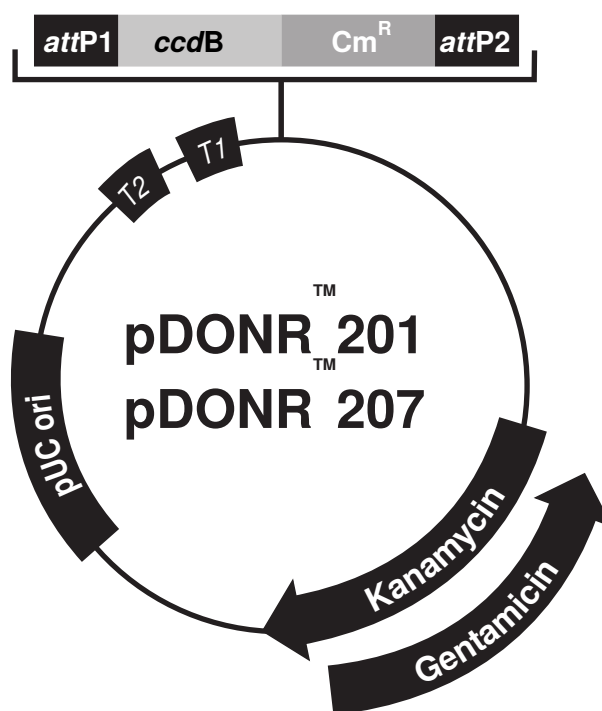
Comments for:	pDONR™201 4470 nucleotides	pDONR™207 5585 nucleotides
*rrn*B T2 transcription termination sequence (c):	73-100	73-100
rrnB T1 transcription termination sequence (c):	232-275	232-275
Recommended forward priming site:	300-324	300-324
*att*P1:	332-563	332-563
*ccd*B gene (c):	959-1264	959-1264
Chloramphenicol resistance gene (c):	1606-2265	1606-2265
*att*P2 (c):	2513-2744	2513-2744
Recommended reverse priming site:	2769-2792	2769-2792
Kanamycin resistance gene:	2868-3677	---
Gentamicin resistance gene (c):	---	3528-4061
pUC origin:	3794-4467	4909-5582

(c) = complementary strand

FIGURE B.2: pLenti 6.3/TO/V5-DEST map
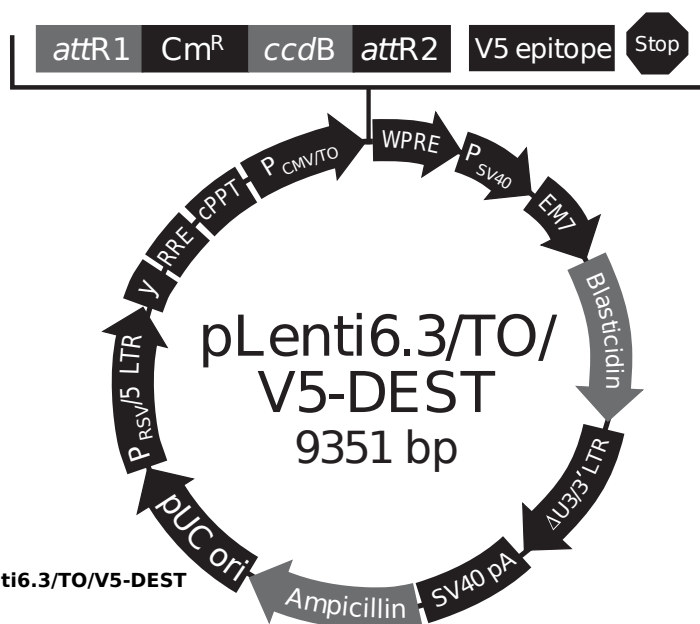
**Comments for pLenti6.3/TO/V5-DEST
9351 nucleotides**

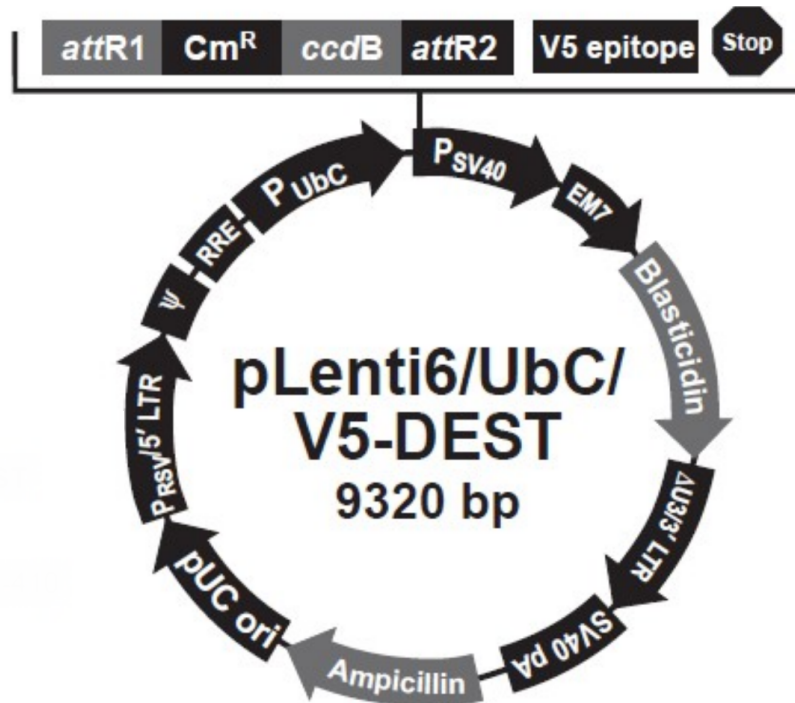RSV/5 LTR hybrid promoter: bases 1-410
    RSV promoter: bases 1-229
    HIV-1 5 LTR: bases 230-410
5 splice donor: base 520
HIV-1 psi (y) packaging signal: bases 521-565
HIV-1 Rev response element (RRE): bases 1075-1308
3 splice acceptor: base 1656
3 splice acceptor: base 1684
cPPT: bases 1801-1923
CMV/TO promoter: bases 1937-2491
    CMV promoter: bases 1937-2436
    TATA box: bases 2436-2442
    Tetracycline operator (2X TetO$_2$) sequences: bases 2452-2491
*att*R1 site: bases 2532-2656
Chloramphenicol resistance gene (Cm^R): bases 2765-3424
*ccd*B gene: bases 3766-4071
*att*R2 site: bases 4112-4236
V5 epitope: bases 4289-4330
WPRE: bases 4349-4946
SV40 promoter: bases 4957-5265
EM7 promoter: bases 5320-5386
Blasticidin resistance gene: bases 5387-5785
DU3/3 LTR: bases 5871-6105
    DU3: bases 5871-5924
    3 LTR: bases 5925-6105
SV40 polyadenylation signal: bases 6177-6308
bla promoter: bases 7167-7265
Ampicillin (*bla*) resistance gene: bases 7266-8126
pUC origin: bases 8271-8944

FIGURE B.3: pLenti 6 UbC/TO-DEST map

Comments for pLenti6/UbC/V5-DEST
9320 nucleotides

RSV/5′ LTR hybrid promoter: bases 1-410
   RSV promoter: bases 1-229
   HIV-1 5′ LTR: bases 230-410
5′ splice donor: base 520
HIV-1 psi (ψ) packaging signal: bases 521-565
HIV-1 Rev response element (RRE): bases 1075-1308
3′ splice acceptor: base 1656
3′ splice acceptor: base 1684
UbC promoter: bases 1798-3016
*att*R1 site: bases 3072-3196
Chloramphenicol resistance gene (Cm^R): bases 3305-3964
*ccd*B gene: bases 4306-4611
*att*R2 site: bases 4652-4776
V5 epitope: bases 4829-4870
SV40 early promoter and origin: bases 4925-5234
EM7 promoter: bases 5289-5355
Blasticidin resistance gene: bases 5356-5754
ΔU3/3′ LTR: bases 5840-6074
   ΔU3: bases 5840-5893
   3′ LTR: bases 5894-6074
SV40 polyadenylation signal: bases 6146-6277
bla promoter: bases 7136-7234
Ampicillin (*bla*) resistance gene: bases 7235-8095
pUC origin: bases 8240-8913

Absolute carbon contribution

The calculation of carbon contribution gives relative information about the contribution of a given carbon source to metabolites. Absolute carbon contribution can be obtained by multiplying the carbon contributions obtained for each tracer with the signal intensity of the corresponding metabolites.

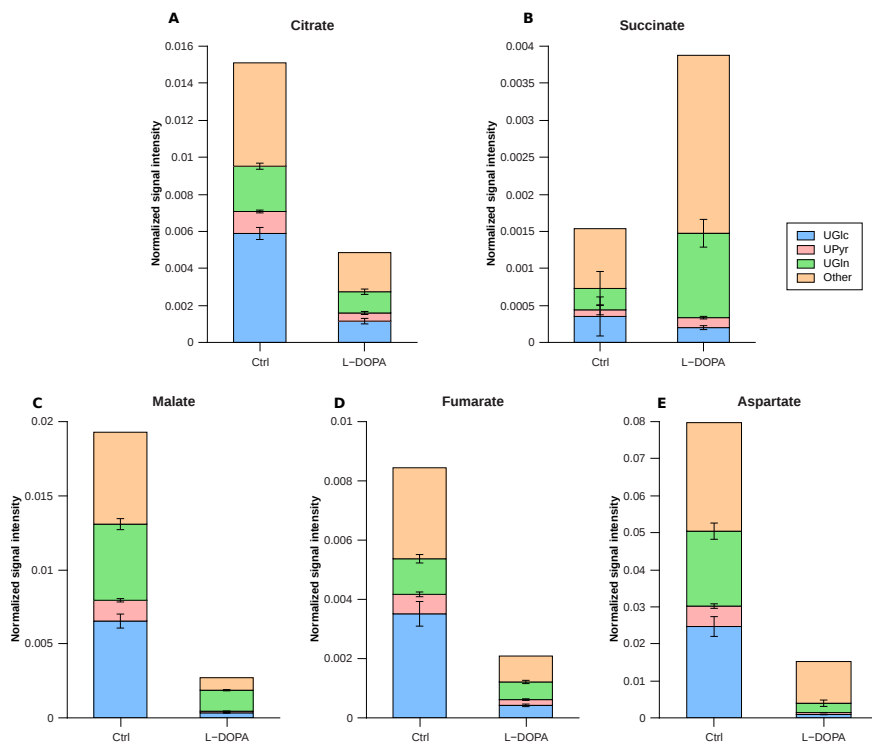FIGURE C.1: **Absolute carbon contributions upon L-DOPA treatment.** LUHMES cells were treated for 24 h with 200 μM L-DOPA and incubated with [U-^{13}C$_6$]glucose (**Glc**), [U-^{13}C$_5$]glutamine (**Gln**) or [U-^{13}C$_3$]pyruvate (**Pyr**) for the same period. Absolute carbon contribution for citrate **(A)**, succinate **(B)**, malate **(C)**, fumarate **(D)** and aspartate **(E)** were calculated for each tracer.

Loss of DJ-1 impairs antioxidant response by altered glutamine and serine metabolism

During my PhD thesis, I contributed to the elaboration of a research article published in Neurobiology of Disease. This article focused on the effects of loss of DJ-1 on the metabolism of tyrosine hydroxylase (TH)-positive LUHMES cells and BV2 cells. In LUHMES cells, silencing of DJ-1 lead to an increased sensitivity to oxidative stress. Data showed that this increased sensitivity was most likely due to a perturbed reduced L-glutathione (GSH) regeneration. Using stable isotope tracers, we showed that serine biosynthesis is decreased, while its uptake is increased in the absence of DJ-1. This metabolite is a precursor of cysteine, the rate-limiting compound in GSH synthesis. Moreover, we observed that glutamine uptake and its contribution to the tricarboxylic acid (TCA) cycle decreased. Glutamine can be used for glutamate synthesis, another component of GSH. Upon treatment with H_2O_2, the increase in glutathione disulfide (GSSG)/GSH was stronger in DJ-1-deficient cells, indicating an impaired GSH regeneration. In mouse microglia, silencing of DJ-1 induced a weak but constitutive inflammatory state. This was evaluated by increased gene expression of Tnfα, Irg1 and iNos as well as by increased intracellular levels of succinate and itaconate.

In summary, we conclude that it is possible that the combination of (1) the decreased anti-oxidant capacity of the neurons as well as (2) the constitutive inflammatory state of microglia contribute to the onset of Parkinson's disease (PD) in patient carrying a DJ-1 loss of function mutation.

Contributions:

In this project, I participated in the generation of the DJ-1 silenced LUHMES cell lines. I performed the cell viability assay comparing LUHMES shCtrl and shDJ-1 cells upon 6-hydroxydopamine (6-OHDA) treatment. I also took part in the $[U^{13}C_6]$glucose and $[U^{13}C_5]$glutamine labeling experiments in LUHMES shDJ-1 and shCtrl cells. In the same cell lines, I evaluated gene expression of the catalytic and modifier domains of glutamate cysteine ligase (GCLC and GCLM, respectively). Finally, I compared protein expression of NRF2 between human A549 lung cancer cells and LUHMES cells.
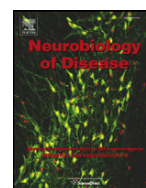
Loss of DJ-1 impairs antioxidant response by altered glutamine and serine metabolism

J. Meiser [a], S. Delcambre [a], A. Wegner [a], C. Jäger [a], J. Ghelfi [a], A. Fouquier d'Herouel [a], X. Dong [a], D. Weindl [a], C. Stautner [c], Y. Nonnenmacher [a], A. Michelucci [a,k], O. Popp [j], F. Giesert [c], S. Schildknecht [b], L. Krämer [a], J.G. Schneider [a,i], D. Woitalla [g], W. Wurst [c,d,e,f], A. Skupin [a,h], D.M. Vogt Weisenhorn [c], R. Krüger [a], M. Leist [b], K. Hiller [a,*]

[a] *Luxembourg Centre for Systems Biomedicine, University of Luxembourg, L-4367 Belvaux, Luxembourg*
[b] *Doerenkamp-Zbinden Chair for In Vitro Toxicology and Biomedicine, University of Konstanz, Konstanz D-78457, Germany*
[c] *Helmholtz Zentrum München, German Research Center for Environmental Health, Institute of Developmental Genetics, Ingolstädter Landstr. 1, 85764 Neuherberg, Germany*
[d] *Deutsches Zentrum für Neurodegenerative Erkrankungen e. V. (DZNE) Standort München, Feodor-Lynen-Strasse 17, 81377 München, Germany*
[e] *Munich Cluster for Systems Neurology (SyNergy), Adolf-Butenandt-Institut, Ludwig-Maximilians-Universität München, Schillerstrasse 44, 80336 München, Germany*
[f] *Technische Universität München-Weihenstephan, Lehrstuhl für Entwicklungsgenetik, c/o Helmholtz Zentrum München, Ingolstädter Landstr. 1, 85764 Neuherberg, Germany*
[g] *Neurology, St. Josef Hospital, Ruhr-University, Gudrunstr. 56, 44780 Bochum, Germany*
[h] *National Center for Microscopy and Imaging Research, University of California San Diego, La Jolla, CA, United States*
[i] *Saarland University Medical Center, Department of Internal Medicine II, Homburg/Saar, Germany*
[j] *Mass Spectrometry Core Facility, Max-Delbrueck Center for Molecular Medicine, Robert-Roessle Strasse 10, 13125 Berlin, Germany*
[k] *NorLux Neuro-Oncology Laboratory, Luxembourg Institute of Health, 84, Val Fleuri, L-1526, Luxembourg*

ARTICLE INFO

ABSTRACT

The oncogene *DJ-1* has been originally identified as a suppressor of PTEN. Further on, loss-of-function mutations have been described as a causative factor in Parkinson's disease (PD). DJ-1 has an important function in cellular antioxidant responses, but its role in central metabolism of neurons is still elusive. We applied stable isotope assisted metabolic profiling to investigate the effect of a functional loss of DJ-1 and show that DJ-1 deficient neuronal cells exhibit decreased glutamine influx and reduced serine biosynthesis. By providing precursors for GSH synthesis, these two metabolic pathways are important contributors to cellular antioxidant response. Down-regulation of these pathways, as a result of loss of DJ-1 leads to an impaired antioxidant response. Furthermore, DJ-1 deficient mouse microglia showed a weak but constitutive pro-inflammatory activation. The combined effects of altered central metabolism and constitutive activation of glia cells raise the susceptibility of dopaminergic neurons towards degeneration in patients harboring mutated *DJ-1*. Our work reveals metabolic alterations leading to increased cellular instability and identifies potential new intervention points that can further be studied in the light of novel translational medicine approaches.

© 2016 The Authors. Published by Elsevier Inc. This is an open access article under the CC BY-NC-ND license (http://creativecommons.org/licenses/by-nc-nd/4.0/).

1. Introduction

DJ-1 (*PARK 7*) is expressed in different organs throughout the body and has first been identified as an oncogene together with activated Ras (Nagakubo et al., 1997). High levels of DJ-1 have been associated with malignancy of tumor development (Nagakubo et al., 1997; Davidson et al., 2008; Kim et al., 2005; Yuen et al., 2008). Mechanically, DJ-1 has been identified as a repressor of the phosphatase PTEN,

which itself is a repressor of PKB/AKT (Stambolic et al., 1998; Sun et al., 1999). In case of *DJ-1* overexpression, PKB/AKT is hyperphosphorylated, promoting cell survival and anaplerotic metabolism needed for proliferation (Kim et al., 2005). In cancer cells, DJ-1 has been identified as a positive regulator of NRF2 (Clements et al., 2006), a master regulator in the antioxidant response. NRF2 has also been shown to influence central metabolism (Hayes and Dinkova-Kostova, 2014). However, its role in neuronal metabolism remains to be elucidated. While *DJ-1* overexpression provokes oncogenesis, loss of function mutations in *DJ-1* have been associated with a familial autosomal recessive form of Parkinson's disease (PD) with an early onset of disease progression (Bonifati, 2003; Bonifati et al., 2003; Van Duijn et al., 2001). PD leads to motor and non-motor symptoms with hallmarks such as

---

elevated levels of reactive oxygen species (ROS) and specifically, a decay of dopaminergic (DAergic) neurons of the *substantia nigra pars compacta* (Antony et al., 2013).

Lack of DJ-1 hampers quenching of cellular ROS, affecting mitochondrial and cellular integrity (Clements et al., 2006; Ariga et al., 2013; Irrcher et al., 2010; Kahle et al., 2009; Krebiehl et al., 2010). Within the brain, *DJ-1* is expressed in neuronal as well as non-neuronal cells (Bader et al., 2005) and is up-regulated with increasing oxidative stress (Baulac et al., 2009). Oxidation of cysteine residues in DJ-1 leads to a shift of the isoelectric point (pI) and subsequent relocation of the protein to the nucleus, as well as the mitochondrial membrane (Canet-Avilés et al., 2004). ROS production and a concomitant shift of the pI have also been shown in cells exposed to lipopolysaccharide (LPS), an inducer of inflammatory responses (Mitsumoto and Nakagawa, 2001) indicating further implications in the context of neuroinflammation and mitochondrial metabolism (Kim et al., 2013; Trudler et al., 2014; Waak et al., 2009). Activation of microglia has been found to correlate with the occurrence of neurodegenerative diseases (Brown and Neher, 2010; Meiser et al., 2013).

Although there is evidence that DJ-1 regulates metabolism directly (Lee et al., 2012) and indirectly (Clements et al., 2006; Aleyasin et al., 2010; van der Brug et al., 2008), a detailed understanding of its role in central metabolism, especially in the context of PD, is still missing.

Here, we investigated the impact of a functional loss of DJ-1 on cellular metabolism. Our study demonstrates that loss of DJ-1 affects central metabolism by decreasing glutamine influx and serine biosynthesis. These two metabolic pathways provide the precursors glutamate, serine and glycine for *de novo* synthesis of glutathione. In line with these metabolic flux changes, we observed decreased glutathione levels in DJ-1 deficient cells.

Additionally, DJ-1 deficient mouse microglia showed a weak but constitutive pro-inflammatory phenotype. We reason that the combination of weak pro-inflammatory activation with metabolic dysfunction renders DAergic neurons more susceptible for early cell death.

2. Results

2.1. Loss of DJ-1 increases susceptibility to oxidative stress

To investigate the effect of loss of DJ-1 on central metabolism, we targeted *DJ-1* by RNAi in the human tyrosine hydroxylase (TH)-positive neuronal cell model LUHMES (Scholz et al., 2011) (Fig. 1a and b; S1). As a control we used non-specific *shRNA* and generated *shCtrl* LUHMES cells in parallel to the *shDJ-1* cells. LUHMES cells are conditionally immortalized and are postmitotic after differentiation (Scholz et al., 2011).

To confirm our working hypothesis that *DJ-1* deficient cells are more susceptible to oxidative stress (Zhou and Freed, 2005), we first performed a viability assay after treating the cells with different concentrations of the ROS-inducing compound 6-hydroxydopamine (6-OHDA) (Fig. 1c). 6-OHDA treated LUHMES cells lacking DJ-1 showed 30–40%
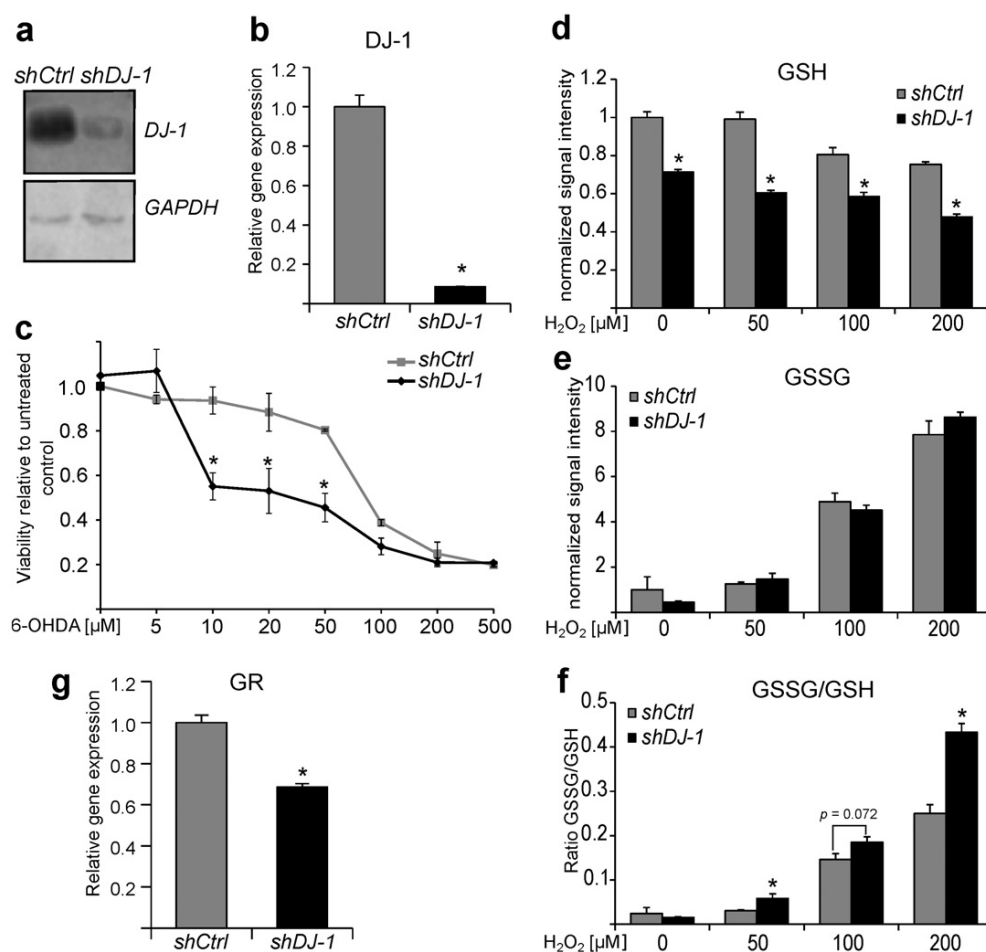
Fig. 1. Loss of *DJ-1* increases sensitivity to oxidative stress and affects glutathione homeostasis. (a–b) Western blot and qPCR analysis demonstrating DJ-1 knockdown. (c) Viability assay of LUHMES cells in response to oxidative stress. Cells were treated for six hours with different concentrations of 6-hydroxydopamine (6-OHDA). (d–e) Relative quantification of (d) GSH and (e) GSSG, 20 min after treatment with H_2O_2. (f) Ratio GSSG/GSH. (g) Gene expression of *GR*. Error bars represent SEM. Asterisks indicate a significant difference to the respective *shCtrl* (Welch's *t*-test, $p < 0.05$; number of biological replicates: $n \geq 3$). See also Supplementary Fig. S1.
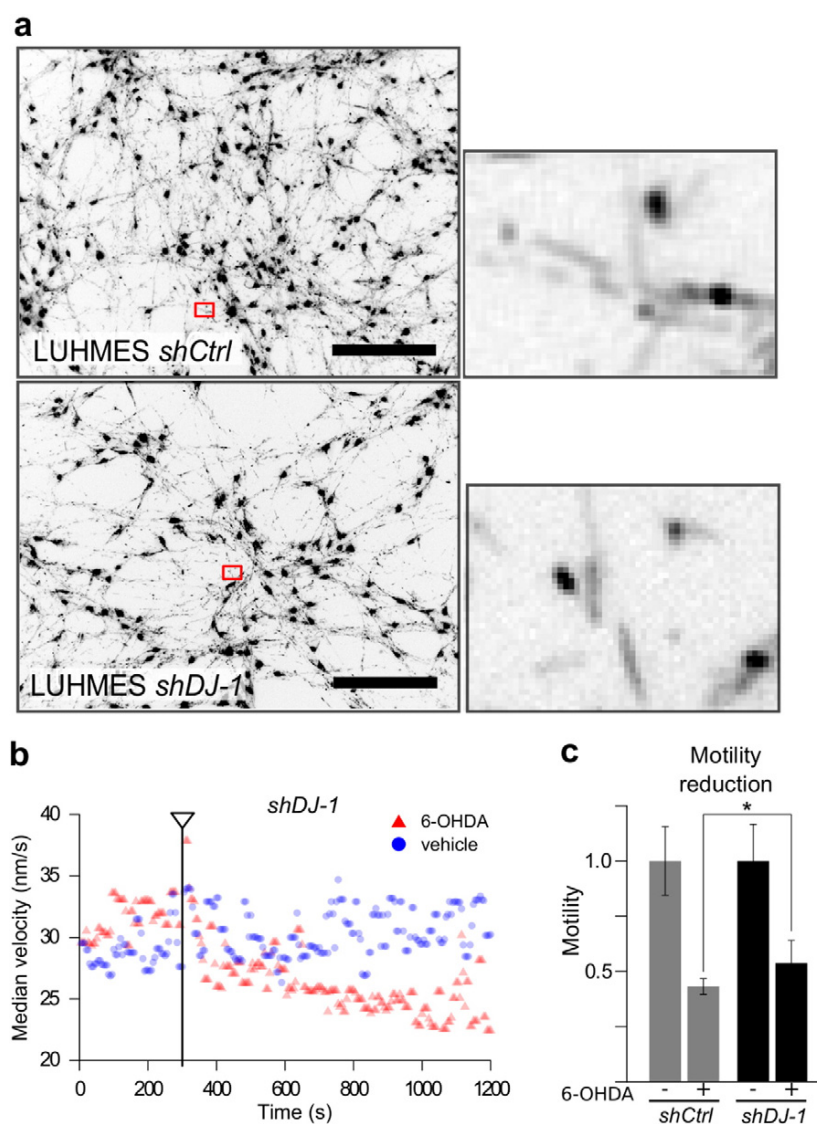
Fig. 2. Loss of DJ-1 affects mitochondrial motility in neurons (a) Fluorescence microscopy image of differentiated LUHMES cells stained with TMRM (scale bar = 100 μM) and a 10× magnification of a selected area (red square). Stain shows the location of mitochondria in soma and neurites. (b) Representative time-course of global mitochondrial motion analysis (in this case *shDJ-1*). Before and after (300 s; grey bar) addition of 200 μM 6-OHDA. Mito motility was reduced due to addition of 6-OHDA (red) compared to control (blue). (c) Parallel measurement of global mitochondrial motion. Shown values were normalized to the mean velocity measured before treatment with 6-OHDA. Error bars in (c) represent SD. Asterisks indicate a significant difference to the respective *shCtrl* cells (Student's *t*-test, $p < 0.05$ number of biological replicates $n = 3$). See also Supplementary movies and Fig. S2.

decreased viability (within the range of 10–50 μM 6-OHDA) compared to *shCtrl*, confirming that loss of DJ-1 increases sensitivity to oxidative stress.

To further analyze the cellular response to ROS, we measured the level of reduced (GSH) and oxidized (GSSG) glutathione after H_2O_2 treatment by UHPLC–MS (Fig. 1d–f). Already without any additional perturbation, GSH levels in *shDJ-1* cells were lower than in the respective *shCtrl* cells. With increasing concentrations of H_2O_2, we detected decreasing GSH levels and a concomitant increase of GSSG and thus an increase in the GSSG/GSH ratio. The GSSG/GSH ratios were more increased in *shDJ-1* cells, pointing to insufficient GSH regeneration from GSSG or a lack of alternative detoxification mechanisms. In line with these observations, we also found decreased gene expression levels of *glutathione reductase* (*GR*) in DJ-1 deficient cells (Fig. 1g).

Insufficient ROS detoxification is likely to affect mitochondrial integrity (Irrcher et al., 2010; Kahle et al., 2009). In neurons, mitochondria

are actively transported through the projections of neuronal cells to directly satisfy axonal and synaptic energy demands (Saxton and Hollenbeck, 2012). Therefore, we investigated whether *shDJ-1* cells exhibit systematically different mitochondrial motion patterns than *shCtrl* cells and whether loss of the gene function would elicit different responses upon 6-OHDA treatment. To that end, we monitored the global motion of fluorescence-stained mitochondria in differentiated LUHMES cells by time-lapse microscopy (Fig. 2, Supplementary Movies and Fig. S2). Without perturbation, there was no significant difference in mitochondrial movement between the two cell types (Fig. 2C).

Consistent with the literature (Chen et al., 2008) we observed a general deceleration of mitochondrial motion in both cell types, following 6-OHDA treatment (Fig. 2b). Surprisingly, deceleration showed a trend to be less in *shDJ-1* cells compared to *shCtrl* cells (Fig. 2c and Supplementary movies and Fig. S2), suggesting that the regulation of mitochondrial transport in response to 6-OHDA-mediated oxidative stress might be affected by loss of DJ-1.

Together with the observation that the treatment did not lead to a significant drop of the mitochondrial membrane potential in the two cell types (Supplementary Movies) this may indicate additional effects of the induced oxidative stress. A direct target would be Ca^{2+} homeostasis (Guzman et al., 2010) that in turn can influence mitochondrial trafficking by Miro1 (Stephen et al., 2015; Nguyen et al., 2014) and TCA cycle activity by polarization (Krols et al., 2016). Furthermore, DJ-1 deficiency is associated with an impaired microtubule dynamics (Sheng et al., 2013) leading to modified cytoskeleton structures that can affect mitochondrial transport.

2.2. Loss of DJ-1 affects central metabolism

To investigate if the observed moderate changes in mitochondrial motility may have an impact on the cellular energy pool, we profiled cellular metabolism by determining uptake and release rates and by analyzing intracellular fluxes using stable isotope labeled tracers. We detected a decrease in alanine release in *shDJ-1* cells (Fig. 3a), whereas differences in glucose, pyruvate and serine consumption and lactate release were not statistically different (Fig. 3b, c, d, e). This reduction in alanine release of shDJ-1 cells, suggests a lower requirement for nitrogen excretion in these cells.

Since shDJ-1 cells are more sensitive to oxidative stress, we investigated if the canonical NADPH producing pathways, the pentose phosphate pathway and the folate mediated one-carbon metabolism are affected. To this end, we analyzed gene expression of *glycine*

dehydrogenase (*GLDC*), the rate-limiting enzyme of the glycine cleavage system, of *glucose-6-phosphate dehydrogenase* (*G6PDH*), the rate-limiting enzyme of the PPP and of 5,10-*methylene tetrahydrofolate* (THF) *dehydrogenase* (*MTHFD*), a key enzyme in folate metabolism. We did not observe significant changes in the expression of *GLDC*, but decreased expression of *G6PDH*, *MTHFD1* and *MTHFD2* (Fig. 3f–h, S3), pointing to decreased carbon flux into these pathways and decreased cellular potential to generate NADPH, needed for antioxidative activities.

To monitor metabolic fluxes through glycolysis, the serine biosynthesis pathway, glycine cleavage and through PDH, we used uniformly labeled ^{13}C glucose as a tracer. We found that relative glucose contribution to serine biosynthesis was decreased in *shDJ-1* cells (Fig. 3j), which is in line with the observed decreased expression of MTHFD1/2. The trend of increased serine uptake (*p*-value = 0.084) might be a consequence of the decreased biosynthetic flux from glucose. Furthermore, based on M2 citrate isotopologues we did not observe any difference in relative glucose oxidation through PDH (Fig. 3k; 3I for atom transitions), suggesting that not glucose oxidation, but serine and folate metabolism are dependent on DJ-1.

DJ-1 has been shown to stabilize NRF2 in cancer cells (Clements et al., 2006). NRF2 is a key transcription factor that regulates cellular antioxidant responses also by activating serine flux and folate-mediated one-carbon metabolism (Mitsuishi et al., 2012). However, by Western Blotting we were unable to detect NRF2 in LUHMES cells (Fig. S3f). Concluding from non-detectable NRF2 levels in LUHMES cells, it is possible
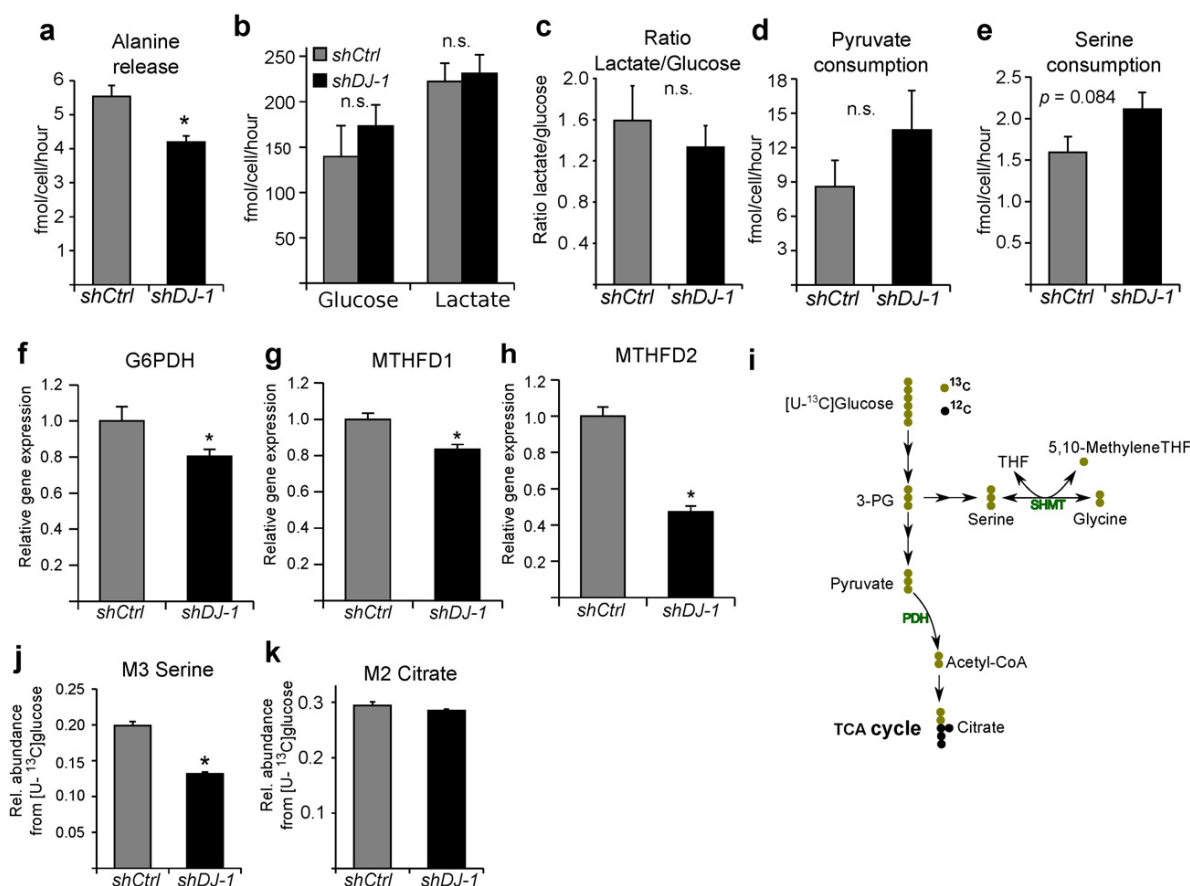
Fig. 3. Metabolic profiling of *DJ-1* silenced LUHMES cells reveals decreased serine biosynthesis flux. (a) Medium consumption and release rates of (a) alanine (release) (b) glucose and lactate. (c) Ratio lactate release/glucose consumption. (d–e) Consumption rates of (d) pyruvate and (e) serine. (f–h) Gene expression (qPCR) of (f) *G6PDH* (g) *MTHFD1* and (h) *MTHFD2*. (i) Schematic of atom transitions in central metabolism using [U-^{13}C]glucose as a tracer. ^{13}C carbons are in green, ^{12}C in black. (j–k) Application of [U-^{13}C]glucose as a tracer in LUHMES cells for determination of MIDs to infer relative intracellular fluxes. (j) M3 serine isotopologue indicating relative serine biosynthesis flux. (k) M2 citrate isotopologue indicating relative PDH flux. Error bars represent SEM. Asterisks indicate a significant difference to the respective *shCtrl* (Welch's *t*-test, $p < 0.05$; number of biological replicates: $n \geq 3$). See also Supplementary Fig. S3.

that the role of DJ-1 in regulating neuronal metabolism in the context of cellular antioxidant responses is even more pronounced, compared to other cell types.

Next, we analyzed TCA cycle fluxes in more detail and we applied uniformly labeled glutamine as a tracer (Fig. 4a for atom transitions). Stable isotope labeling revealed decreased glutamine contribution to the intracellular glutamate pool and to the TCA cycle intermediates alpha-ketoglutarate (aKG), succinate, fumarate, malate, aspartate (as a proxy of oxaloacetate) and citrate (Fig. 4b and c). Analysis of glutamine consumption indicated decreased uptake in *shDJ-1* cells (*p*-value = 0.057) (Fig. 4d). Moreover, we observed decreased gene expression of *glutaminase 2* (*GLS2*) (Fig. 4e), suggesting decreased glutamine-based anaplerosis. To evaluate the importance of glutamine as a carbon source, we calculated its relative carbon contribution to aKG and citrate (Fig. 4f). Providing 45% of carbon to aKG in *shCtrl*, glutamine represents the major precursor of aKG, highlighting the importance of this amino acid to central metabolism. In *shDJ-1*, glutamine carbon contribution

to aKG and citrate was significantly lower than in *shCtrl*, which is in line with our finding of decreased glutamine uptake in *shDJ-1*. Interestingly, we found, that not the contribution of glucose, but that of other carbon sources increased to compensate for the lack of glutamine. Therefore, we quantified the consumption of branched chain amino acids (BCAAs), because their catabolism produces anaplerotic acetyl-coA and succinyl-coA. We observed that the uptake of these three amino acids was indeed elevated in *shDJ-1* cells compared to *shCtrl* (Fig. 4g).

In conclusion, an increased uptake of BCAAs may compensate for the decreased glutamine carbon contribution, but does not prevent increased sensitivity to oxidative stress, which therefore, seems to depend more specifically on serine metabolism and the supply of cysteine via the transsulfuration pathway to generate GSH. Moreover, since glutamine has additional roles in metabolism such as to provide nitrogen for the synthesis of nucleotides it is possible that lack of glutamine represents an additional perturbation to the cell, which makes it more prone to collapse.
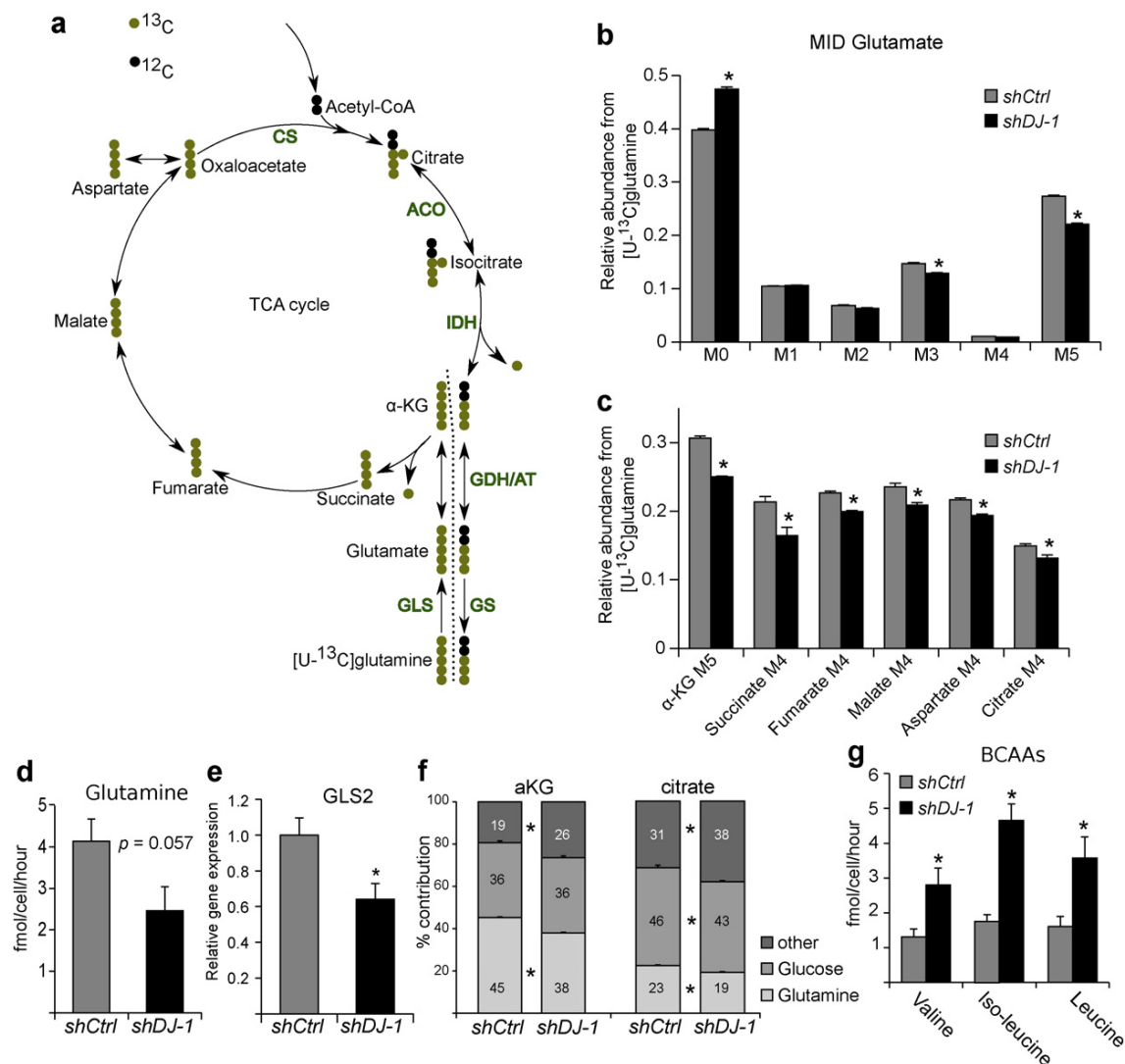
Fig. 4. Metabolic profiling of *DJ-1* silenced LUHMES cells reveals decreased glutamine influx. (a) Schematic of atom transitions in central metabolism using [U-^{13}C]glutamine as a tracer. ^{13}C carbons are in green, ^{12}C in black. ACO: aconitase; AT: aminotransferase; CS: citrate synthase; GDH: glutamate dehydrogenase; GLS: glutaminase; GS: glutamine synthetase; IDH: isocitrate dehydrogenase. The dotted line indicates beginning and end of one cycle. (b–c) Application of [U-^{13}C]glutamine as a tracer in LUHMES cells for determination of MIDs to infer relative intracellular fluxes. (b) MID of glutamate. (c) Relative abundance of M5 aKG, M4 succinate, M4 fumarate, M4 malate, M4 aspartate and M4 citrate. (d) Glutamine consumption from the medium. (e) Gene expression of *GLS2*. (f) Carbon contribution of glucose, glutamine and other carbon sources (%) to aKG and citrate. (g) Branched chain amino acid consumption. Error bars represent SEM. Asterisks indicate a significant difference to the respective *shCtrl*. (Welch's t-test, p < 0.05; number of biological replicates: *n* ≥ 3). See also Supplementary Fig. S4.

2.3. Loss of DJ-1 affects mitochondrial metabolism but does not impair TCA cycle activity

Loss of DJ-1 is often discussed in the context of mitochondrial dysfunction (Clements et al., 2006; Ariga et al., 2013; Irrcher et al., 2010; Kahle et al., 2009; Krebiehl et al., 2010), but how, and more importantly, to what extent this dysfunction manifests on a pathophysiological level remains to be further specified. A strong inhibition of oxidative phosphorylation (OxPhos) caused by ROS would be detrimental for persons carrying a loss of function mutation in *DJ-1*. To analyze this hypothesis in more detail, we inspected TCA cycle activity. In case of OxPhos inhibition, NADH can no longer be oxidized by complex I of the respiration chain, which results in an increased NADH/NAD$^+$ ratio. This altered ratio leads to a thermodynamic shift of IDH activity, resulting in increased reductive carboxylation of aKG (Fendt et al., 2013; Mullen et al., 2014; Wegner et al., 2015). When using [U-^{13}C$_5$]glutamine as a tracer, this inhibition manifests in increased relative abundance of M5 citrate isotopologues, while the relative abundance of M4 citrate isotopologues, decreases (Fig. 5A). To test the effect of OxPhos inhibition and to compare this effect with the metabolic phenotype of *shDJ-1* cells, we treated the cells with MPP$^+$, an inhibitor of complex I of the electron

transport chain, specifically taken up by DAergic neurons through the DA transporter (Javitch et al., 1985; Schildknecht et al., 2015).

Upon MPP$^+$ treatment, we observed a significant increase in fully labeled glutamate and M5 citrate in both cell lines (Fig. 5b, c). As expected, the oxidative route of the TCA cycle was inhibited upon MPP$^+$ treatment, and therefore, relative abundance of M4 citrate was strongly reduced. Although reductive IDH flux was induced in MPP$^+$-treated *shDJ-1* cells, M5 labeling of citrate and glutamate was lower in *shDJ-1*, originating from decreased relative glutamine influx into the TCA cycle. This decrease was also reflected in higher abundances of unlabeled citrate and glutamate as well as in lower M3 glutamate (Fig. 5b, c). Interestingly, compared to shDJ-1, we did not observe a decrease in M0 citrate upon MPP$^+$ treatment in *shCtrl* cells (Fig. 5c). To normalize for the decreased glutamine influx we analyzed the ratio of M5 citrate/M5 glutamate, indicating reductive carboxylation of aKG, M4 citrate/M5 glutamate, indicating glutamine oxidation and M5 citrate/M4 citrate, indicating the ratio of reductively to oxidatively derived citrate from fully labeled glutamine (Fig. 5d–f). These ratios confirmed a strong induction of reductive IDH flux upon MPP$^+$-treatment in both cell lines. However, there was no significant difference between the two cell types.
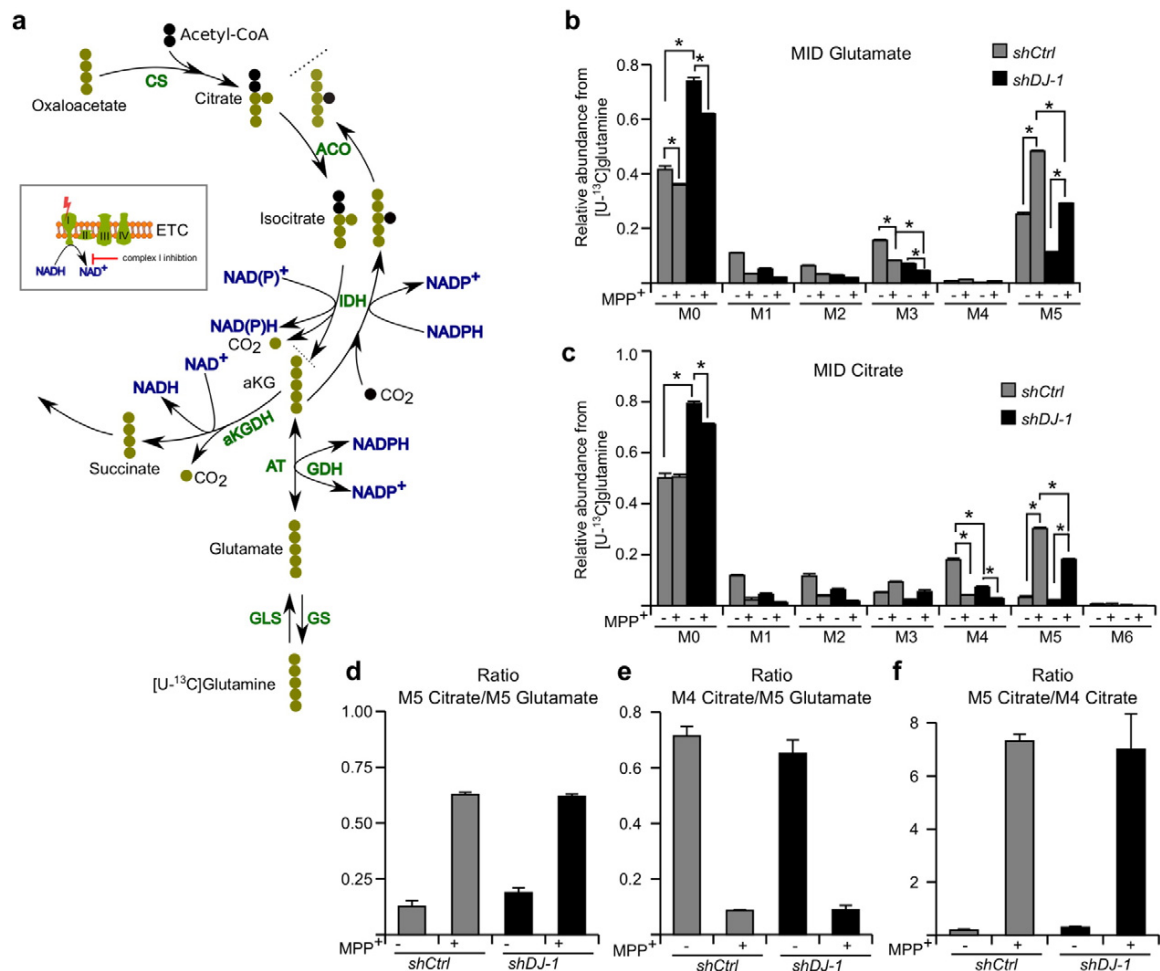
Fig. 5. *DJ-1* silenced LUHMES cells show an active TCA cycle but suffer from decreased glutamine contribution. (a) Schematic of atom transitions in central carbon metabolism using [U-^{13}C]glutamine as a tracer. Shown is reductive carboxylation of M5 aKG to M5 citrate via IDH and ACO. The specific isoenzyme depends on the compartment and is not further considered. For abbreviations see Fig. 4. The dotted line indicates end of one route. In case of complex I inhibition at the electron transport chain (ETC), NADH can no longer be oxidized which leads to a thermodynamic shift in the IDH reaction. (b–c) Application of [U-^{13}C]glutamine as a tracer in LUHMES cells for determination of MIDs to infer relative intracellular fluxes. (b) MID of glutamate. (c) MID of citrate. (d–f) Ratios of (d) M5 citrate/M5 glutamate, indicating reductive carboxylation of aKG (e), M4 citrate/M5 glutamate, indicating oxidation of aKG (f), M5 citrate/M4 citrate, indicating the ratio of reductive to oxidative route. LUHMES *shDJ-1* and *shCtrl* cells were treated with 10 μM MPP$^+$ for 6 h. Error bars represent SEM. Asterisks indicate a significant difference to the respective *shCtrl* (two-way ANOVA, $p < 0.05$; number of biological replicates: $n = 3$).
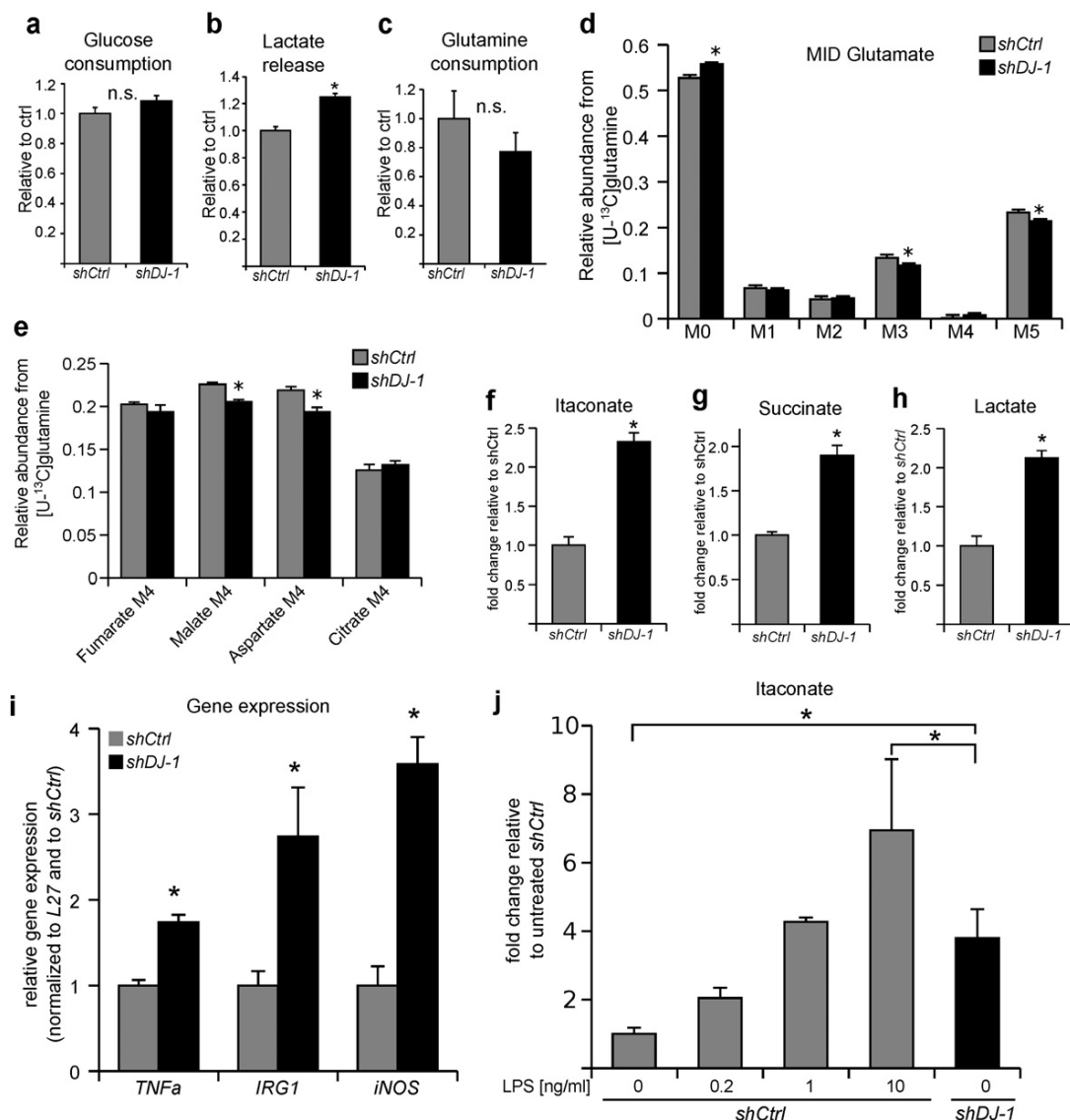
Fig. 6. *Dj-1* silencing affects glutamine metabolism in the mouse microglia cell model BV-2 and causes pro-inflammatory activation. (a–c) Medium consumption and release rates of (a) glucose, (b) lactate and (c) glutamine. (d–e) Application of [U-^{13}C]glutamine as a tracer in BV-2 cells for determination of MIDs to infer relative intracellular fluxes. (d) MID of glutamate. (e) Relative abundance of M4 fumarate, M4 malate, M4 aspartate and M4 citrate. (f–h) Intracellular metabolite levels of itaconate (f), succinate (g) and lactate (h) in BV-2 *shDJ-1* cells compared to *shCtrl*. (i) Gene expression analysis of the inflammatory marker genes *TNFα*, *Irg1* and *iNOS*. (j) Intracellular itaconate levels in *shDJ-1* and *shCtrl* cells. *shCtrl* cells were treated for 6 h with LPS. Error bars represent SEM. Asterisks indicate a significant difference to the respective *shCtrl* (Welch's *t*-test, $p < 0.05$; number of biological replicates: $n = 3$). See also Supplementary Fig. S5.

Analysis of MPP$^+$ treated LUHMES cells leads to the following three conclusions: (1) Lack of DJ-1 does not result in inhibition of OxPhos. Therefore, the general potential to produce ATP via NADH oxidation is still present in DJ-1 deficient cells. (2) The metabolic fate of glutamine between the oxidative and the reductive route is not different between the two cell types upon MPP$^+$ treatment. (3) As a consequence of loss of *DJ-1*, glutamine influx into the TCA cycle is decreased. Whether or not this is solely a result of elevated ROS levels in DJ-1 deficient cells, or if this is rather a mechanistic consequence, needs to be studied further.

2.4. Loss of Dj-1 affects central metabolism in mouse microglia and is sufficient to trigger pro-inflammatory activation

Since neuronal integrity in the central nervous system (CNS) also relies on surrounding glia cells, we investigated the effect of *Dj-1* silencing

in the mouse microglia cell line BV-2 (Fig. S5) (Blasi et al., 1990; Henn et al., 2009).

First, we were interested if the observed metabolic alteration in neuronal cells also occurs in microglia. We did not observe significantly increased glucose consumption but a 20% increase in lactate release (Fig. 6a–b). Although glutamine uptake seemed to be decreased in DJ-1 deficient cells, this difference was not significant (Fig. 6c). Stable isotope labeling of glutamine revealed decreased glutamate labeling in *shDJ-1* BV-2 cells (Fig. 6d). However, the difference in isotopic enrichment was not as pronounced as in LUHMES cells and was only significantly different in the case of malate, aspartate and glutamate (Fig. 6e). Overall, proliferating BV-2 cells showed similar alterations than observed in LUHMES cells but less pronounced.

Recently, it has been reported that loss of Dj-1 leads to increased pro-inflammatory (M1) activation of microglia and astrocytes after perturbation with activating compounds such as the toll like receptor

Appendix D. Loss of DJ-1 impairs antioxidant response

agonist LPS or the cytokine IFNγ (Kim et al., 2013; Trudler et al., 2014; Waak et al., 2009). In this study we wanted to investigate if solely the lack of Dj-1 is already sufficient to trigger M1 polarization, and thus, could be relevant in the context of neuroinflammation. We analyzed levels of the metabolic M1 markers succinate and itaconate (Michelucci et al., 2013; Strelko et al., 2011; Tannahill et al., 2013) as well as expression of *TNFα* and *iNOS*. We observed that a lack of Dj-1 function increased itaconate and succinate levels without an additional perturbation (Fig. 6f, g, S5). Furthermore, we observed increased intracellular lactate levels, most probably a combined result of both, lack of Dj-1 and M1 polarization (Fig. 6h).

To validate the activation, we analyzed gene expression levels of the pro-inflammatory marker genes *Irg1*, *iNOS* and *TNFα*. *Irg1* codes for the enzyme (Cad) that catalyzes the synthesis of itaconate from *cis*-aconitate (Michelucci et al., 2013; Degrandi, 2009; Hall et al., 2013). The increased level of itaconate correlates with a more than twofold increased *Irg1* gene expression in *shDJ-1* compared to *shCtrl*. Moreover, we observed that *TNFα* gene expression was increased twofold and that *iNOS* was more than three times higher expressed than in *shCtrl* (Fig. 6i). To evaluate, how the detected itaconate level in *shDJ-1* cells correlates with different levels of LPS stimulation, we activated the *shCtrl* cells with 0.2 ng, 1 ng and 10 ng of LPS (Fig. 6j). We observed that *shDJ-1* BV-2 microglia constitutively synthesize itaconate amounts corresponding to an activation of *shCtrl* cells with approximately 1 ng of LPS. Since we use 10 ng of LPS to mimic a full activation *in vitro*, we conclude that *shDJ-1* cells show a moderate but constitutive activation.

2.5. Loss of DJ-1 leads to a metabolic shift in primary human and murine immune cells

To validate the observed metabolic alterations in primary cells, we isolated bone marrow-derived cells of *Dj-1* knock-out (KO) mice and differentiated them into macrophages (BMDMs). Since DJ-1 is ubiquitously expressed (Nagakubo et al., 1997), we expected to find the observed metabolic changes also in non-CNS cell types. In line with our previous results in BV-2 cells, BMDMs of *Dj-1* KO mice produced more lactate (Fig. 7a). Moreover, BMDMs of *Dj-1* KO mice consumed significantly less glutamine compared to wild type (WT) BMDMs (Fig. 7B).

Additionally, we applied [U-^{13}C]glutamine as a tracer and observed decreased M5 glutamate fractions in Dj-1 KO cells (Fig. 7c). However, isotopic enrichment in other TCA cycle related metabolites (Fig. 7d) was not significantly different. Compared to LUHMES cells, these differences in isotopic enrichment might be caused by fundamental differences in carbon utilization between the two cell types and/or in a species-specific manner. Although each cell type shows also specific differences, overall, the uptake and release rates of glutamine and lactate point in the same direction when comparing LUHMES, BV-2 and BMDM cells. It is not surprising that cell type specific differences lead to different metabolic phenotypes. However, it is appealing that loss of DJ-1 shows a similar picture in these various cell types.

To further validate our findings, we were interested in analyzing human samples directly originating from patients carrying a *DJ-1* mutation. We analyzed cellular metabolism of peripheral blood derived mononuclear cells (PBMCs)-derived CD14$^+$ macrophages from four patients carrying homozygous and heterozygous loss of function mutations (c.192G > C) in the *DJ-1* gene (Hering et al., 2004). PBMCs are relatively easy to access and could therefore be used as a model in subsequent clinical trials. As controls, we analyzed three independent healthy controls. We applied [U-^{13}C]glucose to provide flux information for both, glycolysis and TCA cycle. Analysis of isotopic enrichment revealed that serine biosynthesis in CD14$^+$ macrophages was close to zero (Fig. S6a). However, the labeling pattern of glutamate showed increased relative abundance of M2 isotopologues in patient-derived macrophages carrying a *DJ-1* mutation (Fig. 7e, f, S6b), indicating increased relative glucose carbon contribution to the TCA cycle and to glutamate. This increase can be a consequence of lower glutamine influx,

resulting in higher relative ^{13}C labeling from glucose. We also observed a relative increase of M2 glutamate in LUHMES *shDJ-1* cells compared to *shCtrl* (Fig. S6c).

In summary, the analysis of human PBMCs indicated that metabolic changes initially observed in a cellular model of the CNS might be diagnosed from patient-derived primary blood cells. Further analyses will clarify if the observed flux changes are common for this mutation and if heterozygous patients show gene-dose dependent effects.

3. Discussion

In this study, we analyzed the metabolic impact of loss of DJ-1. We demonstrated that loss of DJ-1 affects central metabolism, specifically leading to (1) decreased glutamine uptake and decreased glutamine contribution to the TCA cycle, (2) decreased serine biosynthesis, (3) increased sensitivity to ROS and (4) weakly, but constitutively activated microglia. These metabolic alterations coincide with decreased cell survival upon oxidative stress, which may promote early onset of PD. We speculate that these changes are caused by increased sensitivity to ROS as a direct result of loss of DJ-1. Unlike cancer cells, we did not detect NRF2 protein in LUHMES wild type cells which leads us to the assumption that DJ-1 has a more fundamental role in neurons, compared to cancer cells, where NRF2 as a regulator of antioxidant responses is highly abundant (Clements et al., 2006). We conclude that insufficient ROS quenching in DJ-1 deficient neurons is due to decreased GSH levels as well as decreased activity of NADP-reducing enzymes within central metabolism. In line, we observed decreased expression of *G6PDH*, the rate-limiting enzyme of the PPP and decreased expression of MTHFD1 and 2, enzymes of the folate cycle and an alternative route for the generation of NADPH. Moreover, we measured decreased *GR* expression, which is in line with the lower GSH levels and an increased GSSG/GSH ratio upon hydrogen peroxide stress. In conclusion, loss of DJ-1 affects all pathways needed for GSH homeostasis.

DJ-1 has been shown to activate the expression of glutamate cysteine ligase, a key enzyme of GSH synthesis (Zhou and Freed, 2005). However, based on our gene expression analysis, GCLC and GCLM expression was not altered, at least not in LUHMES cells (Fig. S3g, h). We suggest that decreased levels of the rate limiting amino acid cysteine provoke the drop in GSH abundance by altering the net flux towards GSH (Richman and Meister, 1975; Lu, 2013).

Serine can act as a precursor for cysteine and glycine and serves at the same time as a carbon donor for folate-mediated one-carbon metabolism, which has recently been appreciated for its importance in maintaining the cellular NADPH pool (Fan et al., 2014). 5,10-methylene-THF can be oxidized by the NADP-dependent enzyme MTHFD. We observed a moderate, but significantly decreased expression of cytosolic *MTHFD1* and a more strongly decreased expression of mitochondrial *MTHFD2*. Together with glutamate, cysteine and glycine are the building blocks for *de novo* glutathione synthesis. We have demonstrated before that enzymes of serine and folate metabolism as well as the transsulfuration pathway are induced in human neurons upon oxidative stress (Krug et al., 2014). Intriguingly, in the DJ-1 knock-out model, that shows elevated levels of oxidative stress, we observed that serine biosynthesis is decreased and expression of both *MTHFD1* and *2* are reduced. Therefore, DJ-1 is likely to have an important regulatory function in serine and folate metabolism by supporting NADPH and GSH homeostasis. This is especially pronounced due to our observation of no detectable protein levels of NRF2 in post-mitotic neuronal cells. However, we do not exclude the possibility that *in vivo*, neurons are supported by NRF2 mediated protective mechanisms that are derived from surrounding glia cells (Kraft et al., 2004).

The third building block of GSH is glutamate, directly derived from glutamine via glutaminase. We showed that *shDJ-1* cells exhibit decreased *GLS2* expression and lower glutamine influx. The decreased glutamine influx is furthermore reflected in decreased alanine release, suggesting lower glutamine derived anaplerotic reactions. When less
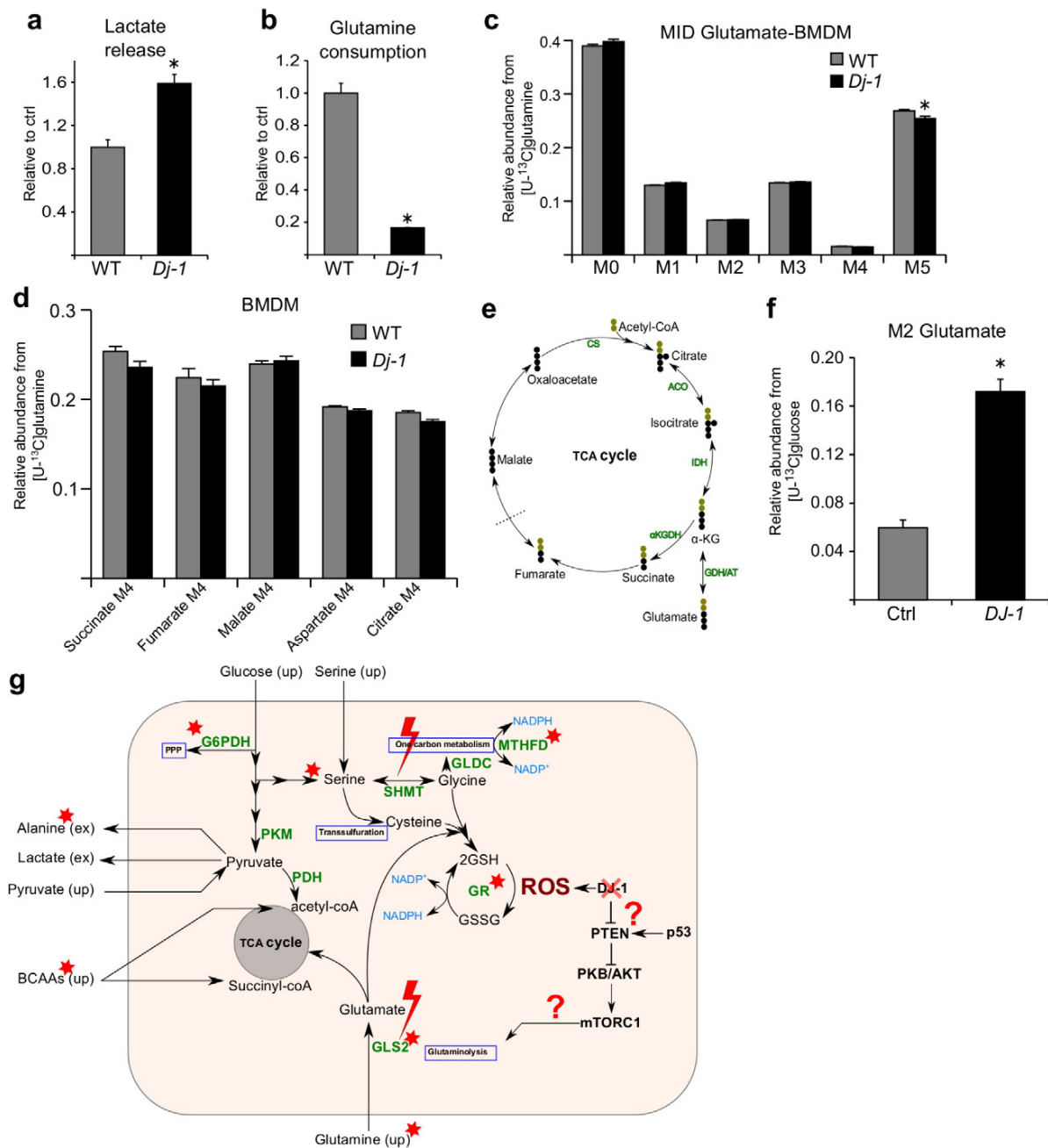
Fig. 7. Stable isotope labeling of BMDMs of *Dj-1* KO mice and PBMCs-derived CD14^{+} macrophages of *DJ-1* patients indicate decreased glutamine contribution to the TCA cycle. (a) Relative lactate release of BMDMs. (b) Relative glutamine consumption of BMDMs. (c) MID of glutamate in BMDMs after application of [U-^{13}C]glutamine. (d) Relative abundance of M4 succinate, M4 fumarate, M4 malate, M4 aspartate and M4 citrate in BMDMs. Error bars represent SEM. Asterisks indicate a significant difference to the respective *shCtrl* (Welch's *t*-test, $p < 0.05$; number of biological replicates: $n = 5$). (e) Schematic of atom transitions in central carbon metabolism using [U-^{13}C]glucose. Illustrated is how M2 glutamate is generated from [U-^{13}C]glucose. The dotted line indicates end of one route. (f) Glutamate M2 isotopologue abundance of *DJ-1* subjects and non-familial healthy controls (Ctrl). Error bars represent SEM. The asterisk indicates a significant difference to the control (Welch's *t*-test, $p < 0.05$; number of individuals: $n \geq 3$). (g) Model highlighting the functional role of DJ-1 and summarizing the affected metabolic pathways as a result of DJ-1 deficiency. Affected metabolites, enzymes or pathways are highlighted with a red star. Loss of DJ-1 leads to decreased glutamine influx, decreased serine biosynthesis and decreased MTHFD expression, needed for glutathione (GSH) homeostasis and antioxidant response. Due to lower GSH levels, DJ-1 deficient cells show increased sensitivity to ROS. Additionally, lower expression of MTHFD and G6PDH suggests decreased potential to generate NADPH, needed for the reduction of GSSG. In cancer cells, DJ-1 acts as a repressor of PTEN, a negative regulator of AKT. Activated AKT can activate mTORC1. Both AKT and mTOR are important to drive metabolic processes needed for cell survival and proliferation, among others, glutaminolysis (for further explanation see discussion). Additionally, the transcription factor p53 can act as an activator on PTEN, thereby antagonizing DJ-1 function. Moreover, p53 can repress mTOR and introduces apoptosis. However, the relevance of these potential nodes of the metabolic network has to be further validated in neuronal cells. See also Supplementary Fig. S6.

glutamate enters the TCA cycle, less nitrogen has to be disposed from the cell. Previous work in cancer cell models demonstrated that a knock-down of *GLS2* results in decreased GSH levels and increased oxidative stress (Suzuki et al., 2010; Hu et al., 2010). However, Richman and Meister showed that not glutamate but cysteine is rate limiting to GSH synthesis (Richman and Meister, 1975). Therefore, we believe that serine and the adjacent transsulfuration pathway play an important role for the generation of GSH. On top of serine metabolism, decreased

expression of *GLS2* and lower glutamine influx adds an additional perturbation to the cell system, which ultimately triggers the observed physiological effects (Fig. 7g). The defect present in *shDJ-1* cells might not only be the result of elevated oxidative stress levels, but DJ-1 might play a role in additional processes. A possible role could be related to the described inhibitory function on PTEN (Kim et al., 2005). When DJ-1 is absent, AKT becomes hypophosphorylated (Aleyasin et al., 2010; Yang et al., 2005) and mTOR, a master regulator of anaplerosis, proliferation and cell survival, becomes less active, which could also favor the activity of p53. The transcription factor p53 is activated upon oxidative stress and can induce apoptosis (Vousden and Ryan, 2009). The role of these fundamental metabolic mechanisms is also relevant during neurogenesis (Rafalski and Brunet, 2011; Vasseur et al., 2009). However, the mechanistic link between DJ-1 and PTEN in regulating the AKT pathway is derived from cancer cells (Kim et al., 2005) and needs additional validation in post-mitotic neurons. Also the interplay between p53 and DJ-1 as well as the role of p53 in activating PTEN in neuronal non-proliferating cells needs additional research to gain a deeper understanding of the metabolic processes that are in place. Another potential link to the mTOR pathway is based on the work by Durán and colleagues (2012) who demonstrated that Rag-mTORC1 signaling is directly regulated by glutaminolysis and that a lack of glutamine results in less mTORC1 phosphorylation and less downstream activation without affecting ATP production (Durán et al., 2012). No difference in ATP production is also in line with our own results indicating functional OxPhos, a major pathway for ATP production, especially in neuronal cells. However, given the example of NRF2 abundance in LUHMES *versus* A549 lung cancer cells (Fig. S3f), comparisons with proliferating cancer cells should be interpreted carefully, since post-mitotic cells have very different metabolic requirements.

An apparent difference was also reflected by the lactate release in LUHMES cells and proliferating, immortalized BV-2 cells. In proliferating cells, increased ROS levels, as present in *shDJ-1* cells, can regulate PKM2 and enhance the Warburg effect. In its metabolically active form PKM2 acts as a tetramer. However, at increased ROS levels, PKM2 is post-translationally modified, stabilizing its dimeric or monomeric form (Anastasiou et al., 2011; Gupta and Bamezai, 2010; Lyssiotis et al., 2012). In this form, PKM2 translocates to the nucleus and influences transcriptional regulation to increase lactate release. In contrast to proliferating cells, post-mitotic neurons express the M1 isoform of pyruvate kinase (Tolle et al., 1976), which is less regulated (Anastasiou et al., 2012; Chaneton et al., 2012). This explains why we did not observe an increase in lactate fermentation in LUHMES cells, but increased lactate release in the proliferating (PKM2 expressing) BV-2 cells.

The reduction of glutamine influx after loss of DJ-1 was weaker in BV-2 cells than in post-mitotic LUHMES cells because BV-2 cells are immortalized with *v-myc/ras* (Blasi et al., 1990), which reprograms cellular metabolism to drive proliferation. A dependency of cancerous and proliferating cells on glutamine is well known (Wise and Thompson, 2010). Moreover, DJ-1 has been shown to activate ERK signaling, promoting cellular protection against oxidative stress (Gu et al., 2009). For that reason, immortalization with *v-myc*, an upstream regulator of ERK1/2 and AKT, might mask underlying metabolic defects by artificially activating the ERK pathway in DJ-1 deficient cells. Thus, the observed decreased glutamine influx and the known increased activation of PTEN due to lack of DJ-1 is at least partially overwritten in immortalized BV-2 cells, leading to re-elevated glutamine uptake. In differentiated LUHMES cells, *v-myc* expression is absent and is therefore not masking decreased glutamine influx (Scholz et al., 2011). Therefore, the metabolic dysfunction in differentiated, post-mitotic neurons is more pronounced and represents a clearer phenotype compared to BV-2 cells.

Besides the described effects in neurons, DJ-1 has been shown to play a role in inflammation by regulating cytokine expression and by interacting with STAT1 signaling (Kim et al., 2013; Trudler et al., 2014; Waak et al., 2009). Here, we demonstrated that solely the loss of DJ-1 results in weakly activated microglia. A constitutive, strong activation would cause immediate detrimental effects in a multicellular environment. However, a weak activation could be tolerated over a longer period of time (*e.g.* several years or decades) but would represent an additional trigger for PD, increasing the sensitivity of DAergic neurons over the course of life.

A metabolic reprogramming of immune cells upon M1 polarization has recently been described (Tannahill et al., 2013; Palsson-McDermott et al., 2015). M1 polarization in immune cells has been shown to induce a Warburg-like metabolic phenotype. A PKM2-mediated regulation in macrophages is possible (Palsson-McDermott et al., 2015). M1 polarized macrophages increase their rate of glycolysis and increase lactate release. In the case of loss of DJ-1, this is an additive effect and explains why the increase in lactate release is more pronounced in BV-2 cells compared to neurons. The metabolic adaptation to inflammation also includes increased glutamine oxidation in the TCA cycle (Tannahill et al., 2013). Therefore, decreased GLS2 activity in immune cells as a result of DJ-1 deficiency can at least be partially overwritten by inflammatory activation and immortalization.

Although TH$^+$-neurons do not proliferate, cellular survival and antioxidant response is even more important since these cells are mostly matured during embryogenesis and need to be functional over the whole life span to supply sufficient dopamine to the *striatum*. Increased oxidative stress during development can result in a lower absolute number of dopaminergic neurons in the midbrain (Pham et al., 2010). In conclusion, it becomes evident that as opposed to cancer therapy, where SHMT2 amplification drives oncogenesis (Kim et al., 2015; Lee et al., 2014) and where a decrease of glutamine uptake is a strategy to stop cell proliferation, a lack of glutamine influx and decreased serine biosynthesis flux seem to be part of the underlying metabolic problem in PD patients carrying a loss of function mutation in *DJ-1*.

4. Methods

4.1. Cell culture

Cells were standardwise tested for mycoplasma contamination in a rhythm of four to eight weeks.

4.2. LUHMES

Cells were kindly provided by the lab of Marcel Leist. Cells were grown in proliferation medium (Advanced DMEM/F12 + 1xN2 supplement (Invitrogen), 40 ng/ml FGF-2 and 2 mM glutamine) at 37 °C and 5% CO$_2$. Further cultivation and differentiation was performed as described in (Krug et al., 2014). For isotopic labeling, medium was replaced by differentiation medium containing 2 mM [U-^{13}C$_5$]glutamine or 17.5 mM [U-^{13}C$_6$]glucose. Cells were extracted at metabolic and isotopic steady state (42 h after labeling start). All experiments were performed with differentiated post-mitotic cells.

4.3. BV-2

Cells were kindly provided by the lab of Wolfgang Wurst. Cells were grown in DMEM (D5796) (Invitrogen) containing 5 mM glutamine, 25 mM glucose, 10% FBS and 1% P/S at 37 °C and 5% CO$_2$. For isotopic labeling medium was replaced by the same medium containing 5 mM [U-^{13}C]glutamine or 25 mM [U-^{13}C]glucose and dialysed FBS. Cells were extracted at metabolic and isotopic steady state (24 h after labeling start).

4.4. Extraction of intracellular metabolites

Cells were cultivated in 12-well plates and washed with 1 ml of 0.9% NaCl and quenched with 0.2 ml −20 °C methanol. After adding an equal volume of 4 °C cold water, cells were collected with a cell scraper and transferred to tubes containing 0.2 ml −20 °C chloroform. The extracts

were shaken at 1400 rpm for 20 min at 4 °C (Thermomixer Eppendorf) and centrifuged at $16,000 \times g$ for 5 min at 4 °C. 0.2 ml of the upper aqueous phase was collected in specific glass vials with micro inserts and evaporated under vacuum at -4 °C using a refrigerated CentriVap Concentrator (Labconco).

4.5. Liquid chromatography–tandem mass spectrometry to measure GSH and GSSG

Cells were cultured in 12-well plates (500,000 cells per well) and washed once with $1 \times$ PBS before adding 40 μl of 5% TCA, followed by an equal volume of cold H_2O. 2 wells were pooled for one sample to increase abundance of GSSG in the sample. Cells were scraped, transferred into 1.5 ml Eppendorf tubes and centrifuged for 5 min at $13,000 \times g$ at 4 °C. Supernatant was transferred into LC–MS glass vials with insert and stored at -80 °C until measurement. Measurement was performed using an Agilent 1290 Series LC coupled to an Agilent 6550 iFunnel Q-TOF MS system equipped with a Dual Agilent Jet Stream ESI source. The columns used in this study were a Waters ACQUITY UPLC HSS T3 1.8 μm (length, I.D., particle size: 100 mm × 2.1 mm × 1.8 μm) and a Phenomenex Kinetex 2.6 μm C18 100 A (length, I.D., particle size: 150 mm × 2.1 mm × 2.6 μm). The autosampler was kept at 4 °C and the column compartment at constant temperature of 45 °C. The LC conditions were optimized to achieve the best chromatographic parameters for both analytes. The flow rate was set to 0.3 ml/min and the mobile phases consisted of 0.1% formic acid in water (eluent A) and 0.1% formic acid in 60% methanol (eluent B). The run consisted of a isocratic delivery of 1% eluent B over 10 min, followed by a linear gradient to 99% eluent B over 2 min, isocratic delivery of 99% eluent B for 7 min, and a re-equilibration phase on starting conditions with 1% eluent B for 5 min. The eluent from the column was only introduced into the mass spectrometer within the first 10 min. The injection volume was 20 μl.

All the MS experiments were performed using electrospray ionization in positive mode ($+ESI$).

The identity of both GSH and GSSH were confirmed by MS/MS and standard addition experiments. Full scan spectra were acquired from m/z 150…1000 (1 spectra/s).

The protonated molecules of both GSH and GSSG were monitored in high resolution mode with following Q-TOF MS conditions: drying gas temperature: 225 °C, drying gas flow: 14 l/min (nitrogen), nebulizer: 35 psig, sheath gas temperature: 350 °C, sheath gas flow: 11 l/min, fragmentor: 400 V, skimmer: 65 V, Oct. RF Vpp: 750 V.

All data were acquired with Agilent MassHunter Workstation Software, version B.05.01 and analyzed with Agilent Qualitative Analysis, version B.06.00. Signal intensities were normalized to cell number.

4.6. Gas chromatography–mass spectrometry

Metabolite derivatization was performed using a Gerstel MPS. Dried polar metabolites were dissolved in 15 μl of 2% methoxyamine hydrochloride in pyridine at 40 °C under shaking. After 60 min an equal volume of MTBSTFA was added and held for 60 min at 40 °C. 1 μl sample was injected into an SSL injector at 270 °C in splitless mode. GC/MS analysis was performed using an Agilent 7890A GC equipped with a 30 m DB-35MS + 5 m Duraguard capillary column. Helium was used as carrier gas at a flow rate of 1.0 ml/min. The GC oven temperature was held at 100 °C for 2 min and increased to 300 °C at 10 °C/min. After 3 min, the temperature was increased to 325 °C. The GC was connected to an Agilent 5975C inert XL MSD, operating under electron ionization at 70 eV. The MS source was held at 230 °C and the quadrupole at 150 °C. The MS was operated in selected ion monitoring (SIM) (Table S1). The total run time of one sample was 25.00 min. All GC/MS chromatograms were processed by using MetaboliteDetector. MIDs were determined and corrected for natural isotope abundance using MetaboliteDetector (Hiller et al., 2009).

In case of absolute quantification of metabolites, a dilution series of a standard mix containing all relevant metabolites was included in the sequence and measured in duplicates.

Measurement of glucose and pyruvate intensities was performed by derivatization with an equal volume of MSTFA (instead of MTBSTFA) and held for 30 min at 40 °C under continuous shaking. 1 μl sample was injected into an SSL injector at 270 °C in split 10 mode. GC oven temperature was held at 90 °C for 1 min and increased to 300 °C at 15 °C/min for 8 min to 320 °C. The total run time of one sample was 24.3 min.

4.7. Quantification of amino acids

Quantification of amino acids was performed on an Agilent 1100 HPLC System equipped with a Diode Array Detector. Separation was carried out on a ZORBAX Amino Acid Analysis Column (150 × 4.6 mm, 5 μm) with a preceding ZORBAX Amino Acid Analysis Guard Cartridge (Agilent Technologies, Santa Clara, CA, USA) at 40 °C in gradient mode. The eluents used were 40 mM Na_2HPO_4 (pH 7.8, eluent A) and a mixture of Acetonitrile, Methanol and Water (45:45:10, eluent B). 0.02% sodium azide was added to eluent A to prevent microbial growth. Primary amines were automatically derivatized with ortho-phthalaldehyde (OPA) in borate buffer (0.4 N in water, pH 10.2) and diluted in eluent A prior to injection. The resulting OPA-derivatives were subsequently detected at 338 nm (10 nm bandwidth — reference wavelength: 390 nm, 20 nm bandwidth). All medium samples were diluted 1:1 with the internal standard L-2-aminobutyric acid (final concentration: 300 μM) to correct for deviations resulting from the derivatization-process. External calibration standards as well as reference media with known concentrations were measured with every run to determine sample concentrations and ensure stability of the analysis. Gradient profile: 1.9 min: 0% eluent B; 18.1 min: 57% eluent B; 18.6 min: 100% eluent B; 22.3 min: 100% eluent B; 23.2 min: 0% eluent B; 26 min: 0% eluent B.

4.8. cDNA synthesis and gene expression analysis

cDNA synthesis and qPCR was performed as previously described (Michelucci et al., 2013). Briefly, RNA was isolated from the interphase after extraction of metabolites, using the Quiagen RNAeasy Mini Kit. 0.5–1 μg RNA was used for cDNA synthesis using SuperScript III (Invitrogen), following the manufacturer's instructions. qPCR was performed using iQ SYBR Green Supermix (Bio-Rad) as manufacturer's instructions. PCR was carried out on a Light Cycler 480 (Roche). Data analysis was performed using the Roche analysis software. Gene expression was normalized to the housekeeping gene *L27*. Primer sequences are summarized in Table S2.

4.9. Lentivirus mediated shRNA gene silencing

For gene silencing of LUHMES cells, the destination vectors containing shRNA were ordered from Thermo Scientific (http://www. thermoscientificbio.com). Plasmids were amplified and purified by maxiprep in *Escherichia coli* and subsequently used for virus production in HEK298FT cells according to the manufacturer's protocol. Harvested virus was filtered using a 45 μM filter and precipitated with 1/5 volume of sterile PEG10000 over night at 4 °C. Concentrated virus was aliquoted in 10 μl and stored at -80 °C. For virus transduction 10 μl virus was added to 50,000 cells on day 1 and day 2. After medium change on day 3 cells were selected using 200 ng/ml puromycin. Correct concentration of puromycin was evaluated by a kill curve.

4.10. Western blot

For preparation of whole cell extract, 1×10^6 cells were harvested, washed with ice cold $1 \times$ PBS (Invitrogen/Life Technologies Europe BV

Belgium), lyzed in $1\times$ M-PER®, Mammalian Protein Extraction Reagent (Thermo Scientific, Belgium) completed with $1\times$ protease inhibitor cocktail (Complete®, Roche, Luxembourg) and further processed according to manufactures instructons. Bradford assay was used to measure the protein concentration (Bio-Rad Protein Assay Dye Reagent, Bio-Rad, Belgium). Proteins were separated by size using sodium dodecyl sulfate polyacrylamide gel elegrophoresis (SDS-PAGE, 15%) and transferred to an Immobilon-FL PVDF membrane (Merck Millipore) using the Mini-PROTEAN Tetra Cell and PowerPac Basic Power Supply (Bio-Rad, Belgium). The membrane was blocked in 5% non-fat milk in phosphate buffered saline (PBS)-Tween for 1 h at room temperature. Blots were incubated with primary antibodies: anti DJ-1 XP® Rabbit mAb (D29E5) (CellSignaling, Bioke, Netherlands) in 5% BSA in PBS-T (1:1000) for 1 h at room temperature. After incubation with primary antibody, membrane was washed with PBS-T and incubated for 1 h at room temperature with anti rabbit-HRP secondary antibody (1:10,000). For equal loading control of samples monoclonal anti-GAPDH-HRP (mouse) antibody (G9295, Sigma, Belgium), was probed in 5% non-fat milk in PBS-T for 1 h at room temperature. Visualization was done using the ECL Plus Western Blotting Detection System Kit (GE Healthcare, Netherlands).

4.11. Cell viability assay

Cell viability was assayed using Resazurin (Sigma Aldrich, R7017) (O'Brien et al., 2000). Briefly, resazurin, blue and non-fluorescent, is reduced to resorufin, pink and fluorescent, proportionally to the number of living cells. After 1 h incubation with 5 μg/ml resazurin (spiked in medium), fluorescence was measured with a Biotek Synergy Mx microplate reader coupled to the Gen5 software at the excitation wavelength of 570 nm and emission at 590 nm.

4.12. Cell imaging

Predifferentiated LUHMES cells were seeded at a density of 60 k cells/well in 96-well plates. After 96 h the cells were post-mitotic and had formed strongly connected networks. One hour prior to imaging experiments, the wells were carefully washed and filled with 100 μl fresh differentiation medium supplemented with 25 nM tetramethylrhodamine (TMRM) to fluorescently stain mitochondria. Plates were then incubated for 30 min at 37 °C, 5% CO_2, whereafter the medium was replaced by TMRM-free solution. Plates were kept for further 30 min at 37 °C, 5% CO_2. Time-lapse images were acquired on a Nikon Ti Eclipse inverted microscope with motorized stage (Nikon Corporation, Tokyo, Japan) and high intensity mercury short arc lamp with monochromator (Cairn Research, Kent, UK) enclosed in a bench top incubator. Fluorescence excitation filter was 540/15 and emission filter 620/60. Automatic microscope control, stage programming and acquisition were done using OptoMorph (Cairn Research, Kent, UK).

Two types of experiments were performed: i) longitudinal acquisition of a single well with one image taken every 2 s for 20 min, and ii) comparative parallel acquisition by switching between two neighboring wells using the motorized stage and taking images every 5 s for 30 min. Imaged wells were supplemented with 200 μM 6-OHDA or pure water for control after 5 min. Images were taken using a $20\times$ air objective and an EXi Blue camera (Qimaging, Surrey, BC) with an exposure time of 350 ms and saved as 16-bit grayscale TIFFs in 1392×1040 px.

4.13. Global motion analysis

Global motion by particle image velocimetry (PIV) was analyzed, which quantifies correlations between pairs of time-lapse images and infers velocities of the image elements that give rise to differences. Microscopy images were contrast-normalized and converted to 8-bit grayscale using ImageMagick. Particle image velocimetry was performed using the OpenPIV toolbox (Taylor et al., 2010) in sliding windows of

16×16 px with 8 px overlap in both vertical and horizontal direction. Statistical analysis of resulting velocity fields and visualization of results was done in GNU R. Global motion was quantified by calculating median velocities over sliding windows spanning six acquisition frames to reduce impulse noise corruption from imaging artifacts. Average motion was assessed in acquisition windows 1 to 100 (pre-treatment) and 401 to 500 (post-treatment) for longitudinal measurements as well as 1 to 40 (pre-treatment) and 301 to 340 (post treatment) for parallel measurements. Significance of difference in motility reduction was assessed by pooling average velocities before and after treatment from all time-lapse experiments ($n = 3$) and performing Student's t-test on relative velocities, i.e., normalized to untreated control. Propagation of uncertainty when normalizing velocities was taken into account.

4.14. BMDM isolation, cultivation and differentiation

4.14.1. Animals

For bone marrow-derived macrophages cultures, C57BL/6 *DJ-1* KO and age-matched C57BL/6 WT mice were obtained from the Helmholtz Zentrum München (Germany) from Dr. Daniela Vogt-Weisenhorn and Prof. Dr. Wolfgang Wurst. Per group, 5 mice were analyzed and from each mouse three independent samples were obtained. All animal work in Munich was carried out in accordance with the European Communities' Council Directive 2010/63/EU. All efforts were made to minimize animal suffering during the work. All protocols involving animal handling were approved by the committee for the Care and Use of Laboratory animals of the Government of Upper Bavaria, Germany. C57BL/6 mice (obtained from Charles River Germany) were group housed in individually ventilated type IIL cages (four mice per cage) and maintained on a 12 h/12 h light/dark cycle with food and water available *ad libitum*. All animal procedures in Luxembourg, such as handling and euthanasia, have been performed according to the Federation of European Laboratory Animal Science Associations (FELASA) guidelines for the use of animals in research, and were institutionally approved by the Luxembourg Centre for System Biomedicine animal user committee and authorized by the local governmental agencies (Ministry of Health, Ministry of Agriculture, chief veterinarian of the Luxembourg government).

4.14.2. Bone marrow-derived macrophages

Mice were deeply anesthetized by intraperitoneal injection of 50 mg/kg of ketamine hydrochloride and 5 mg/kg xylazine hydrochloride and bone marrows were isolated and cultured as previously described by Zhang and colleagues (Zhang et al., 2008). Briefly, bone marrow was flushed from femurs and tibias of five C57BL/6 DJ-1 KO and five age-matched C57BL/6 WT mice and the resultant cell suspension was passed through a 70 μm filter (Greiner Bio-One). After a 10 min centrifugation step at $250 \times g$, supernatant was discarded and pellet re-suspended in 2 ml hypotonic solution (170 mM NH_4Cl) for 5 min to allow lysis of any remaining extracellular red blood cells. Bone marrow-derived cells were finally plated in 12-well plates (Greiner Bio-One) at 5×10^5 cells per well. Cells were cultured for 6 days in complete macrophage medium (Dulbecco modified Eagle's minimal essential medium DMEM) (Invitrogen) supplemented with 10% fetal bovine serum (FBS) (Invitrogen), 20% conditioned medium from macrophage-colony stimulating factor-secreting L929 fibroblasts and 1% penicillin/streptomycin (Invitrogen) at 37 °C. After 6 days in culture, adherent cells were approximately 95% pure macrophages and cells were used for experiments. Stable isotope tracers were added for 24 h prior extraction of intracellular metabolites.

Per genotype 5 individual mice were sacrificed and from each mouse three replicates of BMDMs were used for the analysis.

4.14.3. PBMC derived $CD14^+$ macrophages

The four *DJ-1* patients were brothers of one family (one homozygous and three heterozygous). The samples were analyzed in a blinded

study; patient samples were given numbers and were identified after the results were completely analyzed. The controls were non-family members with different genetic background (two male, one genotype unknown (blood donation from the red cross)). The $CD14^+$ cells were isolated by a positive selection method using the magnetic activated cell sorting (MACS) method: Blood samples of the patients were separated in 50 ml Leucosept tubes (Greiner) through Ficoll-Paque Premium (GE Healthcare) density gradient centrifugation ($1000 \times g$) for 10 min at room temperature, using no break. After 30 min incubation at 4 °C with 2 µl of $CD14^+$ beads (Miltenyi biotech) per 10^7 PBMCs, the $CD14^+$ cells got purified using a positive LS column (Miltenyi Biotech). The purified $CD14^+$ cells were incubated for 24 h at 37 °C and 5% CO_2 in DMEM D5030 medium (Sigma) containing 11 mM [U-$^{13}C_6$]glucose and 5 mM glutamine for metabolite extraction. Cells were extracted at metabolic and isotopic steady state (24 h after labeling start, (tested before with other blood donations)). Heterozygous and homozygous patients were male, two healthy controls were male, the status of the third healthy control is unknown (blood donation of the red cross).

4.14.4. Statistical analyses

To analyze a significant difference between two groups, the Welch's *t*-test or two-way ANOVA was applied. The level of $p < 0.05$ was considered as significant different. Significance of difference in motility reduction was assessed by pooling average velocities before and after treatment from all time-lapse experiments ($n = 3$) and performing Student's *t*-test on relative velocities, *i.e.*, normalized to untreated control. Propagation of uncertainty when normalizing velocities was taken into account.

Supplementary data to this article can be found online at http://dx.doi.org/10.1016/j.nbd.2016.01.019.

Author contributions

JM planned and performed experiments, analyzed data and wrote the manuscript; SD performed experiments, analyzed data and provided parts of Fig. S3. AW and DW analyzed data and revised the manuscript; JG, XD, and LK performed experiments; SS performed and discussed experiments; AM isolated BMDMs; YN set up the HPLC method and measured medium samples; AF and AS performed microscopy and motility analysis; CJ developed LC–MS methods, measured and analyzed the GSH experiments; CS generated and validated BV-2 *shDJ-1* and BV-2 *shCtrl* cells; FG supervised virus production for BV-2 cells; OP tried to detect NRF2 protein via mass-spectrometry; JS helped to establish the method for the PBMCs experiments; RK helped with PBMCs experiment and revised the manuscript; DWo. takes care for DJ-1 patients and isolated blood of DJ-1 patients; DV-W and WW provided *Dj-1* KO mice and revised the manuscript; ML revised the manuscript and discussed experiments; KH planned and discussed experiments and revised the manuscript.

Competing financial interests

The authors declare no conflict of interest.

Acknowledgments

References

Aleyasin, H., et al., 2010. DJ-1 protects the nigrostriatal axis from the neurotoxin MPTP by modulation of the AKT pathway. Proc. Natl. Acad. Sci. 107, 3186–3191.

Anastasiou, D., et al., 2011. Inhibition of pyruvate kinase M2 by reactive oxygen species contributes to cellular antioxidant responses. Science 334, 1278–1283.

Anastasiou, D., et al., 2012. Pyruvate kinase M2 activators promote tetramer formation and suppress tumorigenesis. Nat. Chem. Biol. 8, 839–847.

Antony, P.M.A., Diederich, N.J., Krüger, R., Balling, R., 2013. The hallmarks of Parkinson's disease. FEBS J. 280, 5981–5993.

Ariga, H., et al., 2013. Neuroprotective function of DJ-1 in Parkinson's disease. Oxidative Med. Cell. Longev. 2013, 1–9.

Bader, V., Ran Zhu, X., Lübbert, H., Stichel, C.C., 2005. Expression of DJ-1 in the adult mouse CNS. Brain Res. 1041, 102–111.

Baulac, S., et al., 2009. Increased DJ-1 expression under oxidative stress and in Alzheimer's disease brains. Mol. Neurodegener. 4, 12.

Blasi, E., Barluzzi, R., Bocchini, V., Mazzolla, R., Bistoni, F., 1990. Immortalization of murine microglial cells by a v-raf/v-myc carrying retrovirus. J. Neuroimmunol. 27, 229–237.

Bonifati, V., 2003. Mutations in the DJ-1 gene associated with autosomal recessive early-onset parkinsonism. Science 299, 256–259.

Bonifati, V., et al., 2003. DJ-1 (PARK7), a novel gene for autosomal recessive, early onset parkinsonism. Neurol. Sci. 24, 159–160.

Brown, G.C., Neher, J.J., 2010. Inflammatory neurodegeneration and mechanisms of microglial killing of neurons. Mol. Neurobiol. 41, 242–247.

Canet-Avilés, R.M., et al., 2004. The Parkinson's disease protein DJ-1 is neuroprotective due to cysteine-sulfinic acid-driven mitochondrial localization. Proc. Natl. Acad. Sci. U. S. A. 101, 9103–9108.

Chaneton, B., et al., 2012. Serine is a natural ligand and allosteric activator of pyruvate kinase M2. Nature 491, 458–462.

Chen, S., Owens, G.C., Edelman, D.B., 2008. Dopamine inhibits mitochondrial motility in hippocampal neurons. PLoS One 3, e2804.

Clements, C.M., McNally, R.S., Conti, B.J., Mak, T.W., Ting, J.P.-Y., 2006. DJ-1, a cancer- and Parkinson's disease-associated protein, stabilizes the antioxidant transcriptional master regulator Nrf2. Proc. Natl. Acad. Sci. 103, 15091–15096.

Davidson, B., et al., 2008. Expression and clinical role of DJ-1, a negative regulator of PTEN, in ovarian carcinoma. Hum. Pathol. 39, 87–95.

Degrandi, 2009. The proinflammatory cytokine-induced IRG1 protein associates with mitochondria. 29, 55–68.

Durán, R.V., et al., 2012. Glutaminolysis activates Rag-mTORC1 signaling. Mol. Cell 47, 349–358.

Fan, J., et al., 2014. Quantitative flux analysis reveals folate-dependent NADPH production. Nature 510, 298–302.

Fendt, S.-M., et al., 2013. Reductive glutamine metabolism is a function of the α-ketoglutarate to citrate ratio in cells. Nat. Commun. 4.

Gu, L., et al., 2009. Involvement of ERK1/2 signaling pathway in DJ-1-induced neuroprotection against oxidative stress. Biochem. Biophys. Res. Commun. 383, 469–474.

Gupta, V., Bamezai, R.N.K., 2010. Human pyruvate kinase M2: A multifunctional protein. Protein Sci. 19, 2031–2044.

Guzman, J.N., et al., 2010. Oxidant stress evoked by pacemaking in dopaminergic neurons is attenuated by DJ-1. Nature 468, 696–700.

Hall, C.J., et al., 2013. Immunoresponsive gene 1 augments bactericidal activity of macrophage-lineage cells by regulating β-oxidation-dependent mitochondrial ROS production. Cell Metab. 18, 265–278.

Hayes, J.D., Dinkova-Kostova, A.T., 2014. The Nrf2 regulatory network provides an interface between redox and intermediary metabolism. Trends Biochem. Sci. 39, 199–218.

Henn, A., et al., 2009. The suitability of BV2 cells as alternative model system for primary microglia cultures or for animal experiments examining brain inflammation. ALTEX 26, 83–94.

Hering, R., et al., 2004. Novel homozygous p. E64D mutation in DJ1 in early onset Parkinson disease (PARK7). Hum. Mutat. 24, 321–329.

Hiller, K., et al., 2009. MetaboliteDetector: comprehensive analysis tool for targeted and nontargeted GC/MS based metabolome analysis. Anal. Chem. 81, 3429–3439.

Hu, W., et al., 2010. Glutaminase 2, a novel p53 target gene regulating energy metabolism and antioxidant function. Proc. Natl. Acad. Sci. 107, 7455–7460.

Irrcher, I., et al., 2010. Loss of the Parkinson's disease-linked gene DJ-1 perturbs mitochondrial dynamics. Hum. Mol. Genet. 19, 3734–3746.

Javitch, J.A., D'Amato, R.J., Strittmatter, S.M., Snyder, S.H., 1985. Parkinsonism-inducing neurotoxin, N-methyl-4-phenyl-1,2,3,6-tetrahydropyridine: uptake of the metabolite N-methyl-4-phenylpyridine by dopamine neurons explains selective toxicity. Proc. Natl. Acad. Sci. 82, 2173–2177.

Kahle, P.J., Waak, J., Gasser, T., 2009. DJ-1 and prevention of oxidative stress in Parkinson's disease and other age-related disorders. Free Radic. Biol. Med. 47, 1354–1361.

Kim, R.H., et al., 2005. DJ-1, a novel regulator of the tumor suppressor PTEN. Cancer Cell 7, 263–273.

Kim, J., et al., 2013. DJ-1 facilitates the interaction between STAT1 and its phosphatase, SHP-1, in brain microglia and astrocytes: A novel anti-inflammatory function of DJ-1. Neurobiol. Dis. 60, 1–10.

Kim, D., et al., 2015. SHMT2 drives glioma cell survival in ischaemia but imposes a dependence on glycine clearance. Nature 520, 363–367.

Kraft, A.D., Johnson, D.A., Johnson, J.A., 2004. Nuclear factor E2-related factor 2-dependent antioxidant response element activation by tert-butylhydroquinone and

sulforaphane occurring preferentially in astrocytes conditions neurons against oxidative insult. J. Neurosci. 24, 1101–1112.

Krebiehl, G., et al., 2010. Reduced basal autophagy and impaired mitochondrial dynamics due to loss of Parkinson's disease-associated protein DJ-1. PLoS One 5, e9367.

Krols, M., et al., 2016. Mitochondria-associated membranes as hubs for neurodegeneration. Acta Neuropathol. (Berl.) http://dx.doi.org/10.1007/s00401-015-1528-7.

Krug, A.K., et al., 2014. Transcriptional and metabolic adaptation of human neurons to the mitochondrial toxicant MPP+. Cell Death Dis. 5, e1222.

Lee, J.-Yy., et al., 2012. Human DJ-1 and its homologs are novel glyoxalases. Hum. Mol. Genet. 21, 3215–3225.

Lee, G.Y., et al., 2014. Comparative oncogenomics identifies PSMB4 and SHMT2 as potential cancer driver genes. Cancer Res. 74, 3114–3126.

Lu, S.C., 2013. Glutathione synthesis. Biochim. Biophys. Acta Gen. Subj. 1830, 3143–3153.

Lyssiotis, C.A., et al., 2012. Cellular control mechanisms that regulate pyruvate kinase M2 activity and promote cancer growth. Biomed. Res. 23, 213–217.

Meiser, J., Weindl, D., Hiller, K., 2013. Complexity of dopamine metabolism. Cell Commun. Signal. 11.

Michelucci, A., et al., 2013. Immune-responsive gene 1 protein links metabolism to immunity by catalyzing itaconic acid production. Proc. Natl. Acad. Sci. 110, 7820–7825.

Mitsuishi, Y., et al., 2012. Nrf2 redirects glucose and glutamine into anabolic pathways in metabolic reprogramming. Cancer Cell 22, 66–79.

Mitsumoto, A., Nakagawa, Y., 2001. DJ-1 is an indicator for endogenous reactive oxygen species elicited by endotoxin. Free Radic. Res. 35, 885–893.

Mullen, A.R., et al., 2014. Oxidation of alpha-ketoglutarate Is required for reductive carboxylation in cancer cells with mitochondrial defects. Cell Rep. 7, 1679–1690.

Nagakubo, D., et al., 1997. DJ-1, a novel oncogene which transforms mouse NIH3T3 cells in cooperation with ras. Biochem. Biophys. Res. Commun. 231, 509–513.

Nguyen, T.T., et al., 2014. Loss of Miro1-directed mitochondrial movement results in a novel murine model for neuron disease. Proc. Natl. Acad. Sci. U. S. A. 111, E3631–E3640.

O'Brien, J., Wilson, I., Orton, T., Pognan, F., 2000. Investigation of the Alamar Blue (resazurin) fluorescent dye for the assessment of mammalian cell cytotoxicity. Eur. J. Biochem. 267, 5421–5426.

Palsson-McDermott, E.M., et al., 2015. Pyruvate kinase M2 regulates hif-1α activity and IL-1β induction and is a critical determinant of the Warburg effect in LPS-activated macrophages. Cell Metab. 21, 65–80.

Pham, T.T., et al., 2010. DJ-1-deficient mice show less TH-positive neurons in the ventral tegmental area and exhibit non-motoric behavioural impairments. Genes Brain Behav. 9, 305–317.

Rafalski, V.A., Brunet, A., 2011. Energy metabolism in adult neural stem cell fate. Prog. Neurobiol. 93, 182–203.

Richman, P.G., Meister, A., 1975. Regulation of gamma-glutamyl-cysteine synthetase by nonallosteric feedback inhibition by glutathione. J. Biol. Chem. 250, 1422–1426.

Saxton, W.M., Hollenbeck, P.J., 2012. The axonal transport of mitochondria. J. Cell Sci. 125, 2095–2104.

Schildknecht, S., et al., 2015. Preferential extracellular generation of the active parkinsonian toxin MPP(+) by transporter-independent export of the intermediate MPDP(.). Antioxid. Redox Signal. 23, 1001–1016.

Scholz, D., et al., 2011. Rapid, complete and large-scale generation of post-mitotic neurons from the human LUHMES cell line. J. Neurochem. 119, 957–971.

Sheng, C., et al., 2013. DJ-1 deficiency perturbs microtubule dynamics and impairs striatal neurite outgrowth. Neurobiol. Aging 34, 489–498.

Stambolic, V., et al., 1998. Negative regulation of PKB/Akt-dependent cell survival by the tumor suppressor PTEN. Cell 95, 29–39.

Stephen, T.-L., et al., 2015. Miro1 regulates activity-driven positioning of mitochondria within astrocytic processes Apposed to synapses to regulate intracellular calcium signaling. J. Neurosci. 35, 15996–16011.

Strelko, C.L., et al., 2011. Itaconic acid is a mammalian metabolite induced during macrophage activation. J. Am. Chem. Soc. 133, 16386–16389.

Sun, H., et al., 1999. PTEN modulates cell cycle progression and cell survival by regulating phosphatidylinositol 3,4,5,-trisphosphate and Akt/protein kinase B signaling pathway. Proc. Natl. Acad. Sci. U. S. A. 96, 6199–6204.

Suzuki, S., et al., 2010. Phosphate-activated glutaminase (GLS2), a p53-inducible regulator of glutamine metabolism and reactive oxygen species. Proc. Natl. Acad. Sci. 107, 7461–7466.

Tannahill, G.M., et al., 2013. Succinate is an inflammatory signal that induces IL-1β through HIF-1α. Nature 496, 238–242.

Taylor, Z.J., Gurka, R., Kopp, G.A., Liberzon, A., 2010. Long-duration time-resolved PIV to study unsteady aerodynamics. IEEE Trans. Instrum. Meas. 59, 3262–3269.

Tolle, S.W., Dyson, R., Newburgh, R., Cardenas, J.M., 1976. Pyruvate kinase isozymes in neurons, glia, neuroblastoma, and glioblastoma. J. Neurochem. 27, 1355–1360.

Trudler, D., Weinreb, O., Mandel, S.A., Youdim, M.B.H., Frenkel, D., 2014. DJ-1 deficiency triggers microglia sensitivity to dopamine toward a pro-inflammatory phenotype that is attenuated by rasagiline. J. Neurochem. 129, 434–447.

van der Brug, M.P., et al., 2008. RNA binding activity of the recessive parkinsonism protein DJ-1 supports involvement in multiple cellular pathways. Proc. Natl. Acad. Sci. 105, 10244–10249.

Van Duijn, C.M., et al., 2001. PARK7, a novel locus for autosomal recessive early-onset parkinsonism, on chromosome 1p36. Am. J. Hum. Genet. 69, 629–634.

Vasseur, S., et al., 2009. DJ-1/PARK7 is an important mediator of hypoxia-induced cellular responses. Proc. Natl. Acad. Sci. 106, 1111–1116.

Vousden, K.H., Ryan, K.M., 2009. p53 and metabolism. Nat. Rev. Cancer 9, 691–700.

Waak, J., et al., 2009. Regulation of astrocyte inflammatory responses by the Parkinson's disease-associated gene DJ-1. FASEB J. 23, 2478–2489.

Wegner, A., Meiser, J., Weindl, D., Hiller, K., 2015. How metabolites modulate metabolic flux. Curr. Opin. Biotechnol. 34, 16–22.

Wise, D.R., Thompson, C.B., 2010. Glutamine addiction: a new therapeutic target in cancer. Trends Biochem. Sci. 35, 427–433.

Yang, Y., et al., 2005. Inactivation of *Drosophila* DJ-1 leads to impairments of oxidative stress response and phosphatidylinositol 3-kinase/Akt signaling. Proc. Natl. Acad. Sci. U. S. A. 102, 13670–13675.

Yuen, H.-F., et al., 2008. DJ-1 could predict worse prognosis in esophageal squamous cell carcinoma. Cancer Epidemiol. Biomark. Prev. 17, 3593–3602.

Zhang, X., Goncalves, R., Mosser, D.M., 2008. The isolation and characterization of murine macrophages. Curr. Protoc. Immunol. http://dx.doi.org/10.1002/0471142735.im1401s83 (Chapter 14:Unit 14.1).

Zhou, W., Freed, C.R., 2005. DJ-1 up-regulates glutathione synthesis during oxidative stress and inhibits A53T α-synuclein toxicity. J. Biol. Chem. 280, 43150–43158.

Bibliography

[1] E. R. Dorsey, R. Constantinescu, J. P. Thompson, K. M. Biglan, R. G. Holloway, K. Kieburtz, F. J. Marshall, B. M. Ravina, G. Schifitto, A. Siderowf, and C. M. Tanner. "Projected number of people with Parkinson disease in the most populous nations, 2005 through 2030." eng. In: *Neurology* 68.5 (2007), pp. 384–386.

[2] A. Wood-Kaczmar, S. Gandhi, and N. W. Wood. "Understanding the molecular causes of Parkinson's disease." eng. In: *Trends Mol Med* 12.11 (2006), pp. 521–528.

[3] J. Parkinson. *An essay on the shaking palsy*. Ed. by Sherwood. Whittingham, Rowland for Sherwood, Neely, and Jones, 1817.

[4] M Angela Cenci. "Dopamine dysregulation of movement control in L-DOPA-induced dyskinesia." eng. In: *Trends Neurosci* 30.5 (2007), pp. 236–243.

[5] M. S. Pollanen, D. W. Dickson, and C. Bergeron. "Pathology and biology of the Lewy body." eng. In: *J Neuropathol Exp Neurol* 52.3 (1993), pp. 183–191.

[6] M. Baba, S. Nakajo, P. H. Tu, T. Tomita, K. Nakaya, V. M. Lee, J. Q. Trojanowski, and T. Iwatsubo. "Aggregation of alpha-synuclein in Lewy bodies of sporadic Parkinson's disease and dementia with Lewy bodies." eng. In: *Am J Pathol* 152.4 (1998), pp. 879–884.

[7] B. Scatton, F. Javoy-Agid, L. Rouquier, B. Dubois, and Y. Agid. "Reduction of cortical dopamine, noradrenaline, serotonin and their metabolites in Parkinson's disease." eng. In: *Brain Res* 275.2 (1983), pp. 321–328.

[8] Ronald B. Postuma, Dag Aarsland, Paolo Barone, David J. Burn, Christopher H. Hawkes, Wolfgang Oertel, and Tjalf Ziemssen. "Identifying prodromal Parkinson's disease: pre-motor disorders in Parkinson's disease." eng. In: *Mov Disord* 27.5 (2012), pp. 617–626.

[9] Christopher G. Goetz, Barbara C. Tilley, Stephanie R. Shaftman, Glenn T. Stebbins, Stanley Fahn, Pablo Martinez-Martin, Werner Poewe, Cristina Sampaio, Matthew B. Stern, Richard Dodel, Bruno Dubois, Robert Holloway, Joseph Jankovic, Jaime Kulisevsky, Anthony E. Lang, Andrew Lees, Sue Leurgans, Peter A. LeWitt, David Nyenhuis, C Warren Olanow, Olivier Rascol, Anette

Schrag, Jeanne A. Teresi, Jacobus J. van Hilten, Nancy LaPelle, and Movement Disorder Society U. P. D. R. S Revision Task Force. "Movement Disorder Society-sponsored revision of the Unified Parkinson's Disease Rating Scale (MDS-UPDRS): scale presentation and clinimetric testing results." eng. In: *Mov Disord* 23.15 (2008), pp. 2129–2170.

[10]   Christine Klein and Ana Westenberger. "Genetics of Parkinson's disease." eng. In: *Cold Spring Harb Perspect Med* 2.1 (2012), a008888.

[11]   Anthony H V. Schapira. "Mitochondria in the aetiology and pathogenesis of Parkinson's disease." eng. In: *Lancet Neurol* 7.1 (2008), pp. 97–109.

[12]   Aleksandar Rakovic, Anne Grünewald, Jan Kottwitz, Norbert Brüggemann, Peter P. Pramstaller, Katja Lohmann, and Christine Klein. "Mutations in PINK1 and Parkin impair ubiquitination of Mitofusins in human fibroblasts." eng. In: *PLoS One* 6.3 (2011), e16746.

[13]   Vanessa A. Morais, Dominik Haddad, Katleen Craessaerts, Pieter-Jan De Bock, Jef Swerts, Sven Vilain, Liesbeth Aerts, Lut Overbergh, Anne Grünewald, Philip Seibler, Christine Klein, Kris Gevaert, Patrik Verstreken, and Bart De Strooper. "PINK1 loss-of-function mutations affect mitochondrial complex I activity via NdufA10 ubiquinone uncoupling." eng. In: *Science* 344.6180 (2014), pp. 203–207.

[14]   Takanori Yokota, Kanako Sugawara, Kaoru Ito, Ryosuke Takahashi, Hiroyoshi Ariga, and Hidehiro Mizusawa. "Down regulation of DJ-1 enhances cell death by oxidative stress, ER stress, and proteasome inhibition." eng. In: *Biochem Biophys Res Commun* 312.4 (2003), pp. 1342–1348.

[15]   L. J. Hsu, Y. Sagara, A. Arroyo, E. Rockenstein, A. Sisk, M. Mallory, J. Wong, T. Takenouchi, M. Hashimoto, and E. Masliah. "alpha-synuclein promotes mitochondrial deficit and oxidative stress." eng. In: *Am J Pathol* 157.2 (2000), pp. 401–410.

[16]   B. J. Day, M. Patel, L. Calavetta, L. Y. Chang, and J. S. Stamler. "A mechanism of paraquat toxicity involving nitric oxide synthase." eng. In: *Proc Natl Acad Sci U S A* 96.22 (1999), pp. 12760–12765.

[17]   R. Betarbet, T. B. Sherer, G. MacKenzie, M. Garcia-Osuna, A. V. Panov, and J. T. Greenamyre. "Chronic systemic pesticide exposure reproduces features of Parkinson's disease." eng. In: *Nat Neurosci* 3.12 (2000), pp. 1301–1306.

[18]   I. Prieur, J. Lunardi, and A. Dupuis. "Evidence for a quinone binding site close to the interface between NUOD and NUOB subunits of Complex I." eng. In: *Biochim Biophys Acta* 1504.2-3 (2001), pp. 173–178.

[19]   Firoj Hossain Khan, Tanusree Sen, Arpan Kumar Maiti, Sirsendu Jana, Uttara Chatterjee, and Sasanka Chakrabarti. "Inhibition of rat brain mitochondrial electron transport chain activity by dopamine oxidation products during extended in vitro incubation: implications for Parkinson's disease." eng. In: *Biochim Biophys Acta* 1741.1-2 (2005), pp. 65–74.

[20]   William Dauer and Serge Przedborski. "Parkinson's disease: mechanisms and models." eng. In: *Neuron* 39.6 (2003), pp. 889–909.

[21]   William M. Pardridge. "Blood-brain barrier delivery." eng. In: *Drug Discov Today* 12.1-2 (2007), pp. 54–61.

[22] Rajesh Pahwa and Kelly E Lyons. *Handbook of Parkinson's disease*. Ed. by Rajesh Pahwa and Kelly E Lyons. CRC Press, 2003.

[23] P. S. Papavasiliou, G. C. Cotzias, S. E. Düby, A. J. Steck, C. Fehling, and M. A. Bell. "Levodopa in Parkinsonism: potentiation of central effects with a peripheral inhibitor." eng. In: *N Engl J Med* 286.1 (1972), pp. 8–14.

[24] P.S. Byrne H.W. Proctor. *A Handbook of Treatment*. Ed. by P.S. Byrne H.W. Proctor. MPT Press Ltd, 1976.

[25] Michael Rezak. "Current pharmacotherapeutic treatment options in Parkinson's disease." eng. In: *Dis Mon* 53.4 (2007), pp. 214–222.

[26] Neha Singh, Viness Pillay, and Yahya E. Choonara. "Advances in the treatment of Parkinson's disease." eng. In: *Prog Neurobiol* 81.1 (2007), pp. 29–44.

[27] Olle Lindvall, Zaal Kokaia, and Alberto Martinez-Serrano. "Stem cell therapy for human neurodegenerative disorders-how to make it work." eng. In: *Nat Med* 10 Suppl (2004), S42–S50.

[28] Wen Li, Elisabet Englund, Håkan Widner, Bengt Mattsson, Danielle van Westen, Jimmy Lätt, Stig Rehncrona, Patrik Brundin, Anders Björklund, Olle Lindvall, and Jia-Yi Li. "Extensive graft-derived dopaminergic innervation is maintained 24 years after transplantation in the degenerating parkinsonian brain". In: *Proceedings of the National Academy of Sciences* (2016). eprint: `http://www.pnas.org/content/early/2016/04/26/1605245113.full.pdf`.

[29] Deep-Brain Stimulation for Parkinson's Disease Study Group. "Deep-brain stimulation of the subthalamic nucleus or the pars interna of the globus pallidus in Parkinson's disease." eng. In: *N Engl J Med* 345.13 (2001), pp. 956–963.

[30] T.H. Champney. *Essential Clinical Neuroanatomy*. Essentials Series. Wiley, 2015.

[31] William J Marks, Raymond T Bartus, Joao Siffert, Charles S Davis, Andres Lozano, Nicholas Boulis, Jerrold Vitek, Mark Stacy, Dennis Turner, Leonard Verhagen, and et al. "Gene delivery of AAV2-neurturin for Parkinson disease: a double-blind, randomised, controlled trial". In: *The Lancet Neurology* 9.12 (2010), 1164–1172.

[32] RaymondT Bartus. "Gene therapy for Parkinson disease: a decade of progress supported by posthumous contributions from volunteer subjects". In: *Neural Regeneration Research* 10.10 (2015), p. 1586.

[33] D. L. Roe. "From DOPA to Parkinson's disease: the early history of dopamine research." eng. In: *J Hist Neurosci* 6.3 (1997), pp. 291–301.

[34] T. Flatmark. "Catecholamine biosynthesis and physiological regulation in neuroendocrine cells." eng. In: *Acta Physiol Scand* 168.1 (2000), pp. 1–17.

[35] Shankar J. Chinta and Julie K. Andersen. "Dopaminergic neurons." eng. In: *Int J Biochem Cell Biol* 37.5 (2005), pp. 942–946.

[36] Anders Björklund and Stephen B. Dunnett. "Dopamine neuron systems in the brain: an update." eng. In: *Trends Neurosci* 30.5 (2007), pp. 194–202.

[37] Shane V. Hegarty, Aideen M. Sullivan, and Gerard W. O'Keeffe. "Midbrain dopaminergic neurons: a review of the molecular circuitry that regulates their development." eng. In: *Dev Biol* 379.2 (2013), pp. 123–138.

[38] David L. Felten and John R. Sladek. "Monoamine distribution in primate brain V. Monoaminergic nuclei: Anatomy, pathways and local organization". In: *Brain Research Bulletin* 10.2 (1983), 171–284.

[39] Boadie W. Dunlop and Charles B. Nemeroff. "The role of dopamine in the pathophysiology of depression." eng. In: *Arch Gen Psychiatry* 64.3 (2007), pp. 327–337.

[40] Oscar Arias-Carrión, Maria Stamelou, Eric Murillo-Rodríguez, Manuel Menéndez-González, and Ernst Pöppel. "Dopaminergic reward system: a short integrative review." eng. In: *Int Arch Med* 3 (2010), p. 24.

[41] Roger Cachope and Joseph F. Cheer. "Local control of striatal dopamine release." eng. In: *Front Behav Neurosci* 8 (2014), p. 188.

[42] G. Eisenhofer, A. Aneman, P. Friberg, D. Hooper, L. Fåndriks, H. Lonroth, B. Hunyady, and E. Mezey. "Substantial production of dopamine in the human gastrointestinal tract." eng. In: *J Clin Endocrinol Metab* 82.11 (1997), pp. 3864–3871.

[43] Ronald F. Pfeiffer. "Gastrointestinal dysfunction in Parkinson's disease." eng. In: *Lancet Neurol* 2.2 (2003), pp. 107–116.

[44] Patricio Soares-da Silva and Maria Paula Serrao. "High- and low-affinity transport of L-leucine and L-DOPA by the hetero amino acid exchangers LAT1 and LAT2 in LLC-PK1 renal cells." eng. In: *Am J Physiol Renal Physiol* 287.2 (2004), F252–F261.

[45] Robert M. Carey. "Renal Dopamine System". In: *Hypertension* 38.3 (2001), 297–302.

[46] S. Basu and P. S. Dasgupta. "Dopamine, a neurotransmitter, influences the immune system." eng. In: *J Neuroimmunol* 102.2 (2000), pp. 113–124.

[47] Rafael Franco, Rodrigo Pacheco, Carmen Lluis, Gerard P. Ahern, and Peta J. O'Connell. "The emergence of neurotransmitters as immune modulators." eng. In: *Trends Immunol* 28.9 (2007), pp. 400–407.

[48] Paul Witkovsky. "Dopamine and retinal function." eng. In: *Doc Ophthalmol* 108.1 (2004), pp. 17–40.

[49] Ari Barzilai and Eldad Melamed. "Molecular mechanisms of selective dopaminergic neuronal death in Parkinson's disease." eng. In: *Trends Mol Med* 9.3 (2003), pp. 126–132.

[50] Asa Abeliovich and Rachel Hammond. "Midbrain dopamine neuron differentiation: factors and fates." eng. In: *Dev Biol* 304.2 (2007), pp. 447–454.

[51] S Colette Daubner, Tiffany Le, and Shanzhi Wang. "Tyrosine hydroxylase and regulation of dopamine synthesis." eng. In: *Arch Biochem Biophys* 508.1 (2011), pp. 1–12.

[52] M. A. Mena, J. Garcia de Yebenes, A. Dwork, S. Fahn, N. Latov, J. Herbert, E. Flaster, and D. Slonim. "Biochemical properties of monoamine-rich human neuroblastoma cells." eng. In: *Brain Res* 486.2 (1989), pp. 286–296.

[53] M. A. Mena, B. Pardo, M. J. Casarejos, S. Fahn, and J. García de Yébenes. "Neu-rotoxicity of levodopa on catecholamine-rich neurons." eng. In: *Mov Disord* 7.1 (1992), pp. 23–31.

[54] Fernanda Martins Lopes, Rafael Schröder, Mário Luiz Conte da Frota Jr, Alfeu Zanotto-Filho, Carolina Beatriz Müller, André Simões Pires, Rosalva Thereza Meurer, Gabriela Delevati Colpo, Daniel Pens Gelain, Flávio Kapczinski, José Cláudio Fonseca Moreira, Marilda da Cruz Fernandes, and Fabio Klamt. "Com-parison between proliferative and neuron-like SH-SY5Y cells as an in vitro model for Parkinson disease studies." eng. In: *Brain Res* 1337 (2010), pp. 85–94.

[55] J. C. Byrd, M. Hadjiconstantinou, and D. Cavalla. "Epinephrine synthesis in the PC12 pheochromocytoma cell line." eng. In: *Eur J Pharmacol* 127.1-2 (1986), pp. 139–142.

[56] E. Mazzio and K F A. Soliman. "Whole genome expression profile in neuroblas-toma cells exposed to 1-methyl-4-phenylpyridine." eng. In: *Neurotoxicology* 33.5 (2012), pp. 1156–1169.

[57] Roger G. Tremblay, Marianna Sikorska, Jagdeep K. Sandhu, Patricia Lanthier, Maria Ribecco-Lutkiewicz, and Mahmud Bani-Yaghoub. "Differentiation of mouse Neuro 2A cells into dopamine neurons." eng. In: *J Neurosci Methods* 186.1 (2010), pp. 60–67.

[58] Diana Scholz, Dominik Pöltl, Andreas Genewsky, Matthias Weng, Tanja Wald-mann, Stefan Schildknecht, and Marcel Leist. "Rapid, complete and large-scale generation of post-mitotic neurons from the human LUHMES cell line." eng. In: *J Neurochem* 119.5 (2011), pp. 957–971.

[59] Peter R. Dunkley, Larisa Bobrovskaya, Mark E. Graham, Ellak I. von Nagy-Felsobuki, and Phillip W. Dickson. "Tyrosine hydroxylase phosphorylation: reg-ulation and consequences." eng. In: *J Neurochem* 91.5 (2004), pp. 1025–1043.

[60] Laura J. Lewis-Tuffin, Patrick G. Quinn, and Dona M. Chikaraishi. "Tyrosine hydroxylase transcription depends primarily on cAMP response element activ-ity, regardless of the type of inducing stimulus." eng. In: *Mol Cell Neurosci* 25.3 (2004), pp. 536–547.

[61] M. F. Czyzyk-Krzeska and J. E. Beresh. "Characterization of the hypoxia-inducible protein binding site within the pyrimidine-rich tract in the 3'-untranslated region of the tyrosine hydroxylase mRNA." eng. In: *J Biol Chem* 271.6 (1996), pp. 3293–3299.

[62] Anna S. Hui, Justin B. Striet, Gary Gudelsky, Galia K. Soukhova, Evelyne Gozal, Dana Beitner-Johnson, Shang-Z. Guo, Leroy R Sachleben Jr, John W. Haycock, David Gozal, and Maria F. Czyzyk-Krzeska. "Regulation of catecholamines by sustained and intermittent hypoxia in neuroendocrine cells and sympathetic neurons." eng. In: *Hypertension* 42.6 (2003), pp. 1130–1136.

[63] N. S. Quinsey, A. Q. Luong, and P. W. Dickson. "Mutational analysis of substrate inhibition in tyrosine hydroxylase." eng. In: *J Neurochem* 71.5 (1998), pp. 2132–2138.

[64] Ernst R. Werner, Nenad Blau, and Beat Thöny. "Tetrahydrobiopterin: biochem-istry and pathophysiology." eng. In: *Biochem J* 438.3 (2011), pp. 397–414.

[65] M. Y. Zhu and A. V. Juorio. "Aromatic L-amino acid decarboxylase: biological characterization and functional role." eng. In: *Gen Pharmacol* 26.4 (1995), pp. 681–696.

[66] M. D. Berry, A. V. Juorio, X. M. Li, and A. A. Boulton. "Aromatic L-amino acid decarboxylase: a neglected and misunderstood enzyme." eng. In: *Neurochem Res* 21.9 (1996), pp. 1075–1087.

[67] Kelly M. Lohr and Gary W. Miller. "VMAT2 and Parkinson's disease: harnessing the dopamine vesicle." eng. In: *Expert Rev Neurother* 14.10 (2014), pp. 1115–1117.

[68] Lee E. Eiden and Eberhard Weihe. "VMAT2: a dynamic regulator of brain monoaminergic neuronal function interacting with drugs of abuse." eng. In: *Ann N Y Acad Sci* 1216 (2011), pp. 86–98.

[69] Jean-Martin Beaulieu and Raul R. Gainetdinov. "The physiology, signaling, and pharmacology of dopamine receptors." eng. In: *Pharmacol Rev* 63.1 (2011), pp. 182–217.

[70] C. Missale, S. R. Nash, S. W. Robinson, M. Jaber, and M. G. Caron. "Dopamine receptors: from structure to function." eng. In: *Physiol Rev* 78.1 (1998), pp. 189–225.

[71] Roxanne A. Vaughan and James D. Foster. "Mechanisms of dopamine transporter regulation in normal and disease states." eng. In: *Trends Pharmacol Sci* 34.9 (2013), pp. 489–496.

[72] Gonzalo E. Torres, Raul R. Gainetdinov, and Marc G. Caron. "Plasma membrane monoamine transporters: structure, regulation and function." eng. In: *Nat Rev Neurosci* 4.1 (2003), pp. 13–25.

[73] Masato Asanuma, Ikuko Miyazaki, Shinki Murakami, Francisco J. Diaz-Corrales, and Norio Ogawa. "Striatal astrocytes act as a reservoir for L-DOPA." eng. In: *PLoS One* 9.9 (2014), e106362.

[74] A. Storch, A. C. Ludolph, and J. Schwarz. "Dopamine transporter: involvement in selective dopaminergic neurotoxicity and degeneration." eng. In: *J Neural Transm (Vienna)* 111.10-11 (2004), pp. 1267–1286.

[75] G. Cohen and N. Kesler. "Monoamine oxidase and mitochondrial respiration." eng. In: *J Neurochem* 73.6 (1999), pp. 2310–2315.

[76] Moussa B H. Youdim and Peter F. Riederer. "A review of the mechanisms and role of monoamine oxidase inhibitors in Parkinson's disease." eng. In: *Neurology* 63.7 Suppl 2 (2004), S32–S35.

[77] G. Cohen, R. Farooqui, and N. Kesler. "Parkinson disease: a new link between monoamine oxidase and mitochondrial electron flow." eng. In: *Proc Natl Acad Sci U S A* 94.10 (1997), pp. 4890–4894.

[78] S. Kaakkola. "Clinical pharmacology, therapeutic use and potential of COMT inhibitors in Parkinson's disease." eng. In: *Drugs* 59.6 (2000), pp. 1233–1250.

[79] Timo T. Myöhänen, Nadia Schendzielorz, and Pekka T. Männistö. "Distribution of catechol-O-methyltransferase (COMT) proteins and enzymatic activities in

wild-type and soluble COMT deficient mice." eng. In: *J Neurochem* 113.6 (2010), pp. 1632–1643.

[80] A. Kastner, P. Anglade, C. Bounaix, P. Damier, F. Javoy-Agid, N. Bromet, Y. Agid, and E. C. Hirsch. "Immunohistochemical study of catechol-O-methyltransferase in the human mesostriatal system." eng. In: *Neuroscience* 62.2 (1994), pp. 449–457.

[81] Arthur G. Fitzmaurice, Shannon L. Rhodes, Aaron Lulla, Niall P. Murphy, Hoa A. Lam, Kelley C. O'Donnell, Lisa Barnhill, John E. Casida, Myles Cockburn, Alvaro Sagasti, Mark C. Stahl, Nigel T. Maidment, Beate Ritz, and Jeff M. Bronstein. "Aldehyde dehydrogenase inhibition as a pathogenic mechanism in Parkinson disease." eng. In: *Proc Natl Acad Sci U S A* 110.2 (2013), pp. 636–641.

[82] H. Fedorow, F. Tribl, G. Halliday, M. Gerlach, P. Riederer, and K. L. Double. "Neuromelanin in human dopamine neurons: comparison with peripheral melanins and relevance to Parkinson's disease." eng. In: *Prog Neurobiol* 75.2 (2005), pp. 109–124.

[83] Robert A. Hauser. "Levodopa: past, present, and future." eng. In: *Eur Neurol* 62.1 (2009), pp. 1–8.

[84] Peter A. LeWitt and Stanley Fahn. "Levodopa therapy for Parkinson disease: A look backward and forward." eng. In: *Neurology* 86.14 Suppl 1 (2016), S3–S12.

[85] O. Hornykiewicz. "L-DOPA: from a biologically inactive amino acid to a successful therapeutic agent." eng. In: *Amino Acids* 23.1-3 (2002), pp. 65–70.

[86] Martin R. Gluck and Gail D. Zeevalk. "Inhibition of brain mitochondrial respiration by dopamine and its metabolites: implications for Parkinson's disease and catecholamine-associated diseases." eng. In: *J Neurochem* 91.4 (2004), pp. 788–795.

[87] Patricia Muñoz, Sandro Huenchuguala, Irmgard Paris, and Juan Segura-Aguilar. "Dopamine oxidation and autophagy." eng. In: *Parkinsons Dis* 2012 (2012), p. 920953.

[88] P. L. Chesis, D. E. Levin, M. T. Smith, L. Ernster, and B. N. Ames. "Mutagenicity of quinones: pathways of metabolic activation and detoxification." eng. In: *Proc Natl Acad Sci U S A* 81.6 (1984), pp. 1696–1700.

[89] C. Nathan. "Nitric oxide as a secretory product of mammalian cells." eng. In: *FASEB J* 6.12 (1992), pp. 3051–3064.

[90] N. Hauptmann, J. Grimsby, J. C. Shih, and E. Cadenas. "The metabolism of tyramine by monoamine oxidase A/B causes oxidative damage to mitochondrial DNA." eng. In: *Arch Biochem Biophys* 335.2 (1996), pp. 295–304.

[91] Todd B. Sherer, Ranjita Betarbet, Claudia M. Testa, Byoung Boo Seo, Jason R. Richardson, Jin Ho Kim, Gary W. Miller, Takao Yagi, Akemi Matsuno-Yagi, and J Timothy Greenamyre. "Mechanism of toxicity in rotenone models of Parkinson's disease." eng. In: *J Neurosci* 23.34 (2003), pp. 10756–10764.

[92] Michael J. Zigmond, Teresa G. Hastings, and Ruth G. Perez. "Increased dopamine turnover after partial loss of dopaminergic neurons: compensation or toxicity?" eng. In: *Parkinsonism Relat Disord* 8.6 (2002), pp. 389–393.

[93]   Ikuko Miyazaki and Masato Asanuma. "Dopaminergic neuron-specific oxida-
       tive stress caused by dopamine itself." eng. In: *Acta Med Okayama* 62.3 (2008),
       pp. 141–150.

[94]   A. Bindoli, M. P. Rigobello, and L. Galzigna. "Toxicity of aminochromes." eng.
       In: *Toxicol Lett* 48.1 (1989), pp. 3–20.

[95]   S. B. Berman and T. G. Hastings. "Dopamine oxidation alters mitochondrial
       respiration and induces permeability transition in brain mitochondria: impli-
       cations for Parkinson's disease." eng. In: *J Neurochem* 73.3 (1999), pp. 1127–1137.

[96]   Sujogya Kumar. "Assay Guided Comparison for Enzymatic and Non-Enzymatic
       Antioxidant Activities with Special Reference to Medicinal Plants". In: *Antioxi-
       dant Enzyme* (2012).

[97]   Yun-Zhong Fang, Sheng Yang, and Guoyao Wu. "Free radicals, antioxidants,
       and nutrition." eng. In: *Nutrition* 18.10 (2002), pp. 872–879.

[98]   E. Niki. "Action of ascorbic acid as a scavenger of active and stable oxygen
       radicals." eng. In: *Am J Clin Nutr* 54.6 Suppl (1991), 1119S–1124S.

[99]   W. Wang and N. Ballatori. "Endogenous glutathione conjugates: occurrence and
       biological functions." eng. In: *Pharmacol Rev* 50.3 (1998), pp. 335–356.

[100] Neil S. Isaacs and Rudi van Eldik. "A mechanistic study of the reduction of
       quinones by ascorbic acid". en. In: *Journal of the Chemical Society, Perkin Transac-
       tions 2* 8 (Jan. 1997), pp. 1465–1468.

[101] J. Mãrtensson, A. Meister, and J. Mrtensson. "Glutathione deficiency decreases
       tissue ascorbate levels in newborn rats: ascorbate spares glutathione and pro-
       tects." eng. In: *Proc Natl Acad Sci U S A* 88.11 (1991), pp. 4656–4660.

[102] Umeo Takahama. "The International Journal of Plant Biochemistry Hydrogen
       peroxide scavenging systems in vacuoles of mesophyll cells of Vicia faba". In:
       Phytochemistry 31.4 (1992), pp. 1127 –1133.

[103] Y. Tomita, A. Hariu, C. Mizuno, and M. Seiji. "Inactivation of tyrosinase by
       dopa." eng. In: *J Invest Dermatol* 75.5 (1980), pp. 379–382.

[104] S. Peuchen, J. P. Bolaños, S. J. Heales, A. Almeida, M. R. Duchen, and J. B. Clark.
       "Interrelationships between astrocyte function, oxidative stress and antioxidant
       status within the central nervous system." eng. In: *Prog Neurobiol* 52.4 (1997),
       pp. 261–281.

[105] H. Padh. "Vitamin C: newer insights into its biochemical functions." eng. In:
       Nutr Rev 49.3 (1991), pp. 65–70.

[106] J. X. Wilson. "Antioxidant defense of the brain: a role for astrocytes." eng. In:
       Can J Physiol Pharmacol 75.10-11 (1997), pp. 1149–1163.

[107] C. T. Lai and P. H. Yu. "Dopamine- and L-beta-3,4-dihydroxyphenylalanine hy-
       drochloride (L-Dopa)-induced cytotoxicity towards catecholaminergic neurob-
       lastoma SH-SY5Y cells. Effects of oxidative stress and antioxidative factors."
       eng. In: *Biochem Pharmacol* 53.3 (1997), pp. 363–372.

[108] Julia E. Raftos, Stephney Whillier, Bogdan E. Chapman, and Philip W. Kuchel.
       "Kinetics of uptake and deacetylation of N-acetylcysteine by human erythro-
       cytes." eng. In: *Int J Biochem Cell Biol* 39.9 (2007), pp. 1698–1706.

[109] Reno C. Reyes, Giordano Fabricio Cittolin-Santos, Ji-Eun Kim, Seok Joon Won, Angela M. Brennan-Minnella, Maya Katz, Graham A. Glass, and Raymond A. Swanson. "Neuronal Glutathione Content and Antioxidant Capacity can be Normalized In Situ by N-acetyl Cysteine Concentrations Attained in Human Cerebrospinal Fluid." eng. In: *Neurotherapeutics* 13.1 (2016), pp. 217–225.

[110] R. Dringen, B. Pfeiffer, and B. Hamprecht. "Synthesis of the antioxidant glutathione in neurons: supply by astrocytes of CysGly as precursor for neuronal glutathione." eng. In: *J Neurosci* 19.2 (1999), pp. 562–569.

[111] M. A. Mena, V. Davila, and D. Sulzer. "Neurotrophic effects of L-DOPA in postnatal midbrain dopamine neuron/cortical astrocyte cocultures." eng. In: *J Neurochem* 69.4 (1997), pp. 1398–1408.

[112] G. Agrup, B. Falck, B. M. Kennedy, H. Rorsman, A. M. Rosengren, and E. Rosengren. "Formation of cysteinyldopa from glutathionedopa in melanoma." eng. In: *Acta Derm Venereol* 55.1 (1975), pp. 1–3.

[113] M. J. LaVoie and T. G. Hastings. "Dopamine quinone formation and protein modification associated with the striatal neurotoxicity of methamphetamine: evidence against a role for extracellular dopamine." eng. In: *J Neurosci* 19.4 (1999), pp. 1484–1491.

[114] J. Smythies and L. Galzigna. "The oxidative metabolism of catecholamines in the brain: a review." eng. In: *Biochim Biophys Acta* 1380.2 (1998), pp. 159–162.

[115] F. Solano, V. J. Hearing, and J. C. García-Borrón. "Neurotoxicity due to o-quinones: neuromelanin formation and possible mechanisms for o-quinone detoxification." eng. In: *Neurotox Res* 1.3 (2000), pp. 153–169.

[116] C. Venkateshappa, G. Harish, Rajeswara Babu Mythri, Anita Mahadevan, M M Srinivas Bharath, and S. K. Shankar. "Increased oxidative damage and decreased antioxidant function in aging human substantia nigra compared to striatum: implications for Parkinson's disease." eng. In: *Neurochem Res* 37.2 (2012), pp. 358–369.

[117] T. L. Perry and V. W. Yong. "Idiopathic Parkinson's disease, progressive supranuclear palsy and glutathione metabolism in the substantia nigra of patients." eng. In: *Neurosci Lett* 67.3 (1986), pp. 269–274.

[118] P. Riederer, E. Sofic, W. D. Rausch, B. Schmidt, G. P. Reynolds, K. Jellinger, and M. B. Youdim. "Transition metals, ferritin, glutathione, and ascorbic acid in parkinsonian brains." eng. In: *J Neurochem* 52.2 (1989), pp. 515–520.

[119] Jolanta Dorszewska, Jolanta Florczak, Agata Rozycka, Bartosz Kempisty, Joanna Jaroszewska-Kolecka, Katarzyna Chojnacka, Wiesław H. Trzeciak, and Wojciech Kozubski. "Oxidative DNA damage and level of thiols as related to polymorphisms of MTHFR, MTR, MTHFD1 in Alzheimer's and Parkinson's diseases." eng. In: *Acta Neurobiol Exp (Wars)* 67.2 (2007), pp. 113–129.

[120] John D. Rogers, Anna Sanchez-Saffon, Alan B. Frol, and Ramon Diaz-Arrastia. "Elevated plasma homocysteine levels in patients treated with levodopa: association with vascular disease." eng. In: *Arch Neurol* 60.1 (2003), pp. 59–64.

[121] S Jill James, Stepan Melnyk, Marta Pogribna, Igor P. Pogribny, and Marie A. Caudill. "Elevation in S-adenosylhomocysteine and DNA hypomethylation: potential epigenetic mechanism for homocysteine-related pathology." eng. In: *J Nutr* 132.8 Suppl (2002), 2361S–2366S.

[122] Gary J. Patti, Oscar Yanes, and Gary Siuzdak. "Innovation: Metabolomics: the apogee of the omics trilogy." eng. In: *Nat Rev Mol Cell Biol* 13.4 (2012), pp. 263–269.

[123] Maud M. Koek, Renger H. Jellema, Jan van der Greef, Albert C. Tas, and Thomas Hankemeier. "Quantitative metabolomics based on gas chromatography mass spectrometry: status and perspectives." eng. In: *Metabolomics* 7.3 (2011), pp. 307–328.

[124] William J. Griffiths, Therese Koal, Yuqin Wang, Matthias Kohl, David P. Enot, and Hans-Peter Deigner. "Targeted metabolomics for biomarker discovery." eng. In: *Angew Chem Int Ed Engl* 49.32 (2010), pp. 5426–5445.

[125] C. W. Russ G. Wells H. Prest. *Signal, Noise and Detection Limits in Mass Spectrometry*. Agilent Technologies Inc.

[126] Yang-Rae Kim, Sungyool Bong, Yeon-Joo Kang, Yongtak Yang, Rakesh Kumar Mahajan, Jong Seung Kim, and Hasuck Kim. "Electrochemical detection of dopamine in the presence of ascorbic acid using graphene modified electrodes." eng. In: *Biosens Bioelectron* 25.10 (2010), pp. 2366–2369.

[127] Zheng Guo, Myeong-Lok Seol, Moon-Seok Kim, Jae-Hyuk Ahn, Yang-Kyu Choi, Jin-Huai Liu, and Xing-Jiu Huang. "Sensitive and selective electrochemical detection of dopamine using an electrode modified with carboxylated carbonaceous spheres." eng. In: *Analyst* 138.9 (2013), pp. 2683–2690.

[128] Ewa Rozniecka, Martin Jonsson-Niedziolka, Anna Celebanska, Joanna Niedziolka-Jonsson, and Marcin Opallo. "Selective electrochemical detection of dopamine in a microfluidic channel on carbon nanoparticulate electrodes." eng. In: *Analyst* 139.11 (2014), pp. 2896–2903.

[129] D. G. Watson, R. A. Baines, J. M. Midgley, and J. P. Bacon. "GC/MS determination of biogenic amines in insect neurons." eng. In: *Methods Mol Biol* 72 (1997), pp. 225–237.

[130] Joerg M. Buescher, Maciek R. Antoniewicz, Laszlo G. Boros, Shawn C. Burgess, Henri Brunengraber, Clary B. Clish, Ralph J. DeBerardinis, Olivier Feron, Christian Frezza, Bart Ghesquiere, Eyal Gottlieb, Karsten Hiller, Russell G. Jones, Jurre J. Kamphorst, Richard G. Kibbey, Alec C. Kimmelman, Jason W. Locasale, Sophia Y. Lunt, Oliver D K. Maddocks, Craig Malloy, Christian M. Metallo, Emmanuelle J. Meuillet, Joshua Munger, Katharina Nöh, Joshua D. Rabinowitz, Markus Ralser, Uwe Sauer, Gregory Stephanopoulos, Julie St-Pierre, Daniel A. Tennant, Christoph Wittmann, Matthew G. Vander Heiden, Alexei Vazquez, Karen Vousden, Jamey D. Young, Nicola Zamboni, and Sarah-Maria Fendt. "A roadmap for interpreting (13)C metabolite labeling patterns from cells." eng. In: *Curr Opin Biotechnol* 34 (2015), pp. 189–201.

[131] Karsten Hiller, Christian Metallo, and Gregory Stephanopoulos. "Elucidation of cellular metabolism via metabolomics and stable-isotope assisted metabolomics." eng. In: *Curr Pharm Biotechnol* 12.7 (2011), pp. 1075–1086.

[132] Nathaniel M. Vacanti, Ajit S. Divakaruni, Courtney R. Green, Seth J. Parker, Robert R. Henry, Theodore P. Ciaraldi, Anne N. Murphy, and Christian M. Metallo. "Regulation of substrate utilization by the mitochondrial pyruvate carrier." eng. In: *Mol Cell* 56.3 (2014), pp. 425–435.

[133] Stefan Schildknecht, Susanne Kirner, Anja Henn, Karlo Gasparic, Regina Pape, Liudmila Efremova, Olaf Maier, Roman Fischer, and Marcel Leist. "Characterization of mouse cell line IMA 2.1 as a potential model system to study astrocyte functions." eng. In: *ALTEX* 29.3 (2012), pp. 261–274.

[134] Anja Henn, Søren Lund, Maj Hedtjärn, Andreé Schrattenholz, Peter Pörzgen, and Marcel Leist. "The suitability of BV2 cells as alternative model system for primary microglia cultures or for animal experiments examining brain inflammation." eng. In: *ALTEX* 26.2 (2009), pp. 83–94.

[135] J. L. Biedler, S. Roffler-Tarlov, M. Schachner, and L. S. Freedman. "Multiple neurotransmitter synthesis by human neuroblastoma cell lines and clones." eng. In: *Cancer Res* 38.11 Pt 1 (1978), pp. 3751–3757.

[136] J. O'Brien, I. Wilson, T. Orton, and F. Pognan. "Investigation of the Alamar Blue (resazurin) fluorescent dye for the assessment of mammalian cell cytotoxicity." eng. In: *Eur J Biochem* 267.17 (2000), pp. 5421–5426.

[137] Karsten Hiller, Jasper Hangebrauk, Christian Jäger, Jana Spura, Kerstin Schreiber, and Dietmar Schomburg. "MetaboliteDetector: comprehensive analysis tool for targeted and nontargeted GC/MS based metabolome analysis." eng. In: *Anal Chem* 81.9 (2009), pp. 3429–3439.

[138] R Core Team. *R: A Language and Environment for Statistical Computing*. ISBN 3-900051-07-0. R Foundation for Statistical Computing. Vienna, Austria, 2013.

[139] A. N. Basma, E. J. Morris, W. J. Nicklas, and H. M. Geller. "L-dopa cytotoxicity to PC12 cells in culture is via its autoxidation." eng. In: *J Neurochem* 64.2 (1995), pp. 825–832.

[140] Marie-Véronique Clement, Lee Hua Long, Jeyakumar Ramalingam, and Barry Halliwell. "The cytotoxicity of dopamine may be an artefact of cell culture." eng. In: *J Neurochem* 81.3 (2002), pp. 414–421.

[141] C. M. Jin, Y. J. Yang, H. S. Huang, M. Kai, and M. K. Lee. "Mechanisms of L-DOPA-induced cytotoxicity in rat adrenal pheochromocytoma cells: implication of oxidative stress-related kinases and cyclic AMP." eng. In: *Neuroscience* 170.2 (2010), pp. 390–398.

[142] E. P. Kable, D. Favier, and P. G. Parsons. "Sensitivity of human melanoma cells to L-dopa and DL-buthionine (S,R)-sulfoximine." eng. In: *Cancer Res* 49.9 (1989), pp. 2327–2331.

[143] D. G. Graham. "Oxidative pathways for catecholamines in the genesis of neuromelanin and cytotoxic quinones." eng. In: *Mol Pharmacol* 14.4 (1978), pp. 633–643.

[144] J. Meiser, S. Delcambre, A. Wegner, C. Jäger, J. Ghelfi, A Fouquier d'Herouel, X. Dong, D. Weindl, C. Stautner, Y. Nonnenmacher, A. Michelucci, O. Popp, F. Giesert, S. Schildknecht, L. Krämer, J. G. Schneider, D. Woitalla, W. Wurst, A.

Skupin, D M Vogt Weisenhorn, R. Krüger, M. Leist, and K. Hiller. "Loss of DJ-1 impairs antioxidant response by altered glutamine and serine metabolism." eng. In: *Neurobiol Dis* 89 (2016), pp. 112–125.

[145]   J. S. Beckman, RL Minor Jr, C. W. White, J. E. Repine, G. M. Rosen, and B. A. Freeman. "Superoxide dismutase and catalase conjugated to polyethylene glycol increases endothelial enzyme activity and oxidant resistance." eng. In: *J Biol Chem* 263.14 (1988), pp. 6884–6892.

[146]   H. Shindo, T. Komai, and K. Kawai. "Studies on the metabolism of D- and L-isomers of 3,4-dihydroxyphenylalanine (DOPA). V. Mechanism of intestinal absorption of D- and L-DOPA-14C in rats." eng. In: *Chem Pharm Bull (Tokyo)* 21.9 (1973), pp. 2031–2038.

[147]   F. Vilhardt, J. Haslund-Vinding, V. Jaquet, and G. McBean. "Microglia antioxidant systems and redox signaling." eng. In: *Br J Pharmacol* (2016).

[148]   Cynthia A. Weber and Michael E. Ernst. "Antioxidants, supplements, and Parkinson's disease." eng. In: *Ann Pharmacother* 40.5 (2006), pp. 935–938.

[149]   Jolanta Dorszewska, Michal Prendecki, Margarita Lianeri, and Wojciech Kozubski. "Molecular Effects of L-dopa Therapy in Parkinson's Disease." eng. In: *Curr Genomics* 15.1 (2014), pp. 11–17.

[150]   A. C. Miller and D. Samid. "Tumor resistance to oxidative stress: association with ras oncogene expression and reversal by lovastatin, an inhibitor of p21ras isoprenylation." eng. In: *Int J Cancer* 60.2 (1995), pp. 249–254.

[151]   Y. Agid. "Levodopa: is toxicity a myth?" eng. In: *Neurology* 50.4 (1998), pp. 858–863.

[152]   Andrew P. Wojtovich, C Owen Smith, Cole M. Haynes, Keith W. Nehrke, and Paul S. Brookes. "Physiological consequences of complex II inhibition for aging, disease, and the mKATP channel." eng. In: *Biochim Biophys Acta* 1827.5 (2013), pp. 598–611.

[153]   Karim Bensaad, Atsushi Tsuruta, Mary A. Selak, M Nieves Calvo Vidal, Katsunori Nakano, Ramon Bartrons, Eyal Gottlieb, and Karen H. Vousden. "TIGAR, a p53-inducible regulator of glycolysis and apoptosis." eng. In: *Cell* 126.1 (2006), pp. 107–120.

[154]   E. Brouillet, B. G. Jenkins, B. T. Hyman, R. J. Ferrante, N. W. Kowall, R. Srivastava, D. S. Roy, B. R. Rosen, and M. F. Beal. "Age-dependent vulnerability of the striatum to the mitochondrial toxin 3-nitropropionic acid." eng. In: *J Neurochem* 60.1 (1993), pp. 356–359.

[155]   B. A. McLaughlin, D. Nelson, M. Erecińska, and M. F. Chesselet. "Toxicity of dopamine to striatal neurons in vitro and potentiation of cell death by a mitochondrial inhibitor." eng. In: *J Neurochem* 70.6 (1998), pp. 2406–2415.

[156]   B. A. McLaughlin, D. Nelson, I. A. Silver, M. Erecinska, and M. F. Chesselet. "Methylmalonate toxicity in primary neuronal cultures." eng. In: *Neuroscience* 86.1 (1998), pp. 279–290.

[157]   Peethambaran Arun, John R. Moffett, and Aryan M A. Namboodiri. "Evidence for mitochondrial and cytoplasmic N-acetylaspartate synthesis in SH-SY5Y neuroblastoma cells." eng. In: *Neurochem Int* 55.4 (2009), pp. 219–225.

[158] John R. Moffett, Brian Ross, Peethambaran Arun, Chikkathur N. Madhavarao, and Aryan M A. Namboodiri. "N-Acetylaspartate in the CNS: from neurodiagnostics to neurobiology." eng. In: *Prog Neurobiol* 81.2 (2007), pp. 89–131.

[159] C. Demougeot, P. Garnier, C. Mossiat, N. Bertrand, M. Giroud, A. Beley, and C. Marie. "N-Acetylaspartate, a marker of both cellular dysfunction and neuronal loss: its relevance to studies of acute brain injury." eng. In: *J Neurochem* 77.2 (2001), pp. 408–415.

[160] W. T. Lee, C. S. Lee, Y. L. Pan, and C. Chang. "Temporal changes of cerebral metabolites and striatal lesions in acute 3-nitropropionic acid intoxication in the rat." eng. In: *Magn Reson Med* 44.1 (2000), pp. 29–34.

[161] Maike M. Schmidt and Ralf Dringen. "Differential effects of iodoacetamide and iodoacetate on glycolysis and glutathione metabolism of cultured astrocytes." eng. In: *Front Neuroenergetics* 1 (2009), p. 1.

[162] K. Sakai, K. Hasumi, and A. Endo. "Two glyceraldehyde-3-phosphate dehydrogenase isozymes from the koningic acid (heptelidic acid) producer Trichoderma koningii." eng. In: *Eur J Biochem* 193.1 (1990), pp. 195–202.

[163] S. Przedborski, V. Jackson-Lewis, U. Muthane, H. Jiang, M. Ferreira, A. B. Naini, and S. Fahn. "Chronic levodopa administration alters cerebral mitochondrial respiratory chain activity." eng. In: *Ann Neurol* 34.5 (1993), pp. 715–723.

[164] Andrew J. Worth, Sankha S. Basu, Nathaniel W. Snyder, Clementina Mesaros, and Ian A. Blair. "Inhibition of neuronal cell mitochondrial complex I with rotenone increases lipid β-oxidation, supporting acetyl-coenzyme A levels." eng. In: *J Biol Chem* 289.39 (2014), pp. 26895–26903.

[165] L. Tretter and V. Adam-Vizi. "Inhibition of Krebs cycle enzymes by hydrogen peroxide: A key role of [alpha]-ketoglutarate dehydrogenase in limiting NADH production under oxidative stress." eng. In: *J Neurosci* 20.24 (2000), pp. 8972–8979.

[166] M. Yudkoff, D. Nelson, Y. Daikhin, and M. Erecińska. "Tricarboxylic acid cycle in rat brain synaptosomes. Fluxes and interactions with aspartate aminotransferase and malate/aspartate shuttle." eng. In: *J Biol Chem* 269.44 (1994), pp. 27414–27420.

[167] Shinji Oikawa, Hatasu Kobayashi, Yuki Kitamura, Hong Zhu, Kumi Obata, Yoshio Minabe, Maryia Dazortsava, Kyoko Ohashi, Saeko Tada-Oikawa, Hitoshi Takahashi, Kenichiro Yata, Mariko Murata, and Tetsumori Yamashima. "Proteomic analysis of carbonylated proteins in the monkey substantia nigra after ischemia-reperfusion." eng. In: *Free Radic Res* 48.6 (2014), pp. 694–705.

[168] Yuichiro J. Suzuki, Marina Carini, and D Allan Butterfield. "Protein carbonylation." eng. In: *Antioxid Redox Signal* 12.3 (2010), pp. 323–325.

[169] Anna Stincone, Alessandro Prigione, Thorsten Cramer, Mirjam M C. Wamelink, Kate Campbell, Eric Cheung, Viridiana Olin-Sandoval, Nana-Maria Grüning, Antje Krüger, Mohammad Tauqeer Alam, Markus A. Keller, Michael Breitenbach, Kevin M. Brindle, Joshua D. Rabinowitz, and Markus Ralser. "The return of metabolism: biochemistry and physiology of the pentose phosphate pathway." eng. In: *Biol Rev Camb Philos Soc* (2014).

[170] Markus Ralser, Mirjam M. Wamelink, Axel Kowald, Birgit Gerisch, Gino Heeren, Eduard A. Struys, Edda Klipp, Cornelis Jakobs, Michael Breitenbach, Hans Lehrach, and Sylvia Krobitsch. "Dynamic rerouting of the carbohydrate flux is key to counteracting oxidative stress." eng. In: *J Biol* 6.4 (2007), p. 10.

[171] Xiaofei Wang, Evelyn Perez, Ran Liu, Liang-Jun Yan, Robert T. Mallet, and Shao-Hua Yang. "Pyruvate protects mitochondria from oxidative stress in human neuroblastoma SK-N-SH cells." eng. In: *Brain Res* 1132.1 (2007), pp. 1–9.

[172] Li-Zhen Wang, Wan-Chun Sun, and Xing-Zu Zhu. "Ethyl pyruvate protects PC12 cells from dopamine-induced apoptosis." eng. In: *Eur J Pharmacol* 508.1-3 (2005), pp. 57–68.

[173] Penny L. Sappington, Xiaonan Han, Runkuan Yang, Russell L. Delude, and Mitchell P. Fink. "Ethyl pyruvate ameliorates intestinal epithelial barrier dysfunction in endotoxemic mice and immunostimulated caco-2 enterocytic monolayers." eng. In: *J Pharmacol Exp Ther* 304.1 (2003), pp. 464–476.

[174] Jianying Zeng, Jia Liu, Guo-Yuan Yang, Mark J S. Kelly, Thomas L. James, and Lawrence Litt. "Exogenous ethyl pyruvate versus pyruvate during metabolic recovery after oxidative stress in neonatal rat cerebrocortical slices." eng. In: *Anesthesiology* 107.4 (2007), pp. 630–640.

[175] S. Desagher, J. Glowinski, and J. Prémont. "Pyruvate protects neurons against hydrogen peroxide-induced toxicity." eng. In: *J Neurosci* 17.23 (1997), pp. 9060–9067.

[176] J. O'Donnell-Tormey, C. F. Nathan, K. Lanks, C. J. DeBoer, and J. de la Harpe. "Secretion of pyruvate. An antioxidant defense of mammalian cells." eng. In: *J Exp Med* 165.2 (1987), pp. 500–514.

[177] Jianying Zeng, Guo-Yuan Yang, Weihai Ying, Mark Kelly, Kiyoshi Hirai, Thomas L. James, Raymond A. Swanson, and Lawrence Litt. "Pyruvate improves recovery after PARP-1-associated energy failure induced by oxidative stress in neonatal rat cerebrocortical slices." eng. In: *J Cereb Blood Flow Metab* 27.2 (2007), pp. 304–315.

[178] Luc Pellerin, Anne-Karine Bouzier-Sore, Agnès Aubert, Sébastien Serres, Michel Merle, Robert Costalat, and Pierre J. Magistretti. "Activity-dependent regulation of energy metabolism by astrocytes: an update." eng. In: *Glia* 55.12 (2007), pp. 1251–1262.

[179] L. Pellerin and P. J. Magistretti. "Glutamate uptake into astrocytes stimulates aerobic glycolysis: a mechanism coupling neuronal activity to glucose utilization." eng. In: *Proc Natl Acad Sci U S A* 91.22 (1994), pp. 10625–10629.

[180] X. F. Wang and M. S. Cynader. "Pyruvate released by astrocytes protects neurons from copper-catalyzed cysteine neurotoxicity." eng. In: *J Neurosci* 21.10 (2001), pp. 3322–3331.

[181] Weihai Ying, Conrad C. Alano, Philippe Garnier, and Raymond A. Swanson. "NAD+ as a metabolic link between DNA damage and cell death." eng. In: *J Neurosci Res* 79.1-2 (2005), pp. 216–223.

[182] H. Wang, Y. Mao, A. Y. Chen, N. Zhou, E. J. LaVoie, and L. F. Liu. "Stimulation of topoisomerase II-mediated DNA damage via a mechanism involving protein thiolation." eng. In: *Biochemistry* 40.11 (2001), pp. 3316–3323.

[183] Ryan P. Bender, Amy-Joan L. Ham, and Neil Osheroff. "Quinone-induced enhancement of DNA cleavage by human topoisomerase IIalpha: adduction of cysteine residues 392 and 405." eng. In: *Biochemistry* 46.10 (2007), pp. 2856–2864.

[184] Stryer L. Berg JM Tymoczko JL. *Biochemistry. 5th edition. Section 18.5, Many Shuttles Allow Movement Across the Mitochondrial Membranes*. Ed. by W H Freeman. W H Freeman, 2002.

[185] Shanmugasundaram Ganapathy-Kanniappan and Jean-Francois H. Geschwind. "Tumor glycolysis as a target for cancer therapy: progress and prospects." eng. In: *Mol Cancer* 12 (2013), p. 152.

[186] S. B. Berman and T. G. Hastings. "Inhibition of glutamate transport in synaptosomes by dopamine oxidation and reactive oxygen species." eng. In: *J Neurochem* 69.3 (1997), pp. 1185–1195.

[187] Howard Prentice, Jigar Pravinchandra Modi, and Jang-Yen Wu. "Mechanisms of Neuronal Protection against Excitotoxicity, Endoplasmic Reticulum Stress, and Mitochondrial Dysfunction in Stroke and Neurodegenerative Diseases." eng. In: *Oxid Med Cell Longev* 2015 (2015), p. 964518.

[188] Christof Grewer, Armanda Gameiro, Zhou Zhang, Zhen Tao, Simona Braams, and Thomas Rauen. "Glutamate forward and reverse transport: from molecular mechanism to transporter-mediated release after ischemia." eng. In: *IUBMB Life* 60.9 (2008), pp. 609–619.

[189] J. D. Rothstein, L. Jin, M. Dykes-Hoberg, and R. W. Kuncl. "Chronic inhibition of glutamate uptake produces a model of slow neurotoxicity." eng. In: *Proc Natl Acad Sci U S A* 90.14 (1993), pp. 6591–6595.

[190] Sirsendu Jana, Maitrayee Sinha, Dalia Chanda, Tapasi Roy, Kalpita Banerjee, Soumyabrata Munshi, Birija S. Patro, and Sasanka Chakrabarti. "Mitochondrial dysfunction mediated by quinone oxidation products of dopamine: Implications in dopamine cytotoxicity and pathogenesis of Parkinson's disease." eng. In: *Biochim Biophys Acta* 1812.6 (2011), pp. 663–673.

[191] Caroline Rae, Aurélie D. Fekete, Mohammed A. Kashem, Fatima A. Nasrallah, and Stefan Bröer. "Metabolism, compartmentation, transport and production of acetate in the cortical brain tissue slice." eng. In: *Neurochem Res* 37.11 (2012), pp. 2541–2553.

[192] R. A. Waniewski and D. L. Martin. "Preferential utilization of acetate by astrocytes is attributable to transport." eng. In: *J Neurosci* 18.14 (1998), pp. 5225–5233.

[193] Zachary T. Schug, Barrie Peck, Dylan T. Jones, Qifeng Zhang, Shaun Grosskurth, Israt S. Alam, Louise M. Goodwin, Elizabeth Smethurst, Susan Mason, Karen Blyth, Lynn McGarry, Daniel James, Emma Shanks, Gabriela Kalna, Rebecca E. Saunders, Ming Jiang, Michael Howell, Francois Lassailly, May Zaw Thin, Bradley Spencer-Dene, Gordon Stamp, Niels J F. van den Broek, Gillian Mackay, Vinay Bulusu, Jurre J. Kamphorst, Saverio Tardito, David Strachan, Adrian L. Harris, Eric O. Aboagye, Susan E. Critchlow, Michael J O. Wakelam, Almut

Schulze, and Eyal Gottlieb. "Acetyl-CoA synthetase 2 promotes acetate utilization and maintains cancer cell growth under metabolic stress." eng. In: *Cancer Cell* 27.1 (2015), pp. 57–71.

[194]   Shimin Zhao, Wei Xu, Wenqing Jiang, Wei Yu, Yan Lin, Tengfei Zhang, Jun Yao, Li Zhou, Yaxue Zeng, Hong Li, Yixue Li, Jiong Shi, Wenlin An, Susan M. Hancock, Fuchu He, Lunxiu Qin, Jason Chin, Pengyuan Yang, Xian Chen, Qunying Lei, Yue Xiong, and Kun-Liang Guan. "Regulation of cellular metabolism by protein lysine acetylation." eng. In: *Science* 327.5968 (2010), pp. 1000–1004.

[195]   Xinling Gu, Jing Sun, Shen Li, Xiangmei Wu, and Liang Li. "Oxidative stress induces DNA demethylation and histone acetylation in SH-SY5Y cells: potential epigenetic mechanisms in gene transcription in Aβ production." eng. In: *Neurobiol Aging* 34.4 (2013), pp. 1069–1079.

[196]   Joel E. Ulloth, Carlos A. Casiano, and Marino De Leon. "Palmitic and stearic fatty acids induce caspase-dependent and -independent cell death in nerve growth factor differentiated PC12 cells." eng. In: *J Neurochem* 84.4 (2003), pp. 655–668.

[197]   Diego Mastroeni, Andrew Grover, Brian Leonard, Jeffrey N. Joyce, Paul D. Coleman, Brooke Kozik, Denise L. Bellinger, and Joseph Rogers. "Microglial responses to dopamine in a cell culture model of Parkinson's disease." eng. In: *Neurobiol Aging* 30.11 (2009), pp. 1805–1817.

[198]   Li Qian and Patrick M. Flood. "Microglial cells and Parkinson's disease." eng. In: *Immunol Res* 41.3 (2008), pp. 155–164.

[199]   Lynda J. Peterson and Patrick M. Flood. "Oxidative stress and microglial cells in Parkinson's disease." eng. In: *Mediators Inflamm* 2012 (2012), p. 401264.

[200]   Nikenza Viceconte, Miguel A. Burguillos, Antonio J. Herrera, Rocío M. De Pablos, Bertrand Joseph, and José L. Venero. "Neuromelanin activates proinflammatory microglia through a caspase-8-dependent mechanism." eng. In: *J Neuroinflammation* 12 (2015), p. 5.

[201]   Henrik Wilms, Philip Rosenstiel, Jobst Sievers, Günther Deuschl, Luigi Zecca, and Ralph Lucius. "Activation of microglia by human neuromelanin is NF-kappaB dependent and involves p38 mitogen-activated protein kinase: implications for Parkinson's disease." eng. In: *FASEB J* 17.3 (2003), pp. 500–502.

[202]   Mariza Bortolanza, Roberta Cavalcanti-Kiwiatkoski, Fernando E. Padovan-Neto, Célia Aparecida da Silva, Miso Mitkovski, Rita Raisman-Vozari, and Elaine Del-Bel. "Glial activation is associated with l-DOPA induced dyskinesia and blocked by a nitric oxide synthase inhibitor in a rat model of Parkinson's disease." eng. In: *Neurobiol Dis* 73 (2015), pp. 377–387.

[203]   Alessandro Michelucci, Thekla Cordes, Jenny Ghelfi, Arnaud Pailot, Norbert Reiling, Oliver Goldmann, Tina Binz, André Wegner, Aravind Tallam, Antonio Rausell, Manuel Buttini, Carole L. Linster, Eva Medina, Rudi Balling, and Karsten Hiller. "Immune-responsive gene 1 protein links metabolism to immunity by catalyzing itaconic acid production." eng. In: *Proc Natl Acad Sci U S A* 110.19 (2013), pp. 7820–7825.

[204]   G. M. Tannahill, A. M. Curtis, J. Adamik, E. M. Palsson-McDermott, A. F. McGettrick, G. Goel, C. Frezza, N. J. Bernard, B. Kelly, N. H. Foley, L. Zheng,

A. Gardet, Z. Tong, S. S. Jany, S. C. Corr, M. Haneklaus, B. E. Caffrey, K. Pierce, S. Walmsley, F. C. Beasley, E. Cummins, V. Nizet, M. Whyte, C. T. Taylor, H. Lin, S. L. Masters, E. Gottlieb, V. P. Kelly, C. Clish, P. E. Auron, R. J. Xavier, and L A J. O'Neill. "Succinate is an inflammatory signal that induces IL-1β through HIF-1α." eng. In: *Nature* 496.7444 (2013), pp. 238–242.

[205] Johannes Meiser, Daniel Weindl, and Karsten Hiller. "Complexity of dopamine metabolism." eng. In: *Cell Commun Signal* 11.1 (2013), p. 34.

[206] Michael M. Cox David L. Nelson Albert L. Lehninger. *Lehninger Principles of Biochemistry*. Ed. by W. H. Freeman. W. H. Freeman, 2008, 2008.

[207] John D. Fernstrom and Madelyn H. Fernstrom. "Tyrosine, phenylalanine, and catecholamine synthesis and function in the brain." eng. In: *J Nutr* 137.6 Suppl 1 (2007), 1539S–1547S; discussion 1548S.

[208] M. Karobath and R. J. Baldessarini. "Formation of catechol compounds from phenylalanine and tyrosine with isolated nerve endings." eng. In: *Nat New Biol* 236.68 (1972), pp. 206–208.

[209] A William Tank, Lu Xu, Xiqun Chen, Pheona Radcliffe, and Carol R. Sterling. "Post-transcriptional regulation of tyrosine hydroxylase expression in adrenal medulla and brain." eng. In: *Ann N Y Acad Sci* 1148 (2008), pp. 238–248.

[210] Xiqun Chen, Lu Xu, Pheona Radcliffe, Baoyong Sun, and A William Tank. "Activation of tyrosine hydroxylase mRNA translation by cAMP in midbrain dopaminergic neurons." eng. In: *Mol Pharmacol* 73.6 (2008), pp. 1816–1828.

[211] D. G. Wheeler and E. Cooper. "Depolarization strongly induces human cytomegalovirus major immediate-early promoter/enhancer activity in neurons." eng. In: *J Biol Chem* 276.34 (2001), pp. 31978–31985.

[212] Tanjew Dittgen, Axel Nimmerjahn, Shoji Komai, Pawel Licznerski, Jack Waters, Troy W. Margrie, Fritjof Helmchen, Winfried Denk, Michael Brecht, and Pavel Osten. "Lentivirus-based genetic manipulations of cortical neurons and their optical and electrophysiological monitoring in vivo." eng. In: *Proc Natl Acad Sci U S A* 101.52 (2004), pp. 18206–18211.

[213] Franziska Wilhelm, Ulrike Winkler, Markus Morawski, Carsten Jäger, Lisa Reinecke, Moritz J. Rossner, Petra G. Hirrlinger, and Johannes Hirrlinger. "The human ubiquitin C promoter drives selective expression in principal neurons in the brain of a transgenic mouse line." eng. In: *Neurochem Int* 59.6 (2011), pp. 976–980.

[214] Friederike Herbst, Claudia R. Ball, Francesca Tuorto, Ali Nowrouzi, Wei Wang, Oksana Zavidij, Sebastian M. Dieter, Sylvia Fessler, Franciscus van der Hoeven, Ulrich Kloz, Frank Lyko, Manfred Schmidt, Christof von Kalle, and Hanno Glimm. "Extensive methylation of promoter sequences silences lentiviral transgene expression during stem cell differentiation in vivo." eng. In: *Mol Ther* 20.5 (2012), pp. 1014–1021.

[215] Chin-Ho Cho, Miran Seo, Yun-Il Lee, So-Young Kim, Hong-Duk Youn, and Yong-Sung Juhnn. "Dibutyryl cAMP stimulates the proliferation of SH-SY5Y human neuroblastoma cells by up-regulating Skp2 protein." eng. In: *J Cancer Res Clin Oncol* 133.2 (2007), pp. 135–144.

[216]   G. Chen, P. X. Yuan, Y. M. Jiang, L. D. Huang, and H. K. Manji. "Valproate robustly enhances AP-1 mediated gene expression." eng. In: *Brain Res Mol Brain Res* 64.1 (1999), pp. 52–58.

[217]   Mingjie Li, Nada Husic, Ying Lin, Heather Christensen, Ibrahim Malik, Sally McIver, Christine M. LaPash Daniels, David A. Harris, Paul T. Kotzbauer, Mark P. Goldberg, and B Joy Snider. "Optimal promoter usage for lentiviral vector-mediated transduction of cultured central nervous system cells." eng. In: *J Neurosci Methods* 189.1 (2010), pp. 56–64.

[218]   T. Kageyama, M. Nakamura, A. Matsuo, Y. Yamasaki, Y. Takakura, M. Hashida, Y. Kanai, M. Naito, T. Tsuruo, N. Minato, and S. Shimohama. "The 4F2hc/LAT1 complex transports L-DOPA across the blood-brain barrier." eng. In: *Brain Res* 879.1-2 (2000), pp. 115–121.

[219]   R. E. Yee, D. W. Cheng, S. C. Huang, M. Namavari, N. Satyamurthy, and J. R. Barrio. "Blood-brain barrier and neuronal membrane transport of 6-[18F]fluoro-L-DOPA." eng. In: *Biochem Pharmacol* 62.10 (2001), pp. 1409–1415.

[220]   Do Kyung Kim, Yoshikatsu Kanai, Hye Won Choi, Sahatchai Tangtrongsup, Arthit Chairoungdua, Ellappan Babu, Kittipong Tachampa, Naohiko Anzai, Yuji Iribe, and Hitoshi Endou. "Characterization of the system L amino acid transporter in T24 human bladder carcinoma cells." eng. In: *Biochim Biophys Acta* 1565.1 (2002), pp. 112–121.

[221]   Fiona E. Baird, Kevin J. Bett, Catherine MacLean, Andrew R. Tee, Harinder S. Hundal, and Peter M. Taylor. "Tertiary active transport of amino acids reconstituted by coexpression of System A and L transporters in Xenopus oocytes." eng. In: *Am J Physiol Endocrinol Metab* 297.3 (2009), E822–E829.

[222]   O. Yanagida, Y. Kanai, A. Chairoungdua, D. K. Kim, H. Segawa, T. Nii, S. H. Cha, H. Matsuo, J. Fukushima, Y. Fukasawa, Y. Tani, Y. Taketani, H. Uchino, J. Y. Kim, J. Inatomi, I. Okayasu, K. Miyamoto, E. Takeda, T. Goya, and H. Endou. "Human L-type amino acid transporter 1 (LAT1): characterization of function and expression in tumor cell lines." eng. In: *Biochim Biophys Acta* 1514.2 (2001), pp. 291–302.

[223]   B. Sampaio-Maia, M. P. Serrão, and P. Soares-da Silva. "Regulatory pathways and uptake of L-DOPA by capillary cerebral endothelial cells, astrocytes, and neuronal cells." eng. In: *Am J Physiol Cell Physiol* 280.2 (2001), pp. C333–C342.

[224]   S. R. Jones, R. R. Gainetdinov, M. Jaber, B. Giros, R. M. Wightman, and M. G. Caron. "Profound neuronal plasticity in response to inactivation of the dopamine transporter." eng. In: *Proc Natl Acad Sci U S A* 95.7 (1998), pp. 4029–4034.

[225]   Michael Y. Aksenov, Marina V. Aksenova, Janelle M. Silvers, Charles F. Mactutus, and Rosemarie M. Booze. "Different effects of selective dopamine uptake inhibitors, GBR 12909 and WIN 35428, on HIV-1 Tat toxicity in rat fetal midbrain neurons." eng. In: *Neurotoxicology* 29.6 (2008), pp. 971–977.

[226]   Ming Chi Shih, Marcelo Queiroz Hoexter, Luiz Augusto Franco de Andrade, and Rodrigo Affonseca Bressan. "Parkinson's disease and dopamine transporter neuroimaging: a critical review." eng. In: *Sao Paulo Med J* 124.3 (2006), pp. 168–175.

[227]   John G. Nutt, Julie H. Carter, and Gary J. Sexton. "The dopamine transporter: importance in Parkinson's disease." eng. In: *Ann Neurol* 55.6 (2004), pp. 766–773.

[228]   Keiko Sawabe, Kazumasa Yamamoto, Yoshinori Harada, Akiko Ohashi, Yuko Sugawara, Hiroshi Matsuoka, and Hiroyuki Hasegawa. "Cellular uptake of sepiapterin and push-pull accumulation of tetrahydrobiopterin." eng. In: *Mol Genet Metab* 94.4 (2008), pp. 410–416.

[229]   Cary O. Harding, Mark Neff, Krzysztof Wild, Kelly Jones, Lina Elzaouk, Beat Thöny, and Sheldon Milstien. "The fate of intravenously administered tetrahydrobiopterin and its implications for heterologous gene therapy of phenylketonuria." eng. In: *Mol Genet Metab* 81.1 (2004), pp. 52–57.

[230]   Krystof S. Bankiewicz, John Forsayeth, Jamie L. Eberling, Rosario Sanchez-Pernaute, Philip Pivirotto, John Bringas, Peter Herscovitch, Richard E. Carson, William Eckelman, Bryan Reutter, and Janet Cunningham. "Long-term clinical improvement in MPTP-lesioned primates after gene therapy with AAV-hAADC." eng. In: *Mol Ther* 14.4 (2006), pp. 564–570.

[231]   Gabriele Mittermeyer, Chadwick W. Christine, Kathryn H. Rosenbluth, Suzanne L. Baker, Philip Starr, Paul Larson, Paul L. Kaplan, John Forsayeth, Michael J. Aminoff, and Krystof S. Bankiewicz. "Long-term evaluation of a phase 1 study of AADC gene therapy for Parkinson's disease." eng. In: *Hum Gene Ther* 23.4 (2012), pp. 377–381.